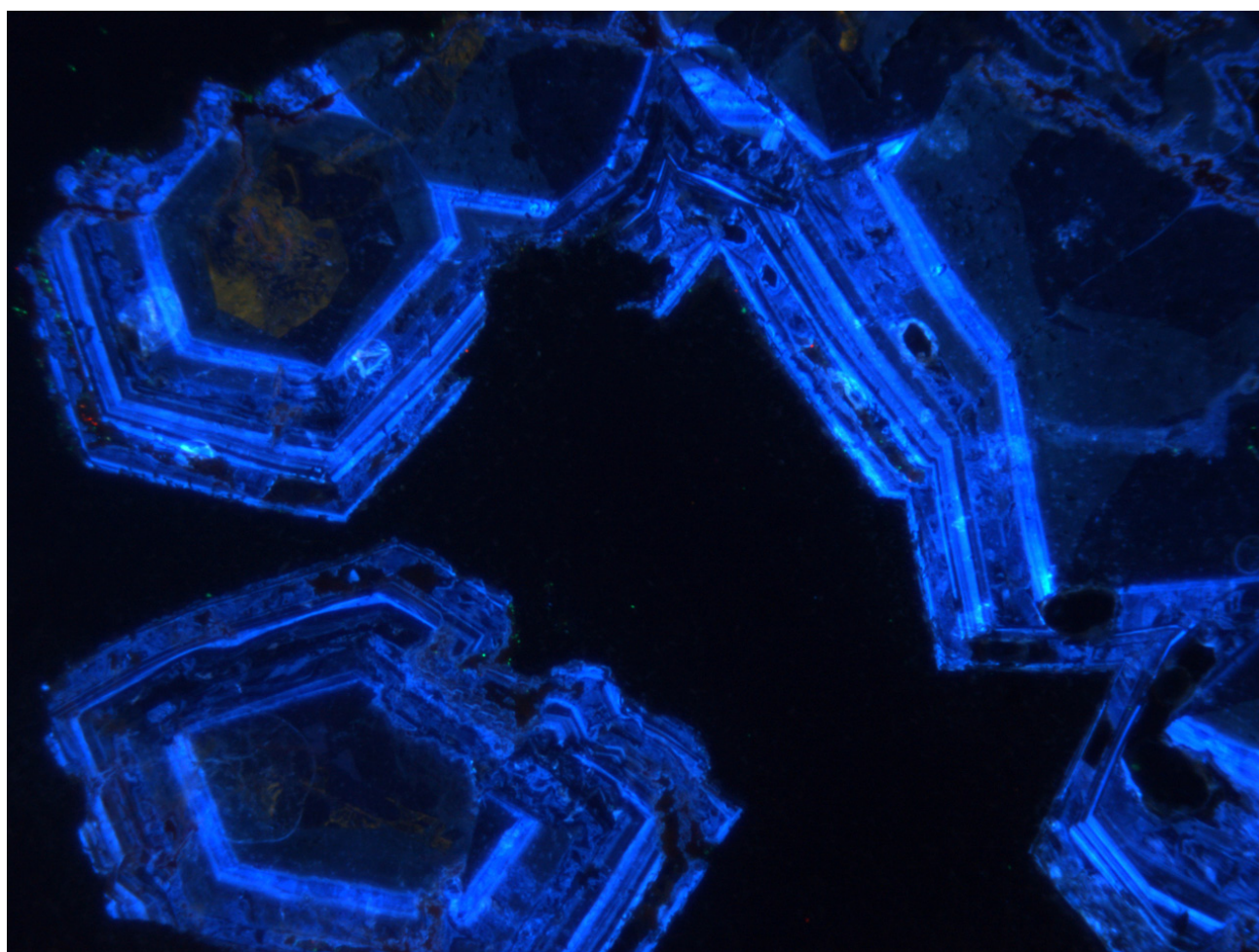


WILLEMITE MINERALISATION IN NAMIBIA AND ZAMBIA

Rosario Terracciano



Dottorato di Ricerca in Scienze della Terra XXI Ciclo

Università degli Studi di Napoli "Federico II"

Facoltà di Scienze MM. FF. NN.

- A.A. 2007/2008 -

WILLEMITE MINERALISATION IN NAMIBIA AND ZAMBIA

MINERALIZZAZIONI A WILLEMITE IN NAMIBIA E ZAMBIA

Rosario Terracciano

Relatore

Prof. Maria Boni
Università degli Studi di Napoli
“Federico II”

Coordinatore

Prof. Stefano Mazzoli
Università degli Studi di Napoli
“Federico II”

Dottorato di Ricerca in Scienze della Terra XXI Ciclo

Università degli Studi di Napoli “Federico II”

Facoltà di Scienze MM. FF. NN.

- A.A. 2007/2008 -

Front page: Kabwe willemite under cathodic light (290 μ A, 12kV), horizontal size ca 1.5mm.

Acknowledgments

This PhD project has gained both direct and indirect support from a few members of the academic world, as well as from many friends that I would like to thank.

First of all, my PhD tutor Prof. **Maria Boni** of the University “Federico II” of Naples (Italy), who introduced me to the ore deposits allowing me, through these years, the opportunity to visit many countries and meet several world famous ore deposit specialists. Without her continual support and encouragement over the last few years I would maybe not have been able to accomplish this work. Also the careful revision of this PhD thesis has greatly benefited of her accurate contribution.

I would like to thank Prof. **Thilo Bechstädt** of the Ruprecht Karls University of Heidelberg (Germany), for his scientific and practical help during the trips to Namibia and my two years stay in Heidelberg. I thank him also for having introduced me to the Laboratories of both Geology and Mineralogy Departments in Heidelberg.

Dr. **Volker Petzel** (formerly Geological Survey of Namibia, now TEAL) helped with the visits and literature of several Namibian willemite deposits. **TEAL** mining company and particularly Dr. **Alex Matthews** are strongly acknowledged for providing technical and operating support during my fieldwork in Zambia and for providing unpublished literature material. I also acknowledge above all the opportunity to sample in the TEAL willemite prospect areas in Kabwe and Lusaka and from the drillcores collections of the same areas.

A special thank goes to the **Society of Economic Geologists**, for having financed my fieldtrip to Chile ore deposits in the spring of 2008, and my participation to the Geocongress in Johannesburg in July of the same year.

The **Deutscher Akademischer Austausch Dienst** (DAAD – German Academic Exchange Service) and the **Ruprecht Karls University of Heidelberg** for their financial support during my stay in Heidelberg are also strongly acknowledged.

I thank all scientists of both Naples and Heidelberg Universities for their constant support while carrying out the mineralogical analyses. In particular, I would like to thank Dr. **Giuseppina Balassone** (Mineralogy Dept. of Naples), Dr. **Ulrich Glasmacher** (Geology Dept. of Heidelberg), Dr. **Ronald Miletich**, Dr. **Hans-Peter Meyer** and Ms. **Ilse Glass** (Mineralogy Dept. of Heidelberg). Many thanks go also to Dr. **Jens Schneider** (Leuven University, Belgium), for providing the ages of some willemite deposits.

Special thanks go to my fellow PhD student in Naples and dear friend Dr. **Vito Coppola**, who encouraged and supported me during the thesis project, being very knowledgeable on the subject of nonsulphide ore deposits. I appreciated particularly his work obstinacy that several times pushed me

to see this journey to its end.

Much appreciation goes to my fellow PhD student in Heidelberg Dr. **Carsten Laukamp** (now in Australia), for introducing me to the Otavi Mountainland geology and for sharing with me both extraordinary field experiences in Namibia (2004) and Zambia (2006), as well as the “long” journey to Victoria Falls.

Dr. **Fabio Lapponi** was one of my Italian “mentors” in Heidelberg, helping me to find a home (his home!) and a bike (his bike!), during his stay in Scotland and Norway for his new job. I will never forget his generosity.

To my room(108)-mate Dr. Thomas Angerer and the other “PhD guys” of the Heidelberg University, goes my gratitude for the unforgettable moments we spent together: Christian Salazar, Eva Lewandowski, Jorham Contreras, Natalia Muñoz, Iris Sonntag and Sonia Pabst. The IPP coordinator Francisco Cueto is fully acknowledged for his didactic, technical and human support. I could really appreciate his “problem-solve” skill.

To all my friends and particularly Dr. Francesco Caruso and Dr. Vittorio Carbone to “brought me back” a piece of Italy when they visited me in Heidelberg. I enjoyed our time spent along the Neckar as much as they enjoyed the Weissbier. A special thank goes to my oldest and dearest friends: Ilaria Canettieri, Carmine Albano, Sabrina Maresca and Eleonora Pistone.

To my brother that kept my working climate light during the writing of this thesis and to my parents, which have been very tolerant with me over the years goes a special thank. Goodbye to my “last” grandmother, who suddenly left us during my stay in Germany: she was 98.

Finally, I fully dedicate this work to Monica just for being her, reminding me who really I am and where really I am going to.

Napoli, 21/11/2008

Rosario Terracciano

CONTENT

ACKNOWLEDGMENTS	3
ABSTRACT.....	7
1 INTRODUCTION AND AIM OF THE THESIS.....	10
2 NONSULPHIDE DEPOSITS.....	12
2.1 CLASSIFICATION AND DEPOSIT TYPES	12
2.2 WILLEMITE: MINERALOGY AND ORE TYPES.....	19
2.3 WILLEMITE MINERALISATION OUT OF AFRICA	22
2.3.1 <i>Vazante</i>	23
2.3.2 <i>Beltana-Aroona</i>	26
2.3.3 <i>Franklin-Sterling Hill</i>	29
3 METHODS.....	32
3.1 SAMPLES COLLECTION AND PREPARATION.....	32
3.2 TRANSMITTED AND REFLECTED LIGHT MICROSCOPY	32
3.3 COLD CATHODOLUMINESCENCE (CL) MICROSCOPY.....	32
3.4 X-RAY DIFFRACTION ANALYSIS (XRPD)	33
3.5 SCANNING ELECTRON MICROSCOPY (SEM) AND ENERGY DISPERSIVE X-RAY SPECTROSCOPY (EDS)	34
3.6 WAVELENGTH DISPERSIVE X-RAY SPECTROSCOPY (WDS).....	35
3.7 WHOLE ROCK GEOCHEMICAL ANALYSES (ICP-MS).....	35
3.8 MICROTHERMOMETRIC ANALYSES OF FLUID INCLUSIONS	36
4 REGIONAL GEOLOGY AND PRIMARY ORE DEPOSITS IN THE STUDIED AREAS.....	38
4.1 OTAVI MOUNTAINLAND, NAMIBIA	38
4.1.1 <i>Geology of the OML</i>	39
4.1.2 <i>Primary ore deposits in the OML</i>	44
4.2 LUFILIAN ARC AND ZAMBEZI, ZAMBIA.....	48
4.2.1 <i>Lufilian Arc</i>	48
4.2.2 <i>Geology of the Kabwe area</i>	50
4.2.3 <i>Primary ore deposits in the Kabwe area</i>	51
4.2.4 <i>Zambezi Belt</i>	53
4.2.5 <i>Geology of the Lusaka area</i>	56
4.3 EVOLUTION OF THE DAMARA-LUFILIAN-ZAMBEZI BELT	58
4.3.1 <i>Deformation phases and metamorphism in the OML</i>	58
4.3.2 <i>Deformation phases and metamorphism in the Lufilian Arc and Zambezi Belt</i>	59
4.3.3 <i>General tectonic evolution of the DLZ</i>	60
5 WILLEMITE MINERALISATION IN THE OTAVI MOUNTAINLAND.....	63
5.1 INTRODUCTION AND MINING HISTORY	63
5.2 BERG AUKAS	64
5.2.1 <i>Northern Ore Horizon</i>	64
5.2.2 <i>Central Orebody</i>	65
5.2.3 <i>Hanging Wall Orebody</i>	66
5.3 ABENAB WEST.....	66
5.4 BALTIKA	66
5.5 MINERALOGY OF THE WILLEMITE ORE IN THE OML	68
5.5.1 <i>Willemite</i>	68
5.5.2 <i>Other minerals</i>	68
5.6 PETROGRAPHY AND PARAGENESIS OF THE WILLEMITE ORE IN THE OML	75
5.6.1 <i>Berg Aukas deposit</i>	75
5.6.2 <i>Abenab West deposit</i>	79
5.7 MAJOR AND TRACE ELEMENTS GEOCHEMISTRY OF WILLEMITE ORES FROM OML	82
5.8 THERMOMETRIC ANALYSIS OF FLUID INCLUSIONS	84
6 WILLEMITE MINERALISATION IN CENTRAL ZAMBIA	90
6.1 INTRODUCTION AND MINING HISTORY	90
6.2 THE KABWE-AREA WILLEMITE DEPOSITS (LUFILIAN ARC)	90

6.2.1	<i>Kabwe Mine</i>	90
6.2.2	<i>Airfield Prospect</i>	93
6.2.3	<i>Kashitu Prospect</i>	94
6.2.4	<i>Millberg prospect</i>	95
6.3	THE LUSAKA-AREA WILLEMITE DEPOSITS (ZAMBEZI BELT)	95
6.4	MINERALOGY, PETROGRAPHY AND GEOCHEMISTRY OF WILLEMITE ORE IN ZAMBIA	97
6.4.1	<i>Mineralogy of willemite ore from Kabwe Area</i>	97
6.4.2	<i>Petrography and paragenesis of willemite ore from the Kabwe Area</i>	107
6.4.3	<i>Major and trace element geochemistry of willemite ore from Kabwe Area</i>	120
6.4.4	<i>Mineralogy of willemite ore from the Lusaka area</i>	125
6.4.5	<i>Petrography and paragenesis of willemite ore from Lusaka area</i>	133
6.4.6	<i>Major and trace element geochemistry of the willemite ore assemblage from Star Zinc</i>	139
6.5	THERMOMETRIC ANALYSIS OF FLUID INCLUSIONS	143
7	AGE CONSTRAINTS OF WILLEMITE MINERALISATION	153
7.1	INTRODUCTION	153
7.2	OML WILLEMITE AGE AND CONSTRAINTS	153
7.3	ZAMBIA WILLEMITE AGE AND CONSTRAINTS	154
8	DISCUSSION	157
8.1	“SUPERGENE” WILLEMITE	157
8.2	“HYPOGENE” WILLEMITE	158
8.3	COMMON AND GENERAL REMARKS	161
8.4	NON AFRICAN WILLEMITE MINERALISATION AGES AND COMPARISONS	161
9	CONCLUSIONS	163
	REFERENCES	164

Abstract

Willemite mineralisation of several Zn-Pb deposits hosted in the Proterozoic carbonates of Namibia and Zambia has been rather neglected in the literature on zinc ores of southern Africa. In fact, willemite (Zn_2SiO_4) is one of the main zinc carriers in several high-grade carbonate-hosted non-sulphide deposits and prospects, located in the southern African subcontinent. These deposits (Berg Aukas, Abenab West and Baltika in the Otavi Mountain Land, Namibia; Kabwe, Excelsior and Star Zinc, Zambia) are currently interpreted (Hitzman *et al.*, 2003) to be all of the same hypogene-hydrothermal origin.

The Otavi Mountain Land (OML) broadly coincides with the Neoproterozoic carbonate platform of the Damara Orogen in Namibia. In the OML several ore deposits and prospects (both sulphides and non-sulphides), are hosted in the shallow-water carbonate successions of the Otavi Group. The primary sulphide ores occurring in the region have been subdivided between the 'Berg Aukas-type' (Zn-Pb MVT) and 'Tsumeb-type' (Pb-Cu-Zn pipes) deposits. A maximum age for 'Tsumeb-type' sulphide ores in the OML is 530 Ma, while the 'Berg Aukas-type' ores seem to be older and related to fluids expelled during the Damaran orogeny. In the few reported occurrences, willemite commonly replaces sphalerite in both ore types, but it may also occur as primary concentrations in the absence of sulphides or replace directly the carbonate host rock.

The Zambian deposits occur in the metasedimentary rocks of the Late Proterozoic Katangan Supergroup. The most important orebodies are located in the Kabwe area (Kabwe n.1-2-3/4-5/6, Airfield and Kashitu) and they contain both sulphides and willemite in dolomite host rocks affected by greenschist facies regional metamorphism. Based on the structural relationships, Zn-Pb sulphide mineralisation in the Kabwe district has been interpreted as having been formed before the last Lufilian deformational phase (ca 650 - 500 Ma) (Kamona and Friedrich, 2006), which would be broadly in the same age range as the OML sulphides. On the contrary, the Star Zinc prospect (Lusaka) is hosted by highly metamorphic lithotypes of the late Proterozoic Zambezi belt sequence. Willemite occurs in both Namibian and Zambian ores in several successive generations and variable paragenetic position. Fluid inclusion studies together with cathodoluminescence petrography and trace element geochemistry are important to distinguish between hypogene, high temperature willemites and low temperature (possibly) supergene ones. In fact in the high-temperature willemite, preferential green luminescent colours indicative of higher Mn values, are more common.

In the Namibian deposits, as well as in the Kabwe orebody, it was possible to detect a typical 'willemitisation' process affecting primary sulphides, where sulphur has been replaced by silica. This process led to an increasingly extended network of needle-thin willemite veins cutting through

sphalerite until a complete removal of Zn-sulphide, whereas early established cerussite rims have preserved galena from total alteration. A hydrothermal dolomite halo, similar to those described at Vazante (Brazil) and Beltana (Australia) by Hitzman *et al.* (2003), is either very limited in space or absent in the African willemite occurrences. However, a further interaction of low temperature acid solutions with the carbonate hosts could have caused the deposition of post-willemite, widespread metal-bearing dolomite cements (Zn+Pb combined up to 10%), closely following a last generation of botryoidal willemite aggregates. In the host carbonates, it is also possible to observe a progressive removal of K and Al from the clay minerals in the stylolite seams, followed by the precipitation of Zn-smectite (sauconite). Smithsonite (ZnCO_3) and hemimorphite [$\text{Zn}_4\text{Si}_2\text{O}_7(\text{OH}) \cdot 2\text{H}_2\text{O}$] occur as late phases filling the remaining porosity of the host rock. In the Star Zinc and Excelsior prospects (Lusaka area) willemite is associated with specular haematite and locally replaces franklinite and gahnite. This mineralogical association has many similarities with that occurring in the Franklin-Sterling Hill deposit (USA). Based on the occurrence of Zn-bearing spinels and other high-temperature minerals, the above-mentioned prospects should be considered of hypogene origin.

The fluid inclusions in the willemites in the Kabwe area, as well as in all the examined specimens from the Namibian mines, are monophase. A preliminary fluid inclusion study of the Star Zinc willemite by Sweeney *et al.* (1991) had produced temperatures ranging between 150-250° C, and salinities around 7-12 eq wt%. Our thermometric analyses roughly confirm the above homogenisation temperatures (Star Zinc and Excelsior Th: 200 - 250°C) and salinities (10 to 16 eq. wt% NaCl). Even if these temperatures are still well below those reached during the regional metamorphism of the Zambezi belt, they point to a hydrothermal origin for the willemite ores in the Lusaka area. The temperatures of the secondary inclusions range from 140 to 190°C for both deposits and the salinities are lower than in the primary ones (2 to 10 eq. wt% NaCl).

The mineralisation timing for most willemite ores is generally poorly constrained, because precise geochronological information on this kind of ore is rare. However, indirect evidence for the timing of the willemite deposits at Vazante (Brazil) and Beltana (Australia) may indicate mineralisation events in the range of ca 490 - 550 Ma (Hitzman *et al.*, 2003). In the general absence of direct radiometric data, the first reliable Rb-Sr isochron model ages have been obtained for the willemite from Namibian deposits by Schneider *et al.* (2008). The measured willemites cover a possible interval of 490 - 550 Ma: these ages are consistent with the late stages of the Damaran orogeny and the uplift phases in the OML. Currently, Rb-Sr geochronology applied to Zambian willemites is still in progress, but the first results are also in the range of an Upper Proterozoic-Cambrian age. The assumed ages may point to a global period of willemite mineralisation extending from Uppermost Proterozoic to lower Ordovician in the southern hemisphere, under special tectonic and climatic

conditions that favoured a circulation of low-temperature hydrothermal, oxygenated waters carrying Zn derived from supergene weathering phenomena. The precipitation of the hypogene high temperature Zn mineralisation occurring in the Lusaka mining area may be of the same age, but in this case the hydrothermal circulation of Zn-carrying fluids was associated with the waning stages of the regional metamorphism in the Zambezi belt.

1 Introduction and aim of the thesis

The aim of this PhD thesis is to characterize the willemite (Zn_2SiO_4) mineralisation from various Zn/Pb mines and prospects of the Otavi Mountainland area (Namibia) and of the Kabwe and Lusaka mining areas (Zambia) (Figure 1.1). To reach this result I have carried out microscopic, mineralogical, petrographic and geochemical investigations on several samples, which have been integrated with field evidence and existing literature. More than 200 samples were examined: mainly willemite and “Zn oxide” (carbonates and silicates) ores, as well as primary sulphides and related hostrock and cements. Three series of samples were collected in July 2003 and 2004, and June 2006 respectively, under the supervision of the Geological Survey of Namibia and Teal Exploration & Mining Company. The samples consist of willemite and “Zn oxides” ore collected *in situ* and from several dumps of already exploited mines. Selected samples have been collected from drillcores.

In regard to Namibia I concentrated on the willemite occurrences of Berg Aukas, Abenab West and Baltika, while in Zambia I sampled the Kabwe orebodies denominated nos. 2 and 5/6, the Airfield and Kashitu prospects, as well as the ores of the Millberg prospect, located approximately 40km north of the Kabwe mine. The other samples were collected in the Star Zinc and Excelsior pit G prospect (10km north of Lusaka). The analytical part of this PhD study has been carried out mainly at the Geologisch-Paläontologisches and Mineralogisches Institut of the Heidelberg University (Germany).

The present study will be developed along the following points:

1. Review of the present knowledge and a classification of the willemite deposits throughout the world;
2. Characterization of the geology, mineralogy and petrography of the chosen areas in Namibia and Zambia, followed by a description of each sampled deposit;
3. Mineralogy and petrography of the willemite ores, and geochemical characterisation and properties of the mineralizing fluids;
4. Possible age constraints for the deposits;
5. Correlation with other willemite occurrences of the southern hemisphere;
6. Models for willemite deposition in the pre-Gondwana geological context.

From the scientific point of view, this thesis represents a complete study on the largest willemite mineralisations occurring in the southern African subcontinent. As a further practical implication, the full mineralogical and petrographic characterisation of such an ore deposit (especially

considering the complex and diversified mineral assemblages of the willemite bodies) plays a very important role, in order to establish how to process the extracted ore and decide on the metallurgy.

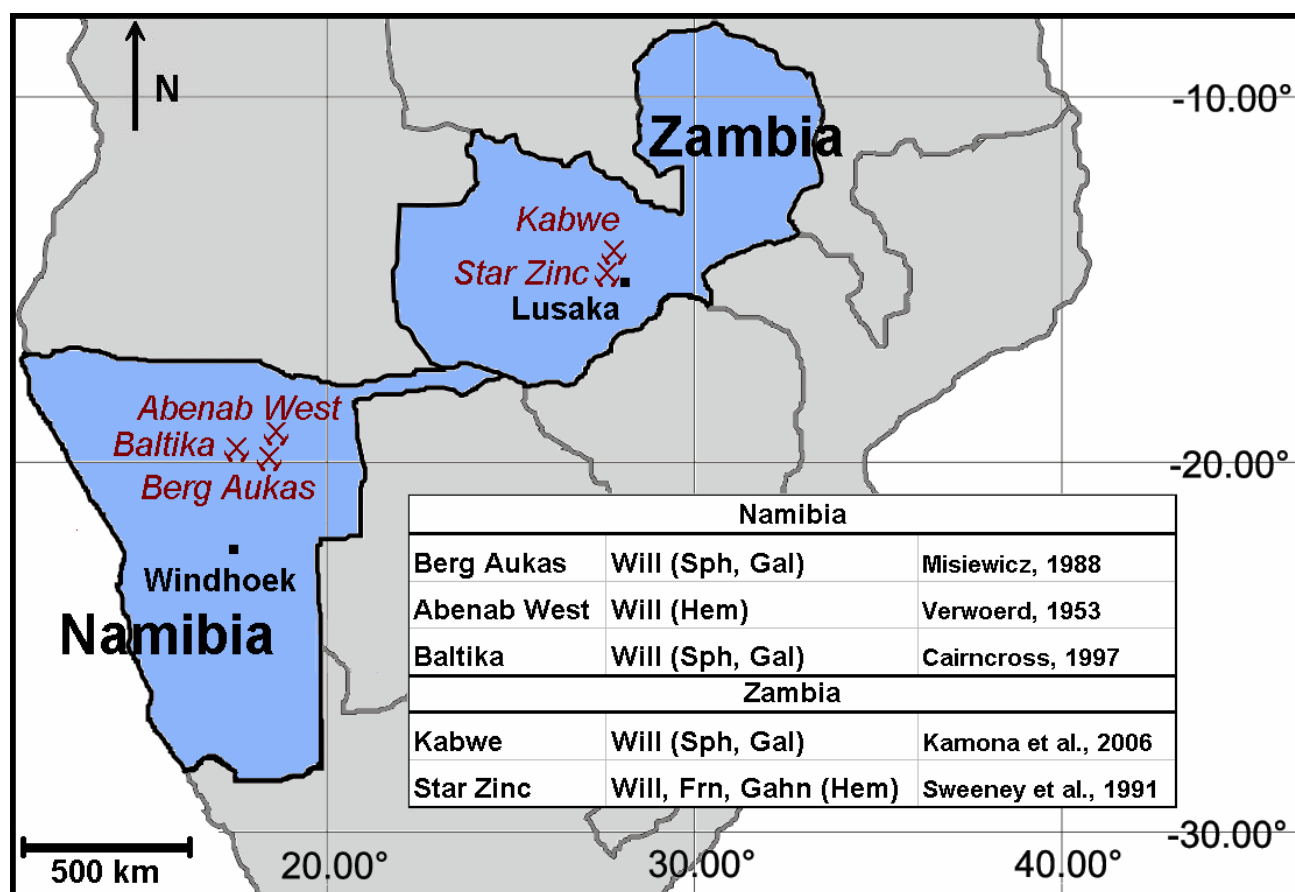


Figure 1.1: Location and schematic mineralogy of the most important willemite deposits and prospects in Namibia and Zambia (Will = willemite, Sph = sphalerite, Gal = galena, Hem = hematite, Frn = franklinite, Gahn = gahnite).

2 Nonsulphide deposits

2.1 *Classification and deposit types*

Nonsulphide Zn-Pb deposits were the prime source for zinc and lead metal production for hundreds of years. They consist mainly of a mixture of Zn-carbonates and silicates with associated Pb-carbonates, oxides and clay minerals (Hitzman et al., 2003, Boni, 2005). They lost their economic importance at the beginning of the twentieth century due to the development of flotation and smelting techniques for zinc sulphides resulting in the exploitation of gigantic Pb-Zn sulphide deposits such as SEDEX and MVT-type. Small productions lasted in Europe until the sixties especially in the Iglesias base-metal district of southern Sardinia (Italy), Belgium and southern Poland.

Even if sulphide ores account still today for most of the zinc production, during the last years nonsulphide Zn-Pb deposits have gained renewed attention and are now considered to be of major importance for the future production of zinc metal (e.g., Large, 2001, Boni, 2003, 2005, Hitzman et al., 2003). This deposit types may contain huge reserves of high grade ores, are mostly easy to exploit, and their ores can now be efficiently processed using improved hydrometallurgical techniques: acid-leaching (LTC), solvent-extraction (SX) and electrowinning (EW) (Woollett, 2005). These techniques allow the extraction of high-grade Zn *in situ* with lower costs. This fact, associated with a higher environmental sustainability, due to the scarcity of non-economic, polluting metals (the so-called “nasties”, as Cd, As and Hg) and the absence of sulphur, is the main reason which promoted a renewed interest of the mining companies towards this kind of ore deposits. However, the paucity of important by-products (Pb, Ag, and Cu) in nonsulphide ores compared with the sulphide ones, lead to consider the nonsulphides economically advantageous only for higher tonnages and grades. Actually nonsulphides represent only the 4.5% of world Zn production (table 2.1). On the base of economic forecasts, they may represent 10% of the annual total zinc production in the next decades.

There are many active projects regarding nonsulphide deposits throughout the world. Their individual tonnage is generally constrained between 1 and 100Mt, with Zn grades ranging between 7% and 30% (Large, 2001, Hitzman et al., 2003, Reynolds et al., 2003, Boni, 2005). Medium to large deposit projects include: Skorpion (Namibia), Mae Sod (Thailand), Lan Ping (China), Angouran (Iran), Mehdiabad (Iran), Shaimerden (Kazakhstan), Jabali (Yemen), Vazante (Brazil). Accha (Peru) and Sierra Mojada (Mexico), while there are a number of other mines producing relatively small tonnages of nonsulphide zinc ores in Vietnam, Turkey, China, Morocco, Tunisia, Zambia and Egypt (Hitzman et al., 2003).

Nonsulphide zinc deposits usually represent the products of supergene oxidation of primary sulphide bodies, but a primary/hydrothermal origin (hypogene) is typical for part of them, including the willemite-dominated types. Many common characteristics, as well as different aspects regarding their mineralogy, geochemistry and emplacement process have been observed in the nonsulphide deposits throughout the world (Figure 2.1).

The mineralogical assemblage of Zn nonsulphides includes a whole number of minerals, but the main economic phases present are Zn-silicates (willemite, hemimorphite, Zn-bearing clays), Zn- Pb-carbonates (smithsonite, cerussite), hydrated Zn- Pb-carbonates (hydrozincite, hydrocerussite) and Zn- Mn- Fe- oxides (zincite, franklinite, gahnite). Relicts of primary sulphides or neo-formed secondary sulphide phases can also occur. Carbonate rocks, both dolomite and limestone, are the most common host rock observed. Substantial differences are recorded in the mineralogy of supergene and hypogene deposits (tables 2.2 and 2.3).

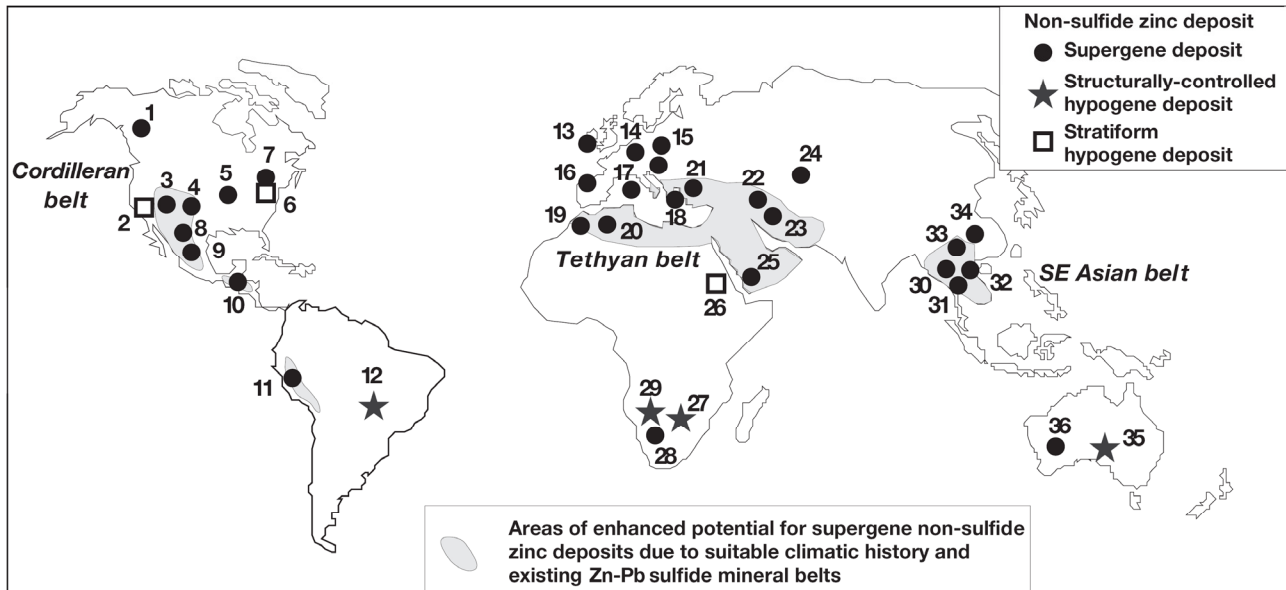
Two classifications for this group of deposits have been proposed so far. The first was compiled by Large (2001) and is based on mineralogical features as well as geological setting of the ores. Zn nonsulphide deposits have been divided into three main groups:

1. “Calamine”-dominated deposits. They occur in Mississippi Valley-type and other stratiform sulphide protorres in carbonate rocks; nonsulphide mineralisation is related to primary sulphides oxidation. The preservation of the newly formed ore takes place in karst-cavity infillings, as well as replacement aggregations;
2. Willemite-dominated deposits in late Proterozoic to early Cambrian sedimentary rocks, where the mineralisation occurs in marked shear zones. These deposits might be hydrothermal in origin, formed in an environment of low S- and high O- fugacities;
3. “Gossan”-type deposits, containing hydrated zinc silicates that were formed by surface oxidation of primary sulphides in situ and subsequently preserved by a special geological-environmental set of circumstances (tectonic, climatic etc.).

According to the above classification, the deposits of groups 1 and 3 are considered supergene in origin, while the nonsulphides included in group 2, comprehending the willemite mineralisation, could have a hydrothermal origin.

Table 2.1: World current zinc production and projections (TeckCominco Ltd. 2006)

Type of deposit	1996	Projection 2005-2015	Major minerals
Volcanic hosted (VMS)	30	15	sulphides
Carbonate replacement/skarn (CRD)	20	25	sulphides, silicates and carbonates
Sedimentary-exhalative (SEDEX)	25	40	sulphides
Mississippi Valley-type (MVT)	20	10	sulphides
Zinc oxides (Nonsulphides)	<5	>10	silicates and carbonates

**Figure 2.1:** Location of the main nonsulphide Zn deposits in the world (from Hitzman et al. 2003).

Deposits: 1) Howards Pass; 2) Desert View; 3) Tintic; 4) Leadville; 5) Upper Mississippi Valley district; 6) Franklin and Sterling Hill; 7) Balmat; 8) Sierra Mojada; 9) Santa Eulalia; 10) Torlon; 11) Accha; 12) Vazante; 13) Tynagh and Silvermines; 14) La Calamine; 15) Upper Silesian Mississippi Valley-type district; 16) Reocin; 17) Sardinian Zn-Pb district; 18) Larium and Thassos; 19) Touissit; 20) Hamman N'Bails; 21) Zamanti Zn-Pb district; 22) Angouran; 23) Mehdiabad; 24) Shaimerden; 25) Jabali; 26) Abu Samar; 27) Kabwe and Star Zinc; 28) Skorpion; 29) Berg Aukas and Abenab; 30) Padaeng; 31) Long Keng; 32) Cho Dien; 33) Jinding; 34) Qiondong Shen; 35) Beltana-Aroona; 36) Magellan.

Hitzman et al. (2003) presented a slightly modified version of the classification proposed in 1962 by Heyl and Bozion, accounting for distinction between supergene and hypogene nonsulphide deposits (Figure 2.2). The supergene deposits (corresponding to type 1 and 3 of Large), are dominated by smithsonite, hemimorphite and hydrozincite assemblages. Most of the known supergene deposits are positioned between 15° and 45° N latitude, thus pointing to specific climatic conditions. These deposits are the result of supergene oxidation of primary sulphides and account for:

1. *Direct replacement* of sulphide bodies. The Zn-oxide deposits form *gossans* on primary sulphide bodies that are replaced *in situ*. Secondary Zn phases (smithsonite and hydrozincite) replace sphalerite, while cerussite replaces galena. The complex mineralogical assemblage can include a mixture of silicates, carbonates, and oxides;
2. *Wall-rock replacement* resulting in smithsonite-dominated bodies primary sulphides areas. The ore is the result of the buffering effect of carbonate host rock on acidic groundwaters containing zinc derived from dissolution of primary sulphides. The distribution of minerals is regulated by the different mobility coefficients of the metals (separation of Zn from Pb and Fe);
3. *Residual and karst-infilling deposits* including reworked material filling the karst cavities after chemical or mechanical transport. These deposits are typical in uplifted areas under tropical climatic condition where acidic and oxidizing solutions derived from sulphides, together with high water availability, can increase the development of a karst network, which could represent a good receptacle for economic minerals.

The hypogene nonsulphide deposits seem to be not correlated to any supergene oxidation of sulphides and generally show hydrothermal or metamorphic characteristics. A limited number of examples of this type is actually known, located both in the southern and in the northern hemisphere. One of the main features of this group is the presence of the silicate willemite, locally associated with franklinite, gahnite and zincite, whereas smithsonite and hemimorphite are subordinated and represent a late weathering product. This class of deposits has been divided in two sub-groups:

1. *Structurally controlled deposits* forming veins and pipes related to fault systems. Their mineralogical assemblage includes willemite with associated remains of sphalerite, hematite and Mn-(hydr)oxides. The origin of the mineralisation is probably due to mixing between an oxidized-low temperature and a reducing-high temperature (80 - 200° C) fluid, both sulphur poor (Brugger et al. 2003). Intergrowths of willemite and sphalerite may be present, caused by changes in fluid's chemistry, principally due to its variable S-content (i.e. Vazante, Brazil and Beltana-Aarona, Australia);
2. *Stratiform* Mn-rich stratiform bodies of franklinite, willemite, zincite and gahnite. The factors controlling the emplacement of this kind of deposits have not been fully explained (Hitzman et

al., 2003, Brugger et al., 2003). Some of these ores could represent the metamorphic alteration of stratabound sulphide deposits (i.e. Franklin and Sterling Hill, USA and Bryson-Renfrew Region, Canada).

Both Hitzman's and Large's classifications are currently used. Considering the peculiar characteristics of the Namibian and Zambian willemite mineralisation, it is not easy to place them in only one group of the quoted classifications. However, most African willemite ore are actually seen as belonging to the Hitzman "*Structurally controlled deposits*" type. They are commonly genetically associated with the Brazilian and Australian hydrothermal willemite ores, but can display also a few similarities with the supergene ores as it will be discussed in the following chapters.

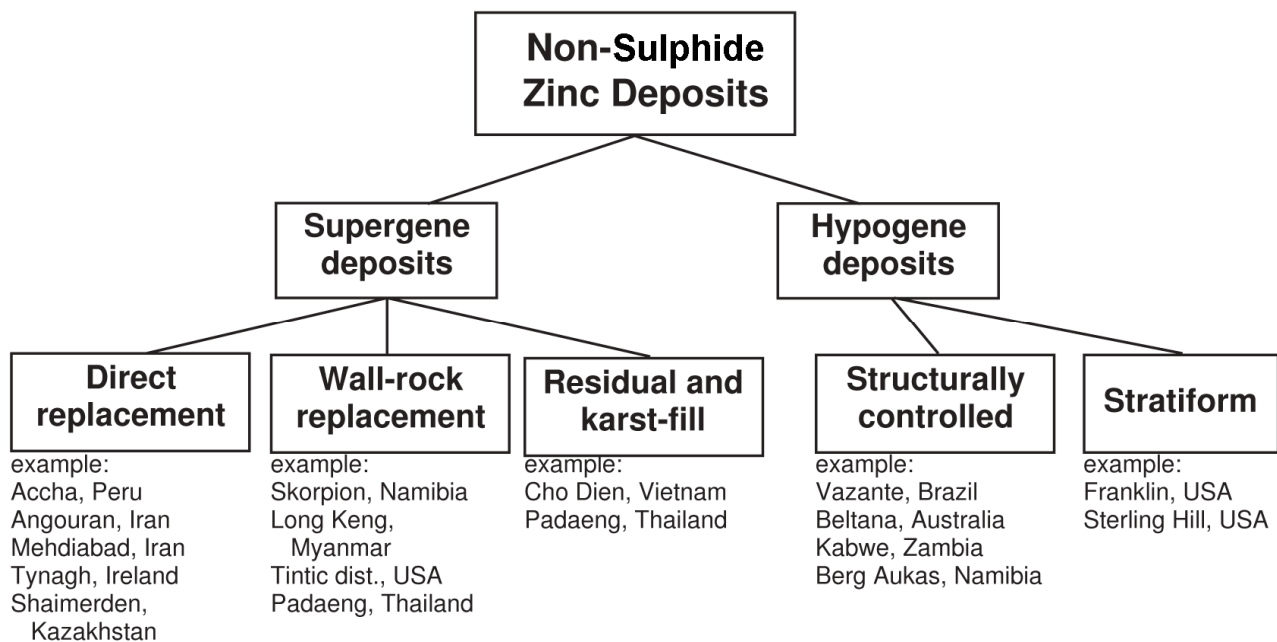


Figure 2.2: Classification of nonsulphide zinc deposits (Hitzman et al., 2003).

Table 2.2: Main supergene nonsulphide Zn deposits in the world: primary ore, mineralogy, resources (Hitzman et al., 2003, modified)

Name	Primary deposit type	Emplacement age	Supergene deposit type*	Major minerals**	Sulphide resources	Mixed nonsulphide resources	Non-sulphide resources	References
Leadville (Colorado - USA)	CRD	Tertiary	WR	sm, hem	8.1Mt @ 5.1% Zn, 4.2% Pb		8.3Mt @ 6% Zn, 2.5% Pb	Thompson & Archart, 1990
Sierra Mojada (Mexico)	CRD	Tertiary	WR(DR)	sm, hem, sa	9Mt @ 5% Zn, 3% Pb, 500g/t Ag		> 3Mt @ 20% Zn	Titley, 1993; Metaline Mining, unpub. company report, 2000
Mapimi (Mexico)	CRD	Tertiary	DR?	sm, hem, sa			6Mt @ 15% Zn, 10% Pb, 500g/t Ag	Titley, 1993
Accha (Peru)	CRD	Tertiary	DR	sm, hem, sa			9Mt @ 9% Zn	Pasminco, unpub. company report, 2000; Hudson et al., unpub. report, 2000
Mina Grand (Peru)	MVT	Tertiary	WR?	sm			1.9Mt @ 19.3% Zn, 2.2% Pb	Solitario Resources, unpub. company report, 1998
Touissit (Morocco)	MVT	Tertiary	DR	sm, ce		70Mt @ 2.5% Zn, 7% Pb		Bouabdellah et al., 1996
Um Gheig (Egypt)	MVT	Tertiary	WR	hem, sm, gos			2Mt @ 10% Zn, 2% Pb	El Aref & Amstutz, 1983
Zamanti (Turkey)	MVT?	Cretaceous - Tertiary	WR	sm, min			6Mt @ 26% Zn	Cerrah, pers. comm, 1999
Jabali (Yemen)	MVT	Cretaceous?	DR	sm			9.4Mt @ 10.8% Zn, 2.3% Pb, 77g/t Ag	ZincOx resources, unpub. company report, 2002
Mehdiabad (Iran)	MVT?	Tertiary?	DR, WR	sm, hem		218Mt @ 7.2% Zn, 2.3% Pb, 51 g/t Ag		Union Capital Limited, unpub. company report, 2001

Table 2.2: *continue*

Irankuh (Iran)	MVT	Tertiary?	WR	sm	15Mt @ 4% Zn, 2% Pb	4Mt @ 7% Zn, 1% Pb	14Mt @ 12% Zn+Pb	Ghazba et al., 1994;
Kuh-e-Surneh (Iran)	MVT	Tertiary?	WR	sm	2Mt @ 7% Zn, 4% Pb		0.8Mt @ 19% Zn, 7% Pb	Liaghat et al., 2000
Padaeng (Thailand)	MVT	Tertiary	WR/karst	hem, sm			5.1Mt @ 12% Zn	Reynolds et al., 2003
Long Keng (Myanmar)	MVT?	Tertiary	WR	sm			0.5Mt @ 38% Zn	Griffith, 1956
Cho Dien (Vietnam)	CRD	Triassic	karst	hem, sm, hyd	1.1Mt @ 11% Zn, 3% Pb		1.6Mt @ 15% Zn, 3% Pb	Fediuk & Kusnir, 1967
Jinding (China)	MVT	Tertiary	DR	hem, sm	90Mt @ 7.8% Zn, 1.6% Pb		50Mt @ 8% Zn, 1% Pb	Li and Kyle, 1997
Qindong Shen Shen (China)	MVT	?	WR?	sm		9.9Mt @ 7% Zn, 1.7% Pb	1.7 Mt @ 10.5% Zn, 1.5% Pb	Page, pers. comm., 2000
Shaimerden (Kazakhstan)	Irish type/CRD	Carboniferous	DR, WR	hem, sm, sa			4.3Mt @ 20.9% Zn	Schaffalitzky et al., 2003
Skorpion (Namibia)	VMS	Neo-proterozoic	DR, WR	sm, hem, sa		60Mt @ 6-8% Zn, 1% Pb	24.6Mt @ 10.6% Zn	Corrans et al., 1993; Borg et al., 2003
Balmat (USA)	Isa/sedex	Proterozoic	WR,DR	will	40.8Mt @ 9.4% Zn		0.1 Mt @ 10-29% Zn	deLorraine, 2001
Vazante (Brasil)	Hypogene nonsulphide	Proterozoic	DR	hem, hyd, min			2.6Mt @ 13.3% Zn	Monteiro et al., 2000

* Deposit types are referred to Hitzman's et al. (2003) classification: DR = direct replacement, WR = wall rock replacement, karst = residual and karst filling.

** Abbreviations: az = azurite; ce = cerussite; hem = hemimorphite; mal = malachite; sm = smithsonite; will = willemite; wulf = wulfenite; Zn-do = zincian dolomite.

CRD = high-temperature carbonate replacement deposit; MVT = Mississippi Valley type deposit; sedex = sedimentary exhalative deposit; VMS = volcanogenic sulphide deposit.

2.2 *Willemite: mineralogy and ore types*

Many carbonate-hosted nonsulphide Zn-Pb deposits, especially in the southern hemisphere, contain the zinc nesosilicate willemite (Zn_2SiO_4 , Figure 2.3) in economic concentrations (Hitzman et al., 2003). Willemite was discovered for the first time in 1829 in La Calamine deposit in Belgium and scientifically described by B. Lévy (1843), who dedicated the mineral to King Willem of Orange (hence the name). It is one of the very few silicate minerals to have a trigonal-rhombohedral symmetry (Simonov et al., 1977, Figure 2.4). The average density of willemite is 4.05 and its colour varies from transparent to red-brown and black. It occurs as thin, transparent, mm-sized crystals with hexagonal-prismatic terminations as well as granular masses, which commonly replace associated primary sulphides (Schneider et al., 2008). Pure willemite contains: 58.68% zinc, 12.60% silicon and 28.72% oxygen. Under polarized light in thin section willemite shows high interference colours (Figure 2.5).

Willemite has been traditionally considered in the past as a product of low-temperature supergene alteration of zinc-sulphide ores (Hitzman et al., 2003). However, a number of recent fluid inclusion studies suggest that willemite may form at high temperature (100-250° C) under oxidizing hypogene-hydrothermal conditions (Ypma, 1978, Sweeney et al., 1991, Brugger et al. 2003, Hitzman et al., 2003), both in deposits where willemite replaces primary Zn sulphides and in entirely nonsulphide mineralisation that lack any evidence for pre-existing sulphides (Schneider et al., 2008). In fact, most carbonate-hosted economic willemite deposits in the southern hemisphere (Vazante, Brazil, ca. 28.5 Mt @ 18% Zn; Kabwe and Star Zinc, Zambia, ca. 13 Mt @ 20-25% Zn; Berg Aukas and Abenab West, Namibia, ca. 3.5 Mt @ 15-25% Zn; and Beltana, Australia, ca. 0.86 Mt @ 38% Zn, Hitzman et al., 2003) are now interpreted to be of hypogene-hydrothermal origin (Large, 2001, Brugger et al., 2003, Groves et al., 2003, Hitzman et al., 2003). According to Brugger et al. (2003) and Hitzman et al. (2003), the precipitation of willemite, instead of sphalerite, from saline hydrothermal fluids is favoured under oxidizing (hematite stable) conditions at neutral to basic pH, low HS^- activity and elevated temperatures (>100-150° C) (Figure 2.6). The fact that economic willemite ores may have formed by hypogene-hydrothermal processes as primary concentration not related to any pre-existing zinc sulphides, has ultimate implications for successful exploration strategies, as these largely depend on the predictions provided by genetic models developed for these deposits (Brugger et al., 2003). It is finally crucial to understand the geological factors that control the formation of willemite deposits and whether these nonsulphide ores have formed by supergene or hypogene-hydrothermal processes, or a combination of both.

Table 2.3: Main hypogene (hydrothermal) nonsulphide Zn deposits: host rock, mineralogy, resources (Hitzman et al., 2003, modified).

Name	Location	Deposit type	Age of host rock	Major minerals*	Resources	References
Vazante	Brasil	Structurally controlled	Neoproterozoic	will, sph, frk	28.5Mt @ 18% Zn	F. Oliveira, pers. comm., 2001
Ariense (Masa)	Brasil	Structurally controlled	Neoproterozoic	will, sph	9.9Mt @ 18% Zn	South Atlantic resources 1999, company report
Beltana	Australia	Structurally controlled	Cambrian	will	0.86Mt @ 38% Zn	Groves et al., 2003
Aroona	Australia	Structurally controlled	Cambrian	will	0.17Mt @ 34% Zn	Groves et al., 2003
Reliance	Australia	Structurally controlled	Cambrian	will, sm	0.37Mt @ 28.8 Zn	Groves et al., 2003
Kabwe**	Zambia	Structurally controlled	Neoproterozoic	will, sph, ga	12.5Mt @ 25% Zn, 11% Pb	Kamona, 1993
Star Zinc	Zambia	Structurally controlled	Neoproterozoic	will, frk, zinc, gahn	0.2Mt @ 20% Zn	Sweeney et al., 1991
Berg Aukas**	Namibia	Structurally controlled	Neoproterozoic	will, sph, ga	3.4Mt @ 15% Zn, 4% Pb	Cairncross, 1997
Abenab West**	Namibia	Structurally controlled	Neoproterozoic	will	0.1Mt @ 25% Zn	Cairncross, 1997
Angouran	Iran	MVT	Tertiary	sm	3.2Mt @ 38% Zn, 2% Pb	Boni et al., 2007
Franklin	USA	Stratiform	Mesoproterozoic	will, frk, zinc	21.8Mt @ 19.5% Zn, 0.05% Pb	Fronde and Baum, 1974
Sterling Hill	USA	Stratiform	Mesoproterozoic	will, frk, zinc	10.9Mt @ 19% Zn	Johnson et al., 1990
Abu Samar	Sudan	Stratiform	Proterozoic	sph, wil, frk	3.6Mt @ 4.9% Zn, 0.6% Cu	El Samani et al., 1986
Desert View	USA	Stratiform	Cambrian	frk, het, wil, zinc	small	Leavens & Patton, 2000

* Abbreviations: frk = franklinite, ga = galena, gahn = gahnite, het = heterolite, sph = sphalerite, sm = smithsonite; will = willemite; zinc = zincite

** There are some doubt on the origin of these deposits (hypogene/supergene)

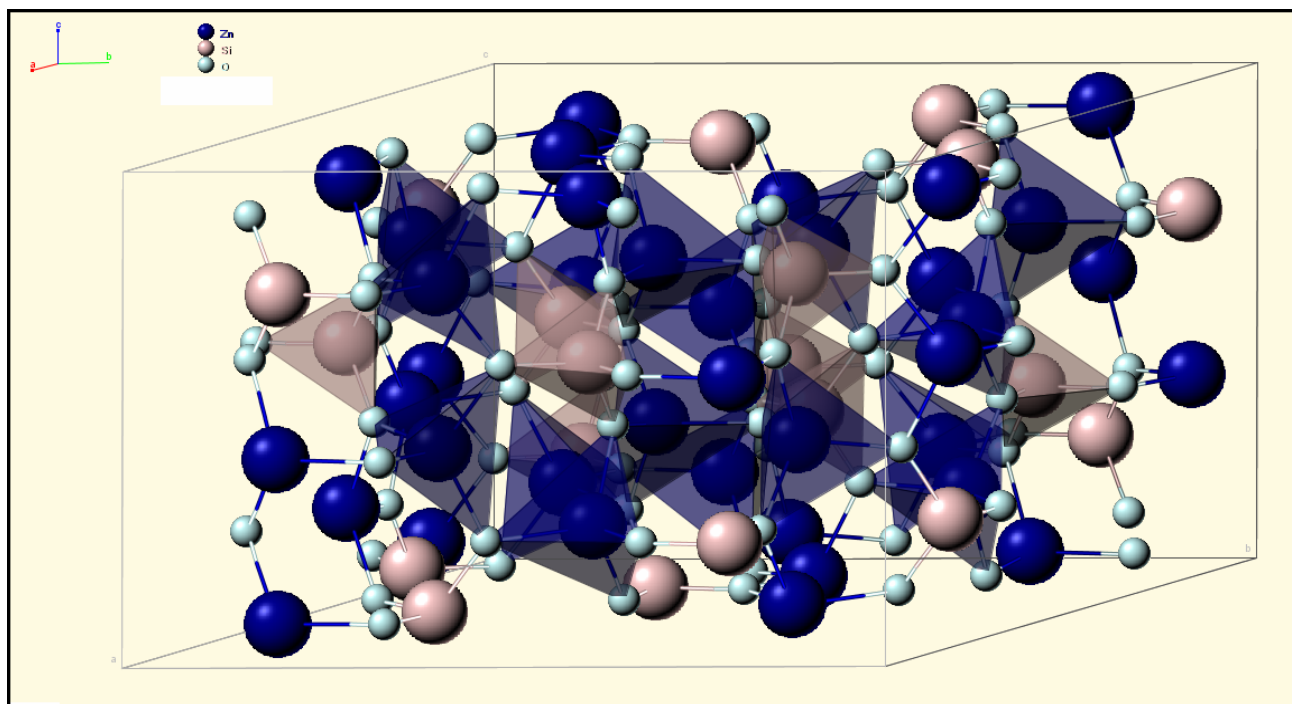


Figure 2.3: Willemite crystal cell (Webmineral.com, 2008).

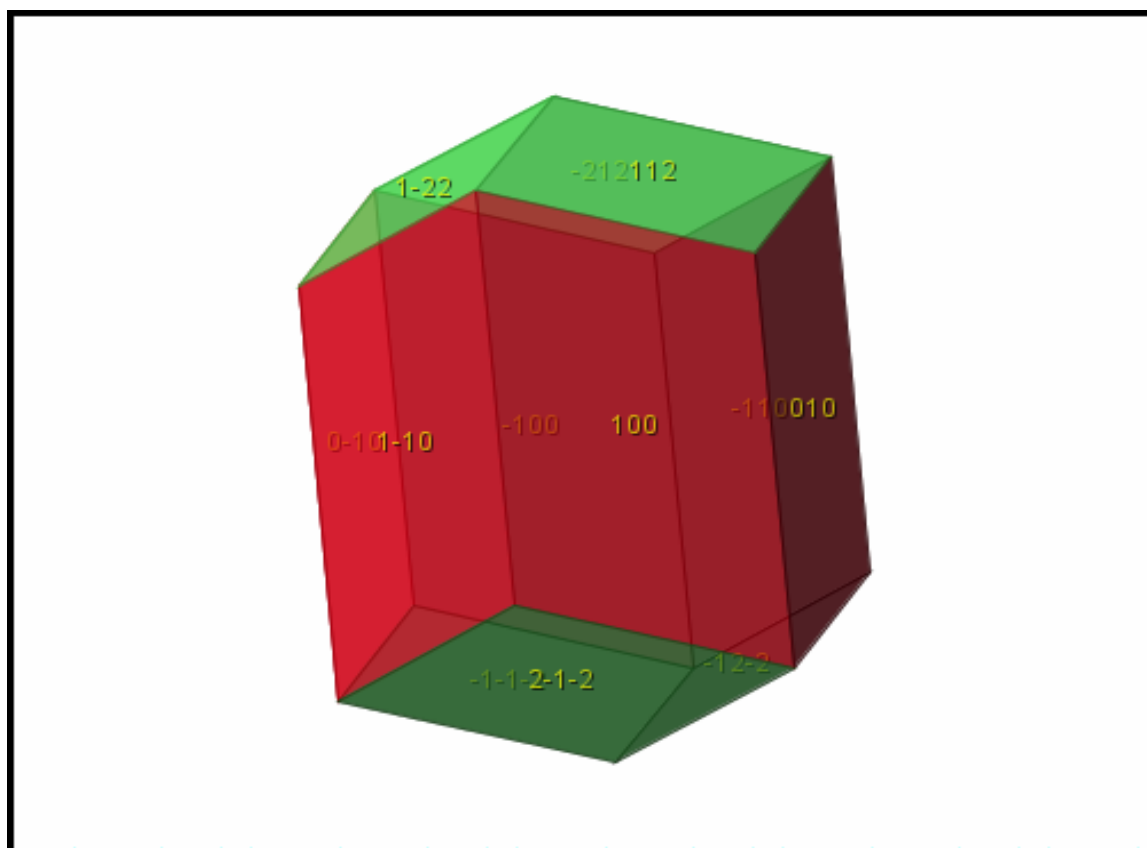


Figure 2.4: Willemite crystal form: $[100][112]$ (Webmineral.com, 2008).

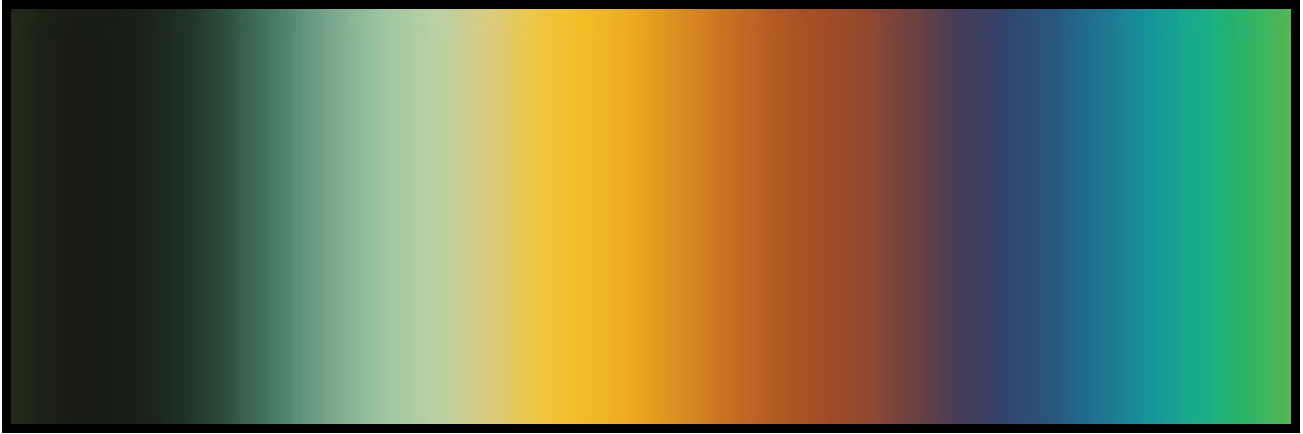


Figure 2.5: Willemite birefringence interference colour range at 30μm thickness (Mindat.org, 2008).

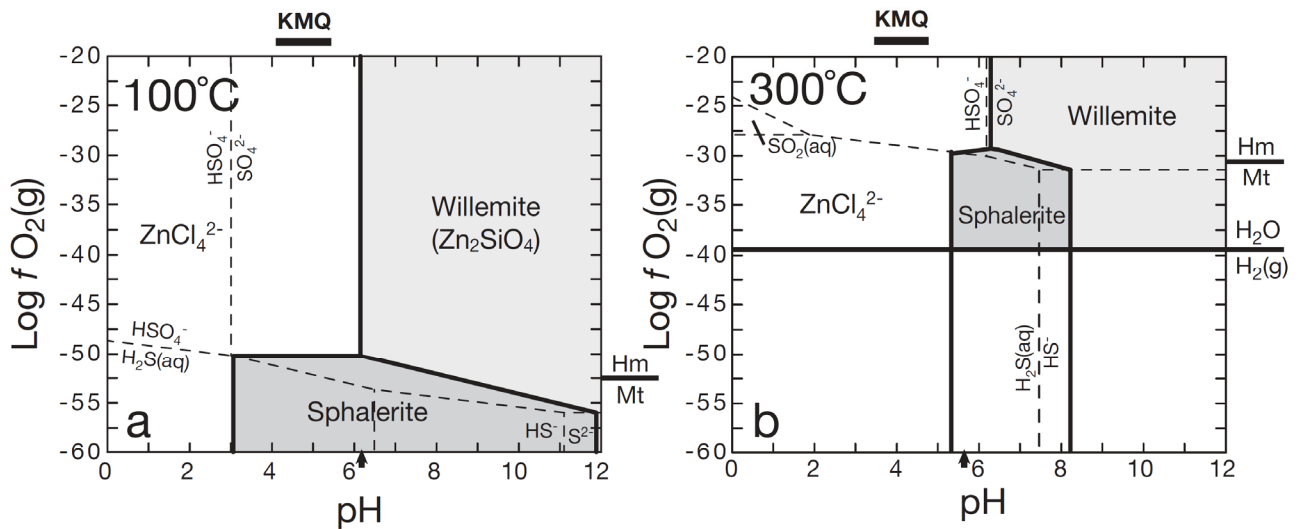


Figure 2.6: Log $fO_2(g)$ vs. pH diagrams illustrating the relative stability of willemite and sphalerite in hydrothermal brines at 100° C (a) and 300° C (b); The hematite-magnetite boundary and a range of pH for K feldspar-muscovite-quartz (KMQ; $0.1 < a_{K^+} < 2$) are plotted for reference. The arrow on the pH axis indicates neutral pH for the temperature of the diagram (Brugger et al., 2003).

2.3 Willemite mineralisation out of Africa

The biggest non-African willemite deposits recognized throughout the world are located in Neoproterozoic to Cambrian host rocks of the southern hemisphere. The Cretaceous-aged willemite ores in Belgium (La Calamine and minor deposits, Coppola et al. 2008) are out of this context and

will not be described here. The African willemite deposits will be exhaustively described in the following chapters.

Following Hitzman et al. (2003), a review of the Proterozoic to Cambrian-hosted deposits suggests that they can be genetically divided into two subtypes: (1) structurally controlled, replacement bodies (Vazante, Brazil; Beltana, Australia) and (2) stratiform, manganese-rich, metamorphic deposits (Franklin-Sterling Hill, US), possibly derived from metamorphic transformation of former exhalative mineralisation.

These deposits contain dominantly willemite locally associated with sphalerite (1) or a willemite franklinite-gahnite-zincite assemblage (2) (table 2.3 and 2.4). Smithsonite, hemimorphite, hydrozincite and sauconite are rare, except in the shallower exposures and may be related to younger weathering phases. In some cases the zinc silicate is apparently intergrown with sphalerite, this suggesting that willemite and sphalerite were possibly co-precipitated (Hitzman et al., 2003).

In most deposits, willemite is known to persist to depths of 300 to 900m below the current topographic surface, far beyond the depth of known oxidation effects. The Vazante and Beltana deposits are surrounded by variably large zones of hydrothermal dolomitisation (Hitzman et al., 2003).

2.3.1 *Vazante*

The Vazante mine, currently the largest zinc producer in Brazil, is located within the Bambuí Group, a Neoproterozoic (approximately 600 Ma, Misi et al., 1997) carbonate sequence belonging to the São Francisco craton (Moore, 1956, Amaral, 1968, Thorman and Nahas, 1979). Measured reserves have been estimated at 28.5 Mt, with an average grade of 18.3% Zn (Monteiro et al., 2006).

Two types of ore are mined at Vazante. The volumetrically most abundant ore type, considered to be hypogene (Hitzman et al., 2003), consists of willemite with subsidiary sphalerite and galena plus traces of franklinite and zincite, all intergrown with silica and hematite (Monteiro et al., 2006). This material occurs as veins within the northeast-trending Vazante fault zone throughout a 10km strike length (Figure 2.7) and is known from drilling to extend to depths of at least 500m (Hitzman et al., 2003). A relatively minor supergene assemblage of hemimorphite, hydrozincite, and minrecordite (termed “calamine”) forms a near-surface (within 50m) direct-replacement cap above the willemite bodies (Hitzman et al., 2003).

The Vazante deposit is comprised within the essentially unmetamorphosed sedimentary rocks of the Bambuí Group (Madalosso, 1979), which display well-preserved sedimentary textures and lack a pervasive foliation. The willemite bodies occur within the approximately 1.3km thick Vazante Formation, which consists of thin- to thick-bedded doloarenites and algal-banded and fenestral

dolomicrites that grade upward to stromatolitic bioherms (Hitzman et al., 2003). The overlying Lapa Formation consists of dark-grey to black carbonate turbidites. The contact between the Vazante Formation and the overlying Lapa Formation is a regional unconformity, which is commonly occupied by a several-meter-thick red conglomerate or paleosoil, indicative of deep weathering processes (Hitzman et al., 2003).

The Vazante fault zone trends N 50° E, sub-parallel to the strike of the rocks, and dips approximately 60° to the northwest at the Vazante mine, with an overall normal displacement (Hitzman et al., 2003). The Vazante fault system is concomitant with the deposition of the Lapa Formation and consists of a structurally dominant basal fault overlain in the hanging wall by a 100m wide, complex array of fault-bounded lozenges and tectonic breccias (Hitzman et al., 2003).

The basal fault is generally occupied by intergrown willemite and (lesser) sphalerite (Hitzman et al., 2003). Willemite also fills many, but not all, of the subsidiary, discontinuous, hangingwall structures. Mineralized bodies occur as cm- to m-wide veins filled with willemite, hematite, and quartz with subsidiary ferroan dolomite, siderite, and fine-grained sphalerite (Hitzman et al., 2003). Minor franklinite (1-2%), zincite, galena, barite, and apatite also occur within the willemite bodies. Willemite intergrown with sphalerite displays euhedral contacts, although it is also observed to cut and, more rarely, be cut by sphalerite (Hitzman, 1997). These textures suggest that both zinc sulphides and zinc silicates were precipitated nearly simultaneously (Hitzman et al., 2003). Galena occupies the contact between willemite and sphalerite in most areas. Hydrothermal alteration (ferroan dolomite) is well developed in and around the mineralized zones (Hitzman et al., 2003). Willemite veins cut ferroan dolomite, but may contain silica and specular hematite.

The age of mineralisation is so far unknown, although Monteiro et al. (2006) suggest that it occurred during the still Neoproterozoic Brasiliano orogeny (between 560 and 550 Ma). Galena intergrown with sphalerite and willemite commonly displays deformation textures and both sphalerite and willemite are commonly fractured and folded. These textures suggest that most of the mineralisation preceded or was concurrent with tectonic displacements.

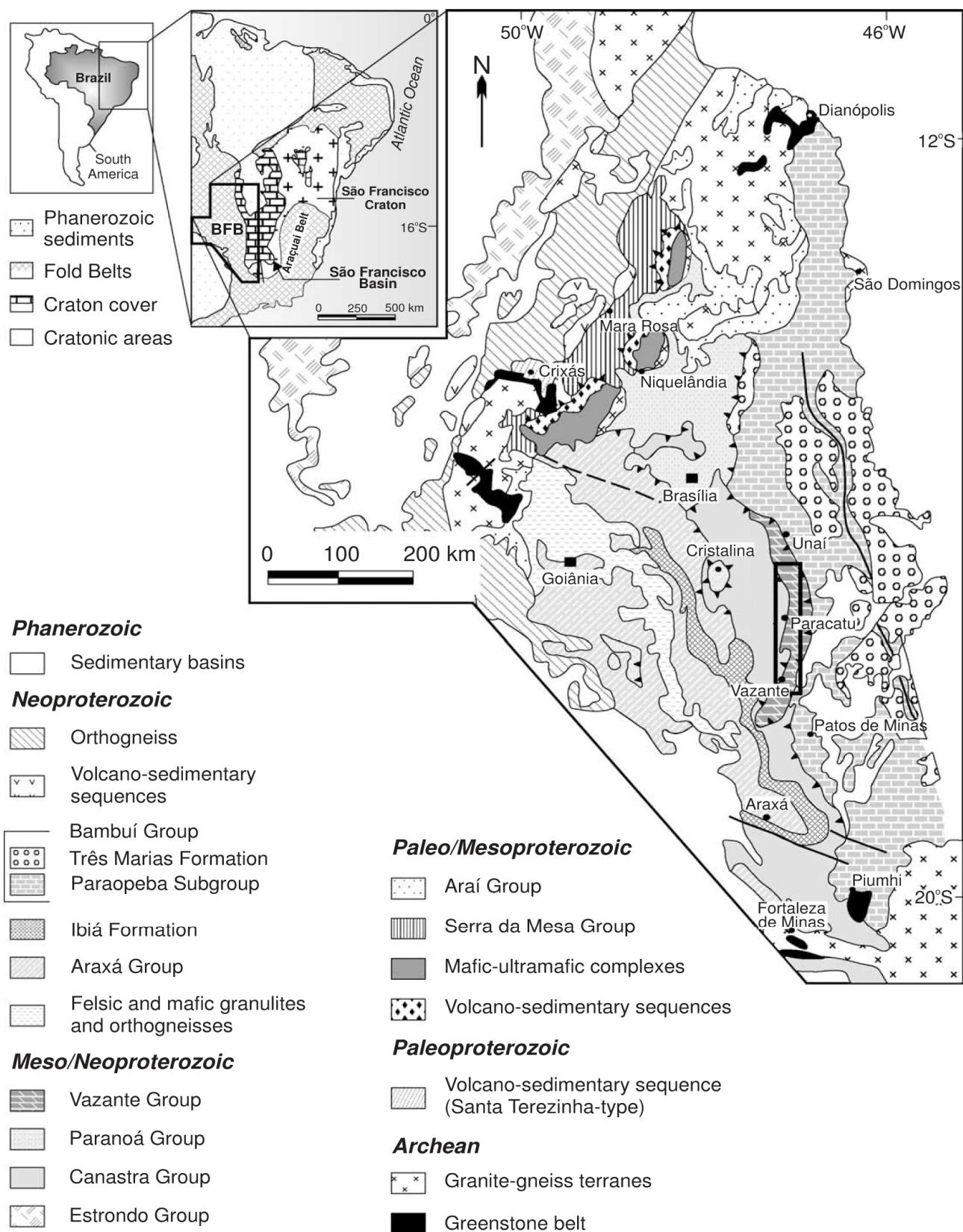


Figure 2.7: Location of Vazante and geological setting of the Vazante Group in the Brasília Fold Belt (BFB) (modified after Monteiro et al., 2006).

2.3.2 *Beltana-Aroona*

Beltana and Aroona are the biggest willemite deposits (Figure 2.8) occurring in the northern Flinders Ranges, South Australia. They are located within the Woodendinna Dolomite and the Wilkawillina Limestone (Groves et al., 2003). These ore deposits are part of an extensive Zn-Pb \pm Cu district located in the northern Flinders Ranges that includes also minor Mississippi Valley-type Zn-Pb occurrences (Groves et al., 2003). The willemite ores are megascopically similar to those at Vazante but the hydrothermal alteration at Beltana lacks silicification; the mineral assemblage consists largely of dolomite with hematite inclusions, rather than ferroan dolomite plus siderite (Hitzman et al., 2003). The willemite bodies at Beltana and Aroona are not known to contain sphalerite, franklinite or zincite. Two models for the genesis of the Beltana orebody have been proposed: supergene enrichment of a sphalerite-galena Mississippi Valley-type massive sulphide orebody (Muller, 1972, Horn, 1975) and hypogene formation of willemite related to salt diapiric intrusions (Grubb, 1971, Burdett, 2000, Hallam, 2000).

The Cambrian Woodendinna Dolomite locally displays algal lamination and contains oolites and mudcracked silt layers indicative of subtidal to supratidal depositional conditions; an early dolomitisation phase in this unit appear to be syndepositional (Hitzman et al., 2003). The conformably overlying deeper water Wilkawillina Limestone is a massive to thickly bedded, locally highly fossiliferous limestone (James and Gravestock, 1990). Sedimentary rocks below these Cambrian carbonates consist of interlayered siltstone, shale, sandstone, and minor dolomite of Neoproterozoic to early Cambrian age, which are interpreted as part of an early rift sequence (Preiss, 1987, Drexel and Preiss, 1995). The Wilkawillina Limestone is unconformably overlain by red shales and siltstones (Hitzman et al., 2003).

After Hitzman et al. (2003) all the willemite occurrences in the northern Flinders Ranges are structurally controlled. The majority of the mineralized zones of the Aroona deposit occur in a narrow fault wedge between the large-displacement Norwest fault and the smaller-displacement Aroona fault (Figure 2.8). The Norwest fault zone is a major inverted normal fault zone, with up to 8 km of normal movement. The Beltana orebody occurs along the Aroona fault zone (where it diverges south from the Norwest fault) and is truncated to the east by the unmineralized Mine fault, a structure subparallel to the main fault (Hitzman et al., 2003).

The orebodies consist of massive white, red, and black willemite, commonly showing complex mm- to cm-scale colloform banding. Willemite colours derive from microinclusions of associated minerals: red willemite contains disseminated hematite, whereas black willemite appears to contain manganese (hydr)oxide minerals such as coronadite (Hitzman et al., 2003). In general, red colloform

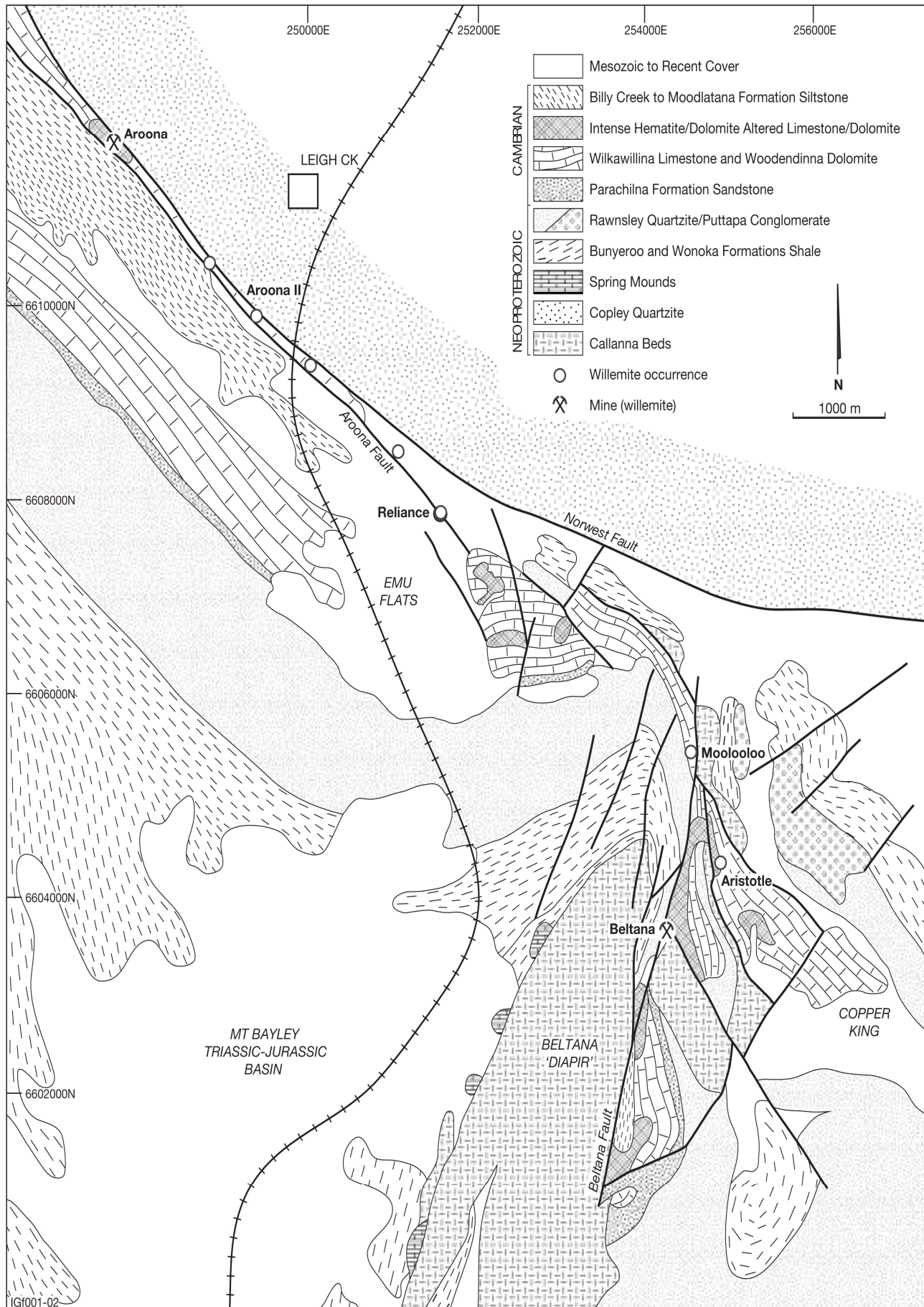
willemite is cut by white colloform willemite. Along the footwall of the Beltana orebody, willemite is locally intergrown with the black Pb-Mn minerals coronadite and hedyphane (Hitzman et al., 2003). No sulphides or remaining boxwork structures after sulphides have been reported from the Australian willemite bodies. Willemite of all colours is then cut and locally replaced by late calcite. The hydrothermal hematitic dolomite extends from tens to more than several hundred meters from the willemite bodies, which cut in turn the dolomite alteration halo. Dolomitisation and hematitisation are best developed at Beltana, where the host rock is the Wilkawillina Limestone. The latter lithotype is more permeable and therefore allowed a better development of the alteration minerals than the Woodendinna Dolomite host rock occurring at Aroona (Hitzman et al., 2003).

A number of researchers (Thomas, 1968, Grubb, 1971, Burdett, 2000, Hallam, 2000, Groves et al., 2002) have proposed a hypogene origin for these deposits on the basis of a variety of textural, geochemical, and isotopic evidences. Thomas (1968) and Grubb (1971) used the lack of boxworks after sulphides and the extremely low sulphur content of the ore and surrounding rocks to conclude that the willemite ores were hypogene in origin.

The age of the Beltana-Aroona ores is not precisely known. Several papers consider the mineralisation having been occurred during the Cambro-Ordovician Delamerian orogeny (e.g., Johns, 1972). Structural analysis indicates that the willemite bodies have been locally sheared, and it is unlikely that such deformation could have taken place recently because the area has not been tectonically active since the Mesozoic (Hitzman et al., 2003). However, K-Ar dating of coronadite intergrown with late willemite gives an age of ~435Ma: this points to a post-Delamerian age for the mineralisation, possibly related to an exhumation event (Groves et al., 2003).

Later oxidation at both Beltana and Aroona resulted in local replacements of the willemite-dominated assemblage by hemimorphite and smithsonite, as well as in the formation of minor smithsonite in the red dolomite outside the willemite bodies (Hitzman et al., 2003). New exploration work in the district has evidenced a deep (>250m) karst morphology associated with the development of wall rock-replacing smithsonite and hemimorphite bodies together with traces of sphalerite, galena, and pyrite in stylolites, near the willemite bodies affected by supergene weathering (Groves et al., 2002).

Figure 2.8: Regional geology of the Beltana district showing the willemite deposits and prospects relative to the Aroona and Norwest fault (Grooves et al., 2003).



2.3.3 *Franklin-Sterling Hill*

The Franklin and Sterling Hill zinc-iron-manganese deposits are located in the exposure of Middle Proterozoic Grenvillian basement within the Appalachian fold belt (Johnson and Skinner, 2003), a belt of Mesoproterozoic rocks 30 to 40 km wide that extends from eastern Pennsylvania to western Connecticut (Figure 2.9). The deposits occur in the Franklin Formation, comprising metasedimentary and metavolcanic rocks, associated with igneous intrusions (Hague et al., 1956), which were metamorphosed to upper amphibolite to granulite facies between 1080 and 1030 Ma (Volkert, 2001). The Franklin and Sterling Hill deposits are located at different stratigraphic positions within the Franklin Marble (Hague et al., 1956). The Franklin Marble occurs within quartzite and gneisses, which are presumed to be metamorphosed siliciclastic sedimentary rocks, with a number of amphibolite lenses that may represent basalt flows (Johnson and Skinner, 1990). The original lithotype is believed to consist of thin beds of clastic sedimentary rocks or volcanic flows that were representing the nucleus of boudins as the host marbles were plastically deformed (Hitzman et al., 2003).

The metasedimentary rocks are intruded by plagioclase-rich orthogneisses, pegmatites and amphibolites (Hitzman et al., 2003). The Proterozoic sequence has been folded repeatedly: both the Franklin and Sterling Hill orebodies occur within synclinal troughs that have not been observed in the overlying gneisses, this suggesting that much of the folding occurred as plastic deformation internal to the marble unit (Fron del and Baum, 1974).

The Franklin and Sterling Hill deposits, that were mined from the middle of the nineteenth century until 1954 and 1987, respectively, are noteworthy because the main ore minerals were willemite (Zn_2SiO_4), franklinite (ZnFe_2O_4) and zincite (ZnO), rather than sphalerite (Johnson and Skinner, 2003). Also noteworthy is the fact that the ores were quite rich, averaging 20 wt percent zinc (Metsger et al., 1958, Fron del and Baum, 1974). The combined production at the two mines was 6.5 million metric tons (Mt) of zinc (Johnson and Skinner, 2003).

The orebodies at Franklin and Sterling Hill comprise a series of discontinuous 1- to 10-m-thick tabular lenses, oriented parallel to the overall shape of the deposit. The ores consist of equigranular, subrounded aggregates of franklinite, willemite, and zincite containing ~20% Zn, ~16% Fe, and ~8% Mn. Individual ore lenses are distinguished by the relative proportions of these minerals. Bedding-concordant bands of sphalerite occur within the primary willemite ore at Sterling Hill but are sparse at Franklin (Fron del and Baum, 1974). Calcite is the principal gangue mineral but manganese silicates, particularly tephroite, are present in small amounts in the ore and in larger quantities in the hanging-wall and footwall rocks (Hitzman et al., 2003). The ore is commonly

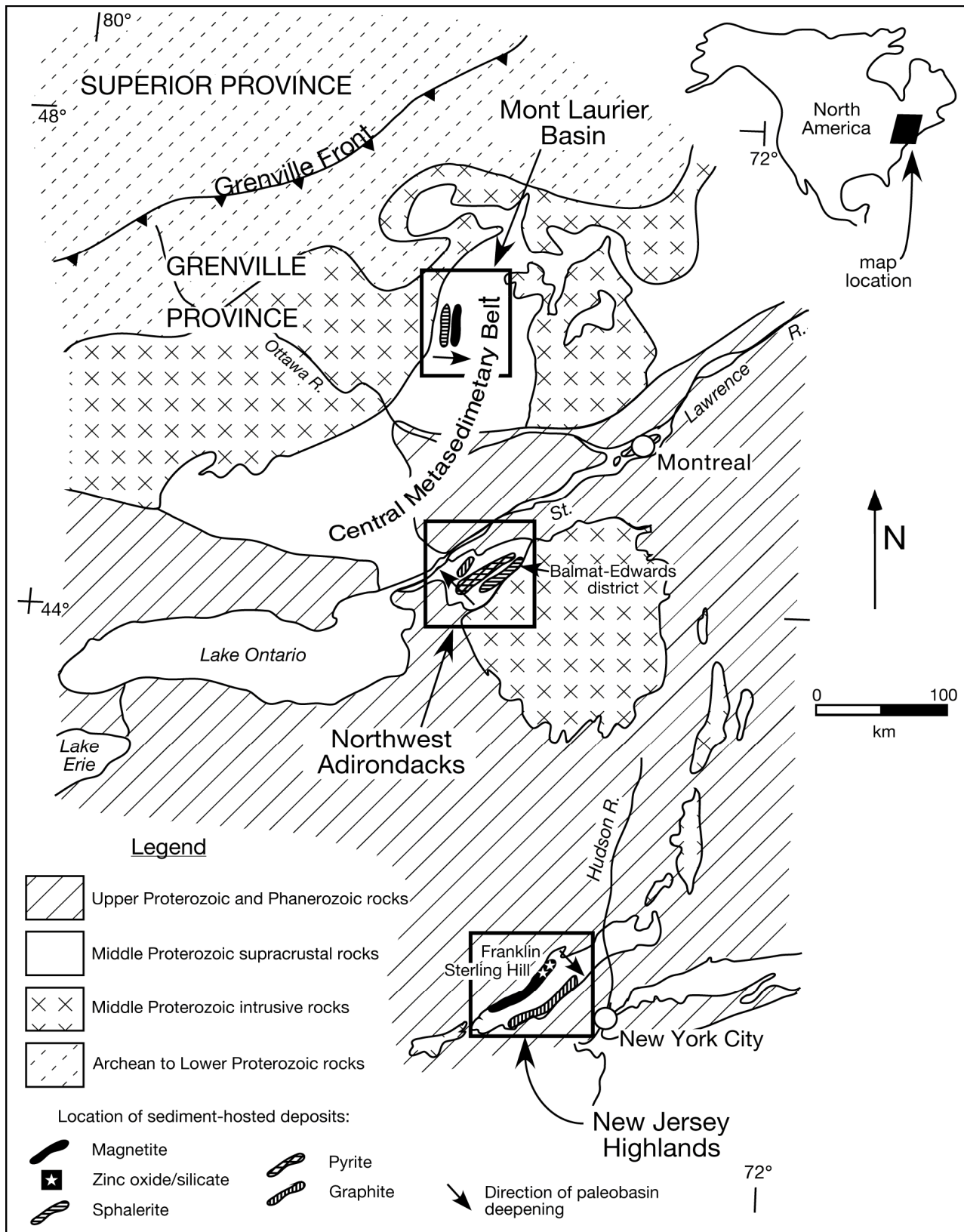


Figure 2.9: Map showing the location of the New Jersey Highlands, the northwest Adirondacks and the Mont Laurier basin with the zinc oxide, sphalerite and magnetite occurrences (Johnson and Skinner, 2003).

surrounded by or interbedded with zinc- and manganese-bearing calc-silicate bands. The Franklin ore zone is underlain by a thin, zinc-free, manganiferous iron formation (Johnson, 2001, Johnson and Skinner, 2003). The New Jersey Highlands also host iron oxide deposits that were mined at hundreds of different locations from the late seventeenth century until the early twentieth century. The deposits were massive magnetite or, rarely, hematite. Especially at the Furnace bed and in the magnetite lens within the Franklin zinc deposit that included magnetite, calcite, dolomite, diopside, tremolite, phlogopite, chondrodite, norbergite, graphite, and fluorite (Johnson and Skinner, 2003). Total production from the New Jersey Highlands deposits was at least 25 Mt of iron (Bayley, 1910, Sims, 1958).

Metsger (1962) has demonstrated that willemite at Sterling Hill is oriented parallel to the regional foliation, this indicating that an accumulation of zinc-bearing minerals must have existed in some form prior to metamorphism and deformation. Johnson and Skinner (2003) proposed an exhalative or early diagenetic model for both the marble-hosted zinc and iron deposits.

3 Methods

3.1 *Samples collection and preparation*

Over 200 rock samples were collected in three different mining/prospecting districts where willemite ores have been exploited: Otavi Mountainland (Namibia), Kabwe area and Lusaka region (Zambia). The main problem encountered during the sampling was to get in most cases mineralized samples *in situ*, due to the closure or inaccessibility of the mines and/or to the absence of characteristic outcrops. Therefore, it was often necessary to carry out the sampling from old dumps located around the old mine sites. Additional samples were collected from drillcores located at the Kabwe ore repository of Teal Mining and from the drillcores of the Zambian Chamber of Mines in Kitwe. In table 3.1 are listed the detailed analytical techniques used on the samples. The investigated samples cover the wide spectrum of willemite mineralisation in all districts, as well as its gangue, mainly consisting of Ca- and Mg- carbonates.

Pure mineral phases for analyses were obtained by hand picking under a stereomicroscope. The samples were then cleaned in a sonic bath for 10 minutes, to remove the impurities deposited on crystal surfaces. Opportunely prepared samples were submitted to several types of mineralogical, petrographic and geochemical investigations.

3.2 *Transmitted and reflected light microscopy*

More than 70 polished thin sections (30µm) were prepared from the most representative samples. Thin sections were observed under transmitted and reflected light using a petrological microscope. A Leica camera was used for obtaining high quality digital images of the samples at the microscopic scale.

3.3 *Cold cathodoluminescence (CL) microscopy*

Cathodoluminescence is an optical and electrical phenomenon whereby a beam of electrons is generated by an electron gun (e.g. cathode ray tube). The further impact on a luminescent material causes the emission of visible light from this material. The electron bombardment of minerals causes excitement of ions, which “jump” to a state of higher energy. After a short delay time the excited ions return to their former energy state and emit a radiation. Emission in the visible spectrum is responsible for the luminescence colour (Pagel et al., 2000)

Cathodoluminescence in rock minerals depends on either crystallographic defects or trace element concentration and distribution. In particular, some elements activate the luminescence whereas others quench it. Depending on the type of mineral and the activator/quencher quantitative ratio,

different colours and/or intensity of brightness may result (Pagel et al., 2000).

CL microscopy was carried out on all thin sections, in order to better characterize the growth features and the relations of the willemite with the other mineral phases. The minerals were distinguished in luminescent and non-luminescent. The first ones were further characterized based on their CL colour, intensity and zoning.

A CITL 8200 Mk3 Cold Cathodoluminescence instrument, coupled with an optical microscope was used at the Geologisch-Paläontologisches Institut of the Universität Heidelberg (Germany). The thin sections were placed on a tray controlled by X-Y manipulators in a vacuum chamber with an upper window for optical observation. A beam with a 12-15kV voltage and a current of 300-350 μ A was used. A Leica digital camera mounted on the microscope was used to obtain high-resolution images.

Table 3.1: Analytical techniques used.

Techniques	No. of samples/analyses	Application
Optical microscopy (transmitted, reflected and cathodic light)	~70	Thin sections
XRPD	~85/~150	Single phase or bulk rock
SEM-EDS	38/~300	Thin sections and single phase
WDS	12/~150	Thin sections
ICP-MS	3/5	Bulk rock
Thermometric analyses of fluid inclusions	10	Thin sections (120 μ m)

3.4 X-ray diffraction analysis (XRPD)

X-ray diffraction (XRPD) on powdered whole rock and selected ore samples has been performed in order to identify the occurring mineral phases. XRPD is a standard method by which crystalline phases of materials can be detected and differentiated even in presence of a multiphase mixture. Further data obtained from XRPD are for instance the crystallinity rate of minerals and a semi-quantitative estimation of compounds in a mixture (based on peak intensity). The minerals can be identified by comparing the obtained peaks with a set of the standard patterns compiled by the Joint Committee on Powder Diffraction Standards (JCPDS). These processes are made easier for the presence of software interfaced with a database.

X-ray powder diffraction analyses (XRPD) of the Namibia and Zambia specimens were carried out in two different laboratories: (1) Dipartimento di Scienze della Terra Università di Napoli “Federico II” (Mineralogy section), and (2) Mineralogisches Institut of the Universität Heidelberg (Germany).

The diffraction data at Dipartimento di Scienze della Terra in Naples were collected with a SEIFERT – GE MZVI automated diffractometer (40kV, and 30mA) equipped with parallel (Soller) slit, a Na(Tl) scintillation detector, and a pulse height amplifier discrimination, and a Cu K α

(1.5418 Å) radiation was selected from the primary beam using a germanium [111] single-crystal monochromator. Powder samples were deposited in the hollow (0.5 mm deep) of a zero background quartz mono-crystal plate. A long scan was performed over $3^\circ < 2\theta < 75^\circ$ with 0.5° $2\theta/\text{min}$ step. Synthetic CaCO_3 (Mallinckrodt analytical reagent) was used as internal standard (position of the 1014 reflection for CaCO_3 taken as 3.035° , JCPDS-ICDD 5-586). The RayfleX software package (GE Inspection Technologies) XDATA program (part of the XDAL 3000 software package from Rich. Seifert & Co.) has been used to evaluate the obtained profiles and to permit the comparison with JCPDS-ICDD database.

At the Mineralogisches Institut of the Universität Heidelberg, a Bragg-Brentano X-ray diffractometer (Siemens D 500) with a Cu tube and graphite monochromator has been used to collect XRD data. The diffractometer operated at 40 kV and 30 μA and scanned the samples in the 2θ range from 2.0° to 70.0° with increments of $0.02^\circ[2\theta]/\text{sec}$. The EVA software (part of the DIFFRACPLUS V5 software suite by the Bruker AXS & Co.) was used to evaluate the obtained profiles and to permit the comparison with JCPDS-ICDD database. Quartz powder was added to the powder samples as internal standard in order to correct the position of the peaks by referring to the known d101 reflection of the internal quartz standard.

All the samples used for XRPD measures have been previously milled in a mortar, in order to obtain granulometrically homogeneous powders (fraction $< 200\mu\text{m}$).

3.5 *Scanning electron microscopy (SEM) and Energy dispersive X-ray spectroscopy (EDS)*

The scanning electron microscope (SEM) is a type of electron microscope able to produce high-resolution images of a sample surface. This technique is based on an incident electron beam focused with magnetic lenses and accelerated by a high potential on the specimen. It is raster-scanned across the sample's surface, and results in the emission of different radiations (backscattered electrons, secondary electrons, X-rays). Secondary electrons provide high-resolution imaging of a fine surface morphology. Alternatively, backscattered electron imaging provides elemental composition variation, as well as surface topography. The efficiency of production of backscattered electrons is proportional to the sample material's mean atomic number, which results in image contrast as a function of composition, for instance material with higher atomic number appears brighter than material with lower atomic number. X-rays, produced by the interaction of the incident electron beam with the specimen, which are in function of the atomic number of element, may also be detected with SEM equipped for energy-dispersive X-ray spectroscopy (EDS). This method permits a point-to-point qualitative and quantitative chemical analysis.

My observations, as well as the qualitative and quantitative analyses were carried out using the LEO

Electron Microscopy LEO440 scanning electron microscope, equipped with an Energy Dispersive X-ray spectrometer. The instrument working conditions were: high vacuum, 12mm objective lens to specimen working distance, 20kV accelerating voltage, 2nA beam current (stabilized and measured with Faraday cup). Backscattered electron images were produced. Quantitative spectra required 50 seconds acquisition time. Silicates, sulphates, sulphides, carbonates, oxides and pure elements were used as standards. Detection limits are in the order of 0.2wt% oxide for EDX-rays. The CO₂ contents in carbonates and water content in hydrated carbonates and silicates were evaluated by stoichiometry. Analyzed samples were coated with a 15µm carbon film.

Secondary electron images of representative samples were also produced. Before analysis, the samples were dried and stuck down onto 12mm Cambridge pin stubs and then coated with 20nm of gold-palladium using a Baltec MED 020 sputter coater. The analyses with LEO440 were carried out mainly at the Mineralogisches Institut of the Universität Heidelberg (Germany). A few observations have been carried out also at the Natural History Museum (NHM) in London (Great Britain).

3.6 *Wavelength dispersive X-ray spectroscopy (WDS)*

Electron microprobe analyses are suitable for high accuracy elemental characterization of major and minor element concentrations on the samples. They can provide qualitative (identification) and quantitative (composition) analyses for most elements. This method is based on an incident electron beam on a polished sample (stub or thin section), opportunely coated with 15nm carbon, which produces an emission of X-rays. Emitted X-rays are detected by a wavelength dispersive spectrometer (WDS). From the wavelength and intensity of the lines in the X-ray spectrum, the elements present may be identified and their concentration estimated. In the quantitative analyses, the intensity of X-ray lines from the specimen of our interest are compared with those derived from standards of known composition.

Chemical analyses of willemite, apatite and gahnite were performed on 6 thin sections using both a Cameca SX50 and SX100 electron microprobe with a gas proportional WDS. Cameca SX50 is at the Mineralogisches Institut of the Universität Heidelberg and the Cameca SX100 at the Electron Microscopy & Mineral Analysis (EMMA) division in the Mineralogy Department of Natural History Museum, London. Instrumental conditions are 15kV, 15nA and 10µm spot size with a X-ray detector. In both cases work conditions were identical. Minerals and pure elements were used as standards. Detection limits are in the order of 0.01 wt%.

3.7 *Whole rock geochemical analyses (ICP-MS)*

Minor and trace elements can be incorporated in the mineral lattice as guest ions, which substitute

for host ions of similar charge and radius. They may also occur interstitially between lattice planes and along crystal boundaries or occupy lattice defects or be included as solid or liquid inclusions. The entrance of an element in a lattice from its mother fluid is governed by the distribution coefficient (k), which describes the behaviour and partitioning of elements between mineral and fluid. Many techniques are used to measure the minor and trace elements in minerals and/or mixtures of minerals. The most common is the ICP-MS (Inductively Coupled Plasma Mass Spectrometry). The ICPMS is a type of mass spectrometry with a elements atomic mass resolution ranging between 7 and 250 and concentrations in the ppm and ppb order. It is based on coupling a inductively coupled plasma for ionization and a mass spectrometer for ions separation and detection. I have used this method only to detect the composition of supergene Zn minerals in the recent karst fillings around the Star Zinc prospect (Zambia). The analyses were performed at the ACME Analytical Laboratories Ltd Canada. on a Perkin Elmer Elan 6000 ICP-MS (ACME whole-rock package 4A) for 20 elements of 7TD Group. Aliquots of several in-house Standard Reference Material like STD GC7 and STD PBC1 were used to monitor accuracy. Procedure details of sample preparation can be obtained from ACME-Lab (www.acmelab.com).

3.8 *Microthermometric analyses of fluid inclusions*

When a crystal grows in the presence of a fluid phase, some of the fluid may be trapped as imperfections in the growing crystal to form fluid inclusions (FIs), sealing small droplets of mother fluid. Different phases may be trapped in inclusions, therefore a distinction of FIs is based on number and types of phases present in the inclusions: (1) *monophase inclusion* with an homogenous fluid (liquid or vapour); (2) *two-phase inclusion*, coexistence of two different fluids (liquid and vapour) from which one is dominant (L-rich and V-rich); (3) *multiphase inclusion* with a liquid, vapour and one or more solid phase (daughter minerals) precipitated during the cooling of high-salinity inclusions; (4) *inclusion with immiscible phases*.

The most useful classifications of fluid inclusions are based on genetic criteria and related to the timing of formation of inclusions relative to that of the host mineral (Bodnar, 1993). Thus, *primary fluid inclusions* are formed during the growth of the surrounding host crystal, *secondary fluid inclusions* are inclusions formed in a later stage from a crack-healing mechanism, *pseudosecondary fluid inclusions* are trapped when fracturing occurs during crystal growth. A group of fluid inclusions that were all trapped at the same time is named *Fluid Inclusion Assemblage* (FIA) (Goldstein & Reynolds, 1994).

The study of FIs gives important clues for understanding the geologic and thermodynamic conditions, as well as the temperature, pressure, density and composition of the fluids, which

precipitated or re-equilibrated with the mineral phases (Goldstein & Reynolds, 1994). The principle of FI microthermometry is based on phase changes, which occur when heating and cooling FIs during experimental work. Microthermometry of FIs allows to measure some of the above-cited parameters (temperature, density and composition).

Each thermometric study on FIs must be preceded by a petrographic observation to detect the different FIAs. Moreover, the reliability of measures is based on the assumption that FI have been kept in a closed system since trapping, but external phenomena (stretching, leakage, necking-down) may have produced exchange with external environment. These inclusions have to be avoided for microthermometric measures.

Ten doubly polished thin sections (120 μ m) were prepared for FIs analyses from the samples of Berg Aukas and Abenab West (Namibia), and Kabwe, Millberg, Star Zinc and Excelsior (Zambia). Sample preparation was conducted with extreme care due to the willemite cleavage along the c axis and with cold techniques, in order to avoid stretching and leakage.

Microthermometric analytical measurements on fluid inclusions have been carried out at the Heidelberg University Fluid Laboratories, using a Linkam MD 600 stage. The stage was regularly calibrated using H₂O and CO₂ inclusion in synthetic quartz, its precision was of ± 1 °C in the temperature range of interest. The samples were positioned in a chamber with an upper window, and controlled with an X-Y manipulator. Observation were carried out also with a camera set on a microscope and connected to a computer. Leaked inclusions were avoided for thermometric measures or discarded when leakage was produced during experiment (increase in bubble size). In order to minimize the risk of inducing stretching and/or leakage, the inclusions were heated and cooled with a small gradient (10 to 5° C/min) to further slow down (1° C/min) in the last phases of the experiment.

4 Regional geology and primary ore deposits in the studied areas

The willemite occurrences studied in this thesis are hosted, both in Namibia and Zambia, by Neoproterozoic terranes (ca 850-550 Ma, cfr. next chapters) involved in the collision of the Kalahari and Sao Francisco/Congo Cratons (figure 4.1). This continental accretion, commonly referred as Pan-African Orogeny, is spanning in age from ca 750-900 (early rifting stage) to ca 550-450 Ma (late orogenic stage). It leads to the formation of the Gondwana Supercontinent and of the Damara-Lufilian-Zambezi Orogenic belts (DLZ) (John et al., 2004).

The collision of the Kalahari and Sao Francisco Cratons and the formation of the Damara-Lufilian-Zambezi Orogen (DLZ) occurred either simultaneously along the whole DLZ or started first in the eastern portion of the cratons boundary (Laukamp, 2006).

The Damara belt (figure 4.2) is located in Namibia and the study area, i.e. the Otavi Mountainland, is in its northern portion (Northern Platform). The Lufilian Arc (figure 4.8) extends from the Northern (Copperbelt area) to Central Zambia (Kabwe area) while the Zambezi belt lays in the southernmost region of Zambia.

4.1 *Otavi Mountainland, Namibia*

The Otavi Mountainland (OML, figure 4.3) represents an area of about 10,000 km², corresponding to the north-eastern foreland of the Damara Orogen in Namibia. Geologically, the OML consists of a Paleo- Mesoproterozoic basement, which is overlain by the sedimentary successions of the Neoproterozoic Damara Supergroup where carbonate rocks are very abundant. The Proterozoic strata are intruded by presumably Karoo age dykes and partly covered by the clastic sediments of the Cambrian to Jurassic Karoo Supergroup, the mainly volcanic Etendeka Group of Cretaceous age and the Cainozoic Kalahari Sequence (Laukamp, 2006).

The platform carbonates of the Damara Supergroup are hosts for polymetallic sulphide and nonsulphide deposits, among which there are world famous deposits such as Tsumeb, Kombat and Berg Aukas. Mining of the base metal deposits was presumably started by the Bergdama tribe, which introduced copper smelting into Namibia (Cairncross, 1997). At the end of the 19th century the region of the Otavi Mountainland was occupied by Europeans, among which the Germans played a dominant role. The first mining concession was granted to the South West Africa Company (SWACO) in 1890 (Misiewicz, 1988). Since then, continuous mining activity on base metal and vanadium deposits in the OML was conducted by several companies.

The first comprehensive overview on the geology of the OML was presented by Schneiderhöhn (1929). Further work on the regional geology of the OML was carried out by Söhne (1957), Hedberg (1979) and Miller (1997). Recent studies concerning the ore deposits of the OML were

published by Lombaard et al. (1986), Innes and Chaplin (1986), Deane (1995), Frimmel et al. (1996), Chetty and Frimmel (2000), Melcher (2003), Melcher et al. (2003, 2006), Boni et al. (2007) and Schneider et al. (2008).

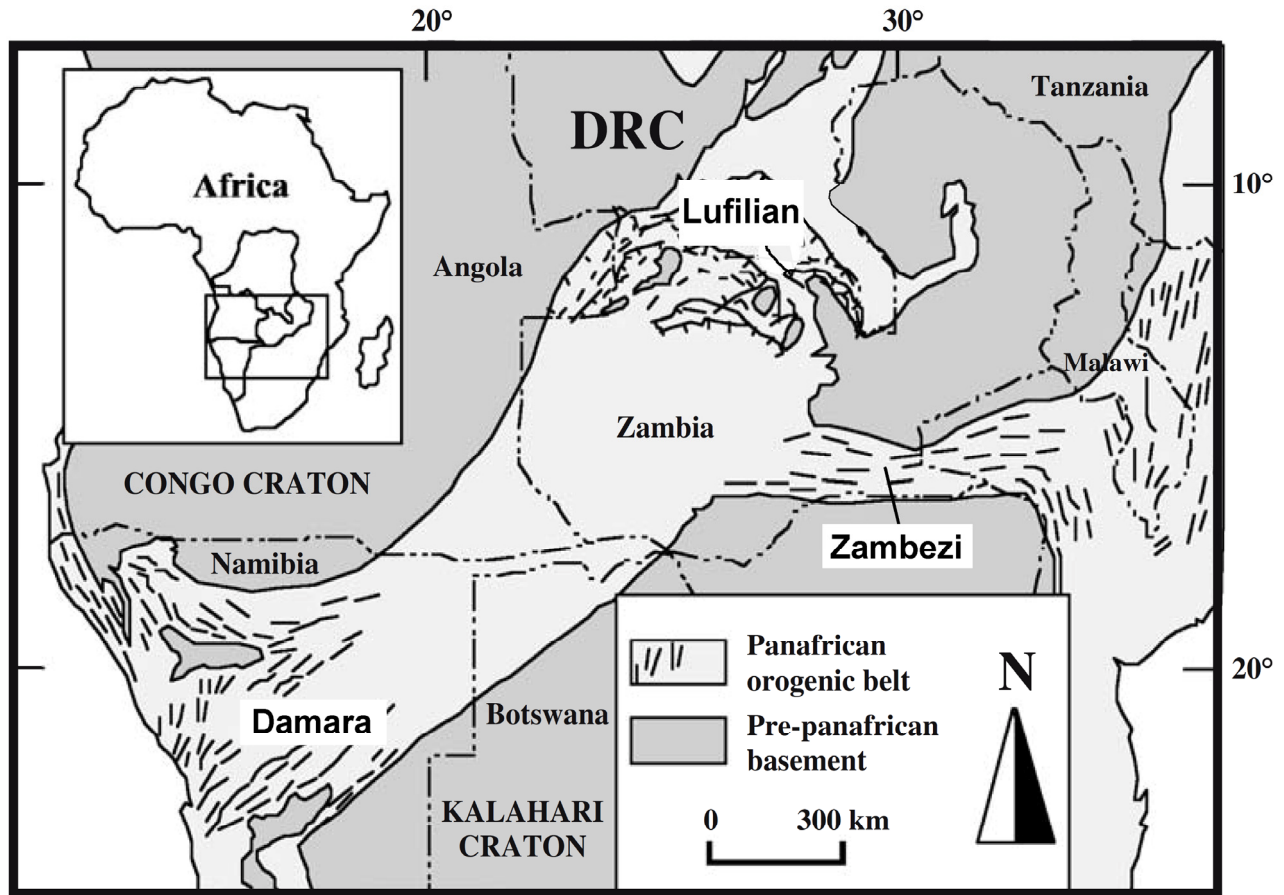


Figure 4.1: Map of southern central Africa showing major Pan-African belts (modified after Schneider et al., 2007).

4.1.1 Geology of the OML

4.1.1.1 Paleoproterozoic basement

The Paleoproterozoic basement (Eburnean, 2.1 to 1.65 Ga, Miller, 1983, Frimmel et al., 2004) of the OML (also referred as the Grootfontein Inlier) is part of the southern Congo Craton (Rainaud et al., 2005). It can be subdivided in the Grootfontein Metamorphic Complex (GMC) and the Grootfontein Mafic Body (GMB) (Laukamp, 2006). The GMC consists mainly of alkaline/calc-alkaline granites and granodiorites (Clifford et al., 1969), whereas the GMB is made of anorthosites, gabbros,

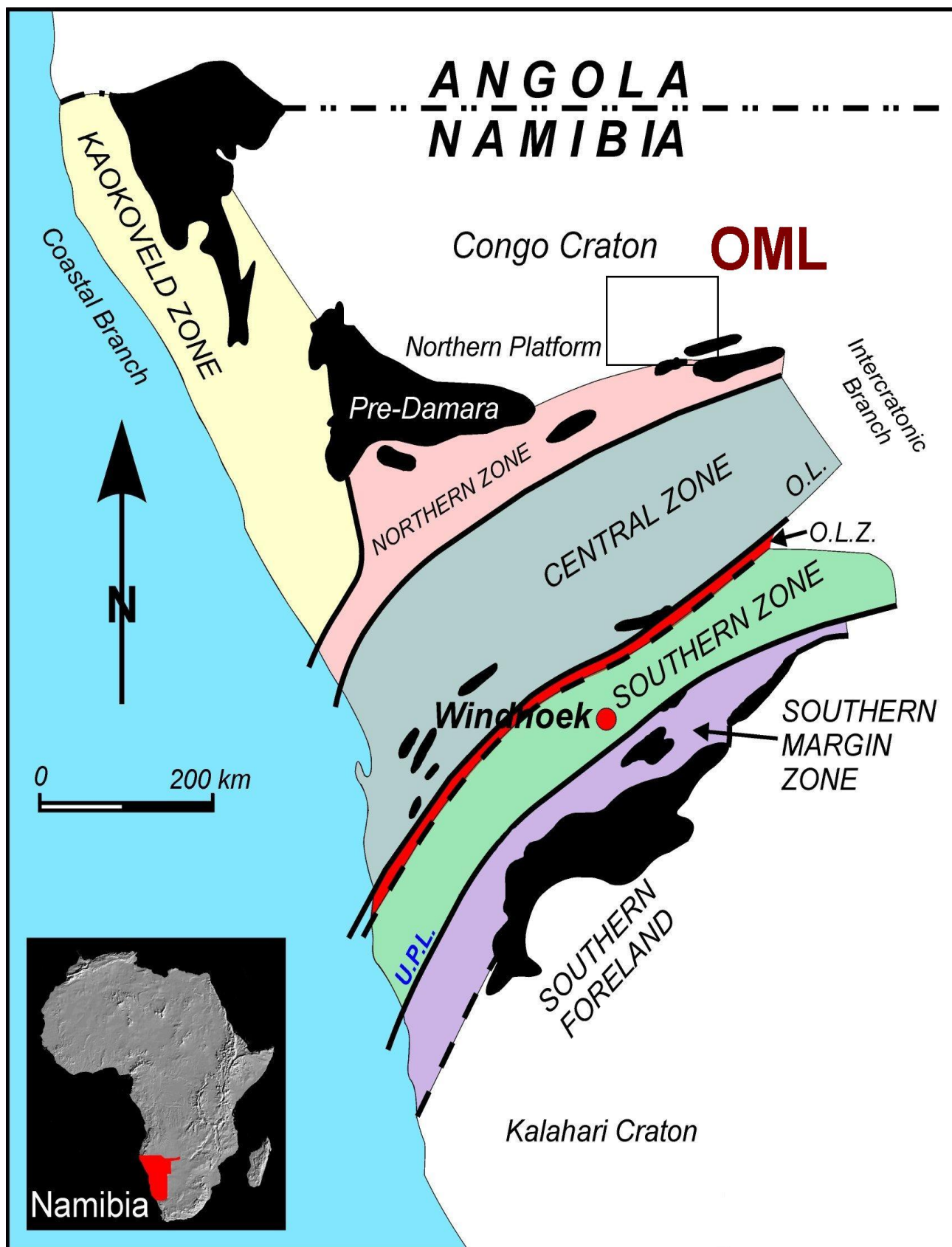


Figure 4.2: Tectonostratigraphic zones and lineaments of the Damara Belt; OL – Okavandija Lineament.

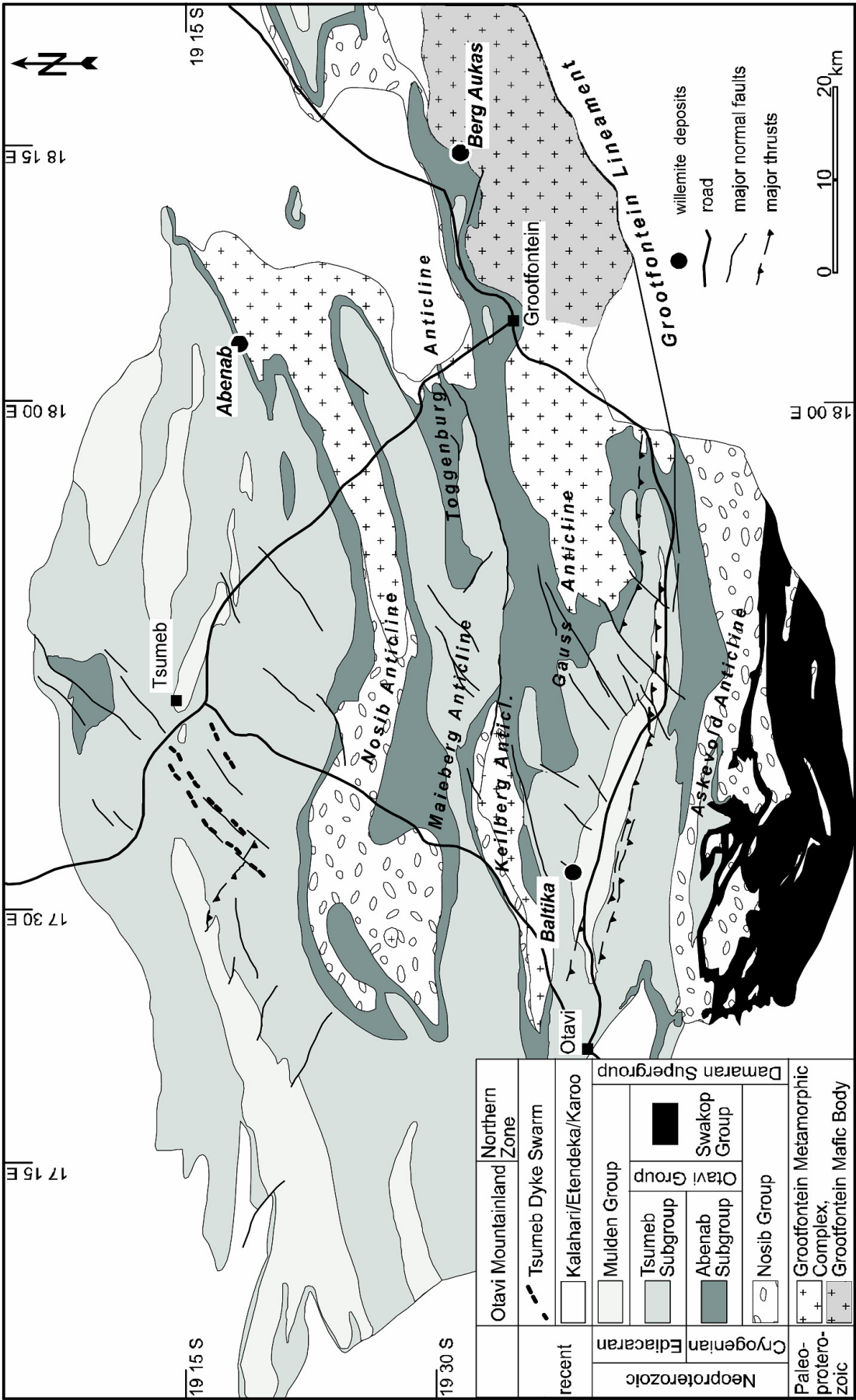


Figure 4.3: Geological map of the Otavi Mountainland with the location of the sampled willerite occurrences (modified after Laukamp, 2006)

micaceous biotite gneisses, granites and amphibolites (Martin, 1965, Söhnge, 1964, Laukamp, 2006). The basement crops out in the nuclei of E-W anticlinal folds (figure 4.3), which have been interpreted as paleotopographic highs predating the deposition of the Damara Supergroup (Schneider et al., 2008).

4.1.1.2 *Damara Supergroup*

The Neoproterozoic successions of the OML are part of the Damara Supergroup (figure 4.4). Up to 4500 m thick platform carbonates of the Otavi Group rest unconformably on the Paleoproterozoic basement of the Grootfontein Inlier and on the Cryogenian rift sediments of the Nosib Group (Laukamp, 2006). The Otavi Group is overlain by the molasse-like Mulden Group.

The Nosib Group consists mainly of siliciclastic sediments of the Nabis Fm, with intercalated metavolcanics of the Askevold Fm. By comparison with the dated volcanic successions of the Naauwpoort Fm in central Namibia, which gave a depositional age of 780-740 Ma, the same age has been assigned to the Nosib Group by Hoffmann et al. (1996). The Chuos Fm (also called Varianto Fm) consists of diamictites, pyroclastics and ironstones, which are interfingering with the Nabis Fm in the central OML (Laukamp, 2006), is considered as part of the Nosib Group. The Nosib Group was deposited in a pre-Pan-African, NE trending horst-graben system that developed due to the Cryogenian break-up of Rodinia (Frimmel et al., 1996).

The Otavi Group is divided by the diamictites of the Ghaub Fm, aged at about 635 Ma (Hoffmann et al., 2004) into lower Abenab and upper Tsumeb Subgroups. The Abenab Subgroup comprises from bottom to top the Berg Aukas, Gauss and Auros Fms. The “cap carbonates” of the Berg Aukas Fm unconformably overly the diamictites of the Chuos Fm (Hoffmann et al., 2004). Massive and bedded dolomites of the Gauss Fm correspond to shallow water carbonates, which were deposited at the margin of the Otavi carbonate platform (Frimmel et al., 1996). The Auros Fm consists of stromatolites and oolites, alternating with bedded limestones and shales. The Tsumeb Subgroup is subdivided in the Ghaub, Maieberg, Elandshoek and Hüttenberg Fms, which can be further subdivided in 8 lithozones (Laukamp, 2006). A second cap carbonate sequence in the OML, represented by limestones and dolomites of the lower Maieberg Fm (T2), overlies the Ghaub diamictites (T1). In the central OML, the dolomites of the upper Maieberg Fm (T3) and the lower Elandshoek Fm (T4) are characterised by synsedimentary brecciation (Laukamp, 2006). The bedded dolomites of the upper Elandshoek and lower Hüttenberg Fms are followed by lagoonal deposits of the middle Hüttenberg Fm (T7) (Söhnge, 1957). Stromatolitic and oolitic dolomites with intercalated cherts occur in the upper Hüttenberg Fm (T8). The Otavi Group was deposited as a carbonate

Reactivation of pre-Damaran lineaments Collision of Kalahari and Congo Plate (D2) Late or post-Damaran uplift in Northern Zone of Damara Orogen (D3) Continental convergence in Kaoko region (D1) Rifting stage (Khomas Trough)	Karstification IV ca.34-14 Ka		Quaternary				aeolian sand		<div>Baltika</div> <div>Abenab</div> <div>Berg Aukas</div>		
	Karstification III	Tertiary	Kalahari	Andoni Fm.		sand, clay, calcrete					
				Olukonda Fm.		sand, calcrete					
				Beiseb Fm.		gravel, sandstone					
	Karoo basalts ca.280 Ma Karstification II ca.450-280 Ma M2 ca. 481-459	Cretaceous	Etendeka Group	undifferentiated		sandstone, basalt, dyke					
		Jurassic to Cambrian	Karoo Supergroup	undifferentiated		sandstone, shale, basalt, dyke					
	M1 ca.535 Ma	Neoproterozoic	Damara Supergroup	Ediacaran	Mulden Group	Kombat Fm. Tschudi Fm.		phyllite, quartzite, greywacke, arkose			
	Karstification I				Otavi Group	Tsumeb Sub-Group	Hüttenberg Fm.	T8		thin-bedded light and dark dolomite, diagenetic chert, phyllite, shale	
								T7			
								T6			
							Elandschoek Fm.	T5		bedded and massive light dolomite	
	T4										
	Maieberg Fm.				T3	thin-bedded and massive dolomite, thin bedded limestone, phyllite					
					T2						
	Ghaub Fm. ca.635.5 Ma				Ghaub Fm.	T1	tillite, dolomite				
	Askevold Fm. ca.742-746 Ma				Cryogenian	Abenab Sub-Group	Auros Fm.			bedded dolomite, massive dolomite, bedded limestone and shale	
							Gauss Fm.			bedded and massive dolomite	
		Berg Aukas Fm.		laminated dark and light dolomite, dark limestone, transition beds							
Chuoss Fm.		tillite, pyroclastics, ironstone									
	Nosib Group	Askevold Fm.		epidosite, agglomerate, chlorite schist, dolomite							
		Nabis Fm.		shale, phyllite, arkose, conglomerate, quartzite							
	Paleo- proterozoic	Grootfontein Metamorphic Complex & Grootfontein Mafic Body				diabase, granite, gneiss, diorite, gabbro, serpentinite					

Figure 4.4: Lithologies and tectonostratigraphic evolution in the Otavi Mountainland and stratigraphic position of the Abenab West, Berg Aukas and Baltika deposits (modified after Schneider et al., 2008). The data have been compiled from the works of: Burger and Coertze (1973), Kröner and Clauer (1979), Haack et al. (1980), Haack and Martin (1983), Frimmel et al. (1996), Hoffman et al. (1996), Bäuml (2003), Frimmel (2004), Frimmel et al. (2004), Goscombe et al. (2004) and Hoffmann et al. (2004).

platform on the southern margin of the stable crust of the Congo Craton (Prave, 1996) even if evidences of large-scale growth faults and synsedimentary breccias in the Tsumeb Subgroup indicate a reactivation of pre-Damaran basement structures (Laukamp, 2006).

In the Mulden Group are comprised the Tschudi and Kombat Fms. The Tschudi Fm consists of conglomerates, sandstones, quartzites and arkoses. The angular unconformity between the Otavi Group and the Tschudi Fm is identified by karst depressions filled by the Tschudi conglomerates (Misiewicz, 1988) and by the Pan-African thrusting of the Otavi carbonates over the siliciclastic rocks (Laukamp, 2006). Also the sedimentary infill of karst pipes observed in several mines throughout the OML (e.g. Tsumeb pipe, Kombat Mine), is correlated with the unconformity of the Mulden Group (Lombaard et al., 1986). The Kombat Fm has been described only in the Otavi Valley and comprises shales and phyllites. It is possible that the Kombat Fm is a low-grade metamorphic equivalent of the Tschudi Fm (Söhnge, 1957).

4.1.1.3 *Post-Damaran successions*

Except in its western areas, the OML is extensively covered by sediments of Paleozoic-Mesozoic, Tertiary and Quaternary age, belonging to the Karoo and Kalahari sequences. Notably, the mainly siliciclastic successions of the Kalahari Sequence occur in deeply eroded, east-trending Pan-African anticlines (King, 1951, Laukamp, 2006). In the northern OML, single calcalkaline lamprophyres (e.g. the kersantites of Tsumeb) as well as other kinds of dykes occur, both types being presumably of Cretaceous age (Söhnge, 1957). The basalts of the Etendeka Group, related to the break-up of Gondwana and the formation of the South Atlantic Ocean in the Early Cretaceous, could have extended to the southern OML (Marsh et al., 2003). Tertiary and Quaternary deposits were accumulated in post-Damaran karst structures (Pickford, 1993, 2000), as well as eolian sands (Kalahari sands) and the ubiquitous calcrete cover.

4.1.2 *Primary ore deposits in the OML*

Over 600 occurrences of base metal ores (figure 4.5) are known from the 10,000 km² extended OML (Cairncross, 1997). Most base metal deposits contain both sulphide and nonsulphide mineralisation and are hosted by shallow-water carbonate successions of the Otavi Group. Based on geological/geochemical criteria, two main mineralisation styles have been distinguished: the Berg Aukas (Zn>Pb>>Cu)- and the Tsumeb (Pb>Cu>Zn)-type deposits (Pirajno and Joubert, 1993, Melcher, 2003). Both are hosted by carbonates of the Otavi Group, with the Tsumeb-type occurring in the upper Tsumeb Subgroup and the Berg Aukas-type predominantly in the upper Abenab and lower Tsumeb Subgroup. A recent summary of the two main types is given in figure 4.6. Currently,



	Berg Aukas-type	Tsumeb-type
Host-rock	Abenab Subgroup and lower Tsumeb Subgroup	Elandshoek and Hüttenberg Formations (dolomites), T4 through T8 zones
Shape of orebody	Stratiform lenses, discordant breccias	Discordant pipe, filled with breccia and sandstone; structural control
Ore mineralogy	Sphalerite, galena (pyrite, chalcopyrite, tennantite)	Tennantite, galena, sphalerite, pyrite, bornite, chalcopyrite, germanite
Ore geochemistry	Zn>Pb; low Cu, Ag, As, Ge, Ga, Cd	Pb>Cu=Zn, Considerable As, Ag, Cd, Ge, Ga, W
Fluid inclusions	ca. 23 wt.% NaCl eq., 137 to 255°C	22.3 wt.% NaCl eq., >212°C (dolomite III)
Fluid source	Basinal brines	Orogenic fluids
Age	635 to 750 Ma ?	460 to 530 Ma?

Figure 4.6: Major types of base metal mineralisation in the OML (modified after Melcher et al., 2006).

this traditional subdivision, based on differences of Pb-isotopes mainly (figure 4.7), has been questioned by Schneider et al. (2008), who relate the different isotope groupings to the original basement composition.

Berg Aukas-type deposits and similar occurrences are located in the central to eastern OML (e.g. Berg Aukas, Abenab Pipe, Harasib. Two models are suggested for the formation of Berg Aukas-type deposits: 1) MVT-style mineralisation prior to the Pan-African orogeny due to basin dewatering processes (Pirajno and Joubert, 1993, Chetty and Frimmel, 2000) and 2) syn Pan-African emplacement (Hughes, 1979).

Tsumeb-type deposits in the OML occur in the type locality of Tsumeb (Lombaard et al., 1986), but also at Kombat (Innes and Chaplin, 1986, Deane, 1993), Khusib Springs (Melcher et al., 2006) and in several small prospects (Tsumeb West, Uris etc.) in the northwestern OML. Most studies on Tsumeb-type deposits suggest that the hydrothermal fluids responsible for ore deposition were generated during prograde metamorphism of the Pan-African orogeny and migrated along Pan-African faults (Pirajno and Joubert, 1993). Based on fluid inclusion studies on massive sulphides occurring in this ore type (Ypma, 1978), Chetty and Frimmel (2000) calculated a formation temperature of ca. 405°C for the Tsumeb-type mineralisation in the Kombat Mine.

The absolute age of primary base metal sulphides in the OML is not well constrained. A minimum age for Berg Aukas-type mineralisation could be deduced by the dating of nonsulphide minerals,

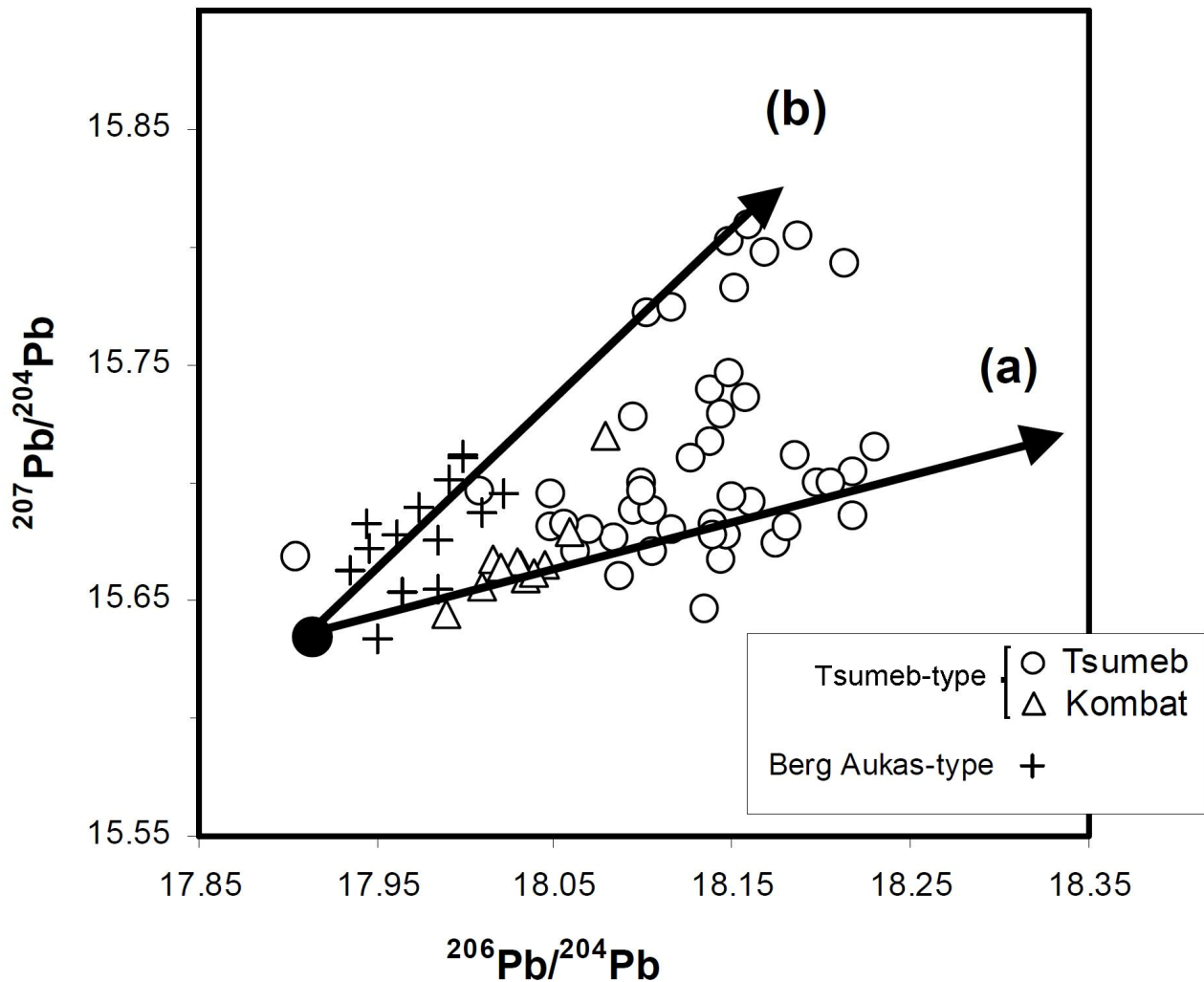


Figure 4.7: Uranogenic lead data result in different trends for Tsumeb type (trend a, Tsumeb and Kombat) and Berg Aukas type (trend b) (modified after Melcher et al., 2006).

which replace sphalerite (Schneider et al., 2008) (cfr § 7.2). Based on preliminary Re-Os analyses of Ge-rich sulphide ores, Melcher et al. (2003) reported an age of 530 Ma for the main ore phase in the Tsumeb Pipe deposit. In general, model ages of ore samples from the Tsumeb Pipe and the Kombat Mine range from 600 to 530 Ma (Allsopp et al., 1981, Hughes et al., 1984, Kamona et al., 1999), but many studies question the reliability of these dates (e.g., Haack, 1993, Frimmel et al., 2004).

Most deposits reflect a multistage evolution and display a strong structural control (Lombaard et al., 1986, Pirajno and Joubert, 1993, Frimmel et al., 1996). Mineralized brittle shear zones indicate the importance of flexural shear folds and small-scale thrusts for mineralisation (Laukamp, 2006). These characteristics are in common between both primary sulphides (e.g., Tsumeb orebody, Lombaard et al., 1986) and also in part of the nonsulphide deposits (Schneider et al., 2008).

Nonsulphide Zn-Pb ores in the OML are mostly associated with, or even clearly replace, primary

base metals sulphides. They partly display complex paragenetic associations, which point to very distinct processes of formation and mineralisation periods (e.g., Lombaard et al., 1986). The economically most important nonsulphide base metal ore minerals are willemite (Schneider et al., 2008) and Pb-Zn-Cu vanadates (descloizite-mottramite) (Boni et al., 2007).

4.2 *Lufilian Arc and Zambezi, Zambia*

The Kabwe area deposits are hosted in Neoproterozoic terranes belonging to the Katangan Supergroup, deformed during the orogeny originating the Lufilian Arc (figure 4.8). The southern margin of the Lufilian arc is separated from the Zambezi belt by the Mwembeshi dislocation (a regional shear zone) (John et al., 2004), that involved the Neoproterozoic terranes of the Zambezi Supracrustal Sequence. To the latter belong the rocks, which are host of the willemite deposits in the Lusaka area (figure 4.8).

4.2.1 *Lufilian Arc*

In the Lufilian Arc, the Katangan Supergroup is deformed into a north verging, thin-skinned, low- to medium-grade, fold-thrust belt (Johnson et al., 2005). The Lufilian Arc consists of four districts, corresponding to north-convex tectonic zones (figure 4.8). These are, from north to south, the following: (1) the External fold and thrust belt (EB), (2) the Domes region (DR), (3) the Synclinorial belt (SB), and (4) the Katanga high (KH) (Selley et al., 2005). The northern margin of the Lufilian arc is defined by the relatively undeformed uppermost Katangan Supergroup strata, and the southern margin by the sinistral, east-northeast trending Mwembeshi shear zone (Selley et al., 2005). Kinematics indicate northwest- to northeast directed thrusting during the Neoproterozoic to Cambrian convergence of the Kalahari and Congo cratons, with displacement vectors radiating perpendicularly with respect to the arcuate trend of the fold belt (Daly, 1986, Kampunzu and Cailteux, 1999).

The External fold and thrust belt is characterised by a thin skinned geometry, with complex, macroscale fragmentation and thrust repetition of the Katangan Supergroup stratigraphy (Selley et al., 2005). Metamorphic grade decreases northward from greenschist to prehnite-pumpellyite facies. The lack of the basement in this zone is commonly considered to reflect widespread decoupling along evaporitic strata at depth (Kampunzu and Cailteux, 1999, Porada and Berhorst, 2000, Jackson et al., 2003). In the DR, the strata of the Katangan Supergroup were deformed with the basement units and underwent upper greenschist to upper amphibolite-facies metamorphism.

The relationship between the outer zones of the Lufilian fold belt (EB and DR) and the Synclinorial and Katangan High remains unclear. Models invoking a fundamental change in basin environment,

broadly coincident with thrust dislocation between DR and SB, were proposed by Cosi et al. (1992) and Porada and Berhorst (2000). According to Porada and Berhorst (2000) this boundary originally represented an abrupt break between a marginal marine platformal-lagoonal setting to north, and a deeper water shelf to the south. Subsequent decoupling along evaporitic horizons accommodated significant north-directed transport (ca 150 km) during Lufilian orogeny, resulting in emplacement of allochthonous thrust sheets containing both basinal and platformal strata (Selley et al., 2005). The Kabwe area deposits are located in the Synclinorial belt (figure 4.8).

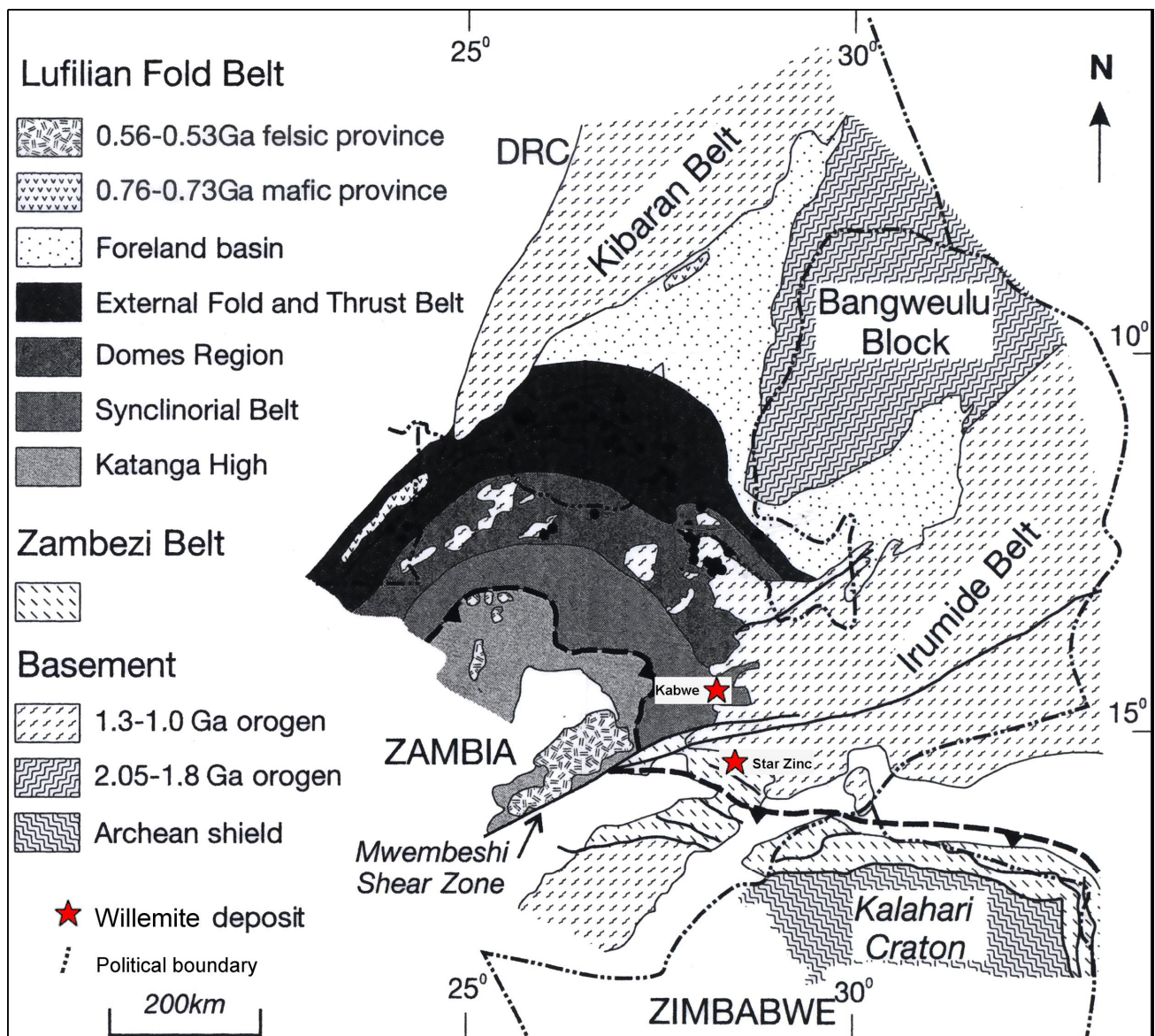


Figure 4.8: Map showing the tectonic zoning in the Lufilian arc and the Zambezi belt. Stars indicate the willemite deposits (modified after Selley et al., 2005).

4.2.2 *Geology of the Kabwe area*

4.2.2.1 *Basement Complex*

The Kabwe region is mostly underlain by the Neoproterozoic metasedimentary rocks (quartzite, schist, ironstone and banded iron formation) of the Muva Supergroup (Kamona and Friedrich, 2007). The Muva Supergroup unconformably overlies a Palaeo- to Mesoproterozoic basement of granite gneiss with minor amphibolite, schist, quartzite, pegmatite and xenolithic metasediments commonly referred to as the “granite-gneiss complex” (Arthurs et al., 1995, Cairney and Kerr, 1998). Quartz-tourmaline conglomerate and volcanic rocks of uncertain age occur within the Muva quartzite (Kamona and Friedrich, 2007). The granite-gneiss of the Basement Complex is part of a Palaeoproterozoic magmatic arc emplaced in a range between 2050 to 1865 Ma, whereas the Muva Supergroup formed between 1941 and 1355 Ma (Cahen et al., 1984, Rainaud et al., 2002).

4.2.2.2 *Katangan Supergroup*

The Neoproterozoic metasedimentary cover rocks consist of meta-arkose, quartzite and conglomerate at the base, followed by phyllite, meta-argillite, metasilstone, quartzite and dolomite-marble with associated tremolite schist, microdiorite, gabbro, amphibolite and epidosite (Moore, 1964, Cairney and Kerr, 1998). These rocks are generally considered to have formed within the same period as the Neoproterozoic Katangan rocks of the Copperbelt (from 877 to 656 Ma, Cahen et al., 1984, Cairney and Kerr, 1998, Armstrong et al., 1999). The Katangan Sequence in the Kabwe area has been subdivided into the Kangomba and Nyama Formations (figure 4.9).


The Kangomba Formation consists of an underlying quartzitic-micaceous member and an overlying, mainly dolomitic member, which correspond to the Lower and Upper Roan Groups in the Copperbelt, respectively (Moore, 1964, Cairney and Kerr, 1998). This correlation of the Kangomba Fm with the Roan Groups suggests that deposition occurred in the Kabwe area in a period spanning from ca. 880 to 765 Ma (Armstrong et al., 1999, Key et al., 2001).

The overlying Nyama Formation consists of dolomite and calcite marble and phyllite, and has been correlated to the Lower Kundelungu Fm in the Copperbelt (Kamona and Friedrich, 2007). It is also possible that the Nyama Fm is partly equivalent to the Upper Roan (Barr et al., 1978).

4.2.2.3 *Post-Katangan successions*

The post-Katangan Karoo Supergroup consists of a series of Carboniferous to Jurassic conglomerate, sandstone and mudstone deposited in a rift environment (Mulcahy, 1991). The sequence is divided between lower and upper Karoo (Drysdaal et al., 1962) and crops out mainly in

877 - 656 Ma	Neoproterozoic	Katanga Supergroup	Kundelungu Group	Nyama Fm	Pelites with minor quartzites and dolomites	
					Pelites an thin limestones with phyllitic partings locally	
			Roan Group	Upper Roan	Kangomba Fm	Pelites; mainly phyllites and metasiltstones with interbedded dolomites, grading locally into interbedded pelites and quatzites
						Lower Roan
				Pelites; indistinguishable from those overlying the Kabwe Dolomite		
				Arkosic sandstones and feldspathic quartzites with minor conglomerates and pelites		

Kabwe Area Deposits

1941-1355 Ma	Neo-Proterozoic	Muva Supergroup		quartzite schist ironstone and bif
--------------	-----------------	-----------------	--	------------------------------------

2050-1865 Ma	Paleo/Meso-Proterozoic	Basement Complex	Mwomboshi Gneiss	Porphyroblastic and granitic gneisses
--------------	------------------------	------------------	------------------	---------------------------------------

Figure 4.9: Lithologies and stratigraphy in the Kabwe area and stratigraphic position of the ore deposits in the Kabwe area (the stratigraphic position of Millberg deposit is still controversial, both Kabwe dolomite or dolomite of the Nyama Fm are considered to host it). The data have been compiled from the works of: Cairney and Kerr (1998) and Kamona and Friedrich (2007).

the Zambezi, Luangwa and Kafue river valleys in western Zambia (Sharad Master, personal communication, 2008). The Lower Karoo is a 2000m sequence of basal conglomerate, tillite and sandstone of fluvioglacial origin followed by deltaic and fluvial sediments. The Upper Karoo consists of 500 to 1000m of basal sandstone (containing uranium ores), overlain by claystone and sandstone (Mulcahy, 1991).

The last part of the sedimentation record in Zambia are carbonates and continental sediments of Cretaceous age followed by unconsolidated sands of Tertiary to Recent (Kalahari) age, found mainly on top of Karoo sediments (Mulcahy, 1991). Thick weathered soils, mainly occurring in river valleys and swamps, cover large areas of the Katangan successions (Geology of quarter degree sheet 1428, NW quarter 1998).

4.2.3 Primary ore deposits in the Kabwe area

Various lithological units of the Kangomba Formation, equivalent to Roan Group in the Copperbelt, contain base metal mineralisation on a regional scale (figure 4.10), including disseminated Cu

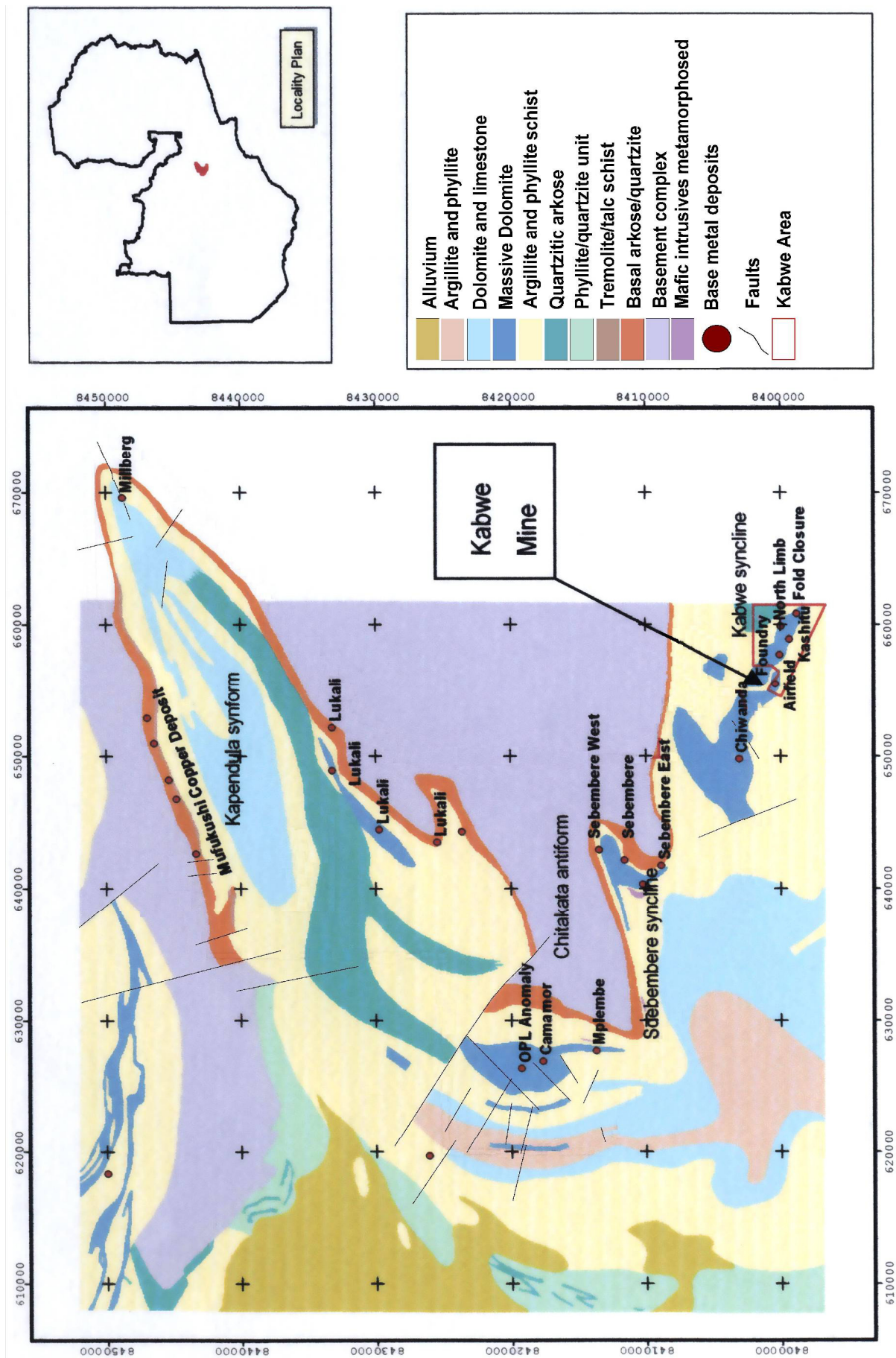


Figure 4.10: Kabwe area regional geology, stratigraphy and mineralisation (modified after Teal unpublished report, 2001).

mineralisation in massive quartzite at Sebembere (Kamona and Friedrich, 2007), and Cu-Zn mineralisation in tremolite schist above the footwall quartzite at Mufukushi (Cairney and Kerr, 1998).

Nevertheless, the most important are the Pb-Zn sulphide mineralisation of the Kabwe-type occurring in dolomitic units of the upper Kangomba Formation (Kamona and Friedrich, 2007), usually referred as the Kabwe Dolomite (geology of quarter degree sheet 1428, NW quarter 1998), and corresponding to the Upper Roan dolomite in the Copper Belt. These carbonate units of the Katangan Sequence, are the principal ore bearing horizons in the district. They comprise crystalline massive dolomite and marble, overlying laminar dolomite, calcareous shale and syn-sedimentary breccias (Billiton unpublished report, 1999). The mentioned Pb-Zn deposits may be described as an epigenetic, moderate to high temperature, carbonate-hosted type, whose origin is associated with the mobilisation of metals and fluid circulation in an intra-continental rift basin (Kamona and Friedrich, 2007). The structurally controlled ore deposition indicate that mineralisation of the Kabwe type is likely to be found in fractured zones controlled by north-east-striking basin margin faults within carbonates of the Kabwe Dolomite Formation. (Kamona and Friedrich, 2007). The source of the metals in the Kabwe orebodies is indicated by the isotopic signature of lead in galena to be the upper continental crust (Kamona et al., 1999), while Kamona and Friedrich obtained negative $\delta^{34}\text{S}$ values with galena, sphalerite and pyrite averaging $-17.43 \pm 0.41\text{‰}$, $-15.23 \pm 0.42\text{‰}$ and $-14.50 \pm 0.50\text{‰}$, respectively, thus pointing to a seawater signature. Fluid inclusions data from Kabwe primary sulphides (250-350°, 30 eq. wt.% NaCl) point to a high-Temp MVT deposit (Kamona and Friedrich, 2007).

4.2.4 Zambezi Belt

The Zambezi Belt (ZB) is part of the Pan-African orogenic system that crosscuts southern Africa, separating the Congo and Kalahari Cratons and their respective Paleo- and Mesoproterozoic units (John et al., 2003). This Pan-African belt was formed during the assembly of the Gondwana Supercontinent. The Zambezi Belt orogeny involved the rocks of the Zambezi Supracrustal sequence (ZSC), crosscutting the Mesoproterozoic parts of Zambia into the Irumide Belt and the Choma-Kalomo Block (figure 4.11).

According to Johnson et al. (2007) the Zambezi Supracrustal sequence (ZSC) of southern Zambia accounts for two major exposures: the “*Nega section*” in the southern portion of the ZB and the “*Lusaka section*” (figure 4.12). Both sedimentary successions can be interpreted as a single succession that was deposited as a result of crustal thinning and extension that began at 880 Ma

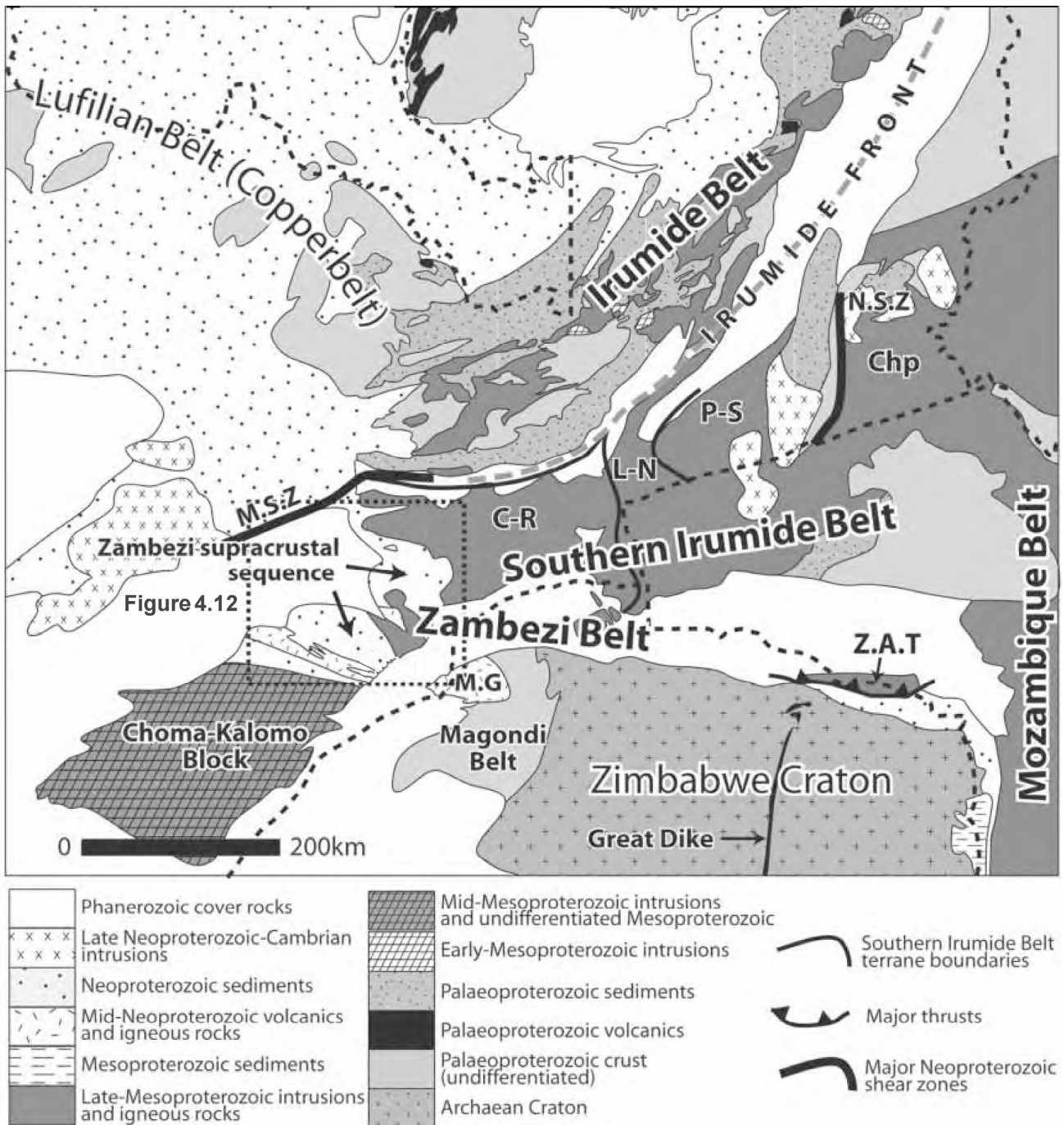


Figure 4.11: Simplified geological map of the central-southern African region showing the location of the various tectonic units, including the Zambezi Supracrustal sequence (modified after Johnson et al., 2007).

(Johnson et al., 2007). The ZSC is a metasedimentary package of clastics and carbonates, with a thick sequence of basal volcanics and lavas (the Kafue Rhyolite Fm, erupted at 880 Ma, Johnson et al., 2007) (figure 4.12). The intrusion of the Lusaka Granite at 820 Ma, provides an upper age limit

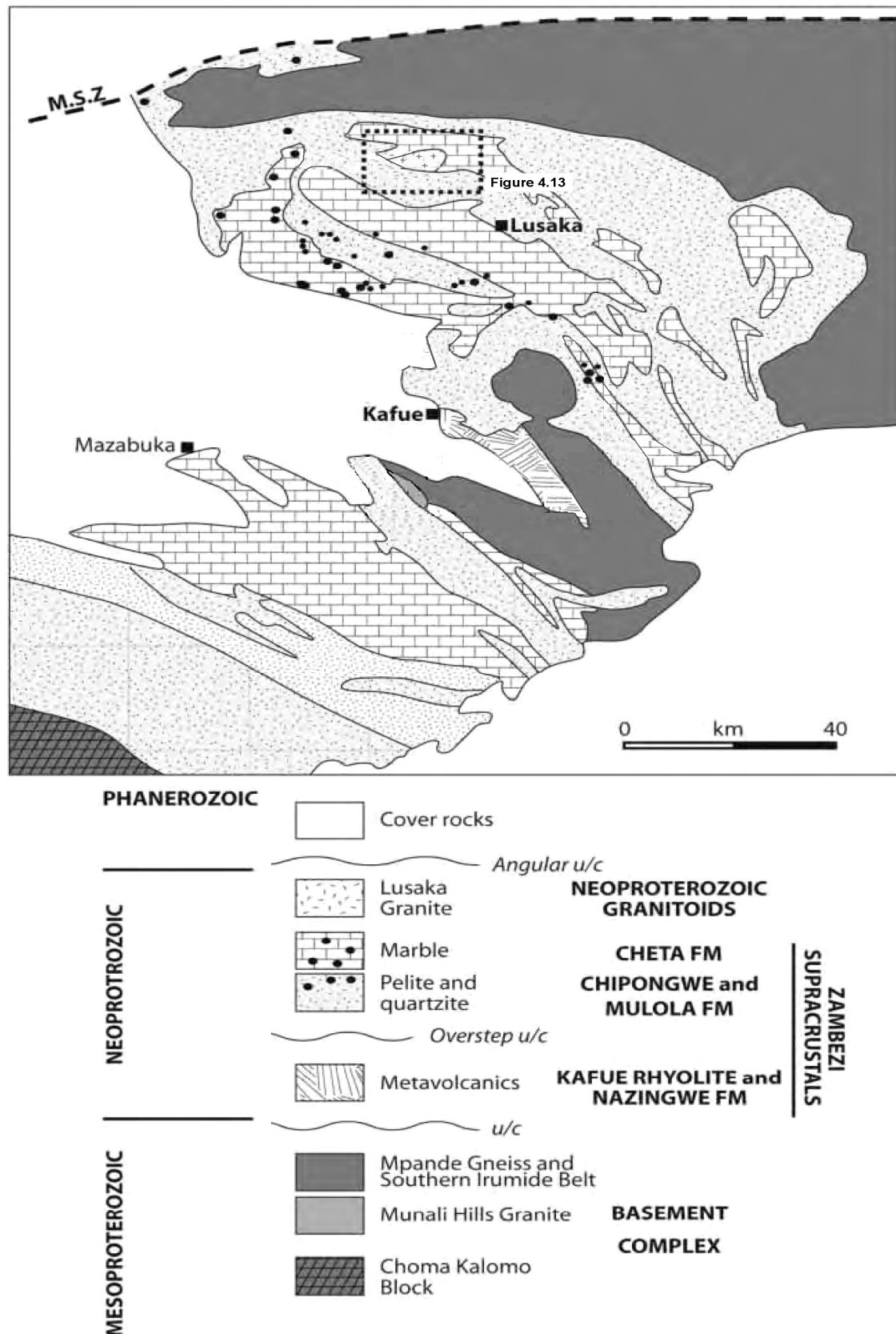


Figure 4.12: Enlarged geological map of the Lusaka area, showing the location of basement outcrops and of the Zambezi Supracrustal lithologies (modified after Johnson et al., 2007).

for the deposition of the ZSC sedimentary succession and, together with the Ngoma Gneiss, geochemically similar (Katongo et al. 2004), represents the final stage of basin development. Both the Lusaka Granite and the Ngoma Gneiss, have metaluminous A-type geochemical characteristics (Katongo et al. 2004) and crystallization ages of ca. 820 Ma (within error), thus providing an upper limit to the age of sedimentation. ZSC has traditionally been correlated with the lowermost Katangan sediments of the Copperbelt Region, the Roan Group (Annels, 1974, Unrug, 1988, Porada, 1989, Binda, 1994, Porada and Berhorst, 2000, Johnson et al., 2005).

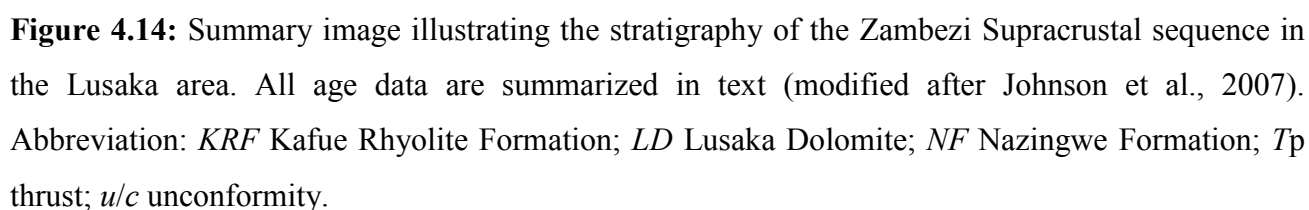
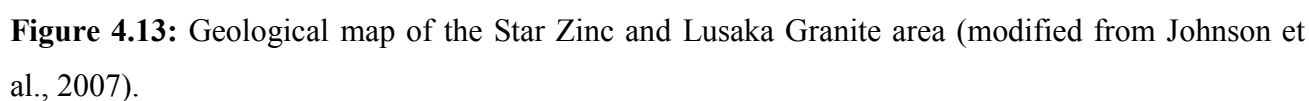
4.2.5 *Geology of the Lusaka area*

The willemite deposits of Star Zinc and Excelsior occur in the Lusaka area. The Lusaka region was mapped in the 1960s by several geologists of the Northern Rhodesia Geological Survey (e.g., Simpson et al., 1963, Smith, 1963) (figure 4.13). The region south of Lusaka is underlain by a variety of metamorphosed gneisses, metasediments, and granitoids (Basement Complex) that are often in tectonic contact with each other. So far, the oldest dated units are the Mesoproterozoic, variably deformed Mpande Gneiss (1106 ± 19 Ma; Hanson et al., 1988, Johnson et al., 2007) and the Munali Hills Granite (1090 ± 1.3 Ma; Katongo et al., 2004, Johnson et al., 2007).

In the Lusaka area the ZSC is floored (figure 4.12 and 4.14) by a thick basal sequence of metarhyolites and minor metabasalts, which have been interpreted as bimodal, continental rift volcanics (the Kafue Rhyolite Formation) (Johnson et al., 2007). The basal Kafue Rhyolite Formation (KRF) is a 2500 m-thick sequence of folded, variably metamorphosed felsic volcanic flows and tuffs with subordinate tuffaceous sediments and extremely rare thin mafic horizons (Smith, 1963, Mallick, 1966). The KRF passes up into the Nazingwe Formation (NF), a ~500m thick sequence of tuffaceous semipelites with intercalated acid and minor mafic volcanic horizons (Smith, 1963, Mallick, 1966). The nature of the boundary of the KRF with the basement rocks is uncertain because of an almost complete lack of exposures; however, Smith (1963) has interpreted it to be an unconformity.

The Kafue Rhyolite and Nazingwe Formations, are overlain by the quartzite-dominated Mulola Formation. At many localities, the latter formation preserves current bedding (Smith, 1963, Mallick, 1966), while its base is marked by a variable thickness of undeformed conglomerates in part consisting of rhyolitic pebbles (Mallick 1966). This being an evidence that this formation is, at least in places, in depositional (rather than tectonic) contact with the underlying basement.

The Mulola Formation passes up into kyanite-bearing, biotite-rich schists and semipelites of the Chipongwe Formation and subsequently into the dolomitic marbles of the Cheta Formation that is



host for Star Zinc willemite deposit (figure 4.13). The Cheta Formation contains thousands of randomly oriented, isolated blocks of variably metamorphosed, some of them up to eclogite facies (John and Schenk, 2003), gabbro, mafic, and ultramafic blocks (Vr̀ana et al., 1975). These blocks have normalized mid-ocean ridge basalt (N-MORB) composition (John et al., 2003, 2004) and are interpreted to represent a tectonically dismembered Neoproterozoic ophiolite (John et al., 2003) or a Neoproterozoic ophiolitic *mélange* (Johnson et al., 2005). The sequence is intruded by various Neoproterozoic within-plate-type granitoid bodies as the Lusaka Granite (Hanson et al., 1988, 1994, Wilson et al., 1993).

It has been suggested that this succession is overlain with a structural break, possibly representing a thrust (Simpson et al., 1963, Porada and Berhorst, 2000), by the Lusaka Dolomite and that this unit was deposited after the intrusion of the Lusaka Granite, currently dated at 846 ± 68 Ma (Barr et al., 1977). Johnson et al. (2007) suggested that the Lusaka Dolomite may be significantly younger than the main ZSC sequence, having been tectonically juxtaposed with the ZSC during Pan-African tectonism. All lithologies have been subjected to the same shearing, folding, and metamorphism that affected the KRF and NF, indicating that this upper sequence of metasediments was deposited before the regional Pan-African event (ca. 550-530 Ma) (Johnson et al., 2007).

4.3 Evolution of the Damara-Lufilian-Zambezi belt

4.3.1 Deformation phases and metamorphism in the OML

The main deformational event of the Pan-African orogeny in the OML (D2) was related to the convergence and collision of the Kalahari and Sao Francisco-Congo Cratons (Laukamp, 2006). The late Pan-African uplift of the Northern Platform (D3), which led to a fragmentation of the OML by extensional normal faults, was due to the waning stages of the convergence between the Kalahari and Sao Francisco-Congo Cratons (Grey et al., 2006). D3 passed over into the post Pan-African uplift and extension, characterised by normal faulting and reactivation of NE-trending structures (Söhne, 1957). D2 was accompanied by a greenschist facies metamorphism (M1) of the Otavi and Mulden Groups with peak conditions aged around 530-535 Ma (Clauer and Kröner, 1979, Goscombe et al., 2004). In the eastern areas of the Northern Zone, 50 km SW of Otavi the metamorphic grade reached the amphibolite facies during D2 (estimated peak conditions: 635° C at 8.7 kbar; Goscombe et al., 2004). This supported a southward increasing syn-D2 metamorphic grade towards the hinterland of the Otavi Mountain fold and thrust belt (Coward, 1981).

Clauer and Kröner (1979) have described a second, low-grade metamorphic event (M2) around 455 Ma (K-Ar, 250 - 300° C at 2 kbar), in the Mulden Group from the Etosha Pan northwest of Tsumeb,

and Haack (1983) published K-Ar cooling ages (at 300° C) around 481 ± 25 Ma. Similar ages of this metamorphic event, ranging from 469 ± 12 to 445 ± 11 , were determined by Ahrendt et al. (1983) by K-Ar in the fine mineral fractions ($< 2\mu\text{m}$) on phyllites of the Kombat Fm, close to the Kombat Mine.

4.3.2 *Deformation phases and metamorphism in the Lufilian Arc and Zambezi Belt*

Three successive deformation phases resulting from the Lufilian orogeny have been recognised within the metasedimentary cover rocks in Zambia (Moore, 1964, Cairney and Kerr, 1998). The earliest (D1) fold phase is characterised by N-S trending isoclinal folds with a shallow to moderate southerly plunge, whereas a later phase (D2) is defined by minor open folds with NNW-SSE axes (Kamona and Friedrich, 2007). The latest deformation phase (D3) resulted in E-W to NE-SW trending regional anticlinal and synclinal structures within both the basement and cover rocks; this final phase generally resulted in refolding and refoliation of older structures. Porada and Berhorst (2000) in their tectogenetic model for the Lufilian and Zambezi belts consider only one major collisional event, the Katanga Orogeny, occurring at ca. 550 Ma (Porada and Berhorst, 2000). However, geological mapping carried out in the Lufilian Arc, including the work of Cosi et al. (1992) and Key et al. (2001) in northwest Zambia, has consistently shown evidence of three deformation phases.

The oldest metamorphic event affecting the Katangan Supergroup is recorded by biotite K-Ar ages in the range of 708 ± 7 to 628 ± 7 Ma in the Domes area (Cosi et al., 1992). More recent SHRIMP U-Pb age data on the monazite from the Chambishi basin indicate three metamorphic events with ages of 592 ± 22 , 531 ± 12 , and 512 ± 17 Ma, respectively (Rainaud et al., 2002). Regional shear zones were developed at the end of the Lufilian Orogeny, when compressive stresses ruptured the basement along the ENE trends that had been already determined by the Paleoproterozoic Irumide orogeny (Kamona and Friedrich, 2007).

Effects of regional metamorphism with greenschist to amphibolite facies have been recognised in the basement (Moore, 1964, Ramsay and Ridgway, 1977, Arthurs et al., 1995, Cairney and Kerr, 1998). The presence of kyanite in quartz-kyanite and quartz-kyanite-garnet schist intercalated with the granitic gneiss in the Lufilian basement indicates a regional amphibolite facies metamorphism of medium-pressure type. Greenschist facies metamorphism occurs in both the metasedimentary and basement rocks, but it is more characteristic of the former (Kamona and Friedrich, 2007). The mineral assemblages in the gneisses indicate retrograde metamorphism from upper amphibolite (muscovite and epidote absent) to epidote-amphibolite facies, as shown by the replacement of hornblende by epidote, whereas the metavolcanic rocks intercalated with the basement quartzite

show a typical greenschist facies mineral assemblage of chlorite, epidote, actinolite and quartz (Arthurs et al., 1995). The regional greenschist facies of the cover rocks is characterised by the chlorite-muscovite-biotite-quartz mineral paragenesis in the phyllite and tremolite-phlogopite-dolomite schist, where poikiloblastic tremolite replaces dolomite (Cairney and Kerr, 1998). Carbonate rocks generally exhibit a lower metamorphic state, as indicated by the presence of talc in a fine-grained recrystallized calcite-dolomite mosaics, whereas quartzite is generally sericite-rich and contains elongated quartz grains as well as fine-grained sutured quartz mosaics with coarser grained, strained quartz (Moore, 1964, Cairney and Kerr, 1998).

In the Zambezi belt, the eclogite facies metamorphism occurred at ca. 600 Ma (John et al., 2003), whereas peak metamorphism during the Kalahari-Congo craton continental collision occurred around 530 Ma ago, with metamorphic P–T conditions reaching the high pressure amphibolite facies (Goscombe et al., 2003, Vinyu et al., 1999, Johnson and Oliver, 2002, John et al., 2003).

4.3.3 *General tectonic evolution of the DLZ*

The tectonic evolution of the Damara-Lufilian-Zambezi (DLZ) belt can be divided in four major stages:

- 1) Formation and generation of the Paleoproterozoic basement during the Eburnean orogeny (Tegtmeyer and Kröner, 1985),
- 2) pre Pan-African rifting,
- 3) Pan-African orogeny with the formation of the DLZ belt,
- 4) post Pan-African uplift and extension.

The suturing of the Rio de la Plata Craton with the Kalahari and Sao Francisco-Congo Cratons respectively, preceded the collision of the latter two cratons (figure 4.14) (Maloof, 2000). According to Laukamp (2006) the collision of the Kalahari and Sao Francisco Cratons and the formation of the Damara-Lufilian-Zambezi Orogen (DLZ), may be occurred either simultaneously along the whole DLZ or started in the east (Lufilian and Zambezi Belts) and propagated to the west (Damara).

The late to post-Cryogenian D1 in the OML comprised NNE and NW-trending folds, accompanied by flexural gliding and terminated before the deposition of the Mulden Group. This first compressional phase in the Otavi Group could be related to the accretion of a Coastal Terrane to the Kaoko region in the west, immediately before the suturing (645-580 Ma) of the Rio de la Plata and Sao Francisco-Congo Cratons (Goscombe et al., 2005).

D2 represents the main deformational event in the OML, which should be divided into two

subphases, due to the apparent cooling of the Damaran successions and a presumable change of the shortening direction from NS (D2a) to NE-SW (D2b) during the collision between the Sao Francisco-Congo and Kalahari Cratons (Laukamp, 2006). D2a was accompanied by the peak metamorphism of the Damaran orogeny in the eastern Northern Zone (535- 530 Ma according to Clauer and Kröner, 1979, Goscombe et al., 2004). This fits roughly with the high-angle, NNE-SSW directed convergence of the Kalahari and Sao Francisco-Congo Cratons in the western inland branch of the Damara Orogen at 535-505 Ma, as suggested by many authors (Coward, 1981, 1983, Goscombe et al., 2005, Miller, 1983).

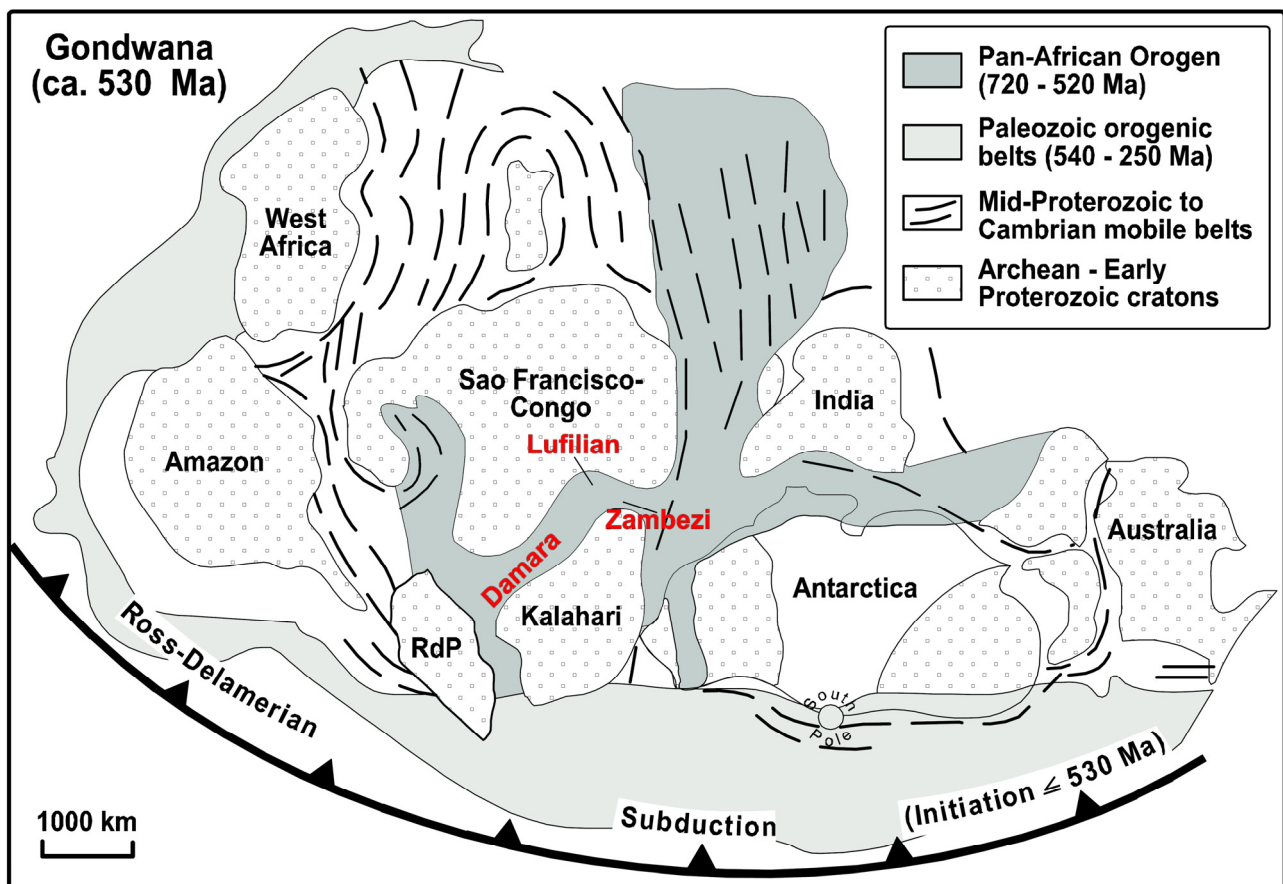


Figure 4.15: Map of the Gondwana Supercontinent between the end of Neoproterozoic and the beginning of Cambrian, showing the extent of the Pan-African Orogeny and the continental margin Ross-Delamerian orogeny. Red letters represent the DLZ belts, D - Damara, L - Lufilian and Z - Zambezi (modified after Laukamp, 2006).

An oblique NE-SW-striking convergence, related to the Mwembeshi Shear Zone (MSZ), is reported from the Lufilian and Zambezi Belt by Johnson et al. (2005), who emphasised the sinistral

displacement along this lineament. The main collision between the Kalahari and Sao Francisco-Congo Cratons in this area took place from 550-520 Ma (Johnson et al., 2005), whereas an age of ca. 551 Ma has been assigned to the Mwembeshi Shear Zone by Hanson et al. (1994). Therefore, the Pan-African continental collision at the eastern end of a Damara-Lufilian-Zambezi Orogen (DLZ) would have preceded the NE-SW directed collision in the west (Laukamp, 2006). The indication of a sinistral movement along the Mwembeshi Shear Zone has been discussed by Porada and Berhorst (2000), which pointed out the changes from sinistral to dextral movement between the different segments (Johns et al., 1989). Dürr and Dingeldey (1996) related sinistral movements along the Pan-African lineaments to an early phase of the convergence between the Kalahari and Sao Francisco-Congo Cratons that was replaced by dextral movements in a later stage. Dextral movements in the OML are distinctly younger than the sinistral ones along the Mwembeshi Shear Zone (Johnson et al., 2005) and are related to the main and late stages of the Pan-African orogeny. Reasons for the different shortening directions along the DLZ during the main phase of the Pan-African orogeny, could be a response to the non-linear shape of the southern margin of the Sao Francisco-Congo Craton, or could have been generated by a later subdivision and offset of the DLZ by a perpendicular lineament (Laukamp, 2006). The late Pan-African uplift (D3) caused predominantly NE- and minor NW-striking normal faults, but also the reactivation of NE- and E-striking dextral strike slip faults (Laukamp, 2006).

A greenschist facies metamorphism during the main phase of the Pan-African orogeny is reported from several areas of the DLZ (Laukamp, 2006). Besides the two early Cambrian ages from the eastern Northern Zone (Goscombe et al., 2004) and the Quangwadum Complex (Singletary et al., 2003), similar ages spanning from 550-520 Ma were described from the Lufilian and Zambezi Belts (Johnson et al., 2005). A similar time frame for a metamorphic period in the Central Zone of the Damara Belt, centred around 494-473 Ma has been assigned by Goscombe et al. (2005) to the well-known NNE-SSW directed shortening between the Sao Francisco-Congo and Kalahari Cratons.

5 Willemite mineralisation in the Otavi Mountainland

5.1 *Introduction and mining history*

The Otavi Mountainland (OML), where more than 600 mines and prospects occur (Melcher, 2003), represents the northern part of the E-W striking Damaran orogenic belt, where most of the Namibian base metal sulphide and nonsulphide deposits (figure 4.1) are located. Based on several geological/geochemical criteria and prevailing metal contents of the primary ores, two main mineralisation types have been distinguished: the Berg Aukas (Zn-Pb>Cu)-type and the Tsumeb (Cu>>Zn-Pb)-type deposits (Pirajno and Joubert, 1993, Melcher, 2003). Both types display very complex paragenetic associations, which probably indicate distinct processes of formation and mineralisation periods (Lombaard et al., 1986).

Most deposits in the OML reflect a multistage evolution and generally display a strong structural control (Laukamp, 2006). Mineralised brittle shear zones indicate the importance of flexural shear folds and small-scale thrusts for both primary sulphide deposits (e.g., Tsumeb orebody, Lombaard et al., 1986) and for at least part of nonsulphide deposits (e.g. Abenab West orebody, Verwoerd, 1953). Nonsulphide Zn-Pb ores in the OML are mostly associated with, or even clearly replace primary base metal sulphides. The economically most significant nonsulphide base metal ore minerals consist of willemite, Pb-Zn-Cu-vanadates and Zn-Pb carbonates.

In the vast literature on the OML base metal ores, willemite has been always considered as a secondary mineral of supergene origin, derived from weathering processes (Verwoerd, 1953, Misiewicz, 1988, Cairncross, 1997). Hitzman et al. (2003) was the first to consider the Namibian willemites as due to hydrothermal processes of unknown age, by comparison with other similar ores occurring in the Proterozoic of southern hemisphere. The economically most important willemite deposits of the OML are located at Berg Aukas, Abenab West and Baltika (figure 4.1).

Other common Zn-Pb nonsulphide minerals, such as cerussite, smithsonite, hemimorphite, hydrozincite and sauconite, clearly represent the product of much younger weathering processes. Moreover, some of the richest vanadium ores in the world, that were exploited also for their base metal content (Verwoerd, 1953, Weilers, 1959), are known to occur in the OML. They consist mainly of the isomorphous series of vanadates descloizite-mottramite $[\text{PbZnVO}_4(\text{OH})\text{-PbCuVO}_4(\text{OH})]$. As the Zn-Pb carbonates, these vanadates significantly postdate both the primary sulphides and willemite phases in the paragenetic sequence throughout the entire district (Cairncross, 1997, Boni et al., 2007).

No reference to the possible age of the supergene mineral assemblages has ever been made, with the only exception of the data published on descloizite/mottramite concentrations. According to

Pickford (1993) the vanadates have a Miocene age based on vanadate-encrusted mammalian fossil remnants discovered in a network of karstic cavities. Recent age dating, using (U-Th)/He descloizite thermochronometry (Boni et al. 2007) have established an age broadly confined to the Tertiary for most deposits, with a distinct period of descloizite formation ranging between 24 and 33 Ma.

5.2 *Berg Aukas*

The Berg Aukas Zn-Pb-V deposit is located in the eastern part of the OML, 20 km northeast of Grootfontein, (Cairncross, 1997). The ore deposit is hosted in Neoproterozoic shallow water microbial dolostones of the Gauss Formation (Abenab Subgroup, figure 4.2), on the northern limb of the E-W trending and westerly plunging, tight Berg Aukas syncline (Misiewicz, 1988).

According to Misiewicz (1988), the deposit is located near a major facies change in the basin, and primary sulphide mineralisation (mainly sphalerite) occurs along a bedding plane-parallel fault, separating different dolostone units (figure 5.1). In contrast to this, Chadwick (1993) proposed the deposition of the Abenab Subgroup in a half-graben setting and a tectonic control for lateral facies changes.

The mine with an average grade of 17% Zn and 5% Pb ceased its operations in 1978. The orebodies have been traced to a depth of 750 m below the surface, but were mined only to a depth of 600 m. The Berg Aukas deposit is one of the largest known accumulations of willemite (and descloizite) in the world (Misiewicz, 1988), where about 40% of the total zinc content occurs in this mineral form. The Berg Aukas deposit consists of three different stratigraphically and structurally controlled orebodies (figure 5.1): *Northern Ore Horizon*, *Central Orebody* and *Hanging Wall Orebody*.

5.2.1 *Northern Ore Horizon*

The Northern Ore Horizon, extending from the surface to the core of the Berg Aukas syncline, consists of three fault-related stratabound lenses of massive, coarse-grained and brecciated sphalerite and minor galena repeatedly modified by oxidation processes (Misiewicz, 1988).

The orebody is zoned, changing upward from its sulphide-rich base into a willemite-rich top (Misiewicz, 1988). Willemite generally forms dark brown to grey masses intergrown with or even replacing sphalerite, but occurs in its latest generations as white to yellow-white needles and concretions (Schneider et al., 2008). The Northern Ore Horizon contains also a late descloizite mineralisation hosted in dolomite breccia, and several cogenetic carbonates (Zn-bearing saddle dolomite) (Laukamp, 2006).

5.2.2 Central Orebody

The Central Orebody forms brecciated, irregular pipe-like lenses of semimassive, mainly weathered sulphides plus willemite, which extend from the surface to a depth of approximately 200m. Other nonsulphide ore minerals are smithsonite, hemimorphite, cerussite, and abundant descloizite and

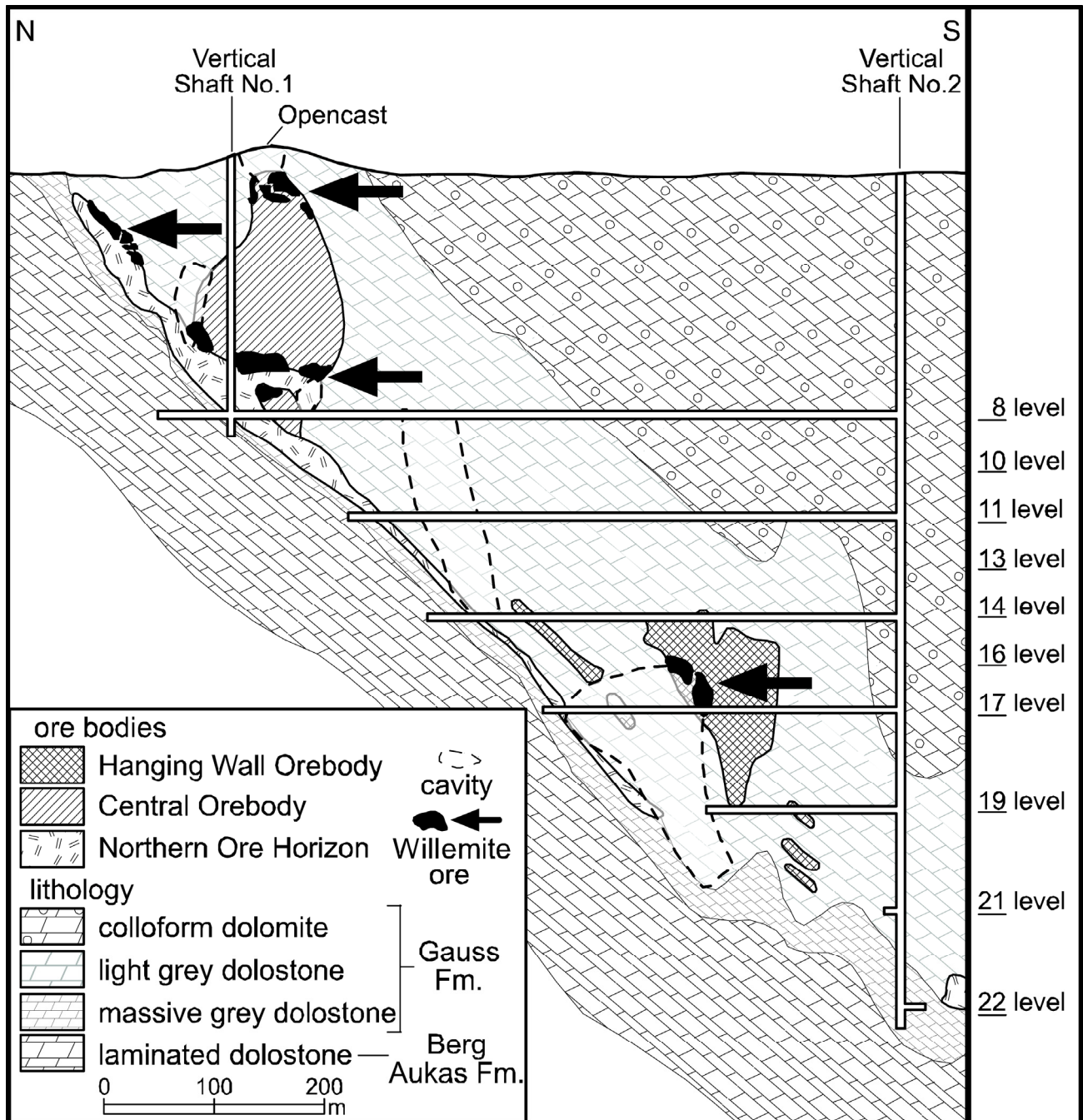


Figure 5.1: Schematic profile of the Berg Aukas mine with the location of the willemite ore (modified from Laukamp, 2006).

vanadinite (Markham, 1958). The orebody was exposed on the top of the Berg Aukas hill with an apex, consisting of a series of vanadiferous mud-filled fractures (“sand sacks” at the top of karst cavities) and descloizite-lined cavities. This outcrop led to the actual discovery of the V-mineralisation in 1913 (Wartha and Schreuder, 1992).

5.2.3 *Hanging Wall Orebody*

The Hanging Wall Orebody is characterized by N-S trending, steeply dipping lenses of ore-bearing fractures. Even if mineralogically not different from the Northern Ore Horizon, very variable ore grades and different structural fabrics made this stratabound orebody more difficult to mine (Misiewicz, 1988).

5.3 *Abenab West*

The Abenab West deposit is located approximately 30 km north of Berg Aukas (figure 4.1) and was exploited between 1922 and 1958 (Cairncross, 1997). The deposit is hosted in the Auros Formation (uppermost Abenab Subgroup, figure 4.2).

The Abenab West deposit consists mainly of secondary base metals ores and vanadates and is located ca. 100 m southwest of the Abenab pipe, the latter referred as the biggest known concentration of vanadate ore in the world. The orebody occurs along a steeply dipping, bedding-parallel structural contact. It is irregular along strike and ceased rapidly at a depth of less than 100 m (Verwoerd, 1953). The main Zn-mineralisation at Abenab West occurs in the so-called “Zinc Reef” (figure 5.2). It consists of a 450 m long replacement zone of red willemite and hematitic clay along a sheared and brecciated contact between laminated limestone and dolostone (Verwoerd, 1953).

The development of bedding-parallel cleavage and tectonic brecciation along this contact predates the formation of the zinc silicates (Schneider et al., 2007). Therefore, willemite mineralisation most probably occurred after the main deformational event of the Damaran orogeny (D2) (Laukamp, 2006).

Willemite in the Zinc Reef occurs also as radially assembled, needle-like crystals in cavities or lining fracture surfaces, possibly as replacement of primary sulphides. The primary sulphides, only reached with a drill core, consist of an association of sphalerite pyrite and galena, with several secondary copper minerals. This association has similarities with those occurring in the Tsumeb-type ores (Verwoerd, 1953).

5.4 *Baltika*

This deposit is located on the northern limb of the Otavi Valley Syncline in the farm area Baltika

515 (Wartha and Schreuder, 1992) (figure 4.1). The mineralisation is hosted in the massive grey dolomite and jasperoidal chert of the Tsumeb Subgroup (figure 4.2). Baltika was discovered in 1931 and was worked until 1942 (Sohnge, 1967) mainly for the abundant V-bearing descloizite ore. This main ore consists of discrete descloizite concentrations associated with calcite occurring in N-S trending veins, but also as cement in collapse breccias and “sand sack” type ore (Wartha and Schreuder, 1992, Boni et al., 2007). Minor stratabound Zn-Pb sulphide concentrations occur, consisting of: sphalerite, galena, tennantite and pyrite (Van der Westhuizen, 1984) with minor bornite and chalcopirite. Only limited information is available for the willemite ore occurring in an east-west fracture system (Wartha and Schreuder, 1992). Minor amounts of smithsonite and

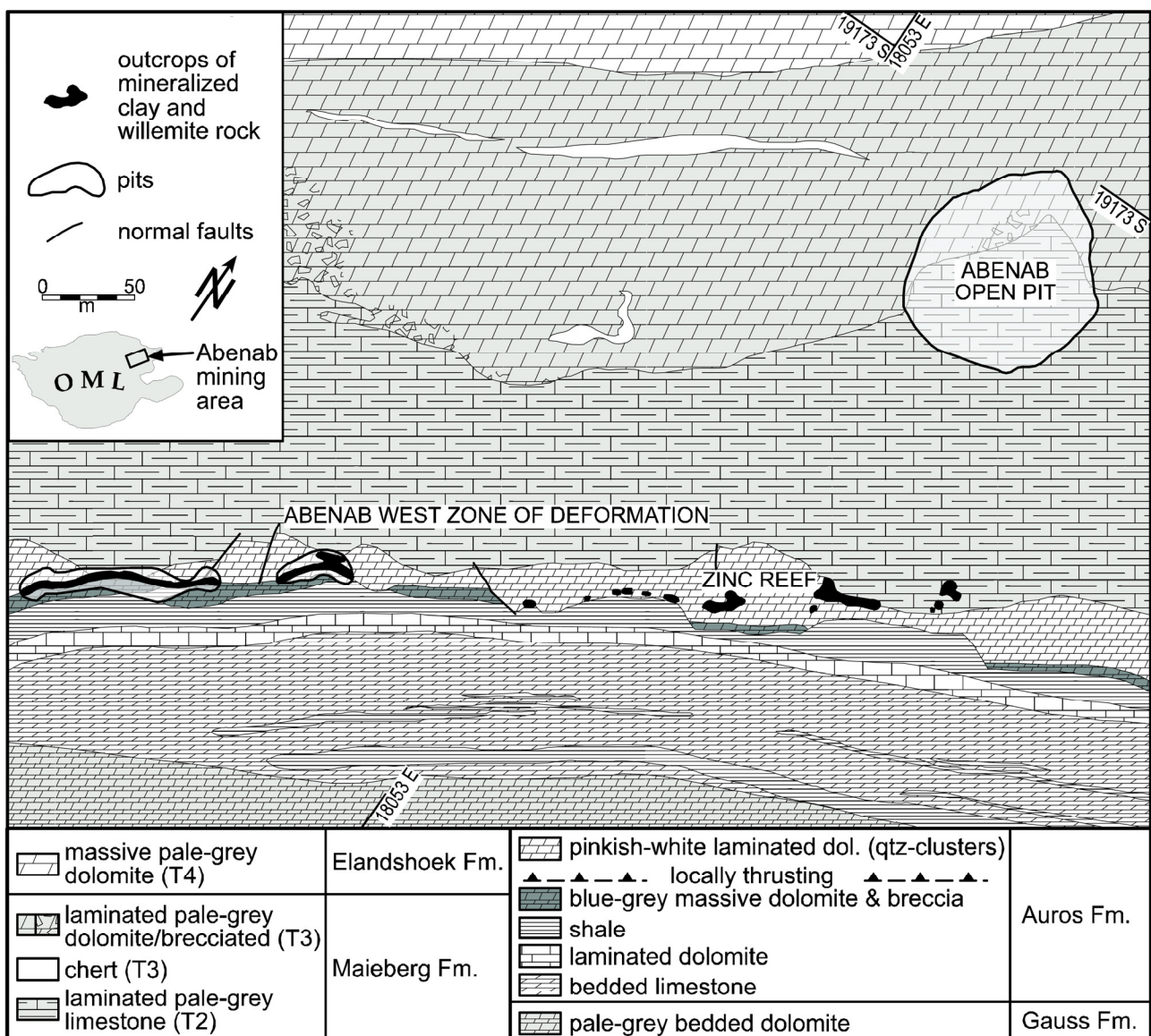


Figure 5.2: Geological map of Abenab West mining area (modified from Laukamp, 2006).

sphalerite accompany the willemite ore (Cairncross, 1997) that generally has a needle-like habit and replaces sphalerite. Other secondary supergene minerals that have been found are: pyromorphite and cerussite.

5.5 *Mineralogy of the willemite ore in the OML*

5.5.1 *Willemite*

Willemite has been detected in most OML base metal deposits with different textures, but always with a good crystallinity and an almost perfect cleavage planes along the c axis ([0001] and [1120]). The prismatic habit is usually best displayed in the open space filling aggregates (figure 5.8c and 5.11g), normally consisting of tiny needle-like crystals that can reach μm to mm size. Cm-sized willemite radial (figure 5.11e) or hexagonal botryoidal aggregates (figure 5.7a and 5.7e) may also be present as host rock replacement. Willemite filling veins (figure 5.7d and 5.8e) commonly consists of microcrystalline grains, while readily indiscernible crystals form massive aggregates (figure 5.10a and 5.10g). Well-formed prismatic or radial willemite crystals are usually white or transparent (figure 5.7a, 5.8c, 5.9g and 5.10c). Reddish-brown (figure 5.3e and 5.9c) to black (figure 5.3b and 5.3d) colours in willemite may be induced either by goethite-hematite or sulphides disseminations. In thin section, willemite may be easily recognized in crossed nicols by its high birefringence colour range, hexagonal habit and uniaxial interference figure. Under cathodic light, the luminescence of the OML willemites does not vary with their different textures. Botryoidal hexagonal crystals (figure 5.7b and 5.7f), vein fillings (figure 5.7d and 5.8b) and massive aggregates of subidiomorphic crystals (figure 5.10e and 5.10g) may show either green or blue colours, with a common dull-bright zonation.

XRD spectra of the typical willemites from Berg Aukas (figure 5.4), Abenab West (figure 5.5) and Baltika (figure 5.6) display patterns close to the ideal values for this mineral, with no appreciable or systematic variations of the crystallographic parameters.

5.5.2 *Other minerals*

Primary sulphides like sphalerite and galena (figure 5.3a and 5.3f) with rare bornite, chalcopyrite and pyrite occur as not-altered remnants mainly at Berg Aukas and Baltika. Secondary idiomorphic galena has been also observed in several samples (figure 5.13a, spot 2).

Appreciable amounts of smithsonite have been observed mainly at Berg Aukas (table 5.1). In cathodic light this smithsonite shows a pinkish luminescence (figure 5.7d and 5.7g). Cerussite is the main alteration product of galena. Minor sauconite (Zn-smectite) has been also detected. This clay

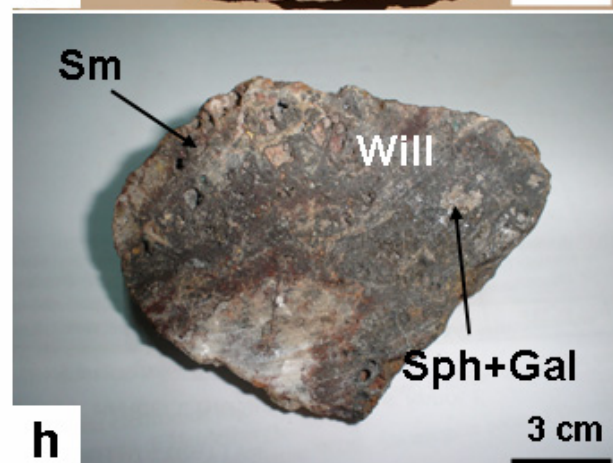
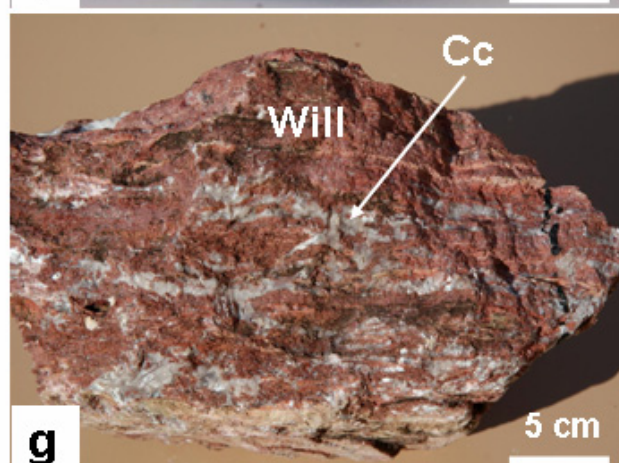
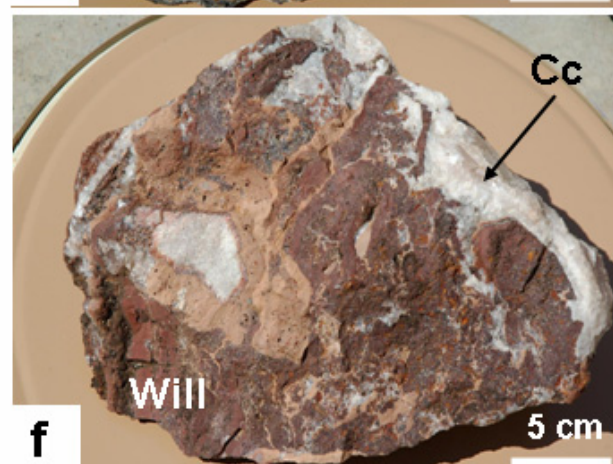
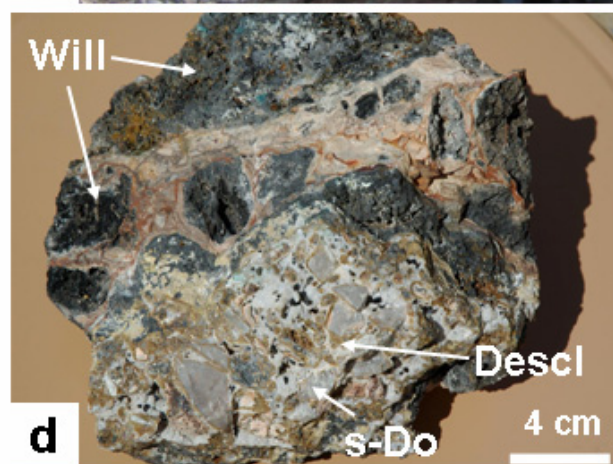
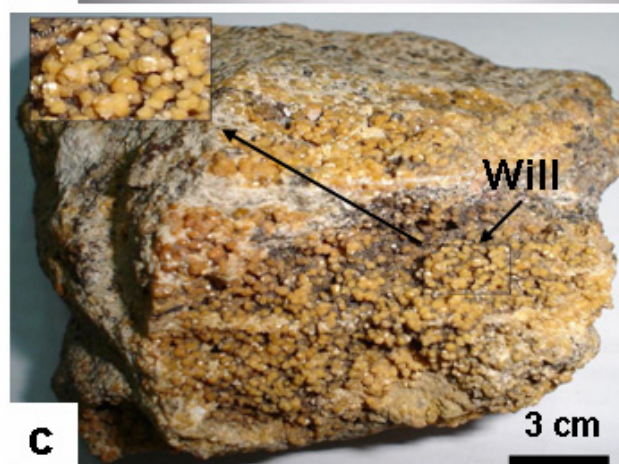
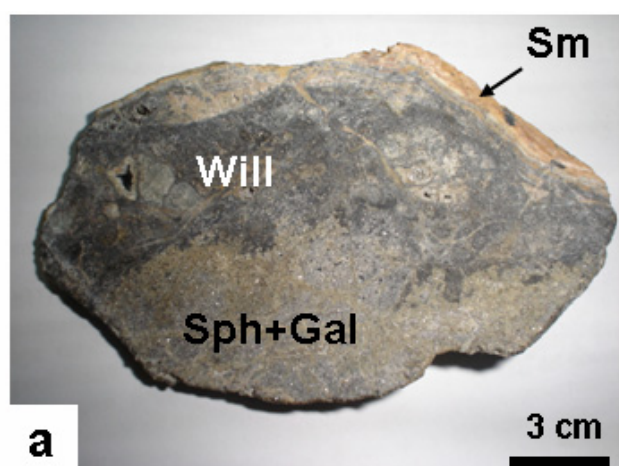


Figure 5.3: Hand specimens from Berg Aukas (a to d), Abenab West (e to g) and Baltika (h) mines. a) Black network of willemite veinlets replacing primary sphalerite-galena; whitish smithsonite is the most recent generation in this sample; b) remnants of an early boxwork of black willemite filled by a younger willemite generation; c) massive euhedral yellowish willemite aggregates replacing dolomite; d) brecciated willemite sample, with late greenish vanadates cementing the breccia, followed by white crystals of saddle dolomite; e) massive red willemite replacing the host rock; late, whitish willemite fills the cavities; f) red willemite ore, followed by late sparry calcite crusts; g) red willemite sample with white, late willemite in veins; h) blackish willemite boxwork replacing primary sulphides; brown supergene smithsonite represents the last generation.

commonly replaces previous barren aluminosilicates hosted in stylolite seams. Several replacement steps could be observed, up to a fillosilicate containing a maximum of 7% sauconite, with an increasing substitution of Zn and Mg respect to K and Al (figure 5.13b, spot 4, 5 and 6).

Calcite and dolomite are also associated with the willemite ore (figure 5.3c and 5.3f). A very late sparry calcite bearing up to 4 wt% Pb is usually one of the last phases (figure 5.8c and 5.11a), while a saddle dolomite phase postdates willemite in most examined mine sites (Berg Aukas, figure 5.7a and 5.7e; Abenab West, figure 5.10g and figure 5.11a). EDS spot analyses of this strongly zoned dolomite have revealed up to 12% of combined Zn-Pb, which replace Mg and Ca respectively in the dolomite lattice.

Fe-(hydr)oxides like hematite and goethite are also very common; Zn-Pb bearing Mn-oxides may be also present. Quartz forms microcrystalline aggregates and spherules throughout the ore.

Zn-Pb vanadates (vanadinite and descloizite) occur especially at Berg Aukas (figure 5.3d and 5.8h) in form of crystalline aggregates, crusts, and tabular brown to reddish crystals. They represent a particular phase of a formerly economic nonsulphide mineralisation, largely widespread in the OML. The vanadates and their genesis have been the subject of a recent study (Boni et al., 2007).

Table 5.1: XRD analyses of samples from OML area deposits; mineral symbols in order of abundance.

Site	Sample No.	Mineral(s)	Site	Sample No.	Mineral(s)
Berg Aukas	BA200310A	DescI, Do, Cc, Qtz	Berg Aukas	BA20037	Do
Berg Aukas	BA200310B	Will	Berg Aukas	NARO474	Will
Berg Aukas	BA200310C	Will, Do, Cc	Berg Aukas	NARO474(1)	Will, Cc, Sph
Berg Aukas	BA200311B1	Will	Berg Aukas	NARO474(2)	Will, Cc
Berg Aukas	BA200311B2	Will, Sm, Cc			
Berg Aukas	BA200311B3	Sm, Will, Qtz	Abenab West	AW20031B	Will, Qtz
Berg Aukas	BA200317	Will, Do, Ce	Abenab West	AW200321	Will, Ce, Qtz
Berg Aukas	BA200317A	Do, Will, DescI, Cc	Abenab West	AW200322	Will, He
Berg Aukas	BA200317B	Will	Abenab West	AW200323	Will, Ce
Berg Aukas	BA20031A1	Will	Abenab West	AW20032A	Will, Qtz
Berg Aukas	BA20031A2	Will, Do	Abenab West	AW20032B	Will, Do, Qtz
Berg Aukas	BA20034	Will, Qtz, Ank			
Berg Aukas	BA20034	Do, Will, Qtz	Baltika	NARO427A	Will, Cc, Sph
Berg Aukas	BA200351	Will, Sm, Do, Cc, Qtz	Baltika	NARO427B	Will, Sph
Berg Aukas	BA200352	Will	Baltika	NARO427C	Will, Sm, Sph
Berg Aukas	BA200353	Sph	Baltika	NARO427C1	Will, Sm
Berg Aukas	BA20036A	Will, Ga	Baltika	NARO427C2	Will, Brn, Cpy, Pyr
Berg Aukas	BA20036A	Will, Do			

Ank = ankerite, Brn = bornite, Cc = calcite, Ce = Cerussite, Cpy = chalcocopyrite, DescI = descloizite, Do = dolomite, Ga = galena, He = hematite, Hem = hemimorphite, Min = minirecordite, Pyr = pyromorphite, Qtz = quartz, Sm = smithsonite, Sph = sphalerite, Will = willemite.

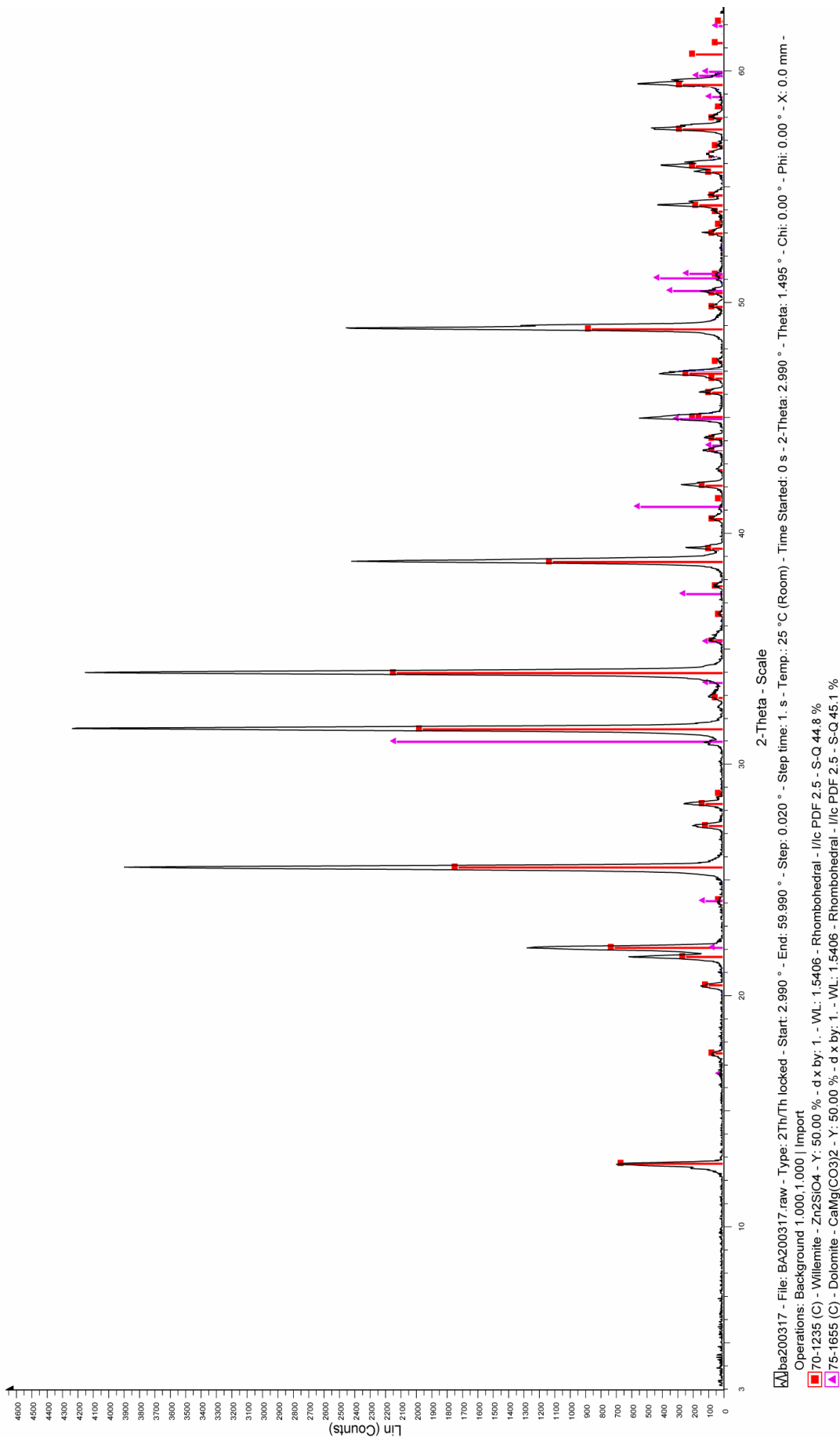


Figure 5.4: Willemite – Dolomite XRD spectra, sample BA200317 from Berg Aukas.

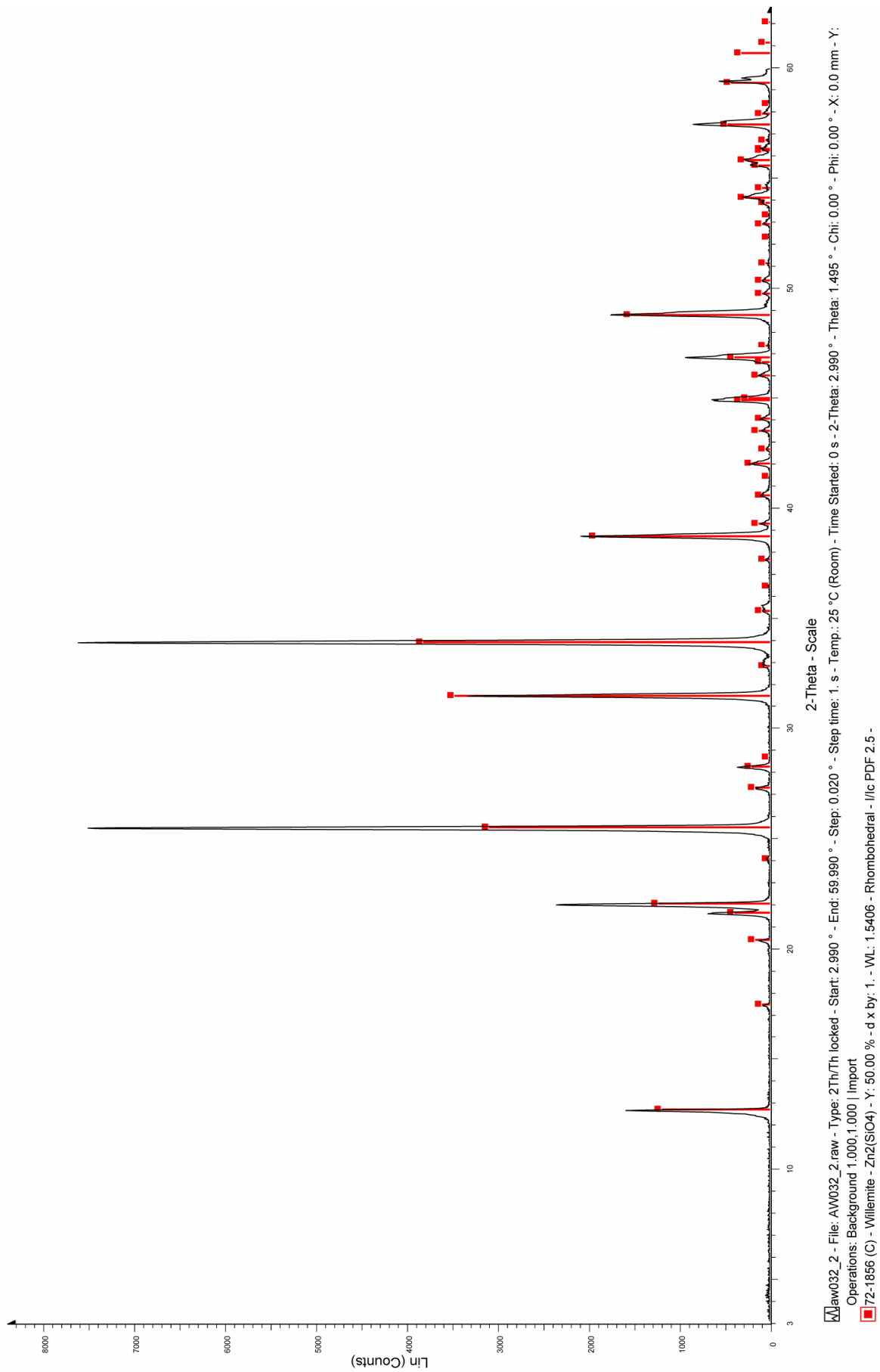


Figure 5.5: XRD spectrum of pure willemite, sample AW20032 from Abenab West.

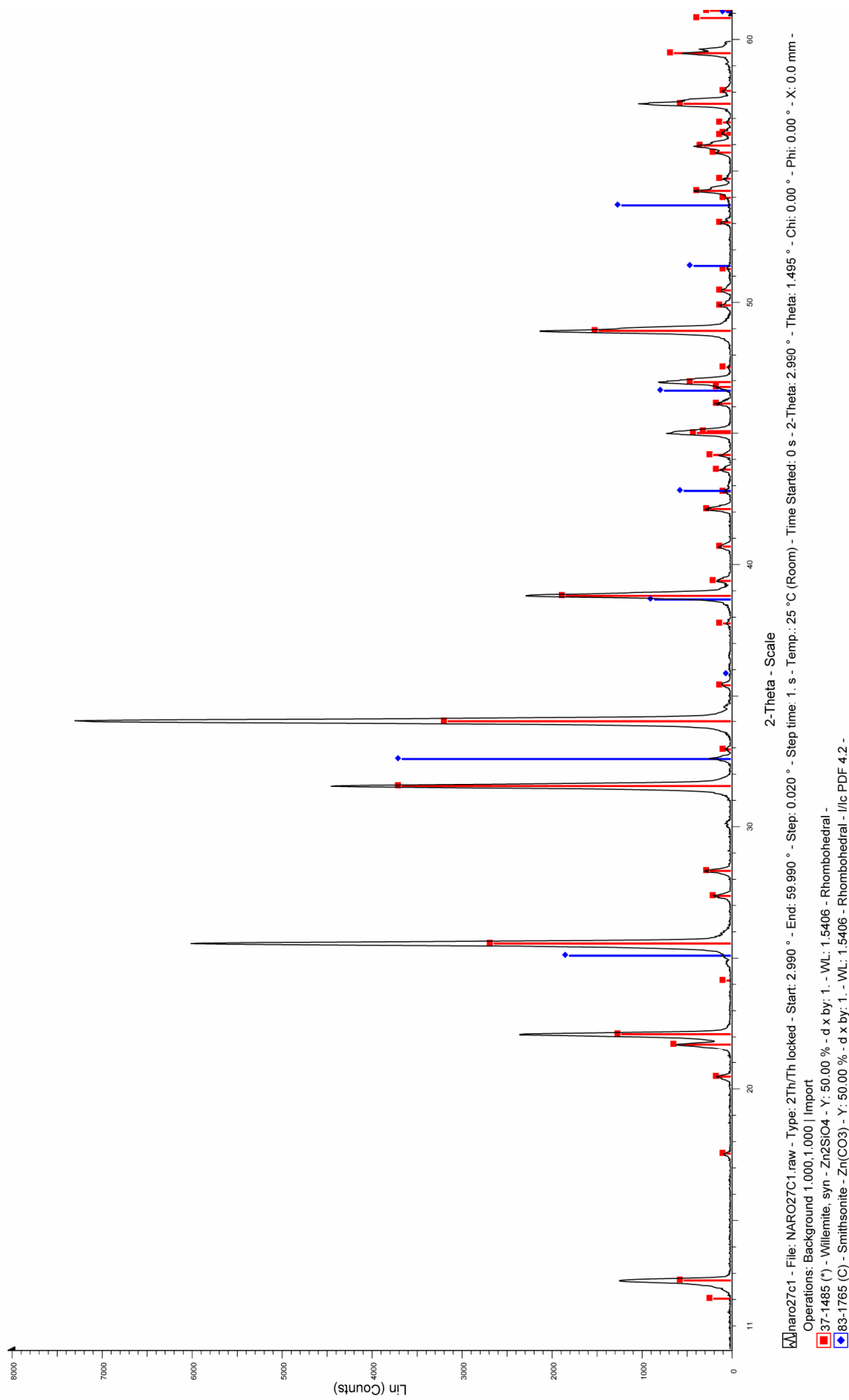


Figure 5.6: Willemite – Smithsonite XRD spectra, sample NARO427C1 from Baltika.

5.6 *Petrography and paragenesis of the willemite ore in the OML*

The zinc nonsulphide ore from the OML accounts for at least three main willemite mineralisation stages. The gangue minerals are mainly carbonates and minor quartz. At least in the Berg Aukas deposit, the late vanadium mineralisation event can be easily distinguished from the main willemite mineralisation stages. A detailed paragenesis will be described for both Berg Aukas and Abenab West mine sites, comprising only the mineralisation stages which occurred after deposition of the main sulphide ores.

5.6.1 *Berg Aukas deposit*

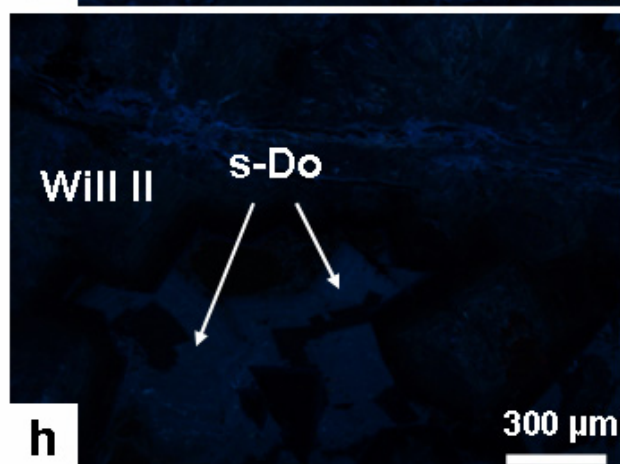
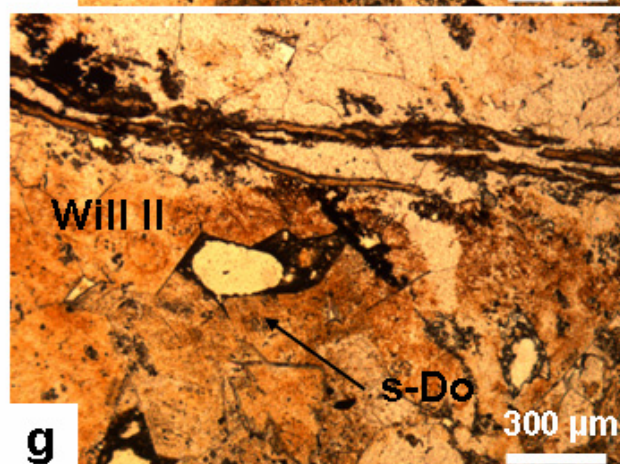
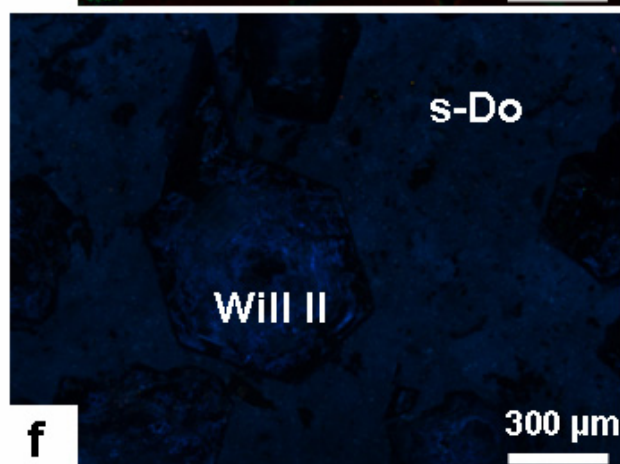
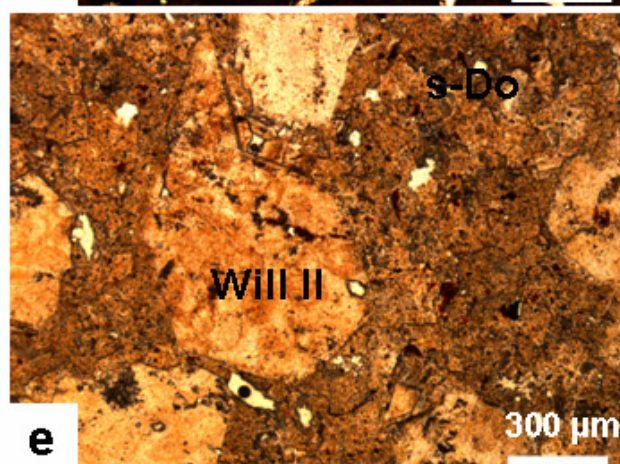
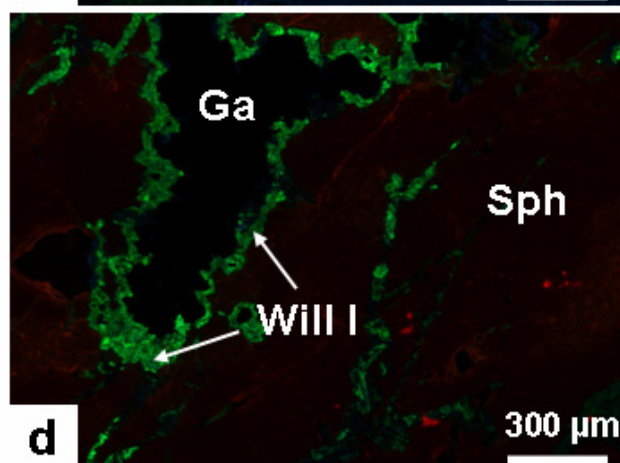
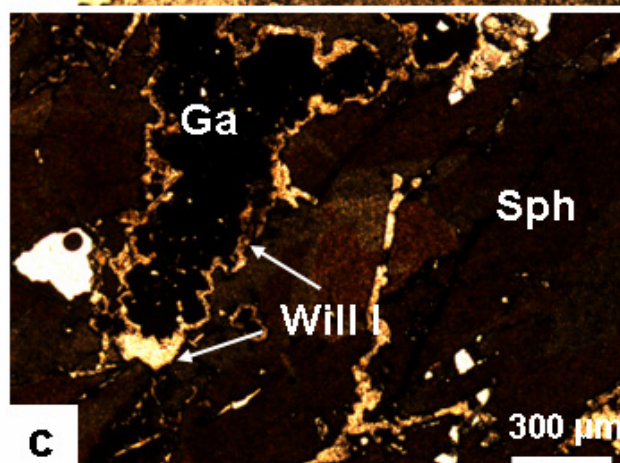
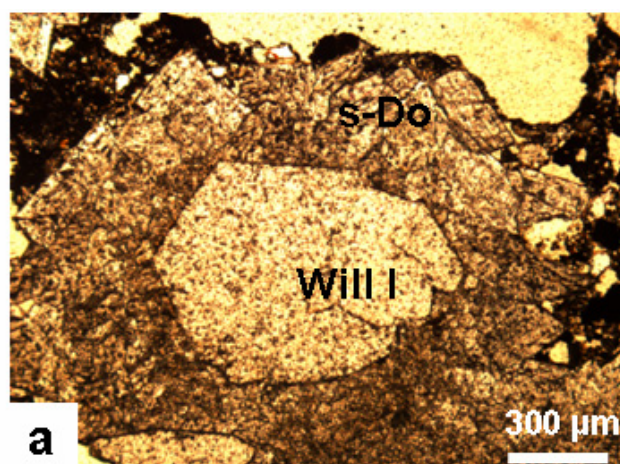
The mineral paragenesis at Berg Aukas is depicted in figure 5.9. Primary sulphides (sphalerite and galena) are at first partially replaced by willemite I generation (figure 5.7c). Willemite I shows a light green luminescence (figure 5.7c), with a dull-bright zonation following the mineral growth and its botryoidal textures (figure 5.7a and 5.7b). The remnants of the willemite I network are usually greenish-blue in CL (figure 5.8b). Secondary galena crystals may precipitate together with the willemite I in small veins (figure 5.13a). A second willemite generation (willemite II) with dull blue CL colour occurs commonly as idiomorphic, not zoned crystals (figure 5.7e and 5.7g); this generation may also be at the rim of willemite I in the veins cutting sphalerite (figure 5.8e and figure 5.8f). Quartz microspheres are disseminated in willemite II.

Willemite II is cut and replaced by smithsonite veinlets and concretions characterized by pinkish CL colours (figure 5.8d and 5.8g). This smithsonite is commonly followed by a willemite III generation in form of tiny needle-like crystals with a bright blue luminescence (figure 5.8b and 5.8d).

In figure 5.8b are depicted the three willemite generations, which follow a clear network pattern while in figure 5.8g micro-collophorm bands of willemite I (green) and II (dull blue) are cut by smithsonite veins. Zn-Pb vanadates (descloizite) overprint the willemite mineralisation and represent the last stage of nonsulphide minerals after the primary sulphide bodies.

At least two major events may be recognized in which vanadium minerals were precipitated: the first

Figure 5.7: Images of willemite ore from Berg Aukas (thin section NII, N+ and CL). a) sub-idiomorphic crystals of willemite I and saddle dolomite (NII); b) same as a in CL; c) willemite I veins replacing sphalerite (brown) and galena (black) (NII); d) same as c in CL; e) idiomorphic crystals of willemite II with microcrystalline saddle dolomite (NII); f) same as e in CL; g) willemite II with light blue zoned saddle dolomite (NII); h) same as g in CL.



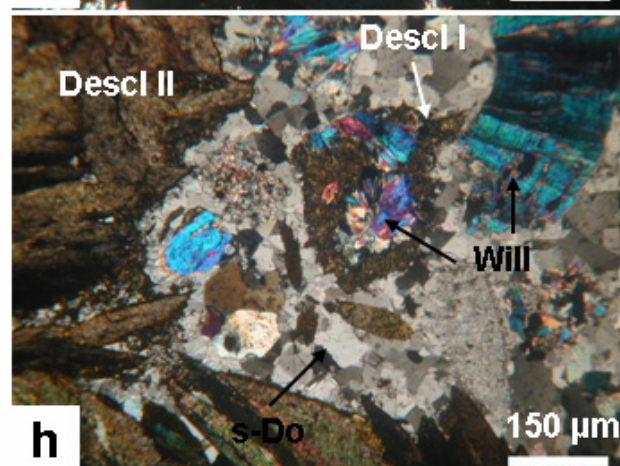
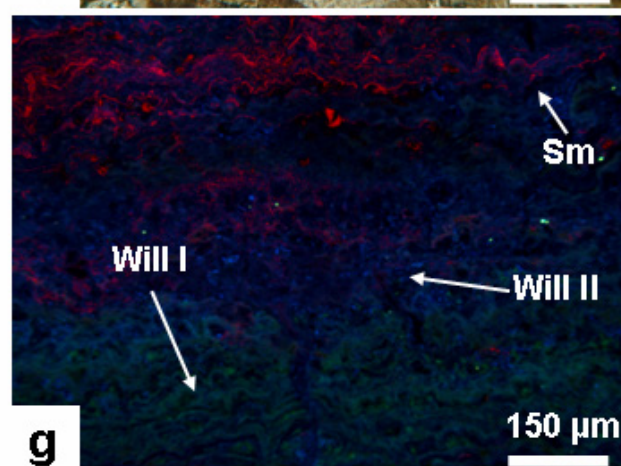
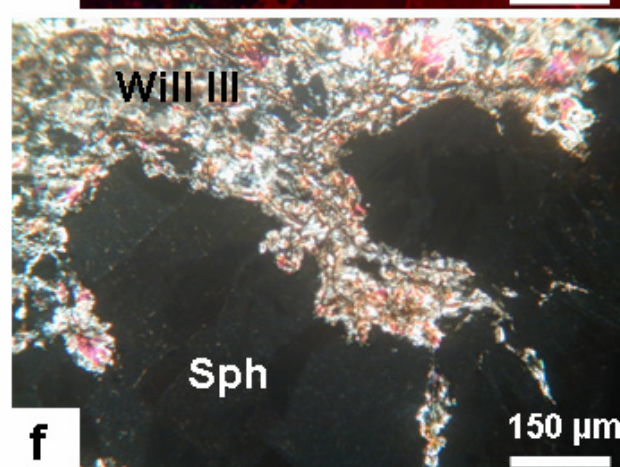
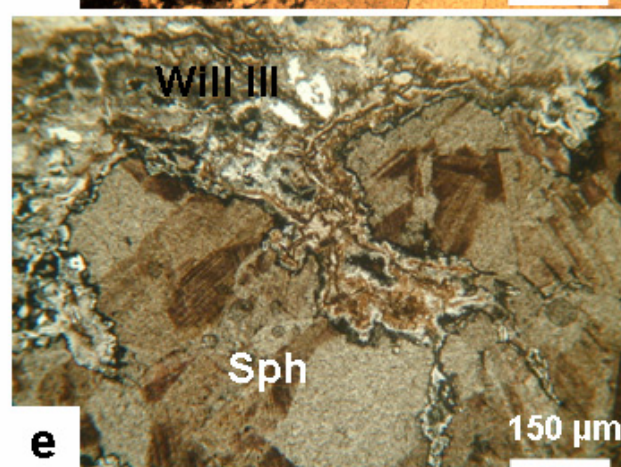
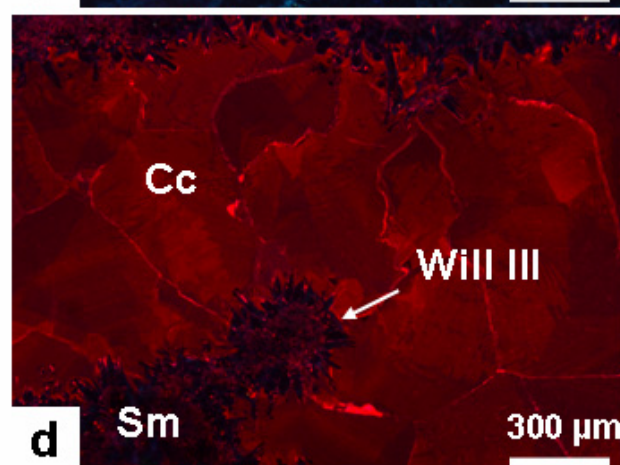
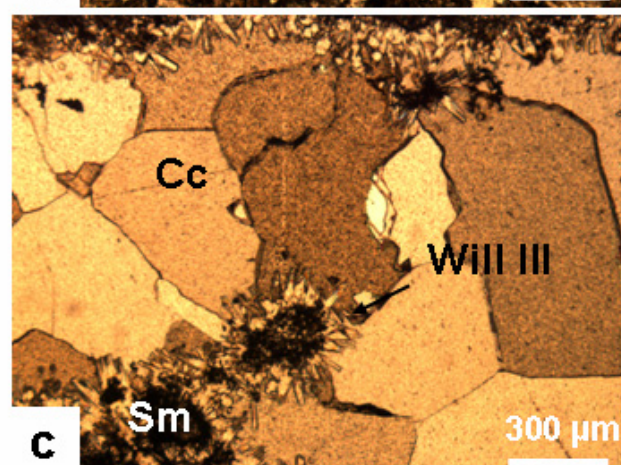
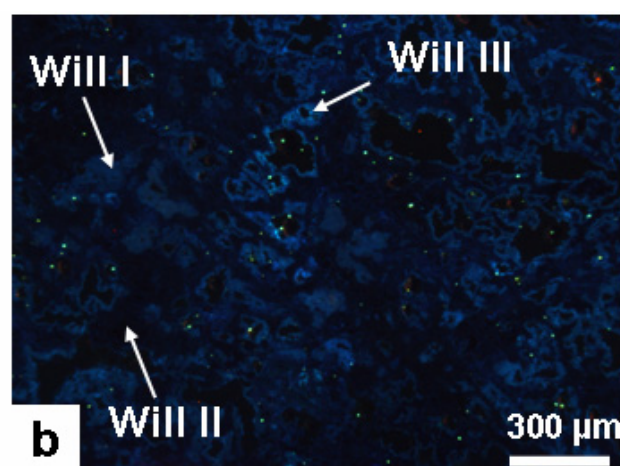
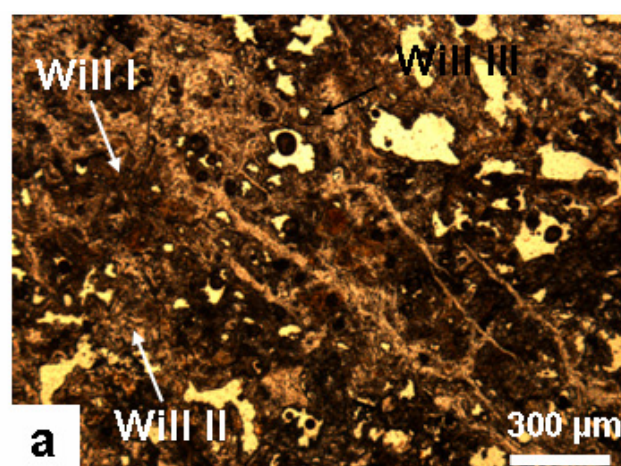


Figure 5.8: Images of willemite ore from Berg Aukas (thin section NII, N+ and CL). a) willemite I, II and III generations in a network of veins (NII); b) same as a in CL: the following generations can be distinguished willemite I (greenish blue), II (dull blue) and III (light blue); c) needle like crystals of willemite III grow on brownish smithsonite centres and are followed by sparry calcite (NII); d) same as c in CL; e) willemite I directly replacing zoned sphalerite (NII); f) same as e in N+; g) collophorm layer of willemite I (green) and II (dull blue), cut by pinkish smithsonite veinlets (CL); h) descloizite I completely rimming willemite ore, postdated by saddle dolomite and descloizite II.

one was responsible for the precipitation of vanadinite and descloizite I (Boni et al. 2007) in the cement of carbonate breccias (figure 5.3d), or at the rim of discrete willemite fragments (figure 5.8h). Zn-Pb bearing saddle dolomite shortly postdates the first vanadates generation. This carbonate contains locally values up to 10-12% of Zn and Pb (figure 5.13a, spot 3). The last phases in the mineralogical assemblage consist of sparry calcite, usually growing as large crystals with Pb bearing layers. This calcite is associated with a last vanadate generation consisting of plume-shaped large descloizite crystals, locally growing in internal karst sediments (figure 5.8h).

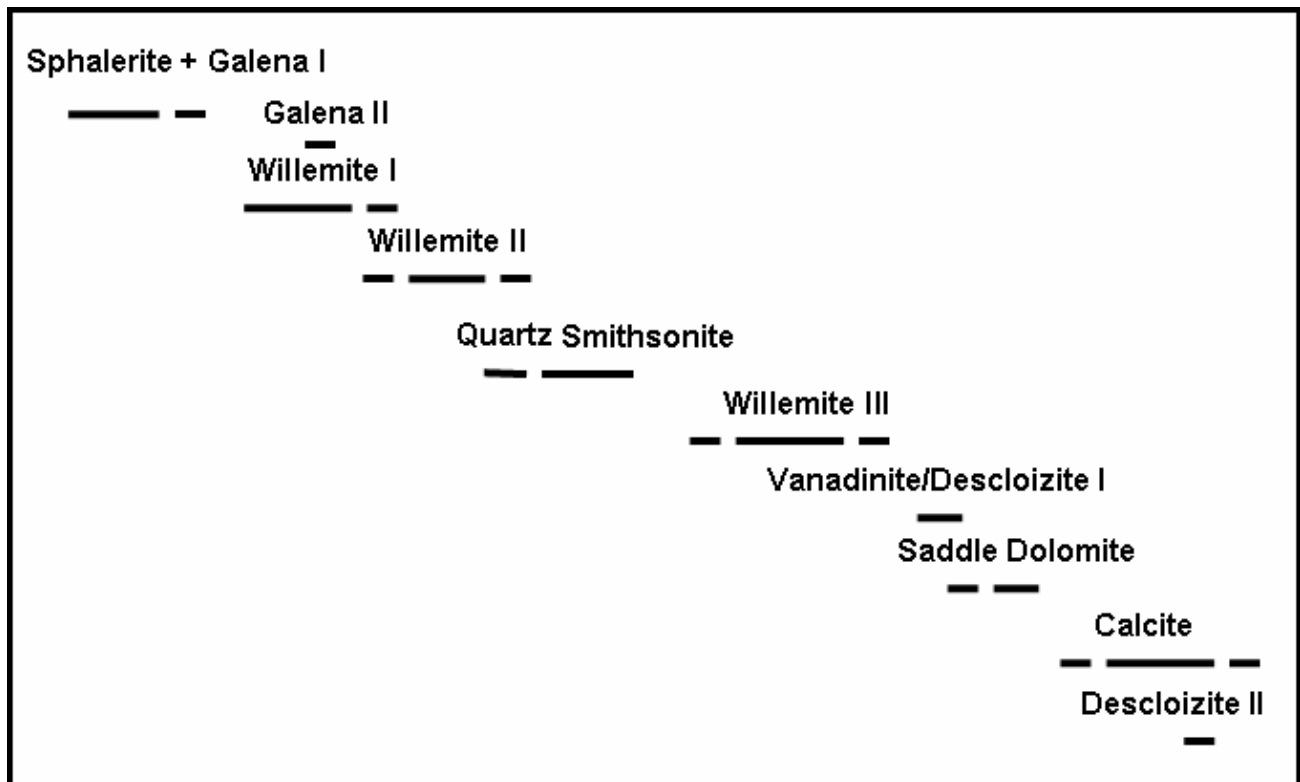


Figure 5.9: Schematic paragenesis of the Berg Aukas deposit.

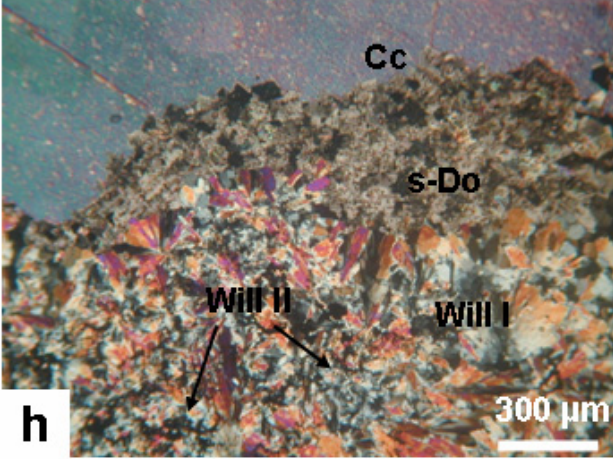
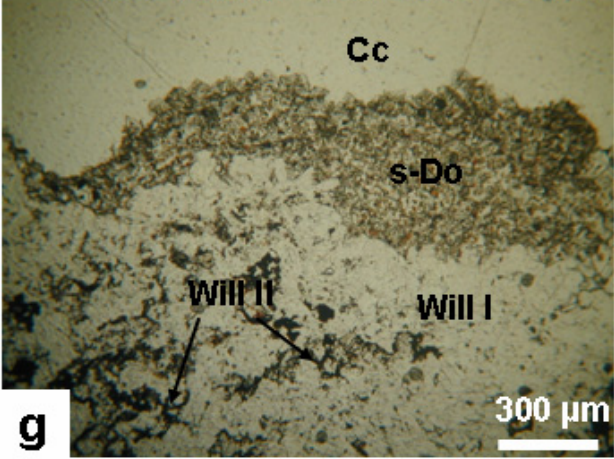
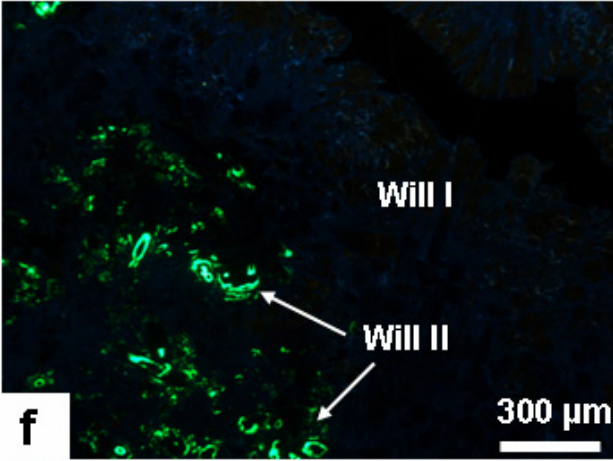
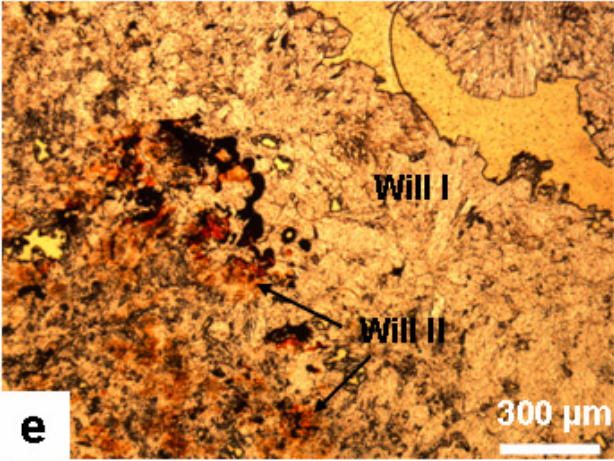
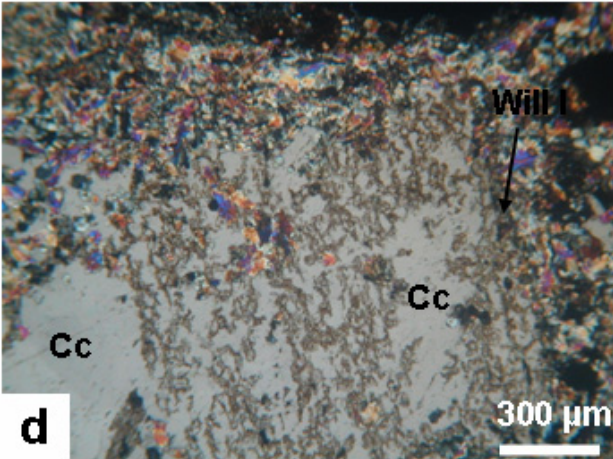
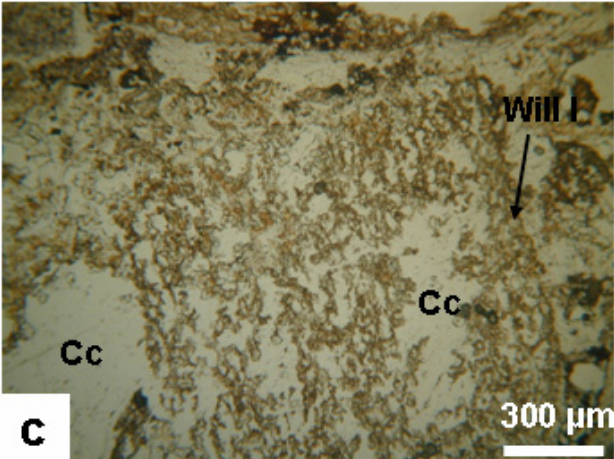
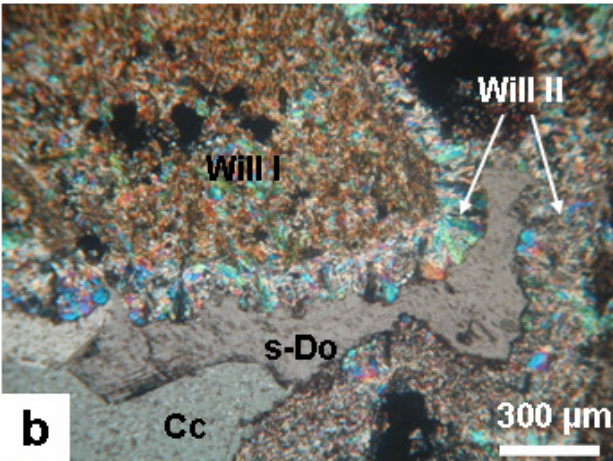
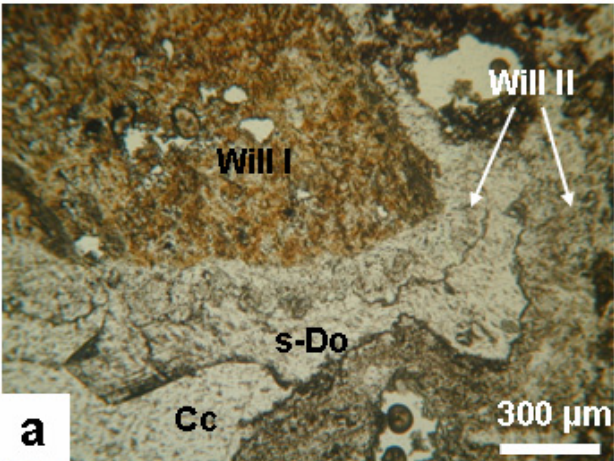
5.6.2 *Abenab West deposit*

At Abenab West the primary sulphides are totally overprinted by massive, red willemite I (figure 5.10a and 5.10c), showing dull blue to bright green cathodoluminescence colours. Willemite I occurs as a replacement network of fine-grained crystals accompanied by newly formed galena or cerussite. A dense dissemination of hematite/goethite microinclusions is responsible for the deep red colour of this willemite phase (figure 5.10e and 5.3e). The fluids precipitating willemite I may have also caused a gradual replacement of the clays in the stylolite seams (from barren clay to sauconite) (figure 5.13b).

Willemite II usually occurs as highly crystalline aggregates rimming (figure 5.10a) or overprinting (figure 5.10g) willemite I. Cm-sized radial crystals show a clear zonation in CL (figure 5.11f), with mainly dull-bright blue colours (figure 5.11g and 5.11h).

Minor vanadates have also been found, spottily disseminated in the willemite ore or as late cavity fillings. As in the Berg Aukas paragenesis, also at Abenab West two main events were produced, in which carbonate minerals occur. Saddle dolomite as discrete crystals (figure 5.11a) was produced in one of these events, while idiomorphic, small dolomite crystals may belong to another one (figure 5.10g); both are postdating willemite II. Even if less commonly than at Berg Aukas, also at Abenab the saddle dolomite contains appreciable amounts of base metals (up to 10 wt% Zn-Pb). The last occurring carbonate phase is sparry calcite (figure 5.3f), growing directly on the massive willemite ore (figure 5.11a), and locally filling the voids (figure 5.10c).

Figure 5.10: Images of willemite ore from Abenab West (thin section NII, N⁺ and CL). a) reddish willemite I, partly replaced and rimmed by willemite II; saddle dolomite and calcite follow (NII); b) same as a in N⁺; c) early network of willemite I replaced by calcite; d) same as c in N⁺; e) reddish willemite I overgrown by white willemite II (NII); f) same as e in CL; g) willemite I reddish dissemination in whitish willemite II followed by idiomorphic dolomite and sparry calcite (NII); h) same as g in N⁺.



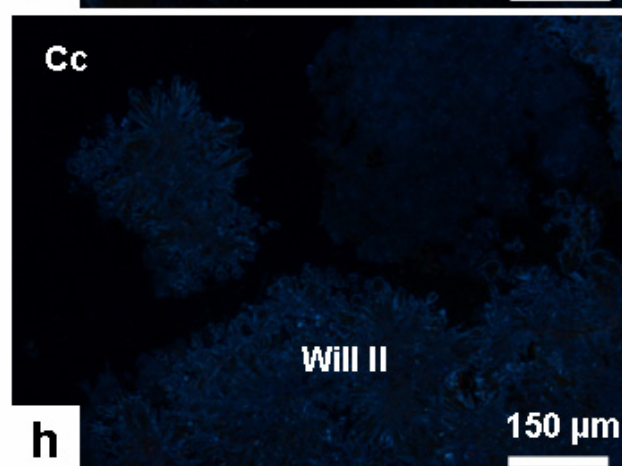
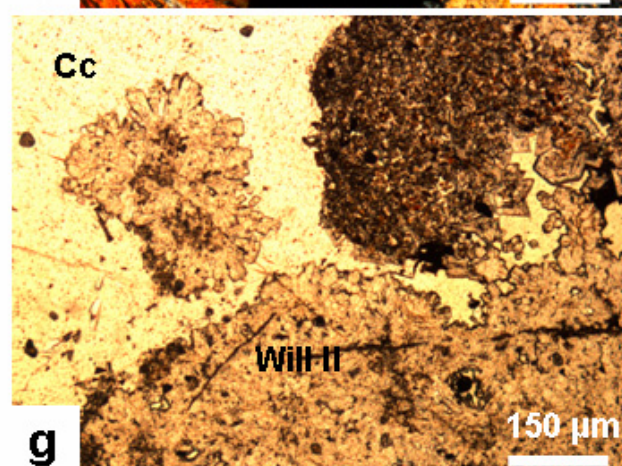
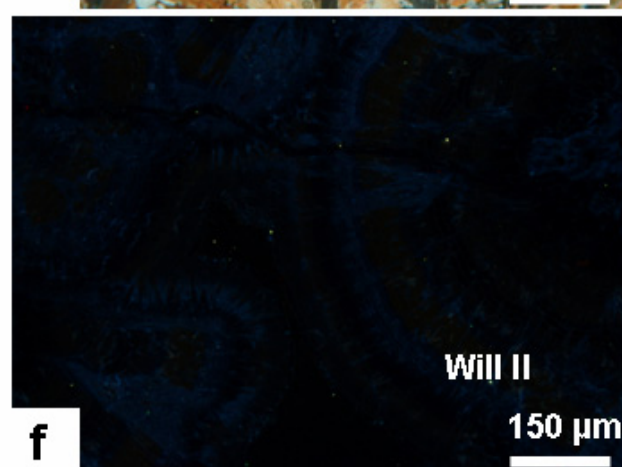
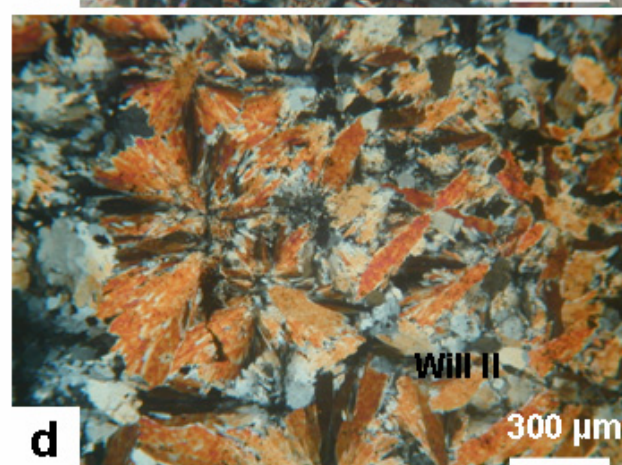
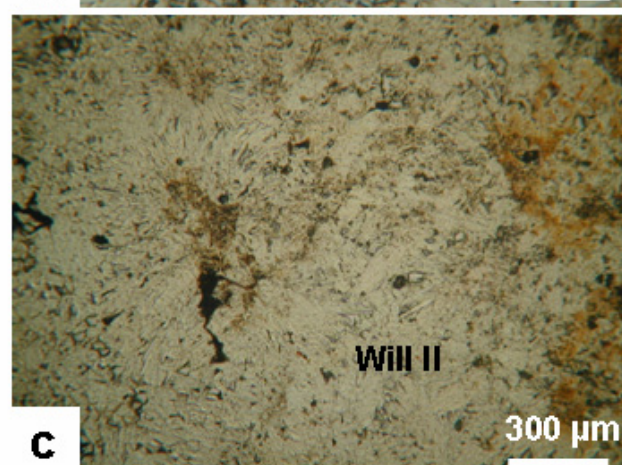
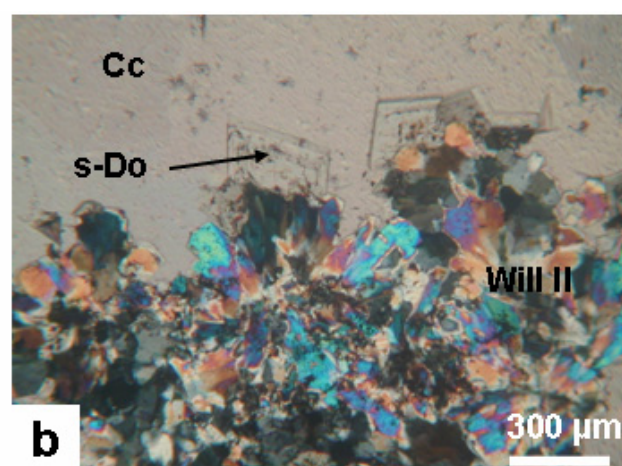
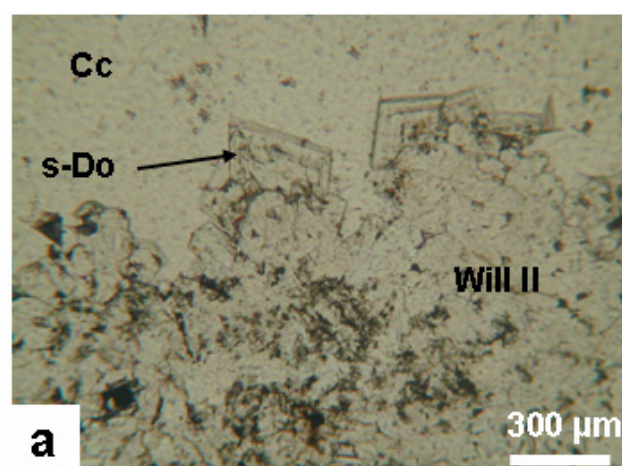


Figure 5.11: Images of willemite ore from Abenab West (thin section NII, N+ and CL) a) idiomorphic dolomite crystals on willemite II (NII); b) same as a in N+; c) massive willemite II (NII); d) same as c in N+; e) radial texture of willemite II (NII); f) same as e in CL; g) rosettes with needle like texture of willemite II (NII); h) same as g in CL.

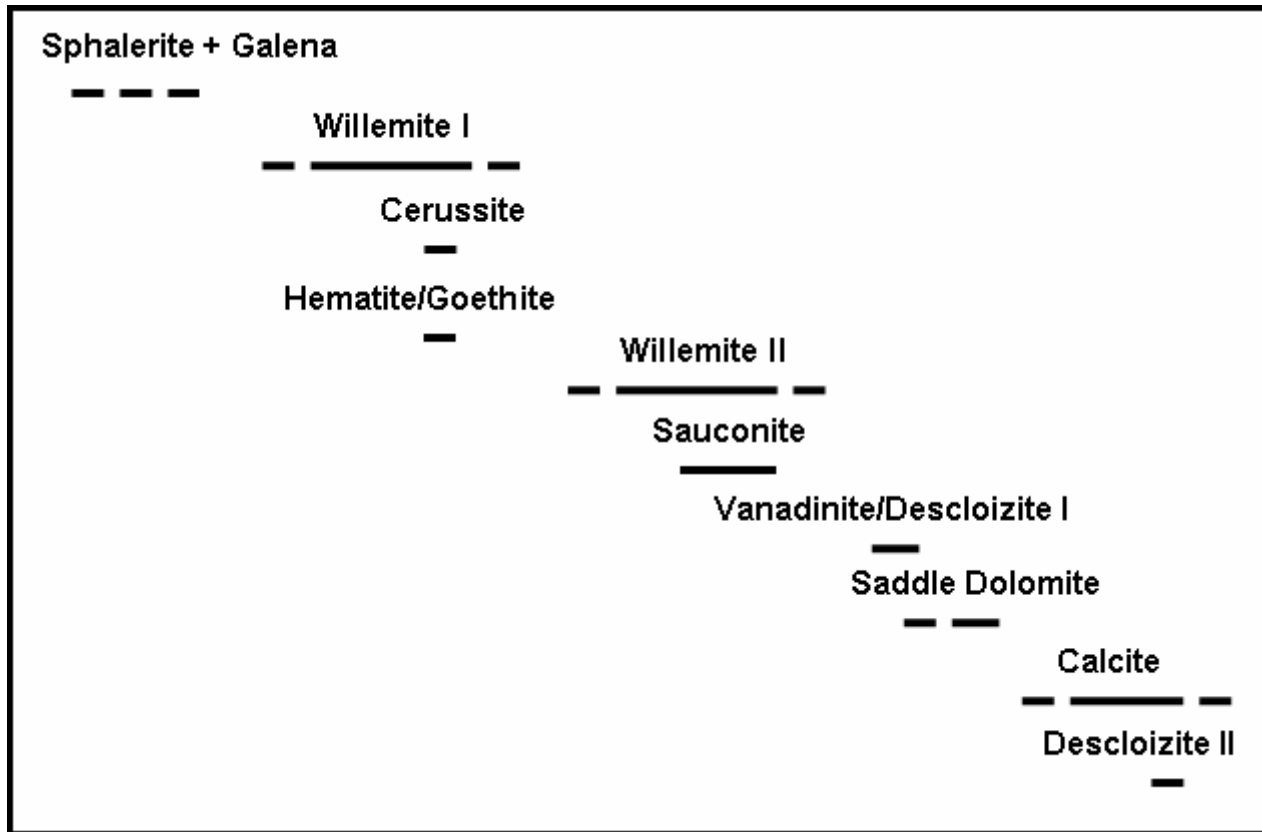


Figure 5.12: Schematic paragenesis of the Abenab West deposit.

5.7 Major and trace elements geochemistry of willemite ores from OML

The willemite ore in the OML is characterized by a variably high Zn grade (>25 wt%). To reach this ore grade, though, a minor contribution of smithsonite should be also considered. The Pb grade (from both primary and neo-formed galena as well as from cerussite) is generally much lower (<5 wt%), thus reflecting a minor Pb content in the primary sulphide ore.

Here below are presented several geochemical analyses of typical OML willemites, performed with the WDS microprobe (table 5.2 and 5.3). Berg Aukas willemites (table 5.2) have ZnO ranging between 68.93% and 73.72%, with a mean value at 72.12%. SiO₂ is less variable between minimum values of 26.15% and maximum of 27.16% (mean 26.79%). FeO can reach a maximum of 2.45%

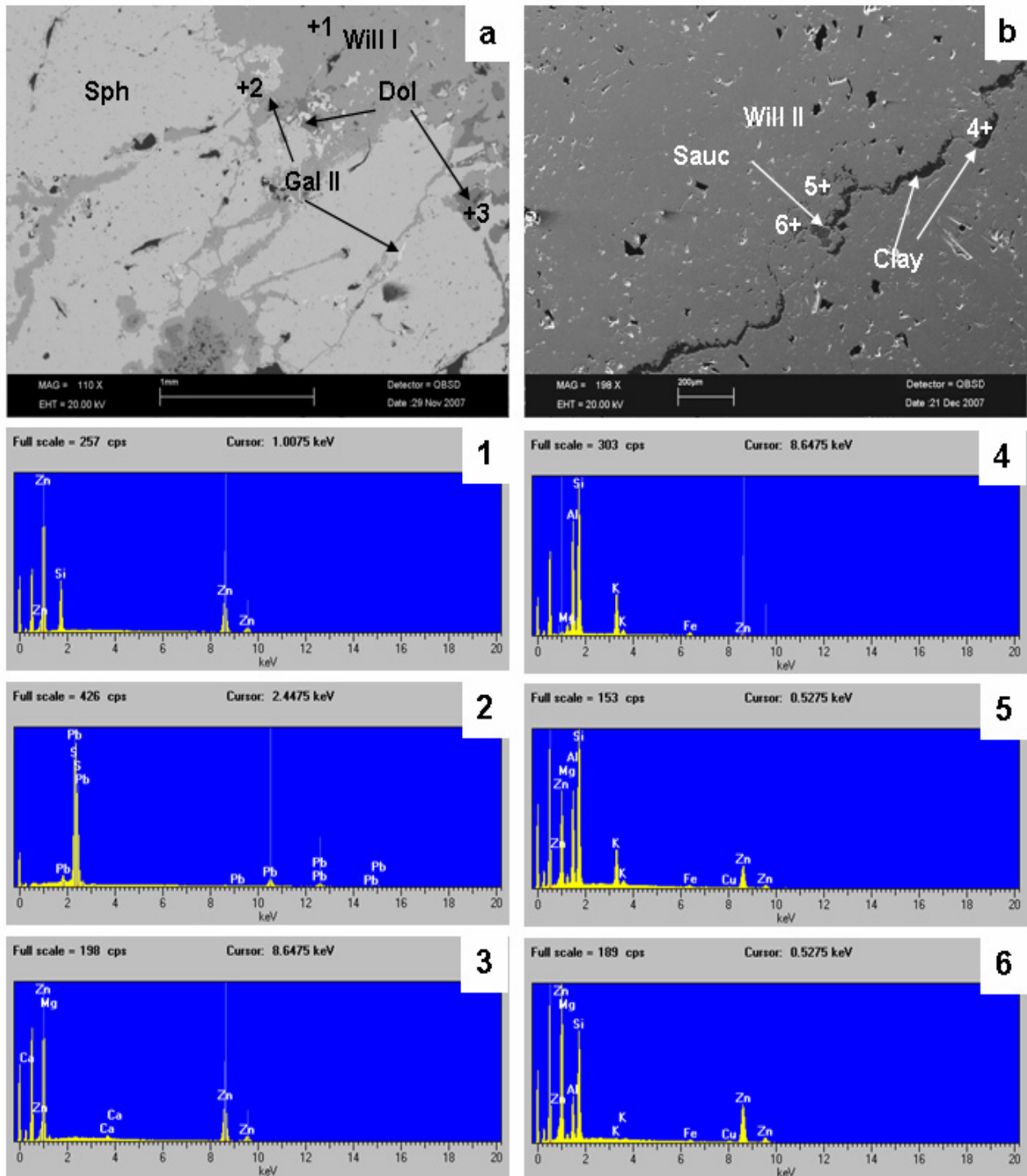


Figure 5.13: BSE images of selected thin sections from OML. a) Berg Aukas, willemite I (spot 1) vein cutting and replacing sphalerite; in the vein also neoformed, idiomorphic galena crystals (spot 2): Late Zn-Pb bearing saddle dolomite (spot 3) is one of the last generations; b) Abenab West, willemite I (grey) replaces the carbonate hostrock; progressive replacement of Zn-Mg over K-Al (spot 4 to 6) in the stylolite (from barren clay to sauconite).

(mean 0.3%, minimum 0.01%). Trace amounts of Cd, Mn and Mg have been also detected. The willemite from the Abenab West deposit (table 5.3) has ZnO values ranging between 70.39% and 72.49%, with a mean set at 71.46%. SiO₂ values vary between 26.19% and a maximum of 29.14% (mean 26.62%). FeO can reach a maximum of 0.5% (mean 0.3%, minimum 0.01%). CdO, MnO and MgO never exceed 0.04% and the mean sum of all analyses is 98.20%. Total stoichiometry has a mean value of 2.996 with Zn = 1.989 apfu, Si = 1.004 apfu and Fe 0.003 apfu as mean values. The structural formula for willemite from Berg Aukas and Abenab West (considering different ore associations) range within a negligible range and are respectively: $[(\text{Zn}^{2+}_{1.92-2.00}\text{Fe}^{2+}_{0.08-0.00}\text{Mn}^{2+}_{0.01-0.00})(\text{Si}_{0.99-1.00})\text{O}_4]$ and $[(\text{Zn}^{2+}_{1.99-2.00}\text{Fe}^{2+}_{0.01-0.00}\text{Mn}^{2+}_{0.01-0.00})(\text{Si}_{0.99-1.00})\text{O}_4]$.

In figures 5.14 and 5.15 are shown the chemical and stoichiometric variations for Berg Aukas and Abenab West, whose results resemble almost perfectly the stoichiometric compositions. Only little covariation can be observed between Zn and Fe (Figure 5.14a). Even if in the current literature on CL, variable Fe and Mn contents are considered to be mainly responsible for the willemite luminescence colours (blue and green, respectively), we could not observe detectable chemical variations among the three willemite types. FeO and MnO amounts are monotonously low and rarely exceeding 0.5% FeO and 0.05% MnO. Instead, the cathodoluminescence colours appear to be related to the strong amount and variety of small mineral disseminations in willemite. Green willemite appears to contain no solid inclusions compared to blue willemite, which is usually disseminated with newly precipitated sulphides and Fe-Mn (hydr)-oxides.

5.8 *Thermometric analysis of fluid inclusions*

A fluid inclusion study was carried out on the OML willemites, in order to obtain direct information on temperature and salinity of the precipitating fluid. Different inclusion groups have been determined in a preliminary petrographic study. At both Berg Aukas and Abenab West sites, willemite occurs in several generations, with associated saddle dolomite and sparry calcite (cfr § 5.6.1 and § 5.6.2). cursory attention has been dedicated to the inclusions assemblage of the carbonate minerals, deposited in later stages of the paragenesis.

Only in the last willemite generations (willemite III at Berg Aukas and willemite II at Abenab West) discernable fluid inclusions occur. The early generations show just primary monophase inclusions (willemite I at Berg Aukas, figure 5.7a), or are too pervasively disseminated by semi-transparent or opaque mineral (willemite I at Abenab West, figure 5.10a), to allow any optical observation at the microscopic scale.

Willemite III at Berg Aukas occurs as tiny needle-like and solid inclusion-free crystals (figure 5.16a) as well as willemite II at Abenab West (figure 5.16b). Secondary two-phase inclusions (L+V) are

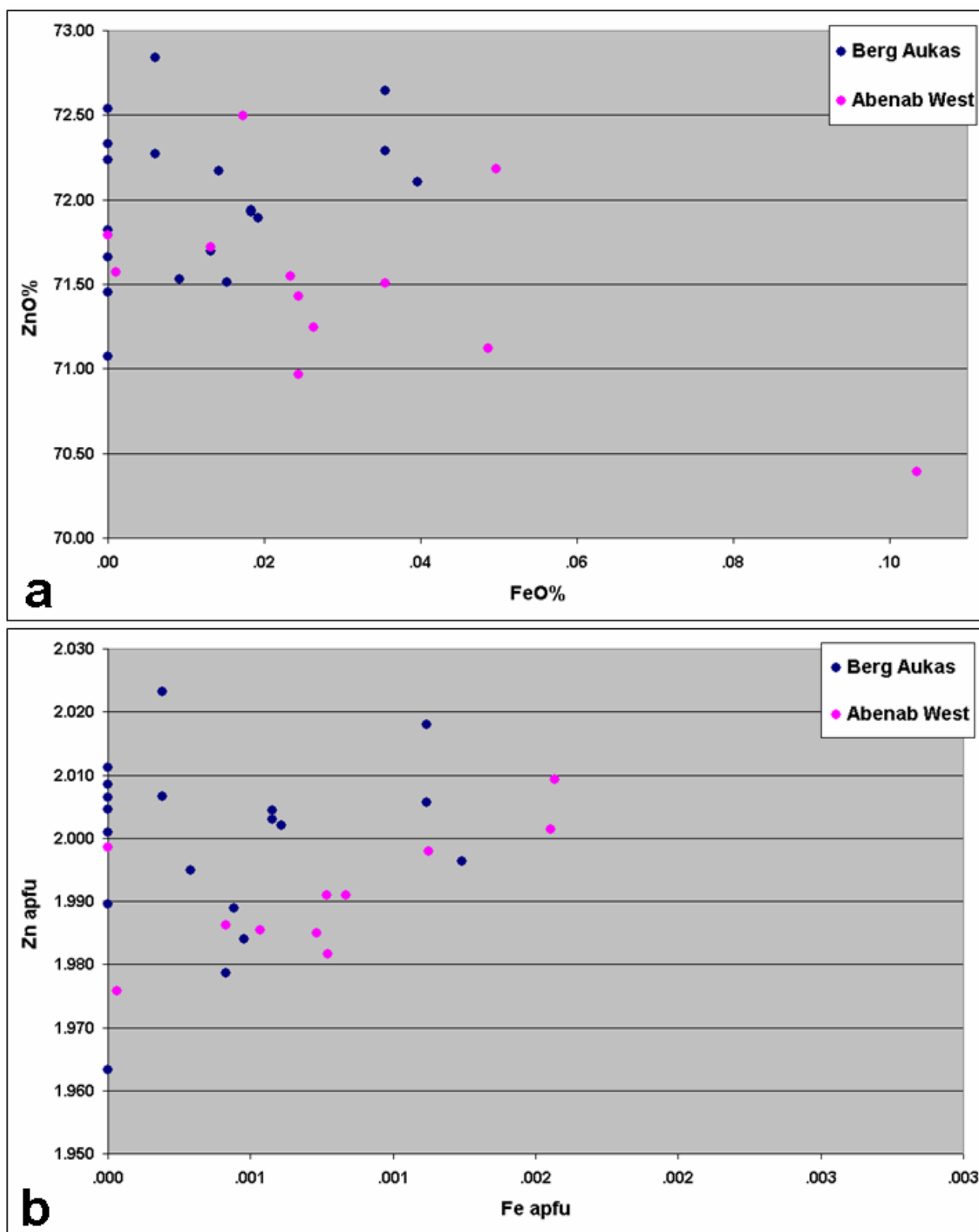


Figure 5.14: OML willemite Fe/Zn chemical and stoichiometric ratios from WDS analyses. a) FeO%/ZnO% ratio, mean ZnO = 72.00% (ideal ZnO% = 73.04%), mean FeO = 0.2%; b) Fe/Zn ratio by stoichiometry, mean Zn = 1.99 apfu (ideal Zn apfu = 2), mean Fe = 0.01 apfu (Zn + Fe = 2 apfu).

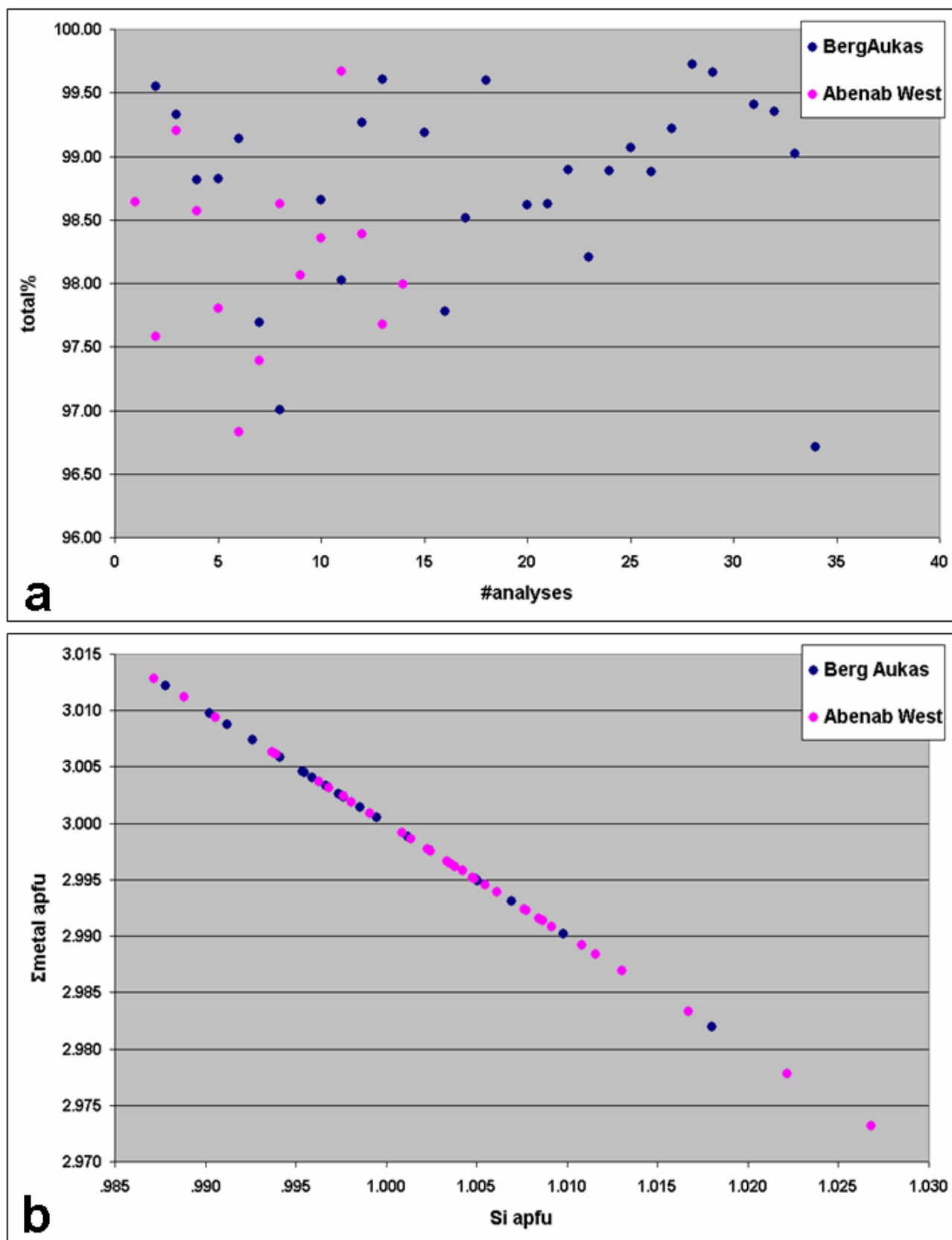


Figure 5.15: OML willemite total chemical/stoichiometric ratios from WDS analyses. a) N of analyses over total %, mean total = 98.50; b) Si/ Σ metal apfu (ideal Si = 1 apfu, Σ metal = 3 apfu).

Table 5.2: WDS analyses (% oxide) of willemite from Berg Aukas (sample BA200317).

	BA17-1	BA17-2	BA17-3	BA17-4	BA17-5	BA17-6	BA17-7	BA17-8	BA17-9	BA17-10	BA17-11	BA17-12
CdO			0.01		0.02	0.01	0.02	0.01	0.02	0.02	0.02	
MnO	0.01	0.02		0.01	0.03	0.06	0.01	0.04			0.01	
FeO	0.77	0.37	0.17	0.43	0.10	0.07	2.45	0.06	0.36	0.05	0.02	0.13
ZnO	72.26	72.02	72.46	71.27	71.68	72.04	68.93	69.88	70.93	71.91	71.04	72.72
MgO	0.02	0.03		0.01	0.02	0.01						0.02
SiO₂	27.09	27.10	26.69	27.08	26.98	26.95	26.28	27.01	26.75	26.69	26.94	26.41
Total	100.14	99.55	99.33	98.81	98.82	99.14	97.69	97.00	98.06	98.66	98.02	99.26

	BA17-13	BA17-14	BA17-15	BA17-16	BA17-17	BA17-18	BA17-19	BA17-20	BA17-21	BA17-22	BA17-23	BA17-24
CdO	0.02	0.01	0.02			0.01		0.01		0.02		0.03
MnO	0.01	0.03	0.04	0.03	0.03	0.01	0.03					
FeO	0.01	0.02	0.06	0.12	0.21	0.03	0.02	0.07	0.03	0.03	0.07	
ZnO	72.84	73.02	72.78	70.56	72.10	72.58	73.72	71.75	71.67	72.02	71.28	71.90
MgO		0.01	0.03	0.04	0.02	0.01				0.02	0.01	0.01
SiO₂	26.73	27.11	26.25	27.03	26.15	26.95	26.91	26.78	26.93	26.81	26.84	26.96
Total	99.60	100.19	99.18	97.78	98.51	99.59	100.68	98.62	98.62	98.89	98.21	98.89

	BA17-25	BA17-26	BA17-27	BA17-28	BA17-29	BA17-30	BA17-31	BA17-32	BA17-33	BA17-34	Mean
CdO	0.03	0.01		0.02	0.02					0.02	0.02
MnO	0.01	0.02	0.04	0.02		0.01	0.03			0.02	0.02
FeO	0.03	0.05	0.12	0.07	0.02		0.03	0.03	0.23	0.06	0.41
ZnO	71.83	71.98	72.55	72.67	72.56	73.32	72.38	72.40	72.15	69.50	71.43
MgO		0.01		0.01							0.02
SiO₂	27.16	26.81	26.51	26.92	27.06	27.02	26.97	26.92	26.63	27.11	26.83
Total	99.07	98.88	99.22	99.72	99.66	100.34	99.41	99.35	99.02	96.71	98.71

Table 5.3: WDS analyses (% oxide) of willemite from Abenab West (sample AW20031).

	AW1-1	AW1-2	AW1-3	AW1-4	AW1-5	AW1-6	AW1-7	AW1-8	AW1-9	AW1-10	AW1-11	AW1-12	AW1-13	AW1-14	Mean
CdO		0.02	0.04			0.01	0.02	0.01			0.01		0.02	0.01	0.02
MnO			0.04					0.01	0.02	0.03		0.03			0.02
FeO		0.50	0.41	0.01	0.03	0.10	0.05	0.05	0.02		0.02	0.02	0.02	0.04	0.11
ZnO	71.57	70.51	72.04	71.72	71.24	70.39	71.12	72.18	71.43	71.79	72.49	71.55	70.97	71.51	71.46
MgO			0.02			0.02									0.02
SiO₂	27.07	26.56	26.66	26.84	26.53	26.30	26.19	26.37	26.59	26.53	27.14	26.79	26.67	26.43	26.62
Total	98.64	97.58	99.20	98.57	97.80	96.83	97.39	98.63	98.06	98.35	99.67	98.39	97.68	97.99	98.20

dominant in both cases (with length commonly exceeding 25 μm), usually aligned along the axis of the crystal (figure 5.16c). Frequent leakage and willemite fracturing prevent to obtain substantial thermometric data. Primary inclusions are very small, ranging between 5 and 10 μm and are generally monophase (liquid-rich). A bubble was obtained from these inclusions through freezing-heating cycle only seldom.

In the saddle dolomite crystals the fluid inclusions are very abundant (figure 5.16d). They are randomly distributed throughout the crystal, arranged along fractures or (mainly) along the dolomite crystalline planes. Only monophase (L) primary inclusions were observed in saddle dolomite and (rare) two phase (L+V) or monophase (L) secondary inclusions. Primary inclusions in saddle

dolomite have sizes rarely exceeding 15 μm , while length of secondary inclusions varies between 10 and 35 μm . Only monophasic (liquid) fluid inclusions were detected in sparry calcite, whose sizes range between 20 and 40 μm . These are predominantly secondary inclusions and after freezing-heating runs did not generate any bubble.

As mentioned above, the brittle nature of willemite and its perfect cleavage represent two major problems hampering a systematic fluid inclusion study. No reliable data were obtained from primary inclusions while secondary two-phase inclusions (80% of the total) display T_h varying between 50 and 80° C and T_m definitely close to 0° C. Widespread necking-down and stretching are very common, as well as leakage phenomena.

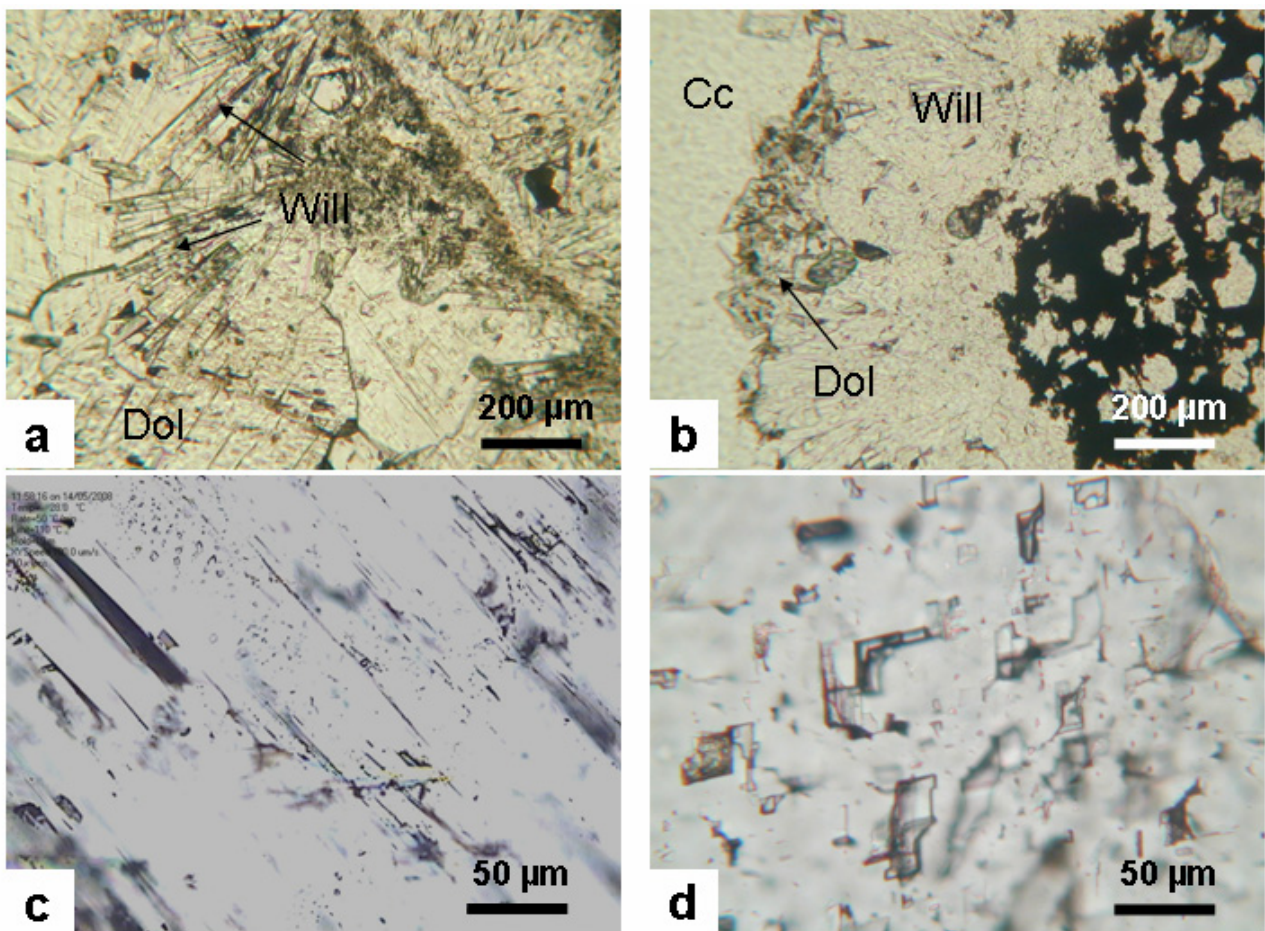


Figure 5.16: Fluid inclusion petrography in willemite ore from OML. a) needle-like willemite III and saddle dolomite (Berg Aukas); b) willemite II and sparry calcite (Abenab West); c) elongated two phase (L+V) secondary fluid inclusions along cleavage plains and primary monophasic (V-dominated) inclusions cloudiness in willemite III from Berg Aukas; d) secondary two phase (L+V) stretched inclusions in saddle dolomite from Berg Aukas.

According to Grooves et al. (2003), the occurrence of primary monophasic fluid inclusions in willemite points to very low formation temperatures ($< 50^{\circ}\text{C}$), in agreement with a possible supergene (or low-T hydrothermal) origin of these late willemite generations, saddle dolomite and calcite.

6 Willemite mineralisation in Central Zambia

6.1 *Introduction and mining history*

After the discovery of the Zn-Pb deposits at Kabwe in 1902, and the opening of the formerly called Broken Hill mine in 1904, an intensive regional exploration took place, which led to the discovery of many other Zn-Pb mineralisations such as Chiwanda, Kabwe West, Carmanor, Lukali and Millberg (Carney and Kerr, 1998). Closer to the mine additional mineralisation was discovered at Airfield (1920), Foundry and Kashitu (1959) prospects (Carney and Kerr, 1998). Up to 1994, about 12.3 Mt @ 25.2% Zn and 10.7% Pb were produced in the Kabwe mine area. More recently (1996), the smelter at Kabwe was re-commissioned to smelt copper industry slags and the old mine dumps, but ceased operating in 1998 (Carney and Kerr, 1998). At Kashitu and Airfield prospects, resources of 2Mt @ 1.2% Zn and 0.1% Pb and 4.56Mt @ 2.5% Zn and 1.4% Pb respectively have been estimated (Hitzman, 1999).

The Star Zinc deposit, in the Lusaka area, was discovered in the early twenties and since then subjected to sporadic exploration (Matthews, 2005). The quoted resources at Star Zinc are the Eastern orebody consisting of 73,000 t @ 16.5% Zn and the Western orebody with 118,200 t @ 21.58% Zn (Matthews, 2005).

6.2 *The Kabwe-area willemite deposits (Lufilian Arc)*

6.2.1 *Kabwe Mine*

The primary Zn-Pb sulphide deposit of Kabwe (figure 6.1) consists of epigenetic sulphides replacing the host Kabwe Dolomite (cfr §4.2.1) in form of irregular bodies (Kamona et al., 2007). The lead-zinc orebodies occur as a series of pipe-like or vein-like bodies cutting the pale grey massive dolomite (Kortman, 1992). They strike east-north-east to west-south-west (approximately at right angles to the strike of the dolomite), dip steeply to the north-north-west at about 80° and plunge to the east-north-east at angles ranging between 30° and nearly vertical (Carney and Kerr, 1994). There are six main orebodies, known as No. 1, 2, 3/4, 5/6, 8 and X (Mulchany, 1996).

The No. 1 orebody was firstly discovered because it originally outcropped as a 15 m high hill (Carney and Kerr, 1996). It is an elongated body striking mainly E-W (Hitzman, 1999). Originally, the Nos. 3/4 and 5/6 ore concentrations were thought to be four separate bodies, but were later found to join in pairs at depth. Nos. 8 and X do not outcrop, but the other bodies originally stood up as small hills up to 25m above the plain (Carney and Kerr, 1998). The 5/6 orebody is the largest, being 800 m in length along the direction of plunge. All the orebodies, except no 2 and 8, have a core of massive sulphides surrounded by an oxidised zone 5 to 10 m wide, which

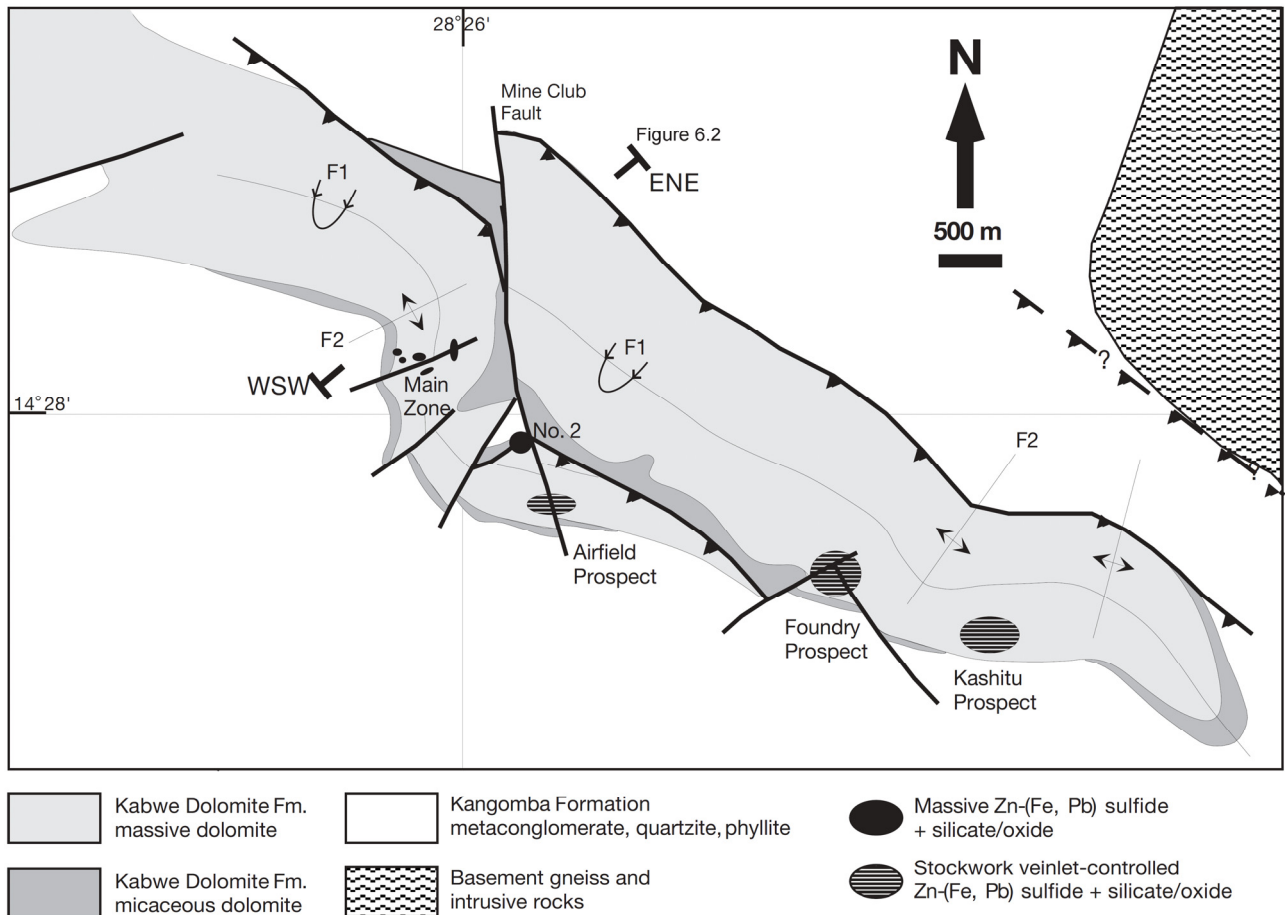


Figure 6.1: Geology and main ore deposits/prospects of the Kabwe area (modified from Hitzman, 2003).

persists to the base of the body (Carney and Kerr, 1998). No. 2 orebody lies about 1 km to the southeast of the others, at the contact between the massive dolomite and the pelitic rocks of the Kangomba Fm (cfr figure 4.9). The contact is along the N-S Club Mine Fault (cfr figure 6.1). This body consists almost entirely of oxidised ore. The sulphide cores of the orebodies consist of sphalerite, galena and pyrite, with minor amounts of chalcopyrite, bornite, tetrahedrite and chalcocite, mainly occurring as minute exsolution laths in sphalerite (Kamona et al., 2007). Sphalerite is predominant over the other ore minerals; gangue minerals are present in very small amounts as minute grains of quartz and dolomite (Carney and Kerr, 1998). Trace elements include iron, manganese and cadmium in sphalerite, and silver and selenium in galena (Kamona et al., 2007). The oxidised ore is fine-grained and mainly red brown due to the iron content. It is commonly banded and ranging from massive to cavernous (Carney and Kerr, 1998).

The main nonsulphide minerals are willemite, smithsonite and cerussite; other minerals include

anglesite, pyromorphite, vanadinite, descloizite, mottramite, quartz, hematite, goethite and limonite (Kamona et al., 2007). Native copper, hopeite, parahopeite and tarbuttite also occur sporadically (Carney and Kerr, 1998). The vanadium content in both sulphide ore and host dolomite is less than 0.01 per cent, whereas that of the outer shell of the oxide zone is 1.87 to 2.43 per cent (Taylor, 1953). It is improbable, therefore, that the sulphides were the source of the vanadium in the oxide zone; it is more likely that the vanadium (as in the OML) was derived from the weathering of the argillaceous sediments, some of which have a vanadium content in excess of 0.02 per cent (Carney and Kerr, 1998). The phosphates occurring in the rare, hydrated zinc phosphate minerals (hopeite, parahopeite and tarbuttite), formerly of common occurrence in the upper levels of the mine, may have been derived from the bones and other organic remains found in karstic cavities (Carney and Kerr, 1998, Avery et al., 2002).

Locally, in the outer parts of the oxidised zone, a brown, hard, jasper-like material, consisting of quartz and limonite with fragments of oxidised ore, was recognised and reported as “lithified mud” (Carney and Kerr, 1998). Rhythmic, varve-like variations of the grain size suggest that the mud was deposited as a late fill of the cavities at the margins of the orebodies (Kortman, 1992).

According to Kamona et al. (2007) (cfr §4.2.3), observed deformation textures of the sulphide ore indicate that ore emplacement occurred prior to the latest deformation phase of the Neoproterozoic Lufilian orogeny. The only age estimate for the Kabwe mineralisation so far is the galena model isotopic age of 680 ± 13 Ma (Kamona et al., 1999). Fluid transport may have been caused by tectonic movements associated with the early stages of the Pan-African Lufilian orogeny, whereas ore deposition within favourable structures should have occurred due to changes in pressure, temperature and pH in the ore solution, during metasomatic replacement of the host dolomite (Kamona et al., 2007).

6.2.1.1 No. 2 Orebody

This No. 2 is a pipe-like body (figure 6.2) located 1 km southeast of the main group of the sulphide orebodies, its former outcrop rising 30 m above the surrounding ground level. (Carney and Kerr, 1996). At the 1050 ft. level, No. 2 orebody splits into two bodies, which merge again at the 1250 ft. level. The hangingwall of the eastern end of the orebody is along an east-west-trending shale/dolomite contact, but most of the mineralisation is hosted by massive dolomite (Hitzman, 1999). Its thickness ranges from 2 to 23 m, averaging 10 m, with a maximum strike length of 260 m on the 1050 ft. level (Carney and Kerr, 1996). The No. 2 orebody has a different geometry from the orebodies of the Main Ore Zone in that it is largely parallel to the foliation/bedding direction of the massive dolomite, rather than forming a discordant pipe or vein (Hitzman, 1999).

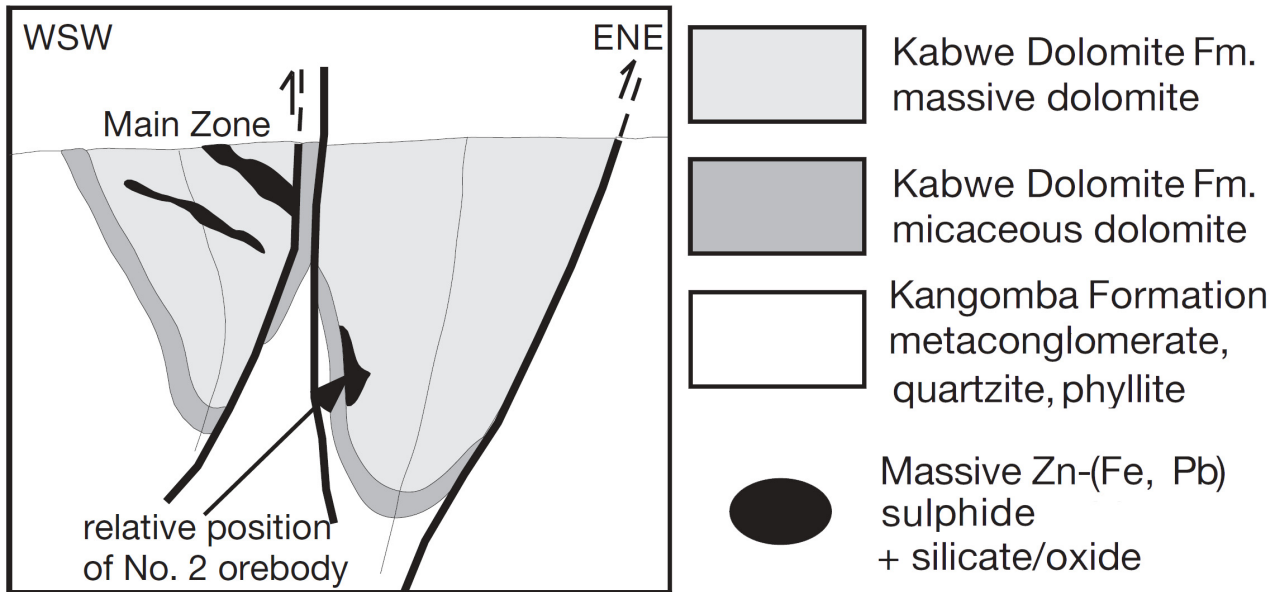


Figure 6.2: WSW-ENE (cfr figure 6.1) vertical section through the No. 2 orebody (modified after Hitzman et al., 2003).

6.2.1.2 No. 5/6 Orebody

The No. 5/6 orebody (figure 6.3), which is the largest in the district, occurs approximately 150 m north of the No. 3/4 orebody (Hitzman, 1999). The No. 5/6 orebody displays a pipe-like shape with vertical dips and plunging at 029° NE to the 1050 ft level (Carney and Kerr, 1996). The body ranges from 16 to 47 m in thickness and has an average strike length of 149 m with a maximum of 245 m on the 950 ft. level; its total plunge length is 670 m (Hitzman, 1999).

6.2.2 Airfield Prospect

The Airfield prospect is located approximately 1 km south of the No. 2 orebody (figure 6.1). Mineralisation occurs within carbonaceous dolomite, which stratigraphically (or even structurally) underlies the massive dolomite hosting the Kabwe orebodies (Hitzman, 1999). The Airfield mineralisation is bisected by the southward extension of the NNW-trending Mine Club Fault. It is bound to the north by a bedding-parallel shear zone (figure 6.1).

The Airfield area contains a large volume of rock (480 m x 80 m and is at least 50 m depth) with disseminated and veinlet- (NE-trending and steeply dipping) controlled sulphide mineralisation (Hitzman, 1999). The width of the veinlets vary from few mm up to 0.5 m (Mulcahy, 1996).



Figure 6.3: SW-NE Vertical section through the No. 5/6 (and No. 2 H/W) orebodies. Cfr figure 6.1 for legend (modified after Hitzman et al., 2003).

Minor narrow, discontinuous, NW-trending, steeply dipping veinlets containing zinc silicate/oxide material are also present (Hitzman, 1999). This volume of rock has been estimated to contain 4.56 million tonnes at 2.5% Zn and 1.4% Pb (Hitzman, 1999). The veins, veinlets and vugs are filled with sphalerite, willemite, and galena, silica and minor pyrite and chalcopyrite (Carney and Kerr, 1996). Four small zones of near-surface zinc silicate/oxide material (referred as *willemite blanket*) occur in the Airfield area above the zone of veinlet-controlled mineralisation; these zones form a 1-3 m thick blanket at the base of the “B” lateritic soil horizon above an irregular karstic dolomite bedrock surface (Haldane, 1989). These zones are estimated to contain a total of 64,000 tonnes of Zn at 15.9% and Pb at 5.6% (Hitzman, 1999).

6.2.3 Kashitu Prospect

The prospect, lying near the south-eastern limit of the Kabwe synform, is contained in massive to mildly arenaceous dolomites, which are interpreted to be the base of the Kabwe dolomite; it was discovered during a reconnaissance soil survey (Hitzman, 1999). The overall trend of the

mineralisation appears to be ENE with a less prominent WNW trend (Carney and Kerr, 1996). Although a tonnage and grade figure was not made available, the inspection of the drill sections suggest that the area contains in excess of 2 million tonnes, grading approximately 1.2% Zn and 0.1% Pb (Hitzman, 1999). In 1969/1970 ca 40 isolated pods of >0.5% Zn consisting primarily of willemite, were discovered at Kashitu. One of these willemite bodies was found at approximately 30 m by 2 to 3 m in extent at the surface and was later mined and yielded 300 tonnes of 50% Zn, primary from willemite (Hitzman, 1999). According to Hitzman (1999) the sulphides occur as disseminations and veins, while the silicates/oxides occur as vug fillings; the vugs were presumably formed by dissolution of the carbonate rock by the acids derived from sulphide oxidation.

6.2.4 *Millberg prospect*

Little information is available on the Millberg prospect that occurs within dolostone which may either be the Kabwe Dolomite or dolomite layers within the Nyama Formation. Unlike other areas, this dolostone contains scapolite (Freeman, 1988). The mineralisation consists of sphalerite and galena (small oxides amount have been reported) in a series of 0.5 to 5 m wide subvertical veins, which crosscut foliation/bedding and have a strike length of up to 200 m. Estimated resources of ore are 315,000 t at 3.7% Zn and 1.7% Pb (Freeman, 1988).

6.3 *The Lusaka-area willemite deposits (Zambezi Belt)*

There is a consistent lack in literature data about the willemite deposits in the Lusaka area. The most consistent (even of small grade) occurrences are Star Zinc (figure 6.4) and Excelsior (Sweeney et al., 1991).

At Star Zinc, willemite is the dominant species with a radial habit, hence the name (Matthews, 2005). Willemite is associated with specular hematite. Recent karst fill deposits on the surface are heavily mineralized with detrital willemite (Matthews, 2005). Although not common, large laths of specular hematite occur within the ores of the Excelsior prospect, where also significant amounts of native silver have been found (Sweeney et al., 1991). Both the Excelsior and Star Zinc occurrences contain traces of germanium and cadmium, but lead or zinc sulphides are totally absent (Sweeney et al., 1991).

The Star Zinc mineralized area is hosted in sediments of the late Proterozoic Zambezi Supracrustal sequence, deposited in a transtensional basin formed during the oblique collision of the Kalahari and Congo cratons at ~820 Ma (Matthews, 2005). The prospect occurs in the Cheta formation (cfr §4.2.5), consisting mainly of limestones and dolomites, with minor quartz-muscovite schists and feldspathic quartzites (Matthews, 2005). According to Sweeney et al. (1991) the host rock, even in

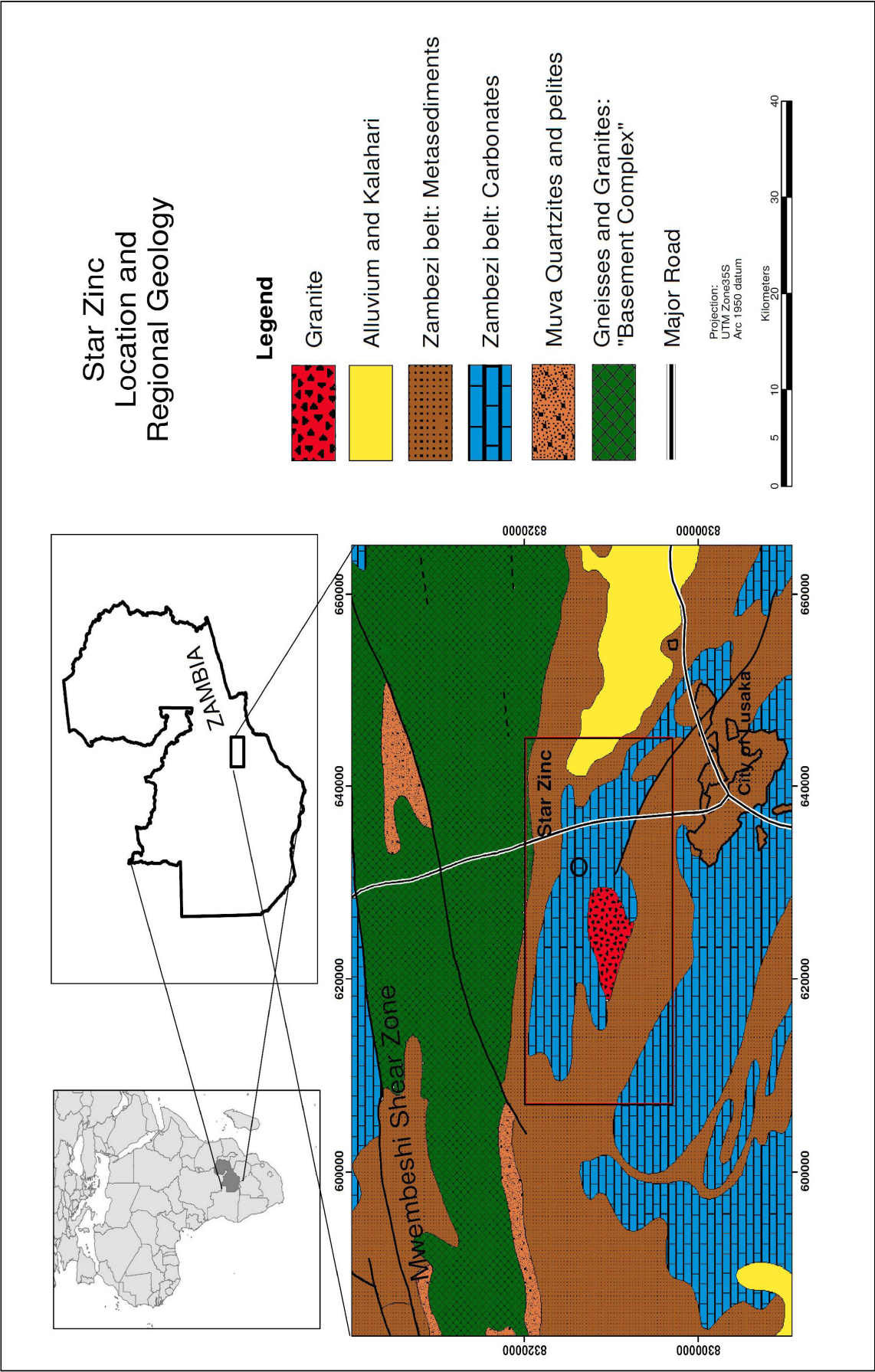


Figure 6.4: Star Zinc location and regional geology (modified after Matthews, 2005).

the immediate vicinity of the mineralisation, is generally barren and does not display significantly recrystallisation. On a local scale, the deposit displays collophorm and vuggy textures as well as open space filling textures at the contact with the host rock; the latter could be regarded as karstic solution features (Sweeney et al., 1991).

Mineralisation both Star Zinc (cfr figure 6.24d) and Excelsior frequently extends beyond the bedded horizons along joints and fissures; the joints are filled with willemite (plus carbonates and barite at Excelsior), thus giving the mistaken impression of vein mineralisation (Sweeney et al., 1991).

6.4 *Mineralogy, petrography and geochemistry of willemite ore in Zambia*

The willemite mineralisation in Zambia occurs in 2 major districts with different characteristics (cfr § 6.2 and § 6.3): Kabwe-area and Lusaka-area. At Kabwe both the primary sulphides, as well as the willemite ores are much better known and described (Kamona et al., 2007, 1999, 1993, Hitzman, 1999, Hitzman et al., 2003). Only poor geological information is available about the willemite deposits in the Lusaka-area, as well as on the geographical location of some of them (only quoted in the old literature from colonial times). For this reasons, I have been able to sample only in the better-known localities of Star Zinc and Excelsior.

In the Lusaka area the occurrence of zinc spinels (typically referred as minerals derived from metamorphic processes in some hypogene nonsulphide deposits as Franklin in USA – Larivière et al., 2007, Johnson et al., 2003, Zheng et al., 1996) and the genetic association of willemite with hematite, are the main differences with the Kabwe-area willemite deposits.

Moreover, in the Kabwe-area deposits the occurrence of supergene nonsulphide minerals such as smithsonite and hemimorphite is much more frequent and widespread, also considering the total size of the deposits (cfr. § 6.2).

6.4.1 *Mineralogy of willemite ore from Kabwe Area*

The mineralogical assemblage (table 6.1) of the willemite ore in the Kabwe mining district (figure 6.5 and 6.6) is usually quite complex and never iterative from site to site. Willemite is the more frequent mineral in the ore. Among the other Zn nonsulphide minerals, smithsonite and hemimorphite prevail.

6.4.1.1 *Willemite*

Willemite has been detected in all considered sites in the Kabwe area, in form of veinlets (figure 6.5a, 6.6d), massive concretions (figure 6.5e, 6.5f and 6.6c) and open-space filling (figure 6.5b). The textures vary from massive/granular, with uniformly indistinguishable willemite aggregates in large

masses, to well-developed prismatic crystals, shaped as slender or squat prisms (figure 6.7a and 6.7b). Well-crystallized willemite grains usually show a vitreous, resinous luster.

Pure, well-shaped willemite crystals are usually white coloured (figure 6.5e). A reddish brown to black (figure 6.5b, 6.5f, 6.6a, 6.6c and 6.6d) colour in willemite may be induced by goethite and hematite disseminations. Under cathodic light, the luminescence of the Kabwe area willemites varies mostly from dull blue (figure 6.8f) in the massive concretions, to bright blue (figure 6.8d) in the botryoidal and zoned crystals. Willemite veins may show both dull and bright blue colour (figure 6.9b and 6.9d). In few cases the willemite luminescence may be spottily dark green (figure 6.11b and 6.11d). The XRD spectra (figure 6.8) display no variations among the different willemite morphologies and locations. Cell parameters randomly measured in a number of willemites throughout the Kabwe area show an almost perfect agreement with the ideal values for this mineral (axial ratios: $a:c = 1:0.67$, $a = b = 13.94$, $c = 9.31$).

6.4.1.2 *Smithsonite and hemimorphite*

Smithsonite (table 6.1) mainly occurs as well-shaped crystalline aggregates (figure 6.5c) but also as earthy concretions (figure 6.5d and 6.6b). Only seldom it occurs in a network of veins replacing primary sulphides (figure 6.5a). Crystalline brownish willemite with translucent quartz veinlets, overgrown by (late) green mottramite aggregates, show usually a massive/botryoidal habit with no visible crystalline affinity and vitreous luster. Earthy smithsonite crusts may consist of the typical trigonal, translucent crystals (figure 6.7c and 6.7d). Smithsonite colours vary from light blue (figure 6.5c) to dark red (due to Fe-(hydr)oxide intercalations). A light purple colour of this smithsonite type is commonly observed under cathodic light (figure 6.9h). XRD spectra (figure 6.6) display almost ideal cell parameters for this mineral ($a = b = 4.653$, $c = 15.028$).

Hemimorphite (table 6.1) occurs usually as well-formed crystalline aggregates (figure 6.7f) of white translucent crystals, forming bushy disseminations (figure 6.5d). Massive hemimorphite masses as open-space filling are also common (figure 6.8h). In figure 6.10 is represented a typical XRD spectrum for the Kabwe hemimorphite.

Table 6.1: XRD analyses of samples from Kabwe area deposits; mineral symbols in order of abundance.

Site	Sample No.	Mineral(s)	Site	Depth (m)	Sample No.	Mineral(s)
Kabwe Camp Plant (5/6?)	ZA0502B-1	Sm, Will	Kabwe No. 2		ZA0508A-1	Hem, Qtz
Kabwe Camp Plant (5/6?)	ZA0502B-2	Sm, Will, Ga, Ce, Sph	Kabwe No. 2		ZA0508A-2	Hem, Cc, Cpy
Kabwe Camp Plant (5/6?)	ZA0502D-1	Sm, Will, Qtz	Kabwe No. 2		ZA0509B-1	Will + He
Kabwe Camp Plant (5/6?)	ZA0502D-2	Sm, Sph, Ga	Kabwe No. 2		ZA0509B-2	Will
Kabwe Camp Plant (5/6?)	ZA0502E-1	Mottr, Qtz	Kabwe No. 2		ZAR611	Sm, Hem, Do
Kabwe Camp Plant (5/6?)	ZA0502E-2	Qtz	Kabwe No. 2		ZAR606-2	Sm, Qtz, Min, Will
Kabwe Camp Plant (5/6?)	ZA0502E-3	Qtz				
Kabwe Camp Plant (5/6?)	ZA0502H-1	Sph, Sm, Py	Airfield pit		ZA0501C	Hem, Sm, Qtz, Ga, Ce
Kabwe Camp Plant (5/6?)	ZA0502H-2	Sm, Hem, Go	Airfield pit		ZA0501E	Sm, Qtz, Do, Sph, Hem
Kabwe Camp Plant (5/6?)	ZA0502H-3	Go, He	Airfield pit		ZAR613	Sm, Ce
Kabwe Camp Plant (5/6?)	ZA0502M-1	Will	Airfield cores	29.3 A12429		Will, Do, Ga, Sph, Qtz
Kabwe Camp Plant (5/6?)	ZA0502M-2	Will	Airfield cores	124.5 A12124.05		Do
Kabwe Camp Plant (5/6?)	ZA0502M-3	Will	Airfield cores	126.5 A1216126B		Will, Min
			Airfield cores	67 A9967		Will, Min
Kabwe No. 2	ZA0509A-1	Sm, Will, Hem				
Kabwe No. 2	ZA0509A-2	Sm, Will, Hem	Kashitu cores	65.8 K3965		Will, Do
Kabwe No. 2	ZA0511-1	Hem, He, Will	Kashitu cores	68.75 K3968		Will, Ce
Kabwe No. 2	ZA0511-2	Cc, Hem	Kashitu cores	69.15 K369.15		Do
Kabwe No. 2	ZA0511-3	Cc, Hem, Ar, Go	Kashitu cores	79.3 K379.30		Do
Kabwe No. 2	ZA0511-4	Hem, Ar, Cc, Go	Kashitu cores	183.15 K4183.15		Do
Kabwe No. 2	ZA0504A1	Hem, Will, Descl	Kashitu cores	185.1 K4185.10		Do
Kabwe No. 2	ZA0504A2	Hem, Will, Descl				
Kabwe No. 2	ZA0505A	Sm, Will, Min	Milberg Pit		ZA0510A-1	Sph, Tr
Kabwe No. 2	ZA0505B	Will, Smith, Descl	Milberg Pit		ZA0510A-2	Sph
Kabwe No. 2	ZA0507-1	Go, Qtz, Tarb	Milberg Pit		ZA0510B	Sph
Kabwe No. 2	ZA0507-2	Go, Qtz, Tarb	Millberg cores	91.25 KM191091		Will, Do, Sph, Qtz
Kabwe No. 2	ZA0507-3	Go, Qtz, Tarb, Dol				

Ar = aragonite, Cc = calcite, Ce = cerussite, Cpy = chalcopyrite, Descl = descloizite, Do = dolomite, Ga = galena, He = hematite, Hem = hemimorphite, Min = minnerdite, Mottr = mottramite, Py = pyrite, Qtz = quartz, Sm = smithsonite, Sph = sphalerite, Tarb = tarbuttite, Tr = tremolite, Will = willemite.

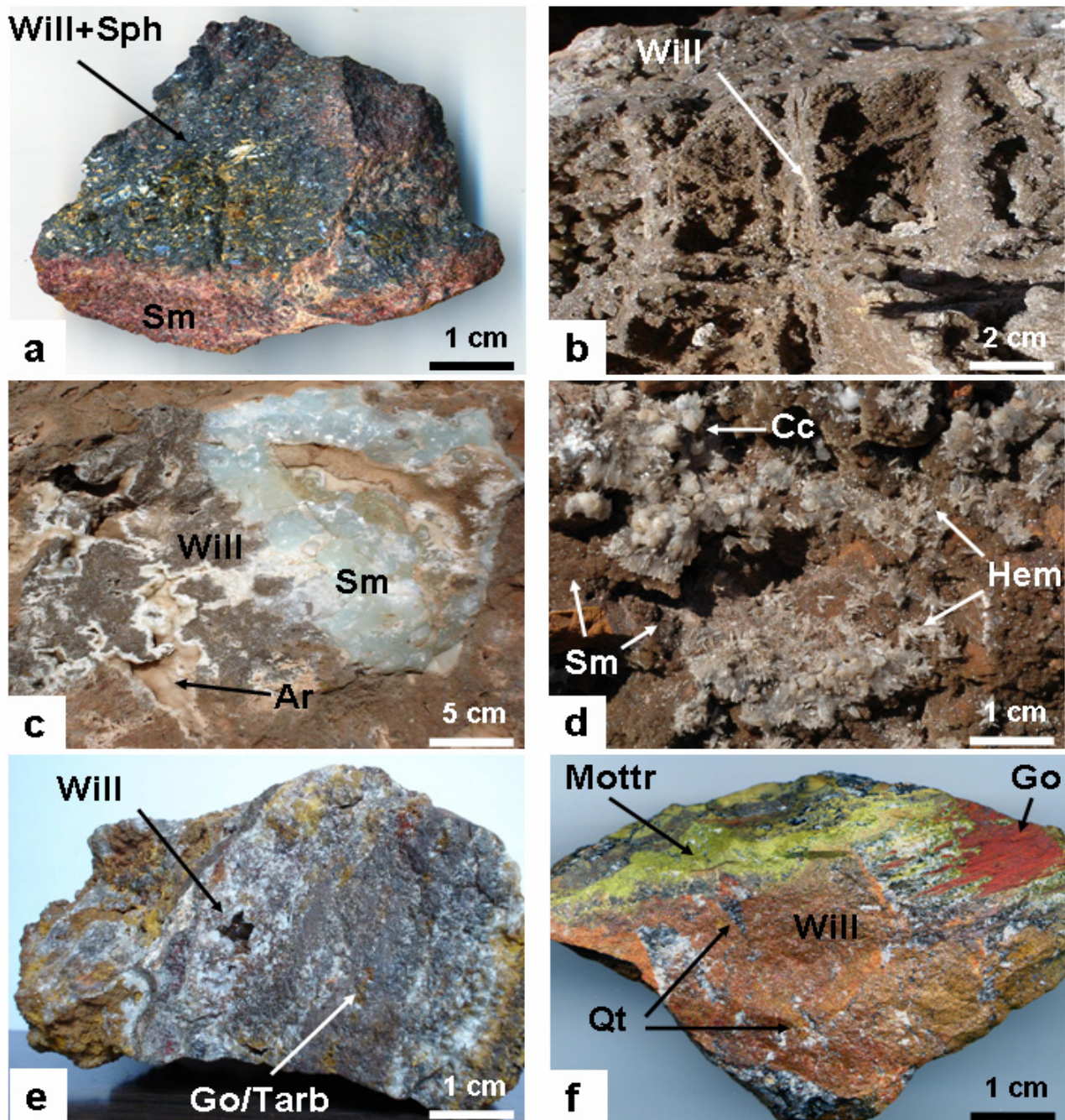


Figure 6.5: Hand specimens from Kabwe no.2 pit (b, c and d) and Kabwe no.5/6 mine dump (a, e and f). a) network of red willemite veinlets replacing yellow sphalerite, covered by late smithsonite aggregates; b) remnants of a well-developed willemite boxwork replacing sphalerite; c) blue reniform smithsonite crust growing on brown willemite; the smithsonite is associated with whitish aragonite concretions filling late cavities; d) white translucent needle-like hemimorphite growing on calcite spherules on brown, earthy smithsonite crusts; e) massive botryoidal willemite streaked by brownish-yellowish goethite and late tarbuttite; f) massive brownish willemite with translucent quartz veinlets, overgrown by (late) green mottamite and reddish late goethite.

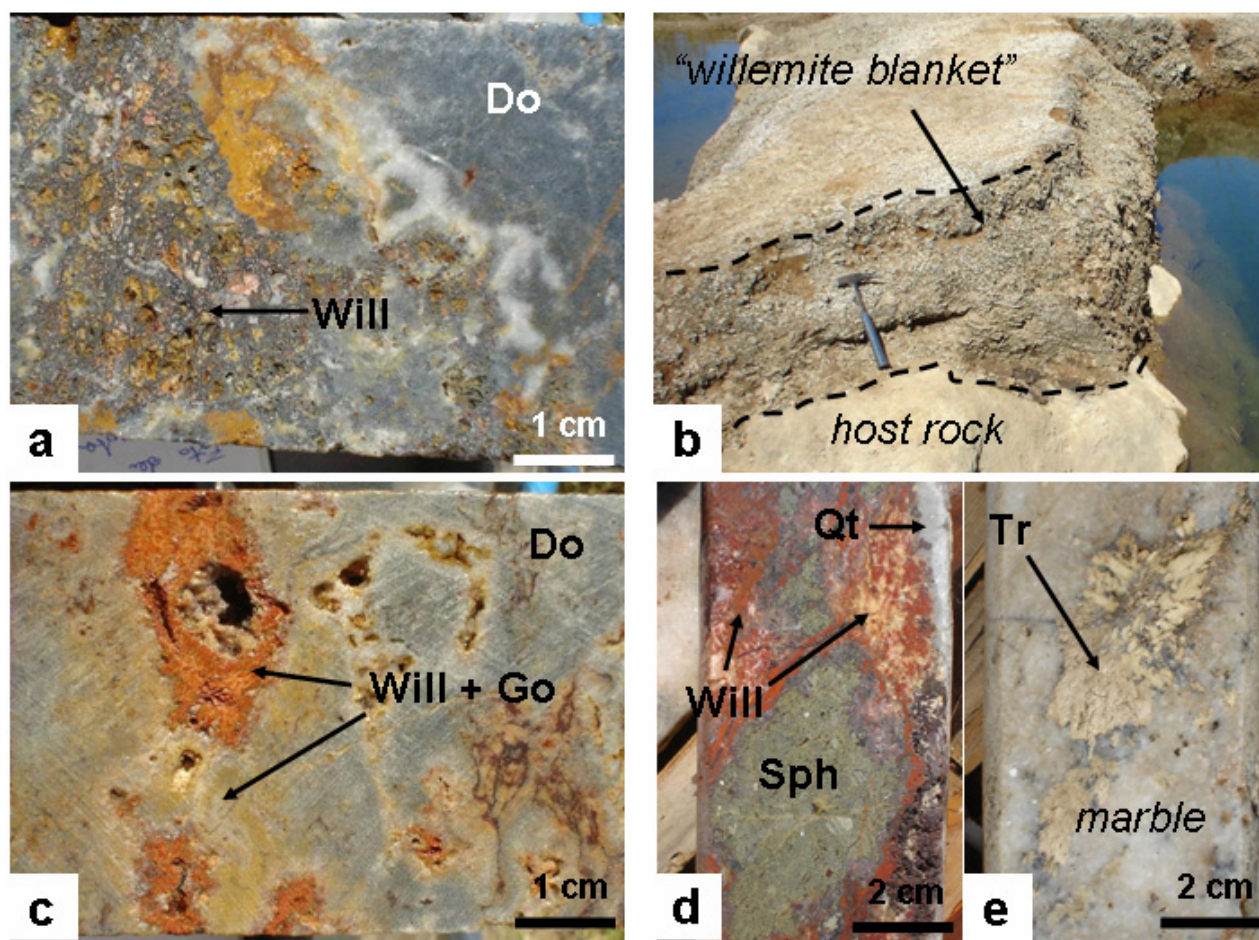
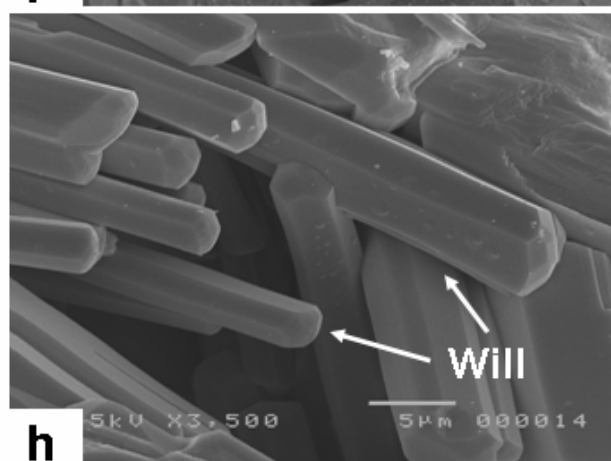
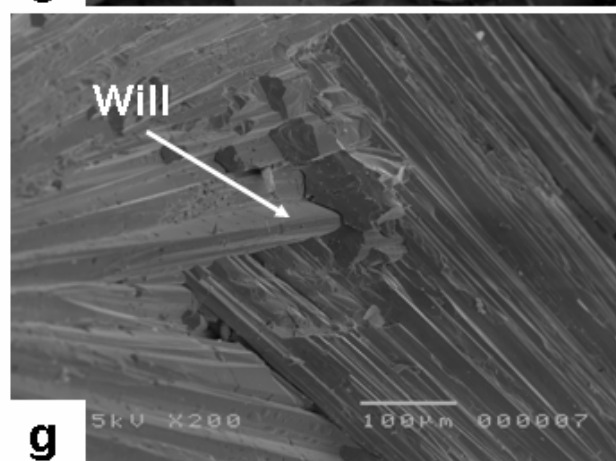
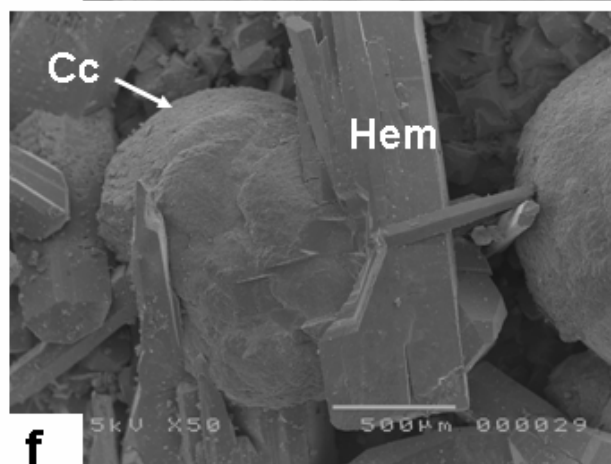
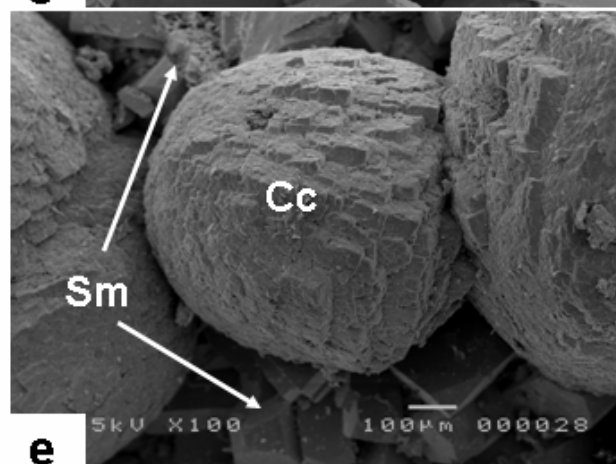
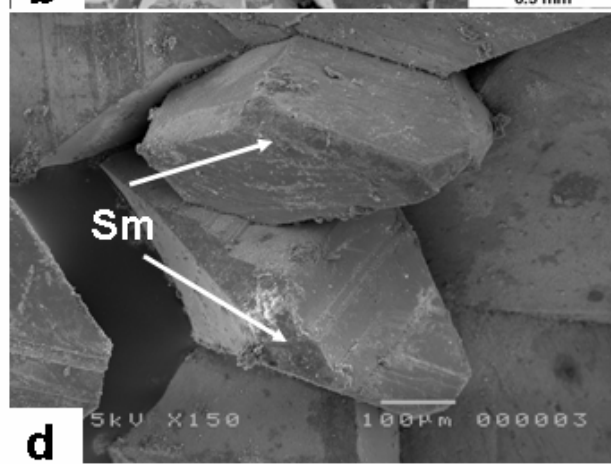
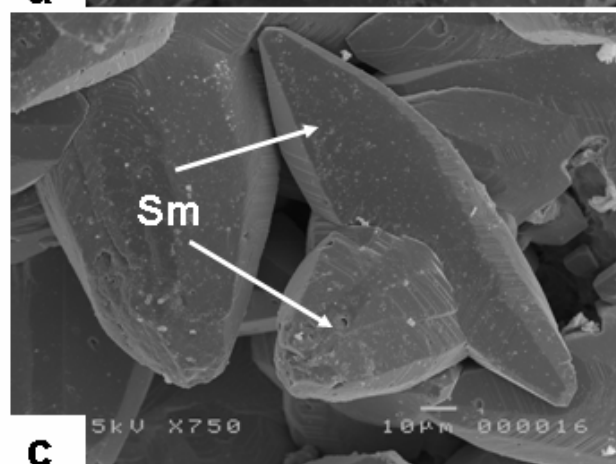
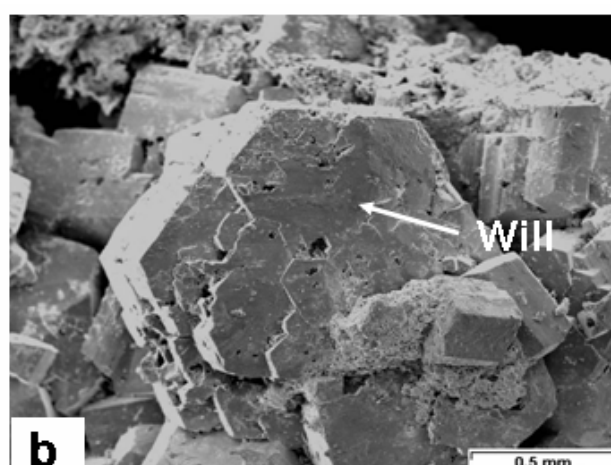
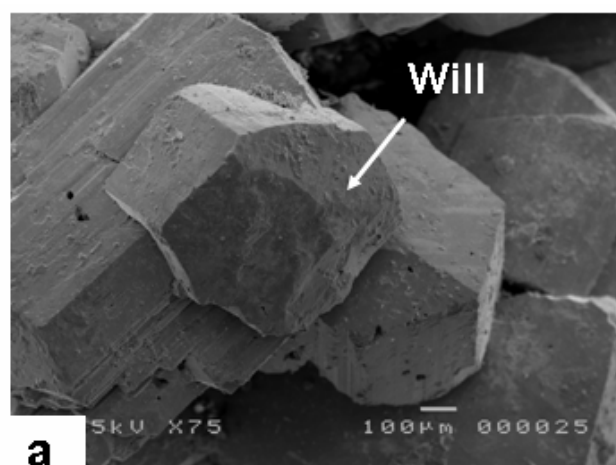


Figure 6.6: Outcrops, hand specimens and drill cores from the Airfield (a and b), Kashitu (c) and Millberg (d and e) prospects. a) black willemite network replacing sphalerite; late cavities are filled with earthy oxide-rich material; b) the typical Airfield “*willemite blanket*” in outcrop: this supergene calcrete-like crust consists mainly of Zn-Pb carbonates, hemimorphite and residual galena. c) red and orange willemite containing goethite disseminations; d) green sphalerite cut by red willemite. White willemite crystallising as open space filling and late black descloizite and white quartz veins; e) hostrock of the Millberg prospect: tremolitic marble.

6.4.1.3 Other minerals

The heterogeneous assemblage in the willemite ore of the Kabwe area deposits (table 6.1) contains also a large number of minor mineralogical phases, both pertaining to the primary sulphide association and to several generations of nonsulphides. The most common phases are the primary Zn-Pb sulphides (sphalerite and galena) as well as minor cerussite, descloizite and mottramite; rare sauconite, minrecordite and tarbuttite have been also found. Calcite, dolomite and aragonite are the most widespread among the gangue minerals, as well as quartz, goethite, hematite and clays.

Figure 9.7: Secondary electron images of selected samples of willemite-smithsonite ore from Kabwe No. 5/6 (a and b), Kabwe No. 2 (c, d, e and f), Star Zinc (g) and Excelsior (h). a): intergrown prismatic crystals of willemite; b) basal hexagonal section of a willemite crystal; c) and d): idiomorphic smithsonite crystals; e): calcite spherules over smithsonite crust; f) needle-like hemimorphite crystals grown on calcite spherules; g) compact needle-like willemite aggregate; h) slender willemite prismatic crystals.



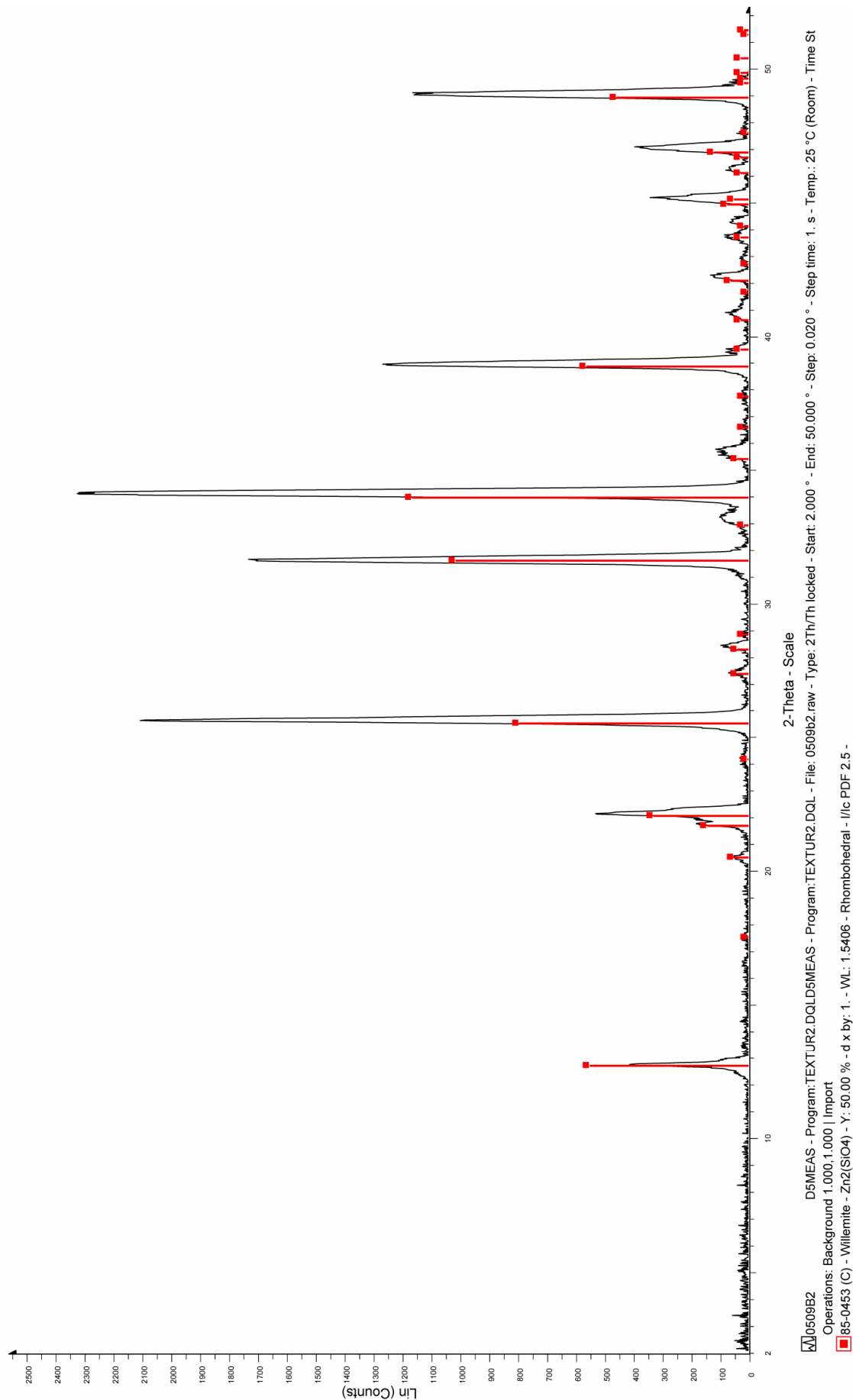


Figure 6.8: Willemite XRD spectrum, sample ZA0509B from Kabwe no.5/6 mine dump.

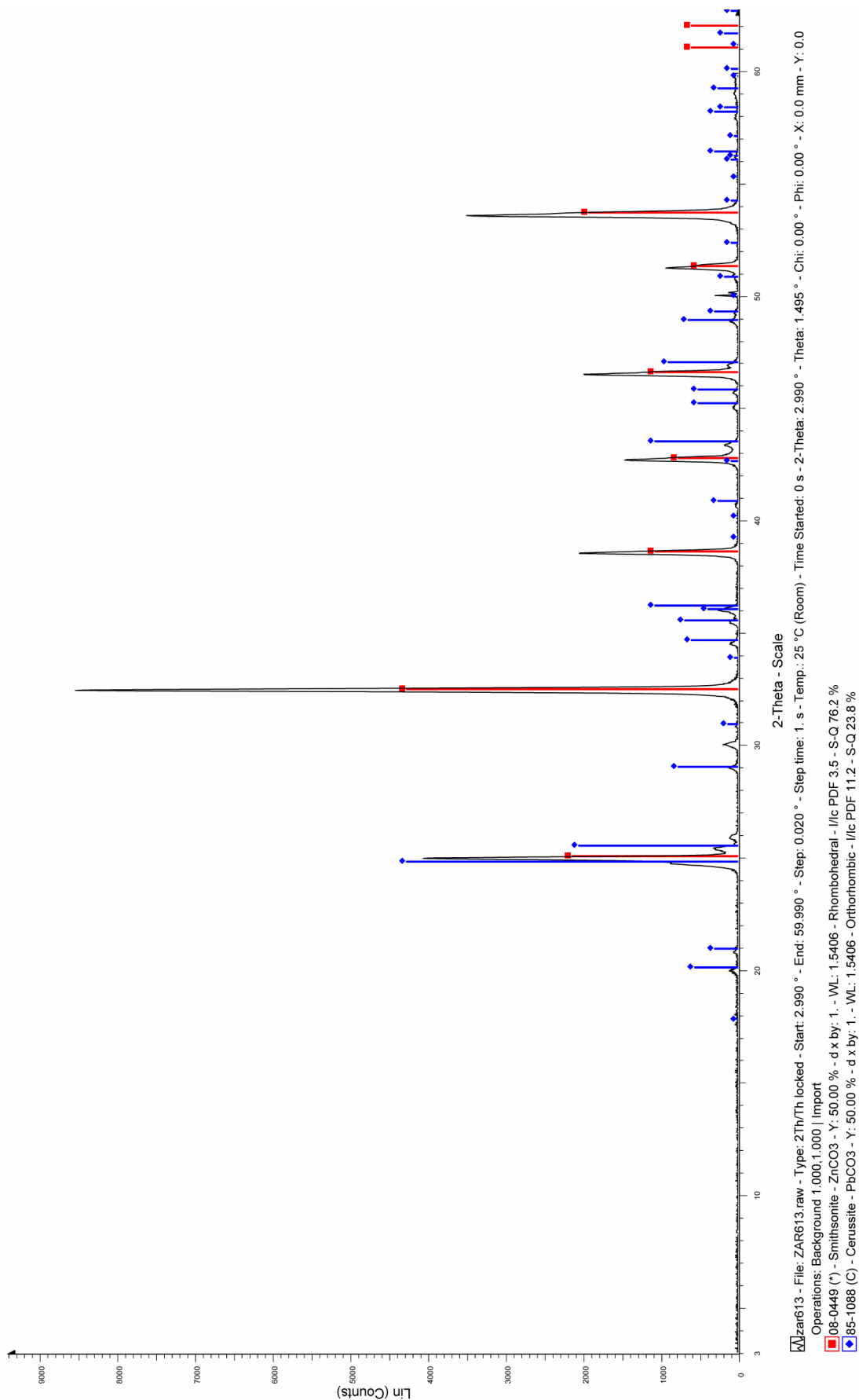


Figure 6.9: Willemite XRD spectrum, sample ZAR613 from Airfield pit.

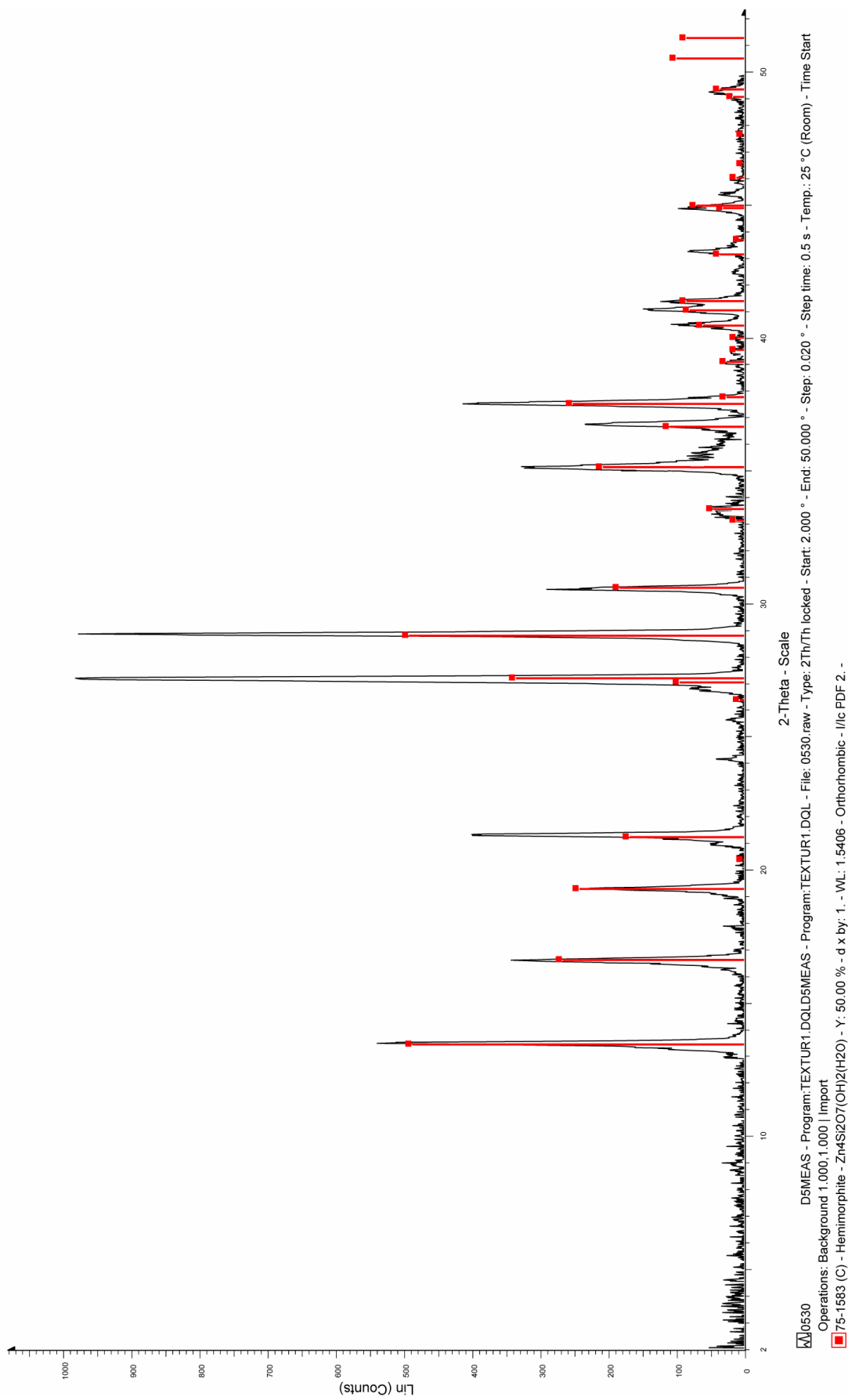


Figure 6.10: Hemimorphite XRD spectrum, sample ZAR611 from Kabwe no.2 pit.

6.4.2 *Petrography and paragenesis of willemite ore from the Kabwe Area*

Two mineralogical associations can be commonly distinguished. The first (usually from the deeper ore zones) consists of willemite as the major phase with economic value, with or without sulphides (sphalerite > galena >> pyrite), accompanied by minor smithsonite. In the second association (usually occurring in the shallower ore zones) willemite is subeconomic, whereas smithsonite and hemimorphite are fairly enriched. Gangue minerals can be carbonates and quartz in both cases. Willemite can be easily distinguished by the second order high interference colours under crossed nicols (XP) and by its blue luminescence under cathodic light (CL).

Lower, but even high, interference colours characterize hemimorphite that show no luminescence in CL. Pinkish luminescence of smithsonite allows to distinguish this one from the other carbonates. A detailed paragenesis will be depicted for each sampled deposit, even if only slight differences were found in the different localities.

6.4.2.1 *Kabwe deposit*

Willemite in the main Kabwe deposit occurs mainly as massive or botryoidal concretions (figure 6.8c and 6.8e). Primary sulphides are firstly replaced by a smithsonite I generation (usually showing a red to slight pinkish CL luminescence) in thin veins (figure 6.8a).

Newly formed galena and covellite may also precipitate as disseminated crystals in this early stage, due to the non-compatibility of Pb and Cu in the smithsonite lattice. A subsequent stage of pervasive willemitisation (figure 6.8e) is causing an only local replacement of primary sulphides, due to armouring effect of early smithsonite around the sulphide grains.

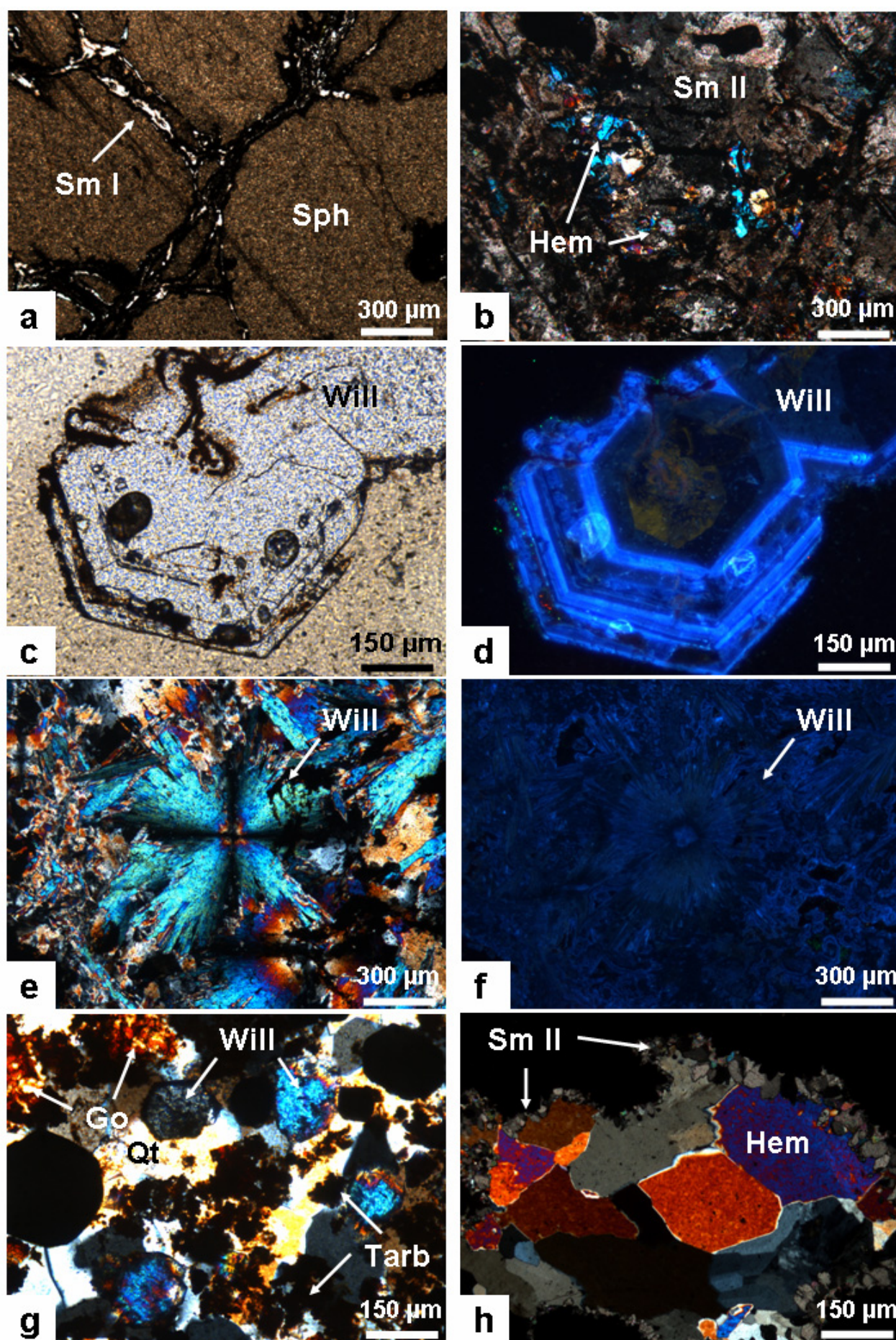
A successive severe willemitisation stage led to the precipitation of massive concretions, locally disseminated with sulphide remnants. Botryoidal textures indicating slow circulation in open space cavities may locally occur.

The multigenetic nature of willemitisation is clearly observed also under cathodic light. Several willemite generations can be distinguished by the variably blue CL colours, clearly defining a perfect zonation in the hexagonal, open-space crystallized willemites (figure 6.8d). Locally it could be observed that early deposited willemites have served as crystallization nuclei for the crystals of younger generations (figure 6.8.f). Anhedral quartz may occur as gangue in the willemite ore, as an evidence of SiO₂ oversaturation in the fluid (figure 6.8g).

Further evidence of even younger secondary mineral phases is given by the goethite and needle-like tarbuttite dissemination (figure 6.8g), as well as by a further smithsonite generation (smithsonite II). Smithsonite II (well crystallised with the typical trigonal shape) usually shows a pink luminescence under CL and may pervasively overprint both the various phases of willemite ore and the carbonate

host (figure 6.8b). Smithsonite II occurs before hemimorphite as late cavity filling (Figure 6.8h). The mineral paragenesis occurring in the Kabwe deposit is depicted in figure 9.12.

Figure 6.11: Thin sections (polarized and cathodic light) of willemite-smithsonite ore from Kabwe No. 5/6 (a to g) and Kabwe No. 2 (h). a) smithsonite I veins cutting sphalerite (N II); b) smithsonite II and hemimorphite (N +); c) idiomorphic willemite crystal (N II); d) same as c (CL), well zoned in blue: in the centre a nucleus of a previous willemite generation with a different CL colour (brown); e) massive willemite aggregates (N +); f) same as e (CL); g) euhedral, hexagonal willemite with quartz, reddish goethite and needle-like tarbuttite (N +); h) smithsonite II lining cavities filled by hemimorphite.



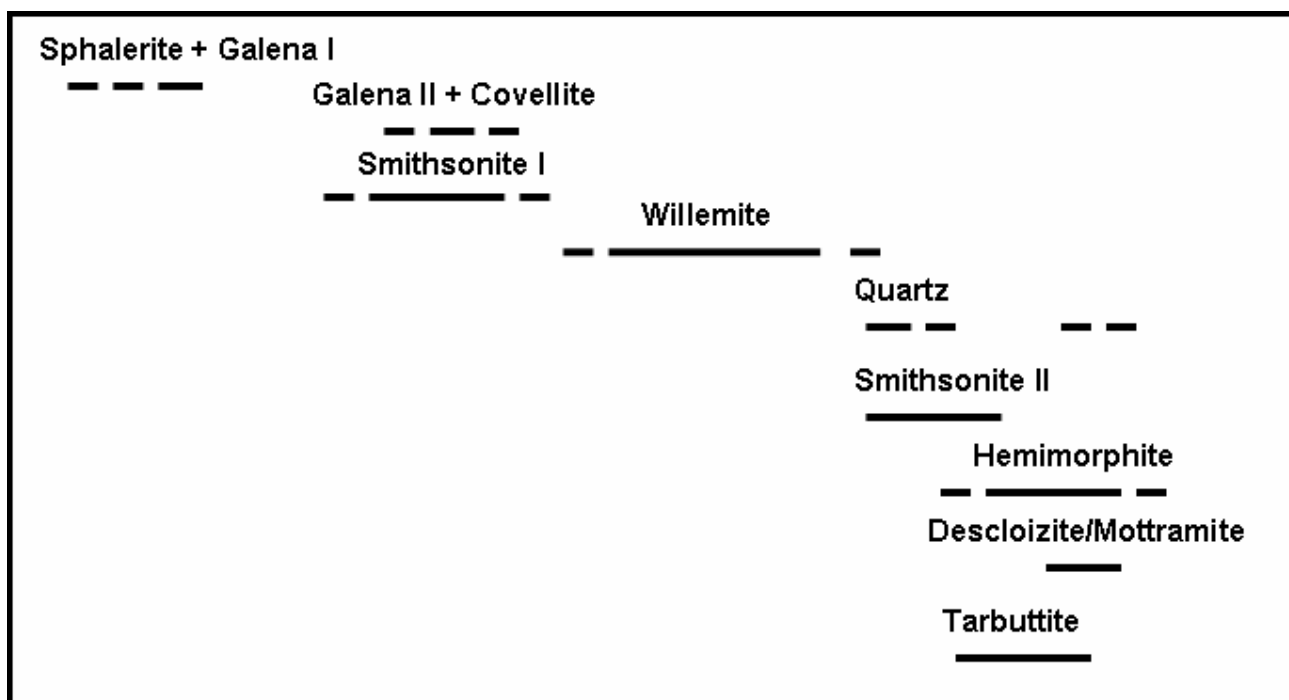


Figure 6.12: Mineral paragenesis post-primary sulphides in the Kabwe deposit.

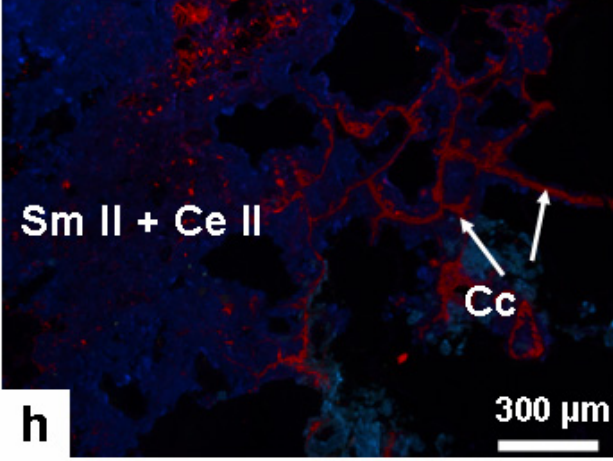
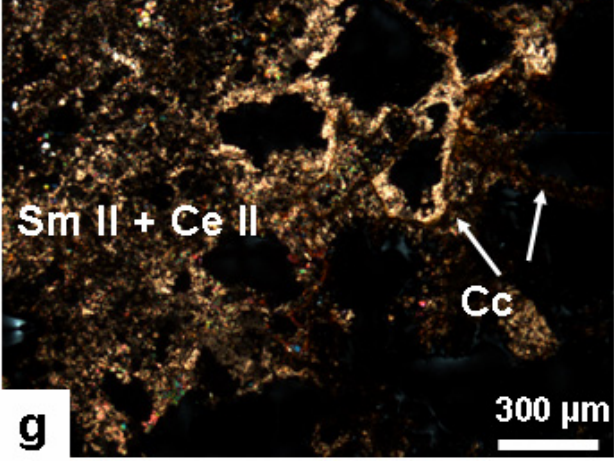
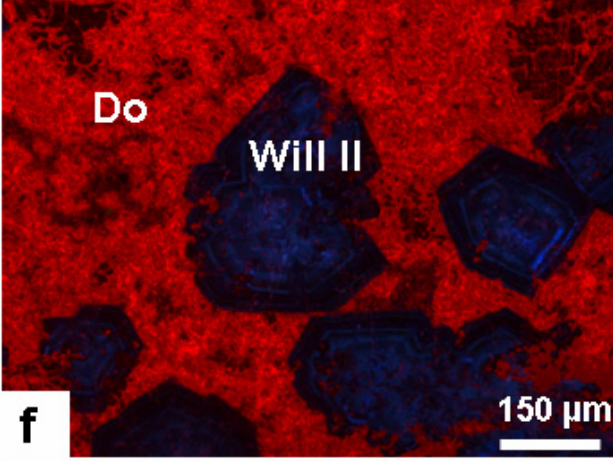
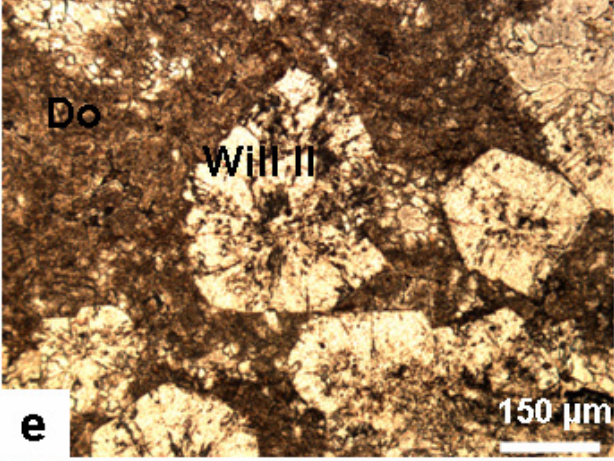
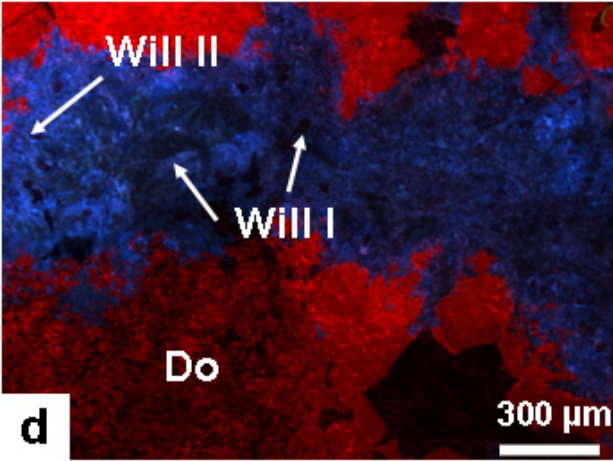
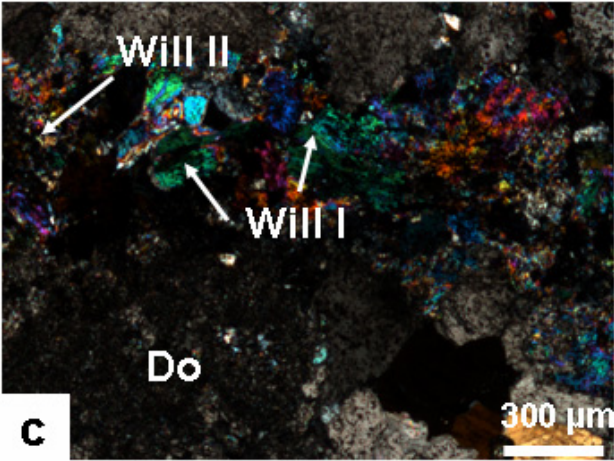
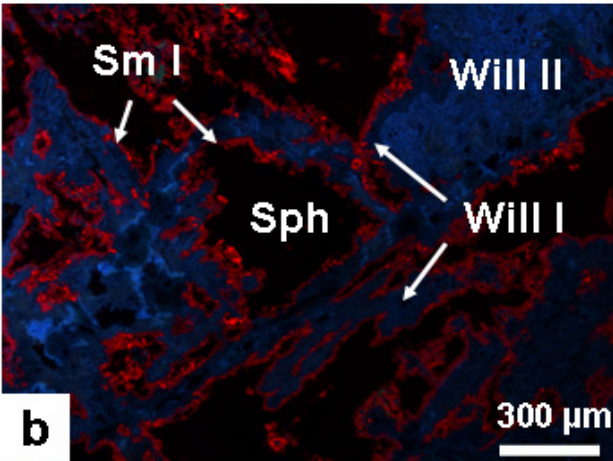
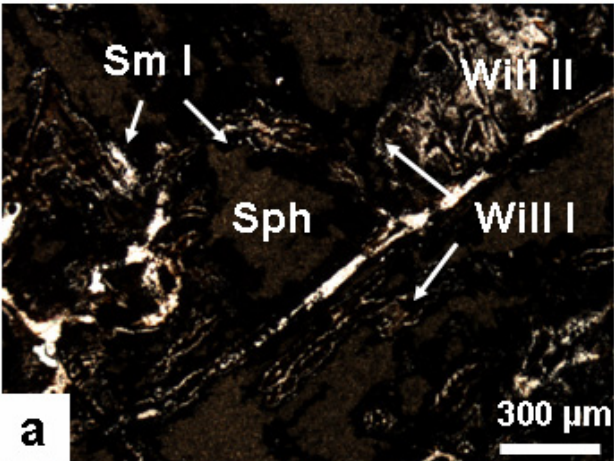
6.4.2.2 *Airfield prospect*

Willemite in the Airfield prospect occurs mainly as veins (figure 6.13a and 6.13b), but also as massive to botryoidal concretions (figure 6.13e and 6.13f). In this small deposit, as in the main Kabwe orebodies the sulphides are firstly replaced by the smithsonite I generation, which shows a red to slight pinkish cathodoluminescence (figure 6.13b). Willemitisation takes place around the pre-altered (by smithsonite I and locally cerussite) sphalerite-galena grains (figure 6.14a). Willemitisation also affects the carbonate host-rock (figure 6.13c and 6.13d).

Under cathodic light willemite appears to have been formed through several mineralisation stages (figure 6.13f). Two main events could be recognized, the first producing a willemite I with dark blue CL colours (figure 6.13b), which replaces directly the sulphides: this willemite locally contains disseminated goethite, which is the cause of its reddish colour under N II. This first willemite generation is followed by willemite II, light blue under CL, which locally replaces willemite I (figure 6.13d). Quartz (figure 6.14b), usually associated with a Zn-rich saddle dolomite (figure 6.14b, ZnO = 8% mean value) may be locally found in the gangue of the willemite ore. Zn-rich saddle dolomite displays a bright red colour under CL. Trigonal smithsonite II may overprint the willemite ore. Smithsonite II generally displays pale pink CL colours and is closely associated with hemimorphite. Together with other secondary carbonates (cerussite and calcite) smithsonite II is the main component of the so-called (by the miners) “*willemite blanket*” (figure 6.13g and 6.13h), a

poorly economic concentration of nonsulphide ore covering subhorizontally the host rock as a strange sort of “zinc-crete” soil (figure 6.6b). The mineral paragenesis of the Airfield deposit has been summarised in figure 9.5.

Figure 6.13: Thin sections (observed under N + and CL) of the willemite ore from the Airfield deposit. a) smithsonite I and willemite I/II network of veins replacing sphalerite (N +); b) same as a under CL; c) willemite II, with internal remnants of willemite I, replacing the carbonate host rock (N +); d) same as c under CL; e) willemite II idiomorphic crystals in a groundmass of saddle dolomite (N +); f) same as e under CL; g) carbonates (smithsonite II and cerussite II) of the “*willemite blanket*” ore (N +); h) same as g under CL.



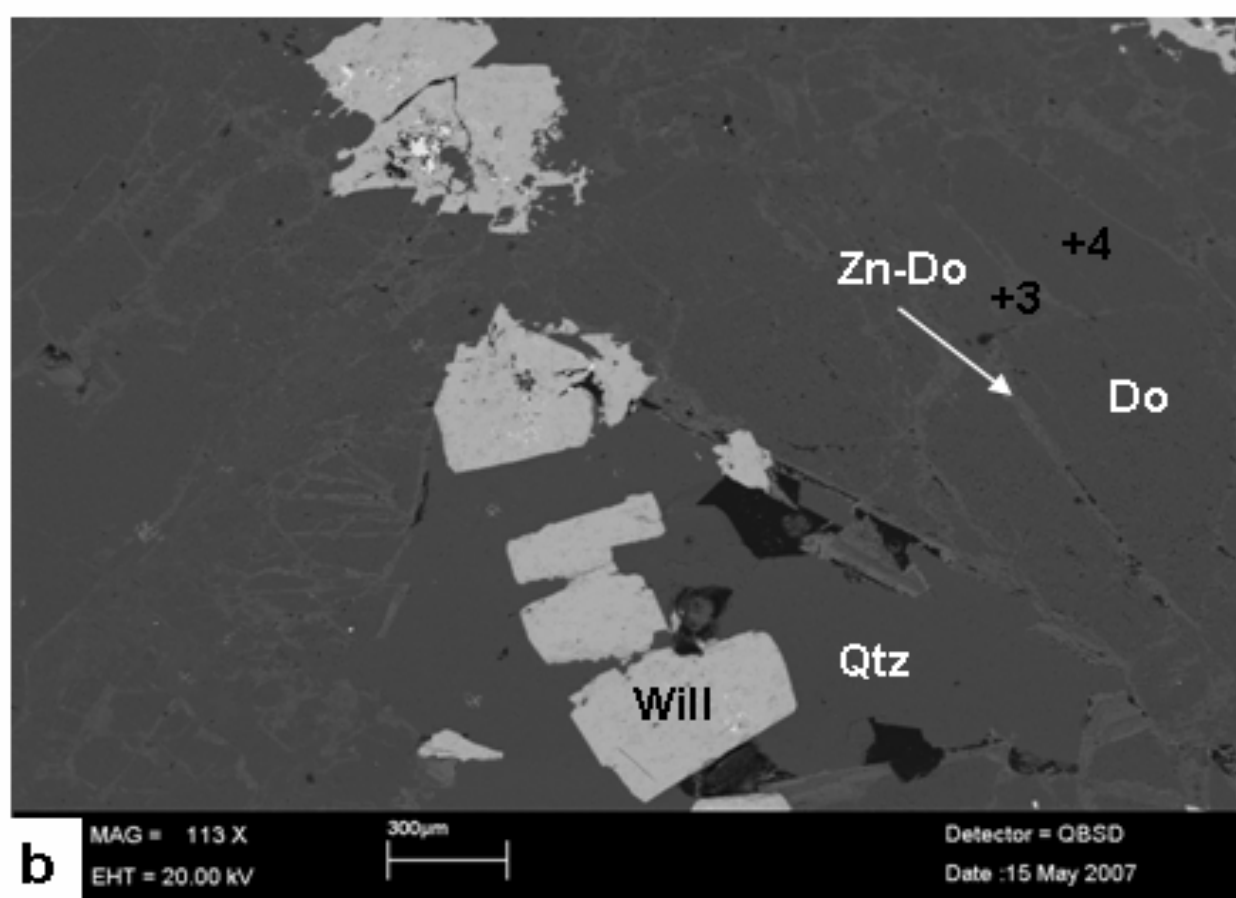
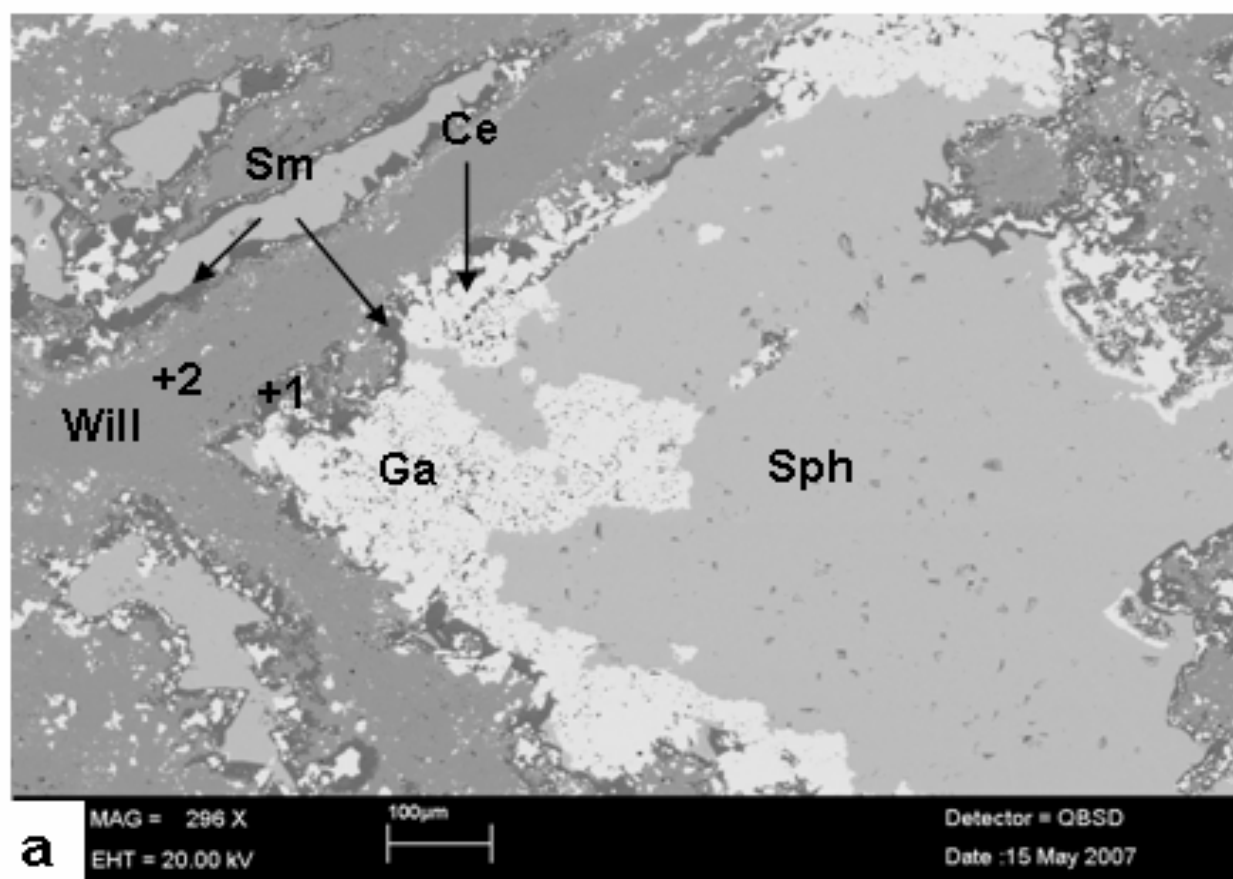


Figure 6.14: BSE images of selected zones of a thin section from the Airfield prospect (sample A12429) a) willemite I veins (spot analysis no.2) lining sphalerite-galena grains previously replaced by smithsonite (spot analysis no.1) and cerussite preventing total dissolution of primary sulphides. During the replacement process, secondary galena crystals (galena II) grow along the primary sulphide grains; b) subidiomorphic crystals of willemite II generation and anhedral quartz, in cavities of coarse-grained dolomite hostrock (spot analyses no. 4, barren). The latter is being replaced by Zn-bearing saddle dolomite (i.e. spot analysis no. 3, ZnO ranging from 6% to 8%) in veins and concretions.

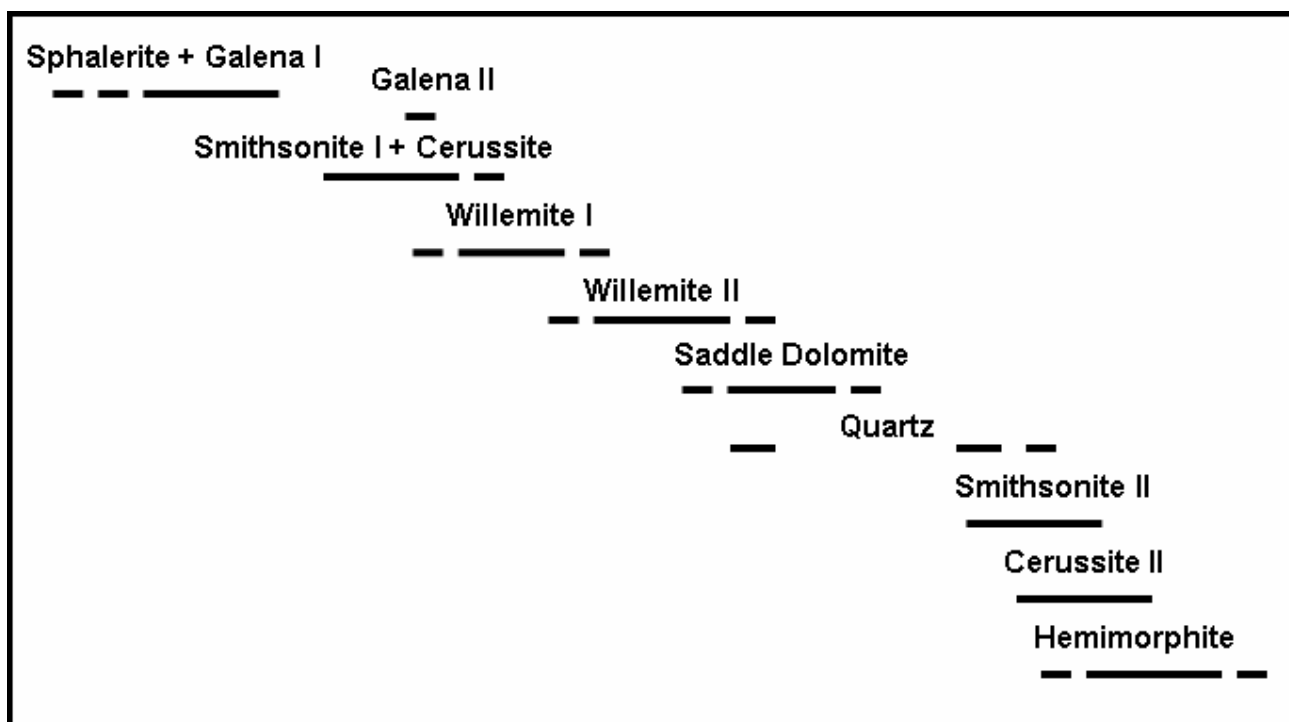


Figure 6.15: Mineral paragenesis at the Airfield prospect.

6.4.2.3 *Kashitu prospect*

No sulphides or smithsonite have been recorded in the cores of the Kashitu prospect, where willemite mainly occurs as massive, locally botryoidal concretions (figure 6.1.7c and 6.17g) replacing the carbonate host-rock. Observed under CL, Kashitu willemite displays three generations (figure 6.17b, 6.17c and 6.17d): willemite I (orange in N II), dark blue-spotted green, willemite II (reddish in N II), dark blue, willemite III (white in N II), light blue. The orange colour of willemite I

is caused by finely dispersed goethite. In willemite II the dissemination of goethite microflakes is increased (hence the reddish colour). Willemite III may occur as euhedral, well defined crystals. Idiomorphic (saddle?) Zn-rich dolomite follows willemite III and is less widespread (ZnO ranging from 4 to 8%, figure 6.18a and 6.18b) than at Airfield (figure 6.17f and 6.17h). Quartz may be locally present. The paragenesis of the Kashitu prospect is summarised in figure 6.16.

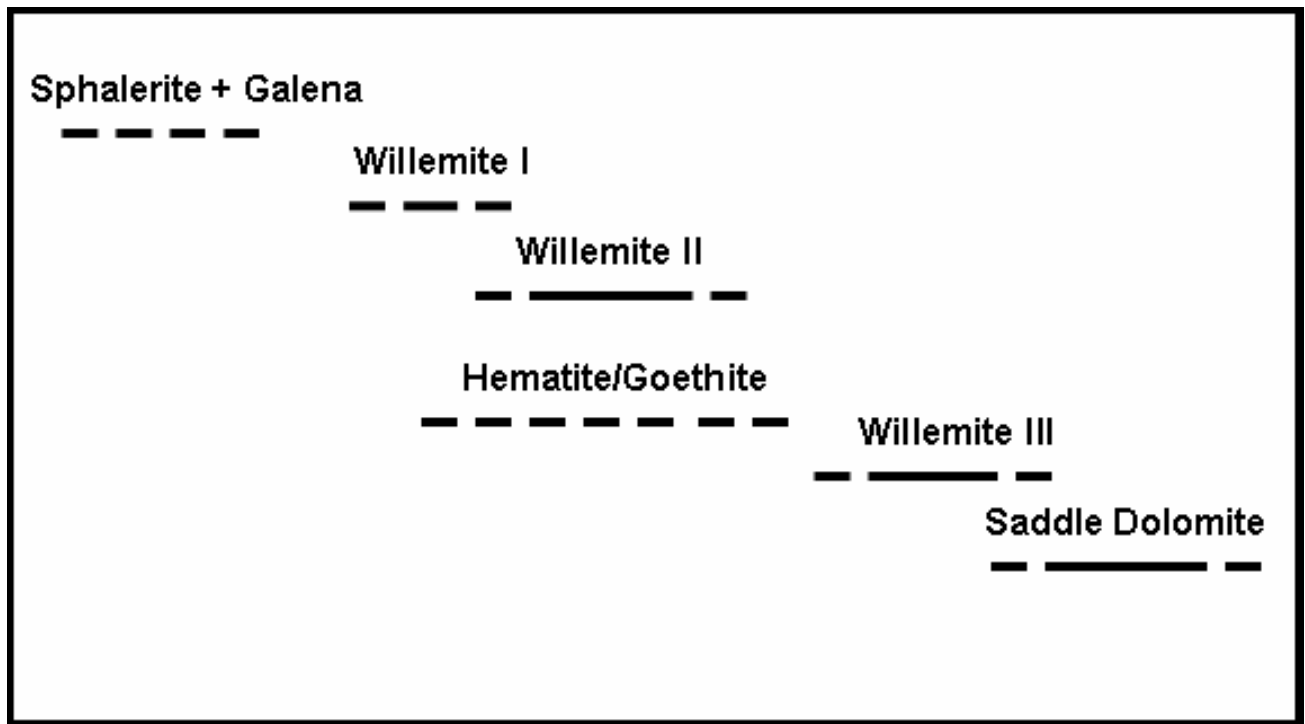
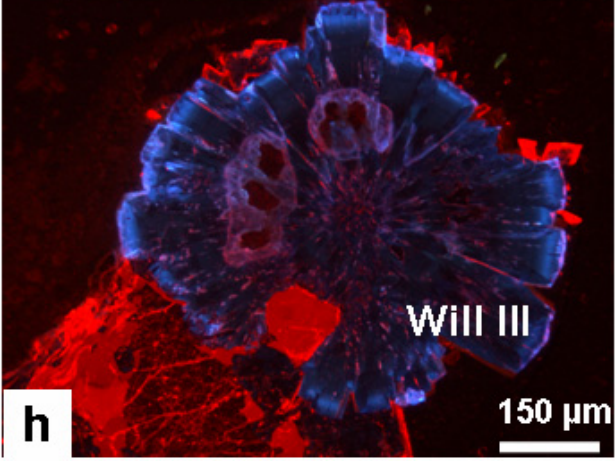
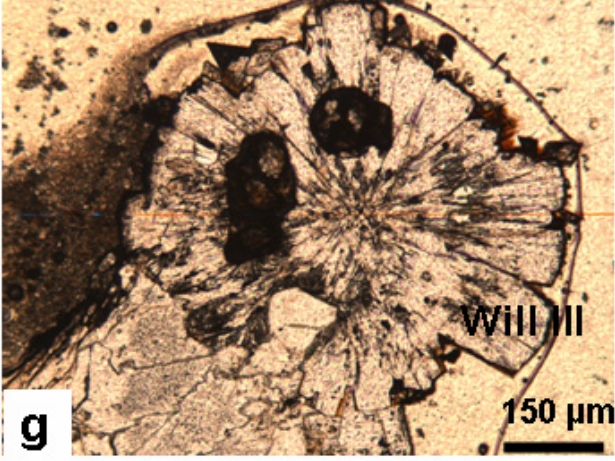
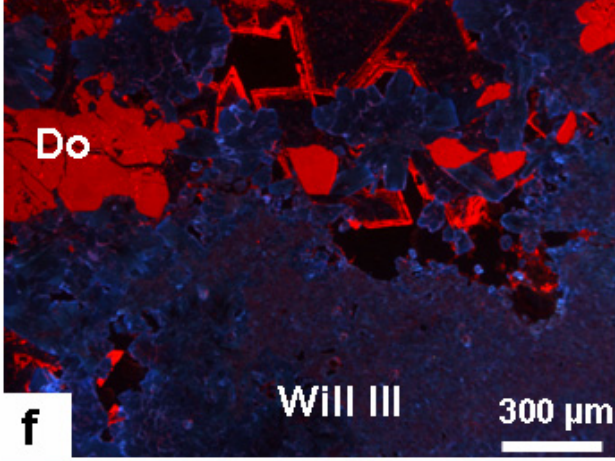
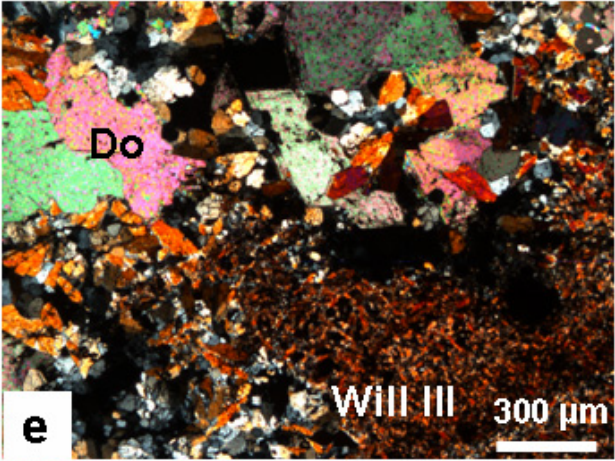
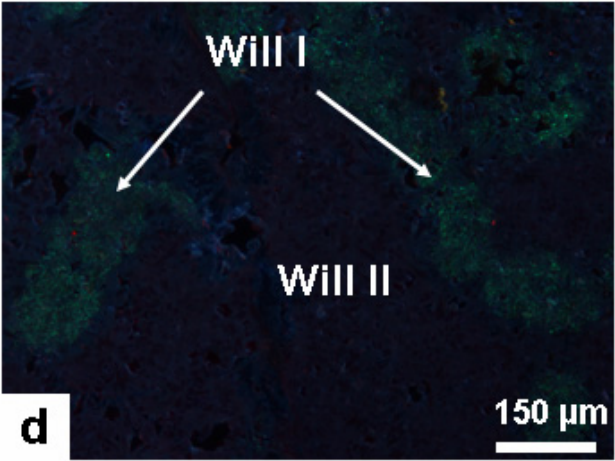
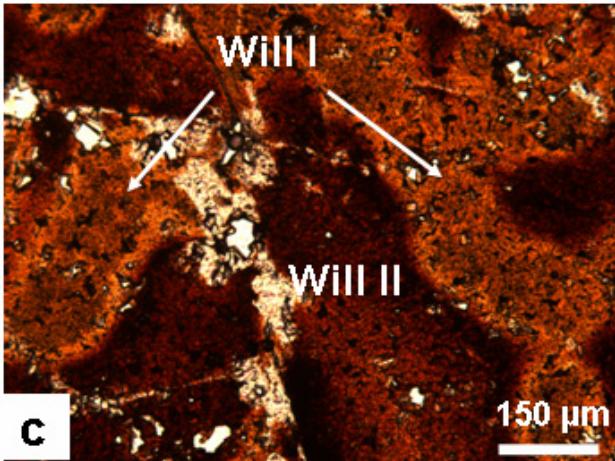
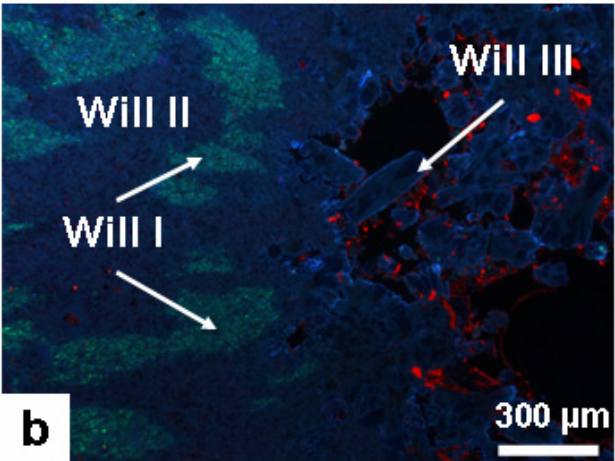
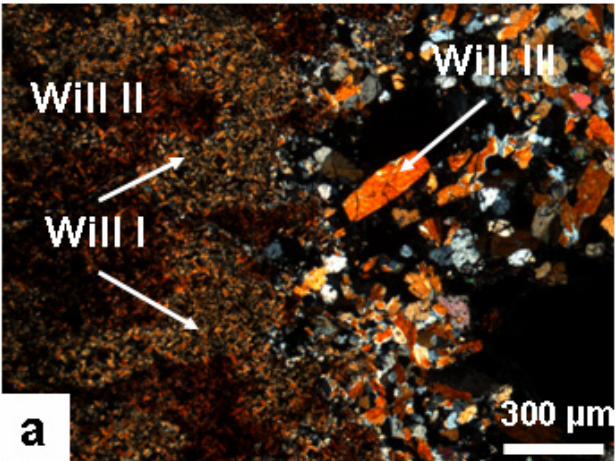


Figure 6.16: Paragenesis of the Kashitu prospect.

Figure 6.17: Thin sections of willemite ore from Kashitu (N II and CL). a) Willemite I, II and III generations (N +); b) same as a in CL with reddish carbonates; c) willemite I and II with disseminations of hematite/goethite (N II); d) same as c in CL; e) willemite III followed by late dolomite; f) same as e in CL; g) radial aggregate of willemite III overgrown by idiomorphic dolomite; h) same as g in CL; in the low left corner the late dolomite cuts and replaces a previous (burial?) dolomite phase.



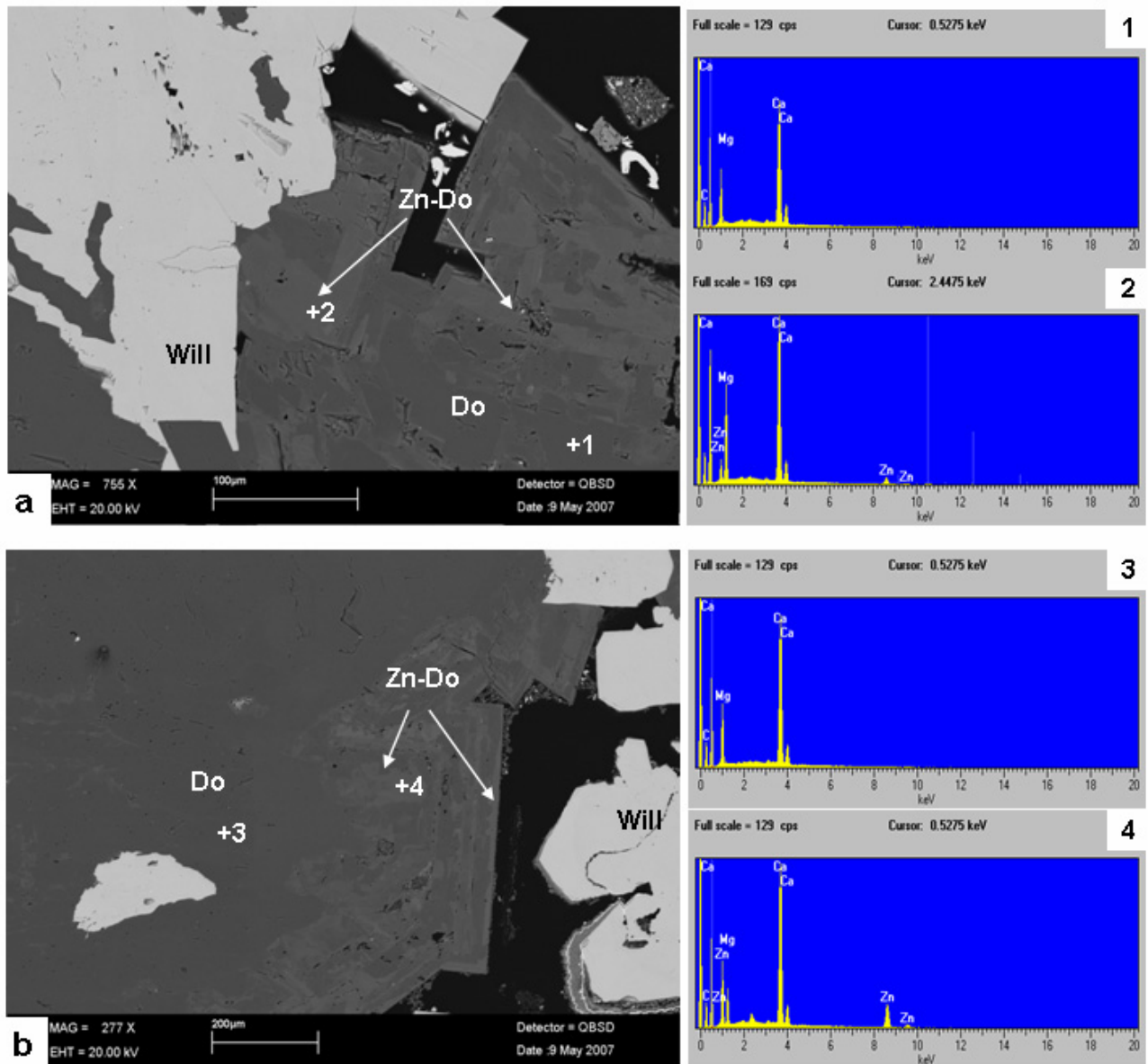


Figure 6.18: BSE images of selected thin sections from the Kashitu prospect. a) willemite III crystals followed by late idiomorphic (saddle?) dolomite. Light grey dolomite horizons contain up to 3% ZnO (spot analysis no. 1); the darker zones are almost barren of metals (spot analysis no. 2); b) zoned saddle dolomite associated with willemite III. The lighter horizons contain ZnO varying from 2% to 6% (i.e. spot analysis no. 3); carbonate in spot 4 same as spot 2.

6.4.2.4 Millberg prospect

Willemite at the Millberg prospect occurs both in veins directly cutting primary sphalerite (figure 6.20a and 6.20b) and as massive aggregates replacing the host rock and growing in cavities (figure 6.20c). No smithsonite occurs here prior than willemite in the replacement process of primary

sulphides. Lead and cadmium mobilized from sphalerite and primary galena may precipitate as small euhedral crystals of secondary galena and greenockite (figure 6.21a). This is due to the incompatibility of lead and cadmium within the willemite lattice.

Under CL willemite shows a multistage nature (figure 6.20e and 6.20f). Three main generations have been recognized: willemite I, light blue in CL (figure 6.20b), which first replaces sphalerite; willemite II, reddish in N II, also light blue in CL, containing disseminations of goethite (figure 6.20c and 6.20e). Willemite III, blue to light green in CL (figure 6.20b), is less abundant and is usually the last phase at the rim of the previous two generations. Barren (saddle?) dolomite (figure 6.20g and 6.20h) is the most common gangue mineral also for the willemite ore at Millberg. Late descloizite associated with quartz in veins (figure 6.21b) represents the last phase deposited. The Millberg mineral paragenesis is depicted in figure 6.19.

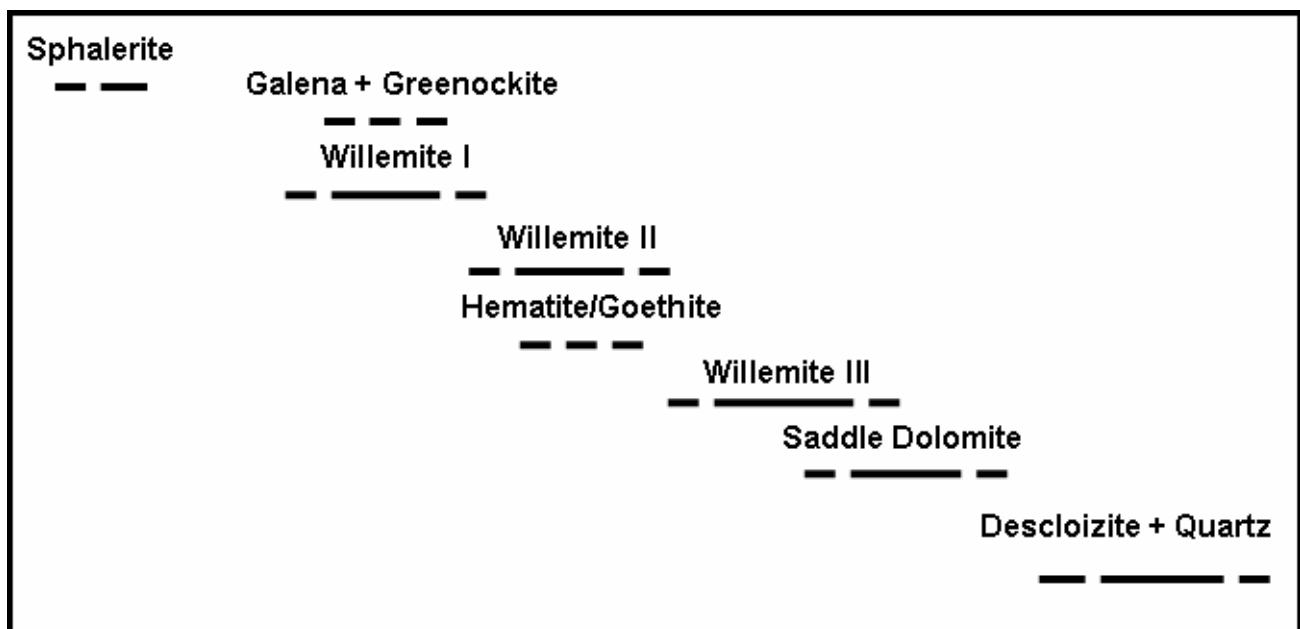
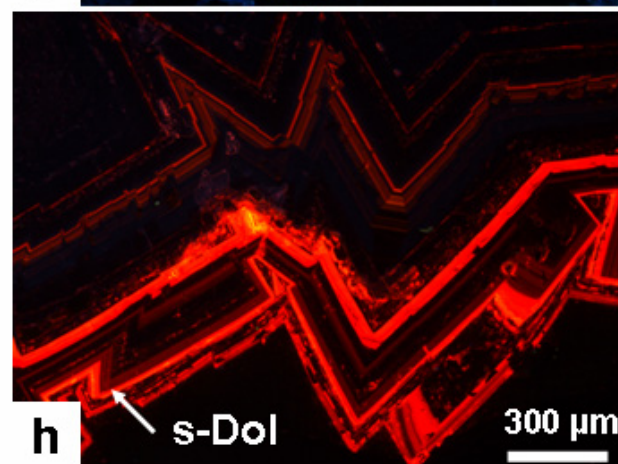
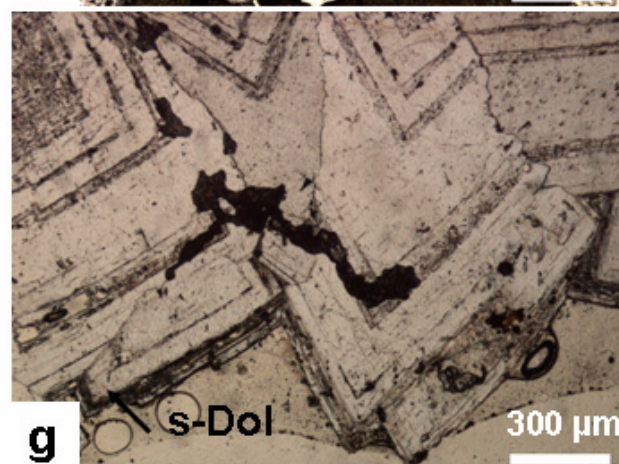
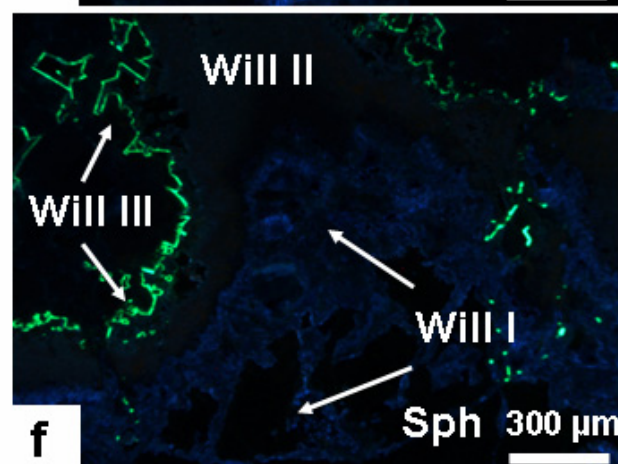
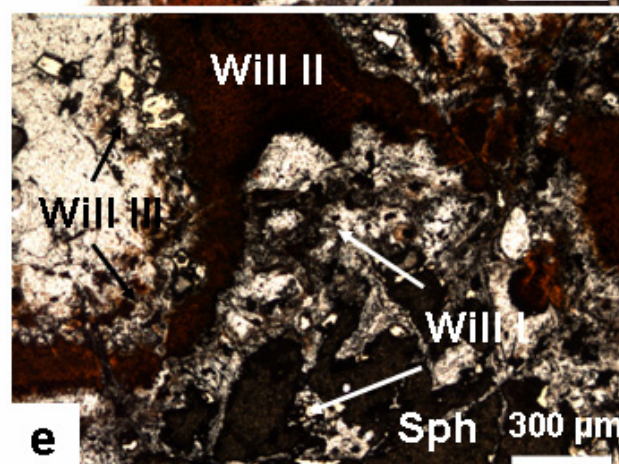
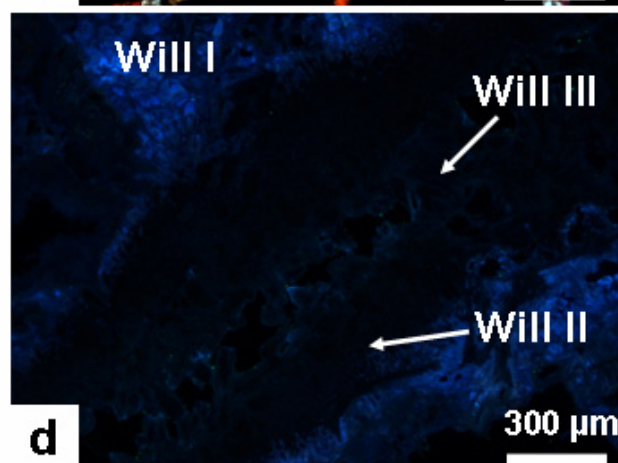
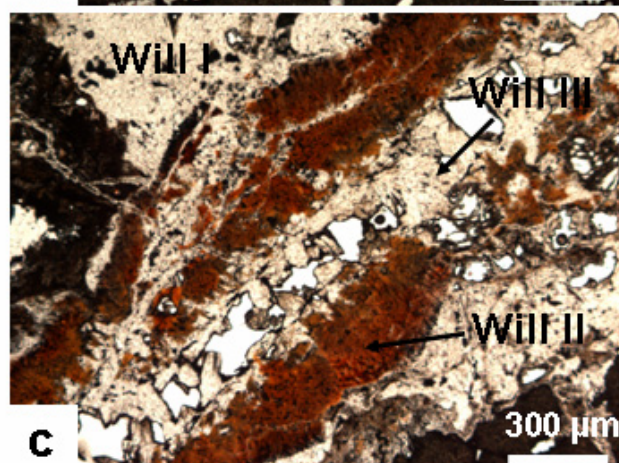
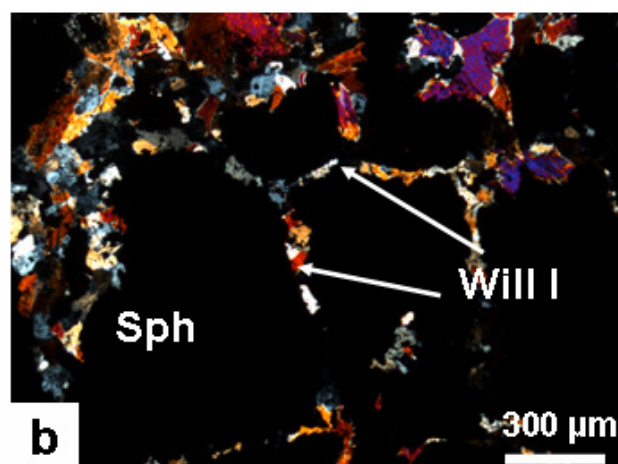
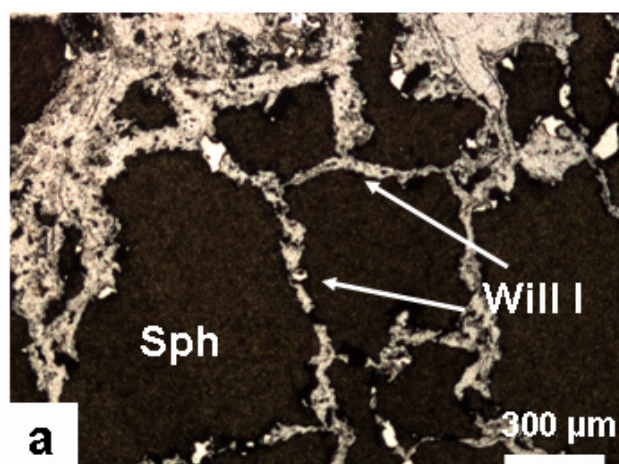


Figure 6.19: Paragenesis of the Millberg prospect.

Figure 6.20: Thin sections (N II, N + and CL) of the willemite ore at Millberg. a) dense network of thin willemite I veins cutting and replacing sphalerite (N II); b) same as a in N +; c) willemite I (as in a-b, right corner down), willemite II (orange) and willemite III (white) (N II); d) same as c under CL (willemite III is here bluish); e) willemite I, II and III; f) same as e in CL: in this case the rim of willemite III shows a green CL; g) late saddle(?) dolomite following the willemitic ore; h) same as g in CL.



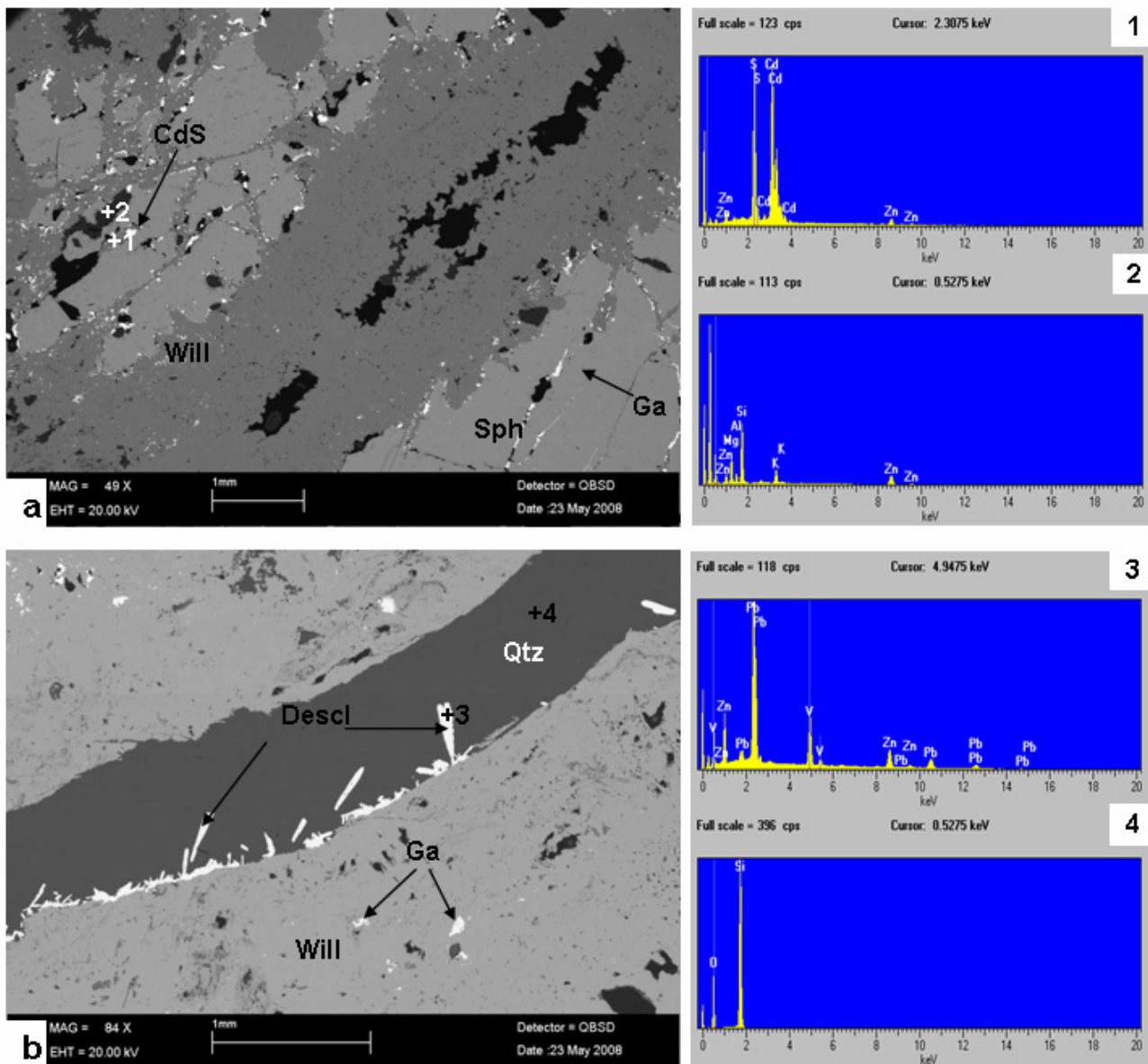


Figure 6.21: BSE images of selected thin sections from the Millberg prospect. a) willemite I, II and III generations with formation of secondary idiomorphic galena and greenockite (spot analysis no. 1); late diagenetic sauconite also occurs in cavities (spot analysis no. 2); b) late descloizite (spot analysis no. 3) and quartz veins (spot analysis no. 4), cutting willemite II.

6.4.3 Major and trace element geochemistry of willemite ore from Kabwe Area

Willemite in the Kabwe area usually occurs as single ore phase or with variable contributions of smithsonite and minor hemimorphite. The total zinc grade of the willemite ore bodies can reach here up to 20 wt% Zn. Pb wt% is generally not exceeding 5%, mainly occurring as several generations of galena (primary sulphides remnants and new precipitations) and as cerussite (minor).

Here below is presented a number of geochemical analyses (WDS) of willemites from the Airfield (table 6.2), Kashitu (table 6.3) and Millberg (table 6.4) prospects. In addition to the Zn and Si contents, also the elements Mn, Mg and Cd have been selected, to investigate their variable amounts in the various willemite generations/localities.

The different willemite generations in each site have been investigated with the aim to establish if there is any difference in their chemical composition that could mirror the broad variability of their optical and morphological range (cfr § 6.4.2.2, §6.4.2.3 and §6.4.2.4). The chemical data thus obtained have been processed, in order to obtain the chemical compositions reflecting the found stoichiometry values, the ideal chemical and stoichiometry values for willemite being as follow: $\text{ZnO} = 73.04\%$; $\text{SiO}_2 = 26.96\%$; with 2 apfu Zn and 1 apfu Si.

Selected willemites from the Airfield prospect have shown ZnO values ranging between 71.50% and 73.50%, with a mean value of 72.40%. FeO has usually values lower than 0.05%, up to a maximum value of 1.04% (mean 0.12). MnO, MgO and CdO mean values never exceed 0.01%, maximum for Mn at 0.04%. The totals of the analyses range between 98.28% and 99.85% (mean 99.33). The total stoichiometry ($\text{Si} + \text{Zn} + \text{Mn} + \text{Mg} + \text{Cd} = 3$ apfu) gives values ranging between 2.99 apfu and 3.01 apfu (mean 3); Zn and Si stoichiometry gives values ranging between 1.97-2.02 apfu (mean 2) and 0.99-1.01 apfu (mean 1) respectively.

The Kashitu willemite has ZnO values varying between 71.52% and 73.26% (mean 72.20). The maximum FeO value is at 0.55% (mean 0.19). MnO, MgO and CdO means are never higher than 0.01%, maximum value recorded for Mn (0.05%). The totals vary between 98.21% and 100.11% (mean 98.92). Total stoichiometry ranges between 3.00 apfu and 3.01 apfu (mean 3); Zn and Si stoichiometry ranges between 2.02-1.99 apfu (mean 2) and 0.99-1 apfu (mean 1) respectively.

Total ZnO at Millberg ranges from a minimum of 70.93% to a maximum of 72.84% (mean 71.91). The maximum FeO value is 1.72% with the majority of values not exceeding 0.05% (mean 0.17). The mean MnO, MgO and CdO amounts are never higher than 0.02% with the Mn highest value of 0.07%. The totals vary between 97.66% and 99.19% (mean 98.67). Total stoichiometry gives values between 2.98 apfu and 3.01 apfu (mean 3); Zn and Si stoichiometry ranges between 2.02-1.96 apfu (mean 2) and 0.99-1.02 apfu (mean 1) respectively.

Chemical variations for Airfield, Kashitu and Millberg are plotted in figures 6.22a. In this diagram is shown that only little covariation exists between Zn and Fe (as it was expected also by the stoichiometry). The analyses totals are plotted in figure 6.22b. It is confirmed that no systematic variation of the analyzed elements, particularly Mn and Fe, has been observed among the different willemite generations, as it might have been hypothesized by their variable cathodoluminescence colours. Systematic low FeO and MnO contents, rarely exceeding 0.5%, have been detected.

Table 6.2: WDS analyses (% oxide) and stoichiometry (apfu) of willemite from Airfield prospect.

	A12-1	A12-2	A12-3	A12-4	A12-5	A12-6	A12-7	A12-8	A12-9	A12-10	A12-11	A12-12	A12-13	Mean
CdO	0.03	0.02		0.01	0.02		0.02		0.01					0.02
MnO	0.01	0.04	0.03	0.01	0.03			0.01	0.03	0.01	0.05	0.01	0.03	0.02
FeO	0.03		0.07	0.01	0.01	0.23	0.03	0.03	0.03	0.02	0.03	0.04	1.04	0.13
ZnO	72.56	72.68	71.52	72.30	72.73	72.01	71.94	73.08	72.65	72.03	72.27	73.51	71.73	72.39
MgO	0.01	0.02	0.01						0.03			0.01		0.01
SiO₂	26.93	27.01	26.64	26.53	26.84	26.98	26.88	26.73	26.84	26.93	26.54	26.65	26.75	26.79
Total	99.57	99.76	98.28	98.86	99.63	99.22	98.87	99.85	99.56	99.02	98.89	100.21	99.55	99.33

Table 6.3: WDS analyses (% oxide) of willemite from Kashitu prospect.

	K39-1	K39-2	K39-3	K39-4	K39-5	K39-6	K39-7	K39-8	K39-9	K39-10	K39-11	K39-12	K39-13	K39-14	Mean
CdO			0.01					0.05	0.02	0.00	0.02			0.02	0.02
MnO	0.01			0.04	0.05		0.04	0.02		0.01	0.03			0.01	0.03
FeO	0.02	0.04	0.16	0.33	0.48	0.55	0.36	0.01			0.04	0.02	0.51	0.09	0.22
ZnO	72.02	72.40	72.25	72.59	72.30	71.52	71.64	72.27	71.65	72.39	72.26	73.26	72.15	72.18	72.21
MgO	0.03			0.01	0.08		0.01			0.01	0.02	0.03			0.03
SiO₂	26.57	26.91	26.40	26.46	26.34	26.25	26.44	26.36	26.53	26.59	26.22	26.80	26.29	26.64	26.49
Total	98.61	99.39	98.82	99.43	99.25	98.32	98.50	98.70	98.21	99.00	98.57	100.11	98.97	98.94	98.92

Table 6.4: WDS analyses (% oxide) of willemite from Millberg.

	KM19-1	KM19-2	KM19-3	KM19-4	KM19-5	KM19-6	KM19-7	KM19-8	KM19-9	KM19-10	KM19-11	KM19-12
CdO	0.02	0.01	0.01							0.03	0.03	
MnO	0.01		0.01		0.07			0.04		0.06	0.02	
FeO		0.04	0.01	1.44	1.72	0.29	0.04	0.01		0.01	0.02	
ZnO	72.54	72.64	72.84	71.23	70.93	72.05	72.10	71.70	71.07	72.27	71.92	71.45
MgO			0.01						0.01			
SiO₂	26.47	26.32	26.26	26.50	26.47	26.50	26.70	27.02	27.21	26.47	26.45	26.21
Total	99.04	99.01	99.12	99.17	99.19	98.84	98.85	98.77	98.29	98.83	98.44	97.66

	KM19-13	KM19-14	KM19-15	KM19-16	KM19-17	KM19-18	KM19-19	KM19-20	KM19-21	KM19-22	Mean
CdO	0.03		0.01		0.01	0.01		0.01	0.01		0.01
MnO		0.01					0.03				0.01
FeO			0.02	0.01		0.02	0.01		0.02	0.04	0.17
ZnO	72.23	71.82	71.89	71.53	71.66	71.94	72.17	72.33	71.51	72.29	71.91
MgO									0.03		
SiO₂	26.43	26.79	26.47	26.54	26.33	26.43	26.92	26.68	26.80	26.52	26.57
Total	98.69	98.62	98.39	98.07	98.00	98.40	99.13	99.02	98.36	98.85	98.67

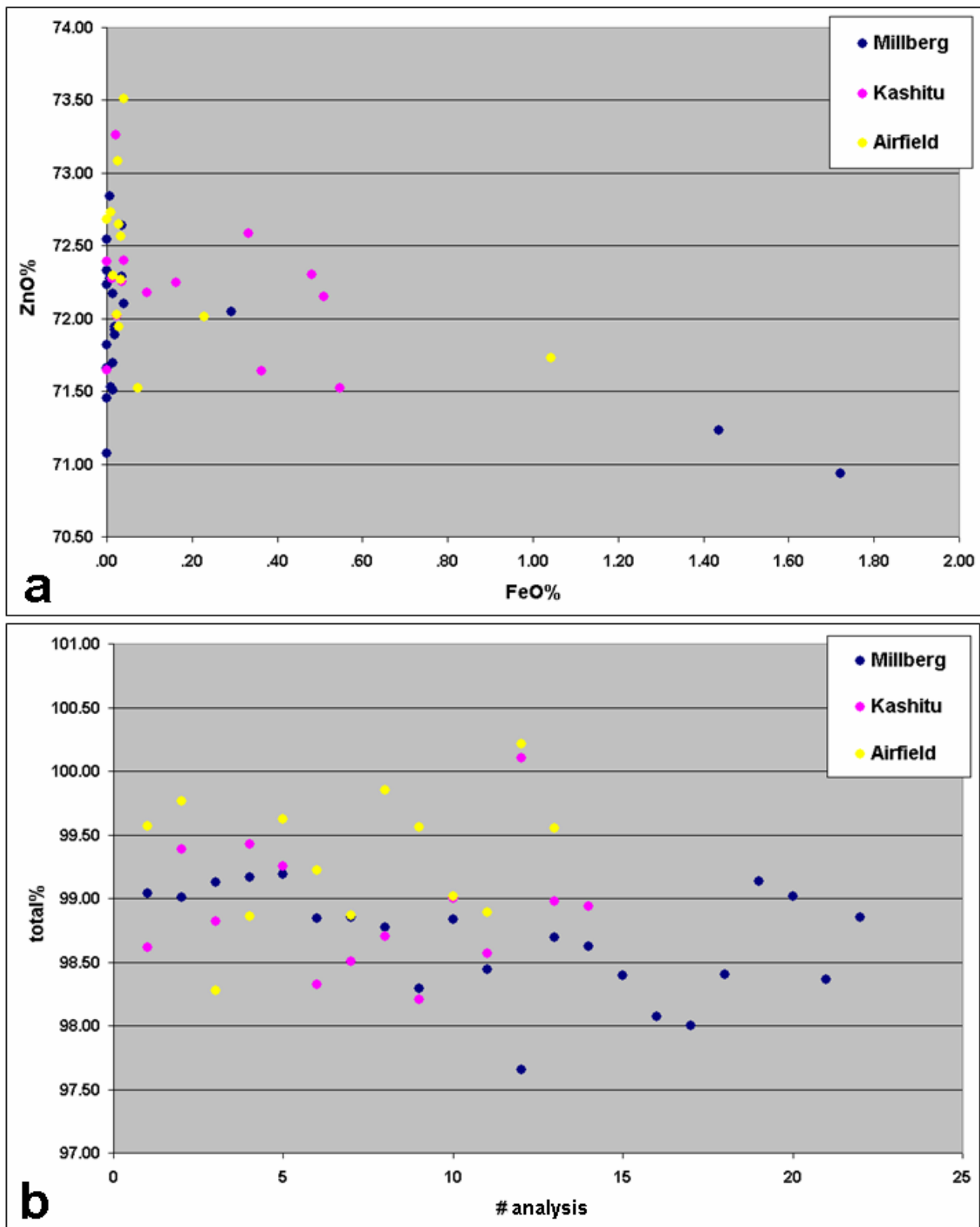


Figure 6.22: a) FeO%/ZnO% ratios measured with WDS for the Kabwe area willemite, mean ZnO = 72.25% (ideal ZnO% = 73.04%), mean FeO = 0.2%; **b)** WDS analyses totals % over no. of analyses ; total mean = 98.75% for 75% of the analysed points.

Therefore, micro disseminations of mainly goethite/hematite, as well as minor galena may be considered responsible for the shifting of the willemite luminescence colours.

The structural formula for the willemite from the Airfield, Kashitu and Millberg shows only negligible variation among the three prospects. Its composition should be considered as follows:

$[(\text{Zn}^{2+}_{1.97-2.00}\text{Fe}^{2+}_{0.03-0.00})(\text{Si}_{0.99-1.00})\text{O}_4]$, $[(\text{Zn}^{2+}_{1.98-2.00}\text{Fe}^{2+}_{0.02-0.00})(\text{Si}_{0.99-1.00})\text{O}_4]$ and $[(\text{Zn}^{2+}_{1.95-2.00}\text{Fe}^{2+}_{0.05-0.00})(\text{Si}_{0.99-1.00})\text{O}_4]$ respectively.

6.4.4 Mineralogy of willemite ore from the Lusaka area

The willemite ore of the Lusaka area was collected for this study almost exclusively from the Star Zinc prospect, with a few more specimens from the small Excelsior permit (figure 6.23). The mineralogical assemblage (table 6.5) is here completely different, but at the same time less complex than the ore assemblage in the Kabwe mining district. Willemite is the major Zn carrier together with Zn spinels (gahnite and franklinite) and abundant haematite. Little amounts of smithsonite, hemimorphite and sauconite occur at Star Zinc in the uppermost part of recent karst infillings.

6.4.4.1 Willemite

Radial-shaped willemite aggregates are predominant at both Star Zinc (hence the name) (figure 6.23a) and Excelsior (figure 6.23h). Willemite masses, where the crystals are difficult to distinguish (figure 6.7g) may also form important accumulations in these localities (figure 6.23c). Discrete veins of massive colophorm willemite are present as well (figure 6.23d). Ore textures vary from radial/globular to well-developed prismatic, with tiny spindly crystals growing in open spaces (figure 6.23e, 6.23h and 6.23c). Discrete crystals of willemite usually show a translucent luster.

Pure, well formed, crystals are usually white (figure 6.23h). A reddish brown (figure 6.23c) colour in willemite may be induced by minute disseminations of hematite or other opaque minerals (i.e. gahnite and franklinite). Willemite with abundant hematite inclusions appears black (figure 6.23e).

The luminescence of the Lusaka area willemites, observed under cathodic light varies from dull to bright green (figure 6.27b, 6.27d, 6.28b and 6.28h) and displays recurrent zonations. Finely zoned willemite crystals usually show an alternation of dull and bright green layers without any periodicity. The brightest colour usually corresponds to the physically purest willemite horizons; in the opaque hematite-rich layers the luminescence may be strongly inhibited (figure 6.27c and 6.27d). The XRD willemite spectra appear monotonously regular with no substantial crystallographic variation. Obtained willemite cell parameters are close to the ideal values for this mineral (mean axial ratios: $a:c = 1:0.63$, $a = b = 13.89$, $c = 9.37$). In figure 6.24 is shown a typical XRD pattern of Star Zinc willemite.

Figure 6.23: Outcrops and hand specimens from Star Zinc (a to g) and Excelsior (h) ore zones. a) radial zoned willemite (white to yellow) over dark calcite aggregate; b) willemite zebra-like mineralisation (Western Orebody); c) massive brownish willemite, with specular hematite and secondary whitish needle-like willemite in druses; d) late willemite fillings joints and fractures of the marble host rock (Eastern Orebody); e) specularite-rich willemite ore with late calcite alteration; f) kidney-like hematite concretion; g) recent mineralized infillings of karstic origin at Star Zinc; h) massive radial willemite over greenish clinocllore.

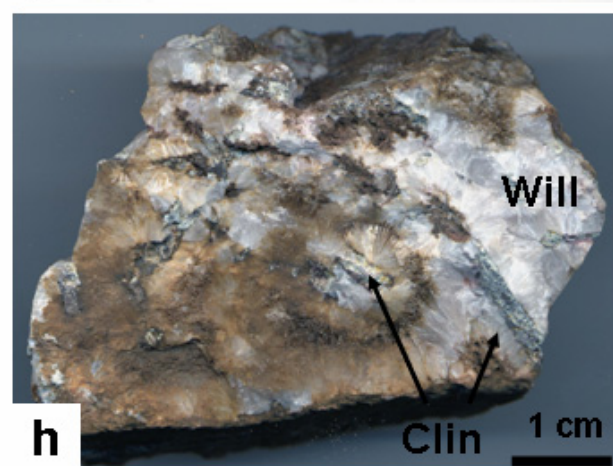
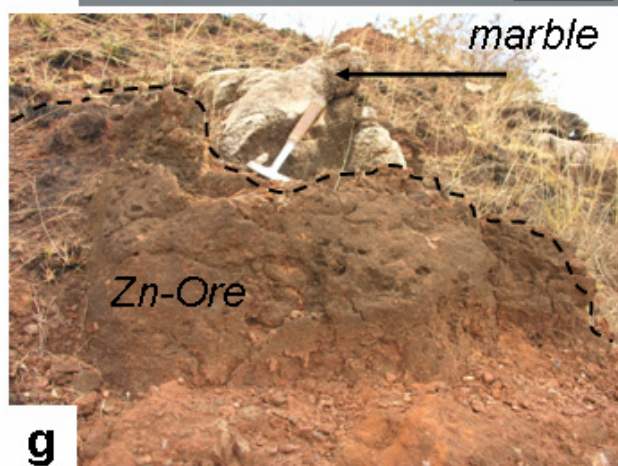
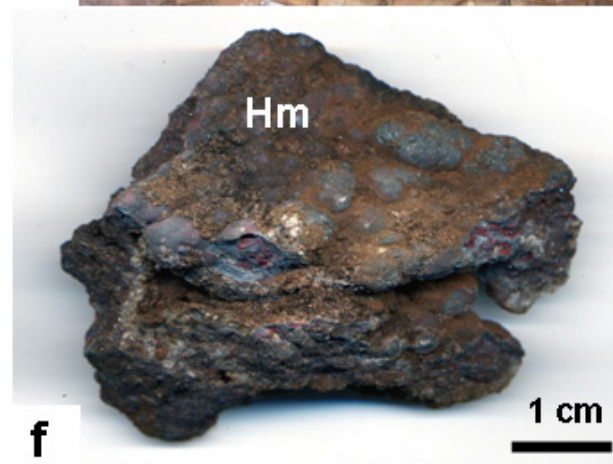
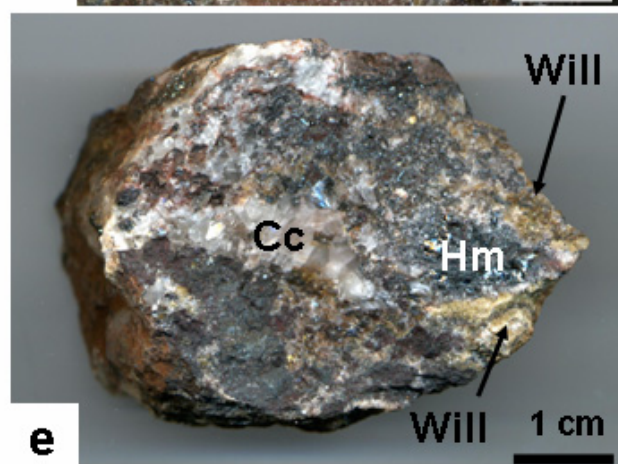
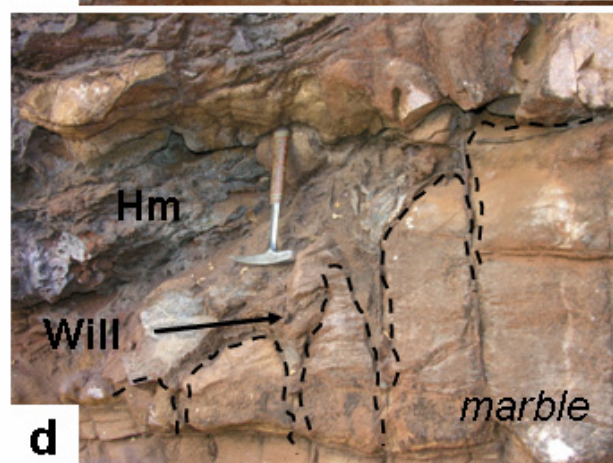
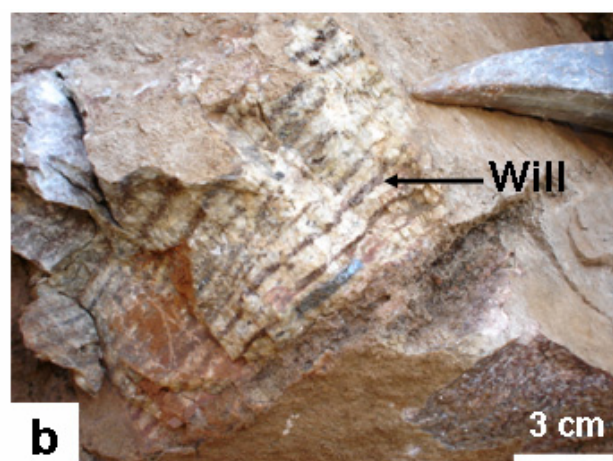
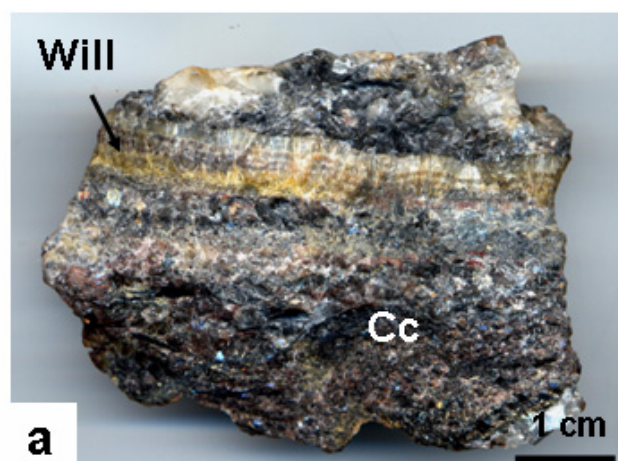


Table 6.5: XRD analyses of samples from Lusaka area deposits; mineral symbol in order of abundance.

Site	Sample No.	Mineral(s)	Site	Sample No.	Mineral(s)
Excelsior	ZA0538	Will, Clin	Star Zinc WOB	ZA0512-1	Will, He, Sph
Excelsior	ZA0538-1	Will, Clin	Star Zinc WOB	ZA0512-2	Will, Sph, He
Excelsior	ZA0540	Will	Star Zinc WOB	ZA0513-1	Cc
Excelsior	ZA0541C-1	Will	Star Zinc WOB	ZA0514-1	Will, Sph
Excelsior	ZA0541C-2	Will, Qtz	Star Zinc WOB	ZA0514-2	Will, Cc, Sph, He
			Star Zinc WOB	ZA0516-1	Will, Cc
Star Zinc EOB	ZA0524A	Will	Star Zinc WOB	ZA0516-2	Cc, Will
Star Zinc EOB	ZA0525-1	Cc	Star Zinc WOB	ZA0532-1	Will, He, Go
Star Zinc EOB	ZA0526-1	Cc	Star Zinc WOB	ZA0532-2	Will
Star Zinc EOB	ZA0528A-1	Will - He, Go, Mt, Ap	Star Zinc WOB	ZA0533-2	Cc, Qtz
Star Zinc EOB	ZA0528B	Will	Star Zinc WOB	ZA0533-1	Cc, Will
Star Zinc Karst	ZA0530	Hem	Star Zinc WOB	ZA0534-1	Will
Star Zinc Karst	ZA0531-1	Hem, Sauc	Star Zinc WOB	ZA0534-2	Will
Star Zinc Karst	ZA0531-2	Qtz, Hem, Do	Star Zinc WOB	ZA0535-1	Will, He
Star Zinc Ore Pile	ZA0518A-1	Will, Qtz	Star Zinc WOB	ZA0535-2	Will, He
Star Zinc Ore Pile	ZA0518A-2	Will	Star Zinc WOB	ZA0536-1	Cc
Star Zinc Ore Pile	ZA0518A-3	Qtz, Do, Will	Star Zinc WOB	ZA0537C-1	Will, He, Qtz
Star Zinc Ore Pile	ZA0518B-1	Will	Star Zinc WOB	ZA0537C-2	Will
Star Zinc Ore Pile	ZA0518B-2	Will, Py, He	Star Zinc WOB	ZA0528b	Will, Frn
Star Zinc Ore Pile	ZA0518B-3	Will, Do			
Star Zinc Ore Pile	ZA0519A-1	Will, Sph			
Star Zinc Ore Pile	ZA0521-1	Will			
Star Zinc Ore Pile	ZA0521-2	Will, Cc			
Star Zinc Ore Pile	ZA0522-1	Will, Sph			

Cc = calcite, Clin = clinocllore, Do = dolomite, Frn = franklinite, Go = goethite, He = hematite, Hem = hemimorphite, Mt = magnetite, Py = pyrite, Qtz = quartz, Sauc = sauconite, Sph = sphalerite, Will = willemite, EOB = Eastern Orebody, WOB = Western Orebody.

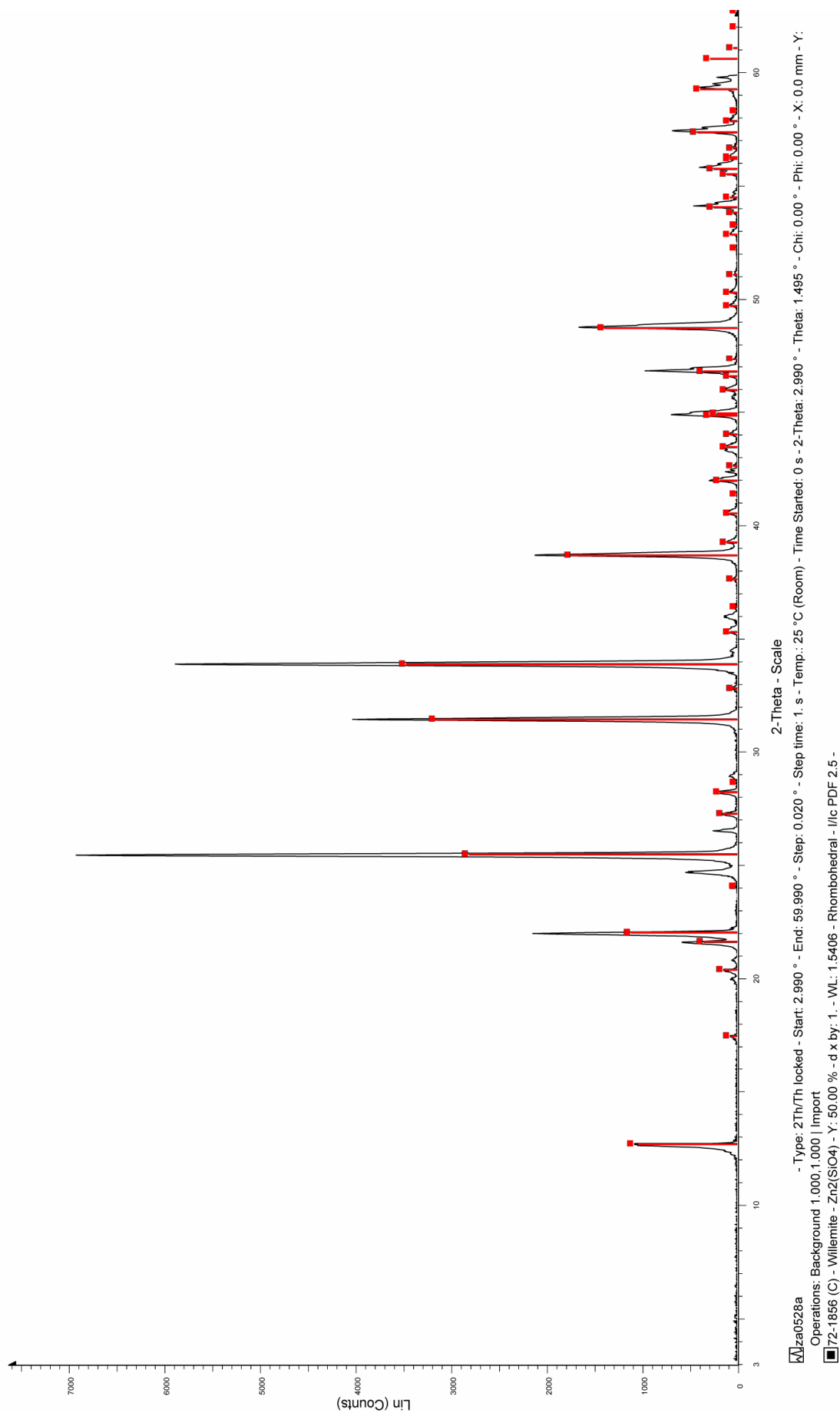


Figure 6.24: Typical XRD willemite spectrum, sample ZA0528A from Star Zinc.

6.4.4.2 *Other minerals*

While Excelsior main ore appears as a monomineralic accumulation of willemite, the ore association at Star Zinc accounts for many different mineral species, the most abundant of which is hematite.

Hematite occurs as an isolated, finely disseminated phase in willemite (figure 6.27a), as distinct tabular aggregates of specular crystals (figure 6.23e, 6.27a and 6.29b) or as massive kidney-like concretions (figure 6.23f). Moreover, in the surroundings of the Star Zinc pit a variably hematised dolomite has been commonly reported in the uppermost portion of the sequence (Matthews, 2005). Earthy hematite/goethite agglomerates are very common in the whole mineralized area. Reniform hematite with a botryoidal texture and commonly opaque with greyish/blackish colour occur occasionally. Specular hematite in tabular crystals has commonly a metallic luster and shows conchoidal fracture.

The second most common phase at Star Zinc corresponds to the association of the Zn spinels franklinite and gahnite. Franklinite generally occurs as perfectly cubic crystals, to be seen both as minute disseminations (figure 6.29c) as well as aggregates of subidiomorphic grains (figure 6.29d) throughout the willemite (figure 6.25). Franklinite may also crystallize as tiny cubes over random apatite grains (figure 6.29f). In polarized light the franklinite cubes (black in N II) stay opaque. Gahnite is less widespread than franklinite and usually occurs as an elongated phase, whose crystals are difficult to distinguish. Commonly gahnite appears olive green in thin section (figure 9.28e) and may contain inclusions of hematite lamellae (figure 9.29e).

The sulphosilicate genthelvite, a Zn-bearing mineral, occurs also as a minor phase. Greyish small masses of genthelvite are easy to detect in polarised light (figure 6.28c). They usually show a blue luminescence under cathodic light (figure 6.28d). Genthelvite never shows its pyramidal habit at Star Zinc, and may be found as irregular (figure 6.29d) aggregates, as well as fine disseminations/mixing halo in willemite (figure 6.29a).

Calcite, which displays a bright zone-like red luminescence under cathodic light, is the main carbonate phase that commonly replaces willemite (figure 6.23a). Apatite and white mica grains may also be present in the willemitic ore with their original mineralogical properties and habits.

Hemimorphite and sauconite are also present at Star Zinc, but just in the terruginous material of the recent karst infilling. They occur with abundant goethite and are optically indistinguishable from the red soil. Their presence can be detected only by XRD analysis (figure 6.26) .

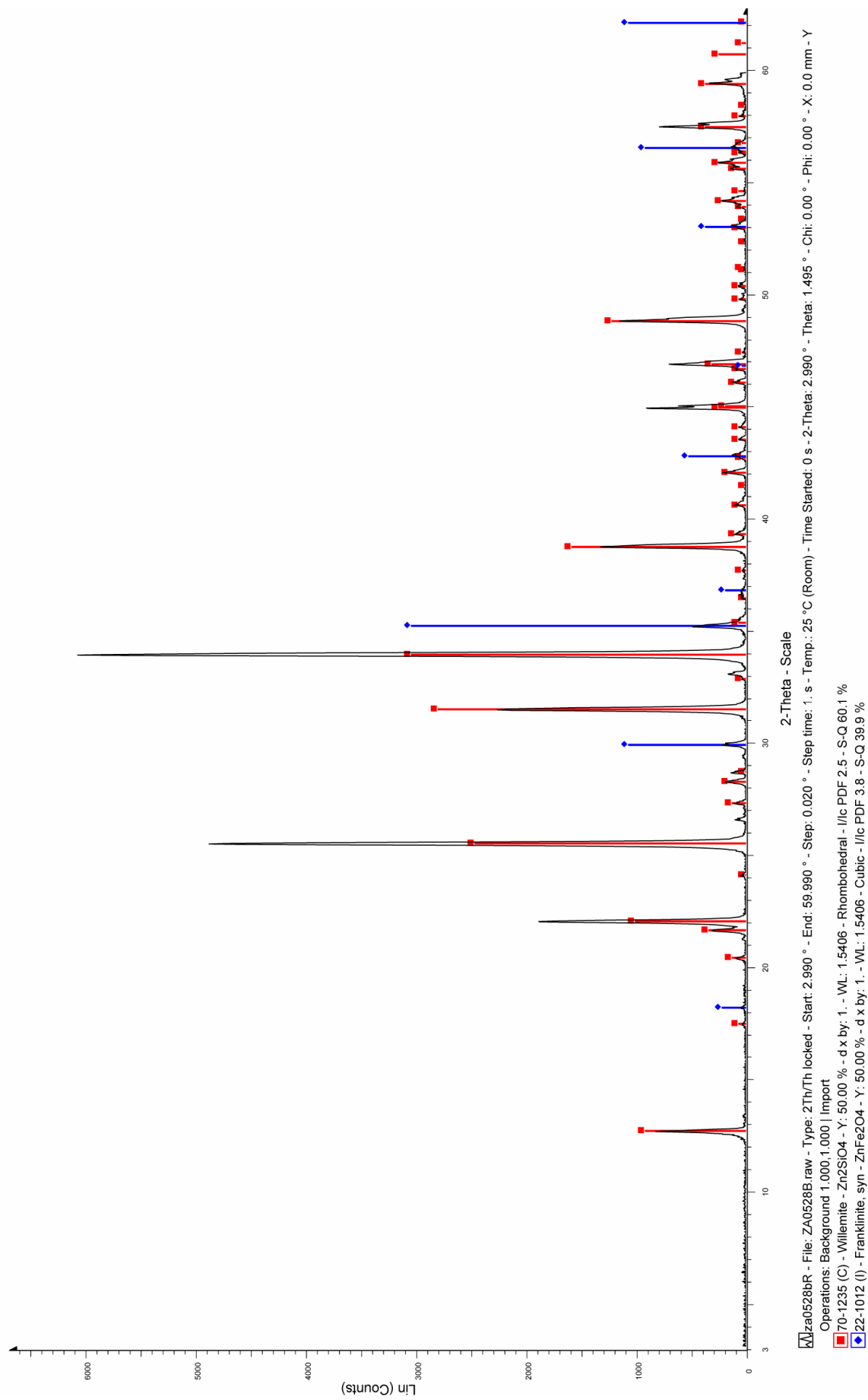


Figure 6.25: Willemite and franklinitite XRD spectra, sample ZA0528B from Star Zinc.

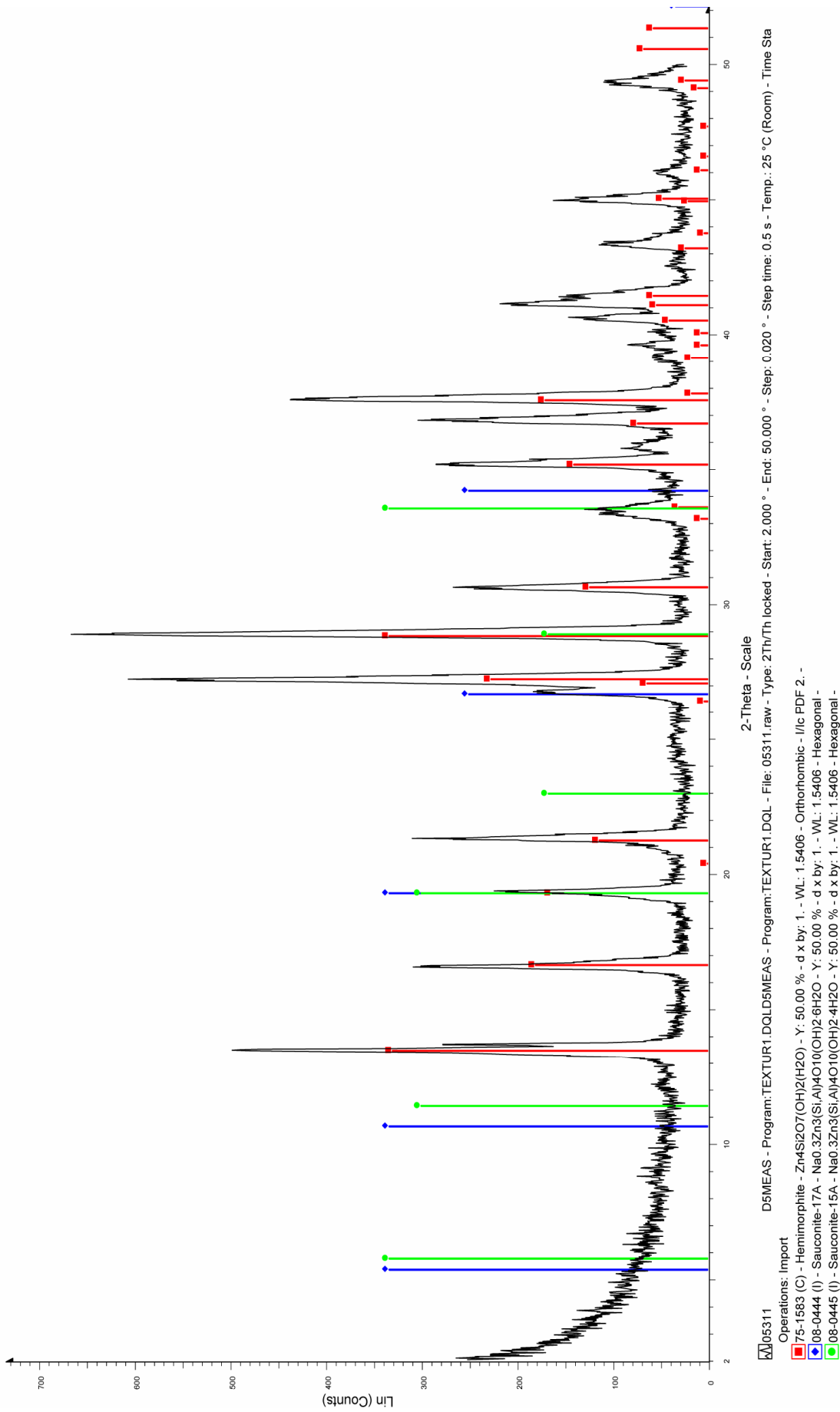


Figure 6.26: Hemimorphite and sauconite XRD spectra, sample ZA0531 from mineralised Star Zinc karst infillings. Goethite peaks are not shown.

6.4.5 *Petrography and paragenesis of willemite ore from Lusaka area*

Also the petrographic evaluation of the willemite ore from the Lusaka area is strictly referred to the Star Zinc deposit, considering the paucity of samples collectable from Excelsior. In the ore samples from the latter prospect, three well-defined willemite generations can be easily differentiated under cathodic light (figure 6.28g and 6.28h). Looking at the basal section of the willemite prism, in thin section, it is possible to identify distinct green-coloured zones. The increased luminescence from crystal core to rim is arranged in three sharps colour zones, corresponding to three successive willemite generations (figure 6.28h). In addition, at the core of each radial willemite aggregate (figure 6.23h), it is common to find clinocllore crystals, in turn almost completely replaced by willemite.

6.4.5.1 *Star Zinc deposit*

Since sulphides have been detected just in the XRD analyses (as sphalerite and pyrite) a negligible occurrence is supposed. The total impossibility to perform direct petrographic observation do not allow to clarify them paragenetic position.

Willemite at Star Zinc is generally replacing a previous mineral assemblage consisting of franklinite and gahnite. The replacement may be extended to the carbonate host rock and take the form of massive bodies (figure 6.23c) or discrete ore veins-like (figure 6.23d).

Franklinite and gahnite are typical spinels of metamorphosed sulphide zinc deposits, occurring i.e. at Vazante in Brazil (Monteiro et al. 2006) and Franklin-Sterling Hill in US (Johnson et al. 2003). At Star Zinc franklinite occurs as discrete crystals or aggregates (figure 6.29c and 6.29d), while gahnite just as not-completely-replaced remnants (figure 6.28e): both these minerals are involved in a first willemitisation event. Franklinite may be found as solid inclusions inside (figure 6.27a), or at the rim (figure 6.27c) of the willemite crystals. Franklinite cubes may be growing on apatite crystals (figure 6.29f). Franklinite may also contain small μm -sized inclusion (exsolution?) of Ag-bearing sphalerite. Differently from franklinite, gahnite seems to have been mostly replaced by willemite (figure 6.28e and 6.28f) and may enclose idiomorphic apatite crystals.

A first willemite generation (willemite I) usually follows a hematite/specularite generation that can affect and replace gahnite (figure 6.29b and 6.29e) as tiny lamellae. Willemite I has well-defined crystals, is generally homogeneously luminescent (figure 6.27b and 6.27d) and may contain several inclusions of rare earth elements phosphates. Willemite I also coexists with apatite and generally shows a reaction rim with the latter (figure 6.29f). Willemite I may have a replacive calcite gangue (figure 6.28a). A second hematite generation also occur postdating willemite I as well formed mm-sized tabular specularite crystals (figure 6.23e) or kidney-like concretions (figure 6.23f).

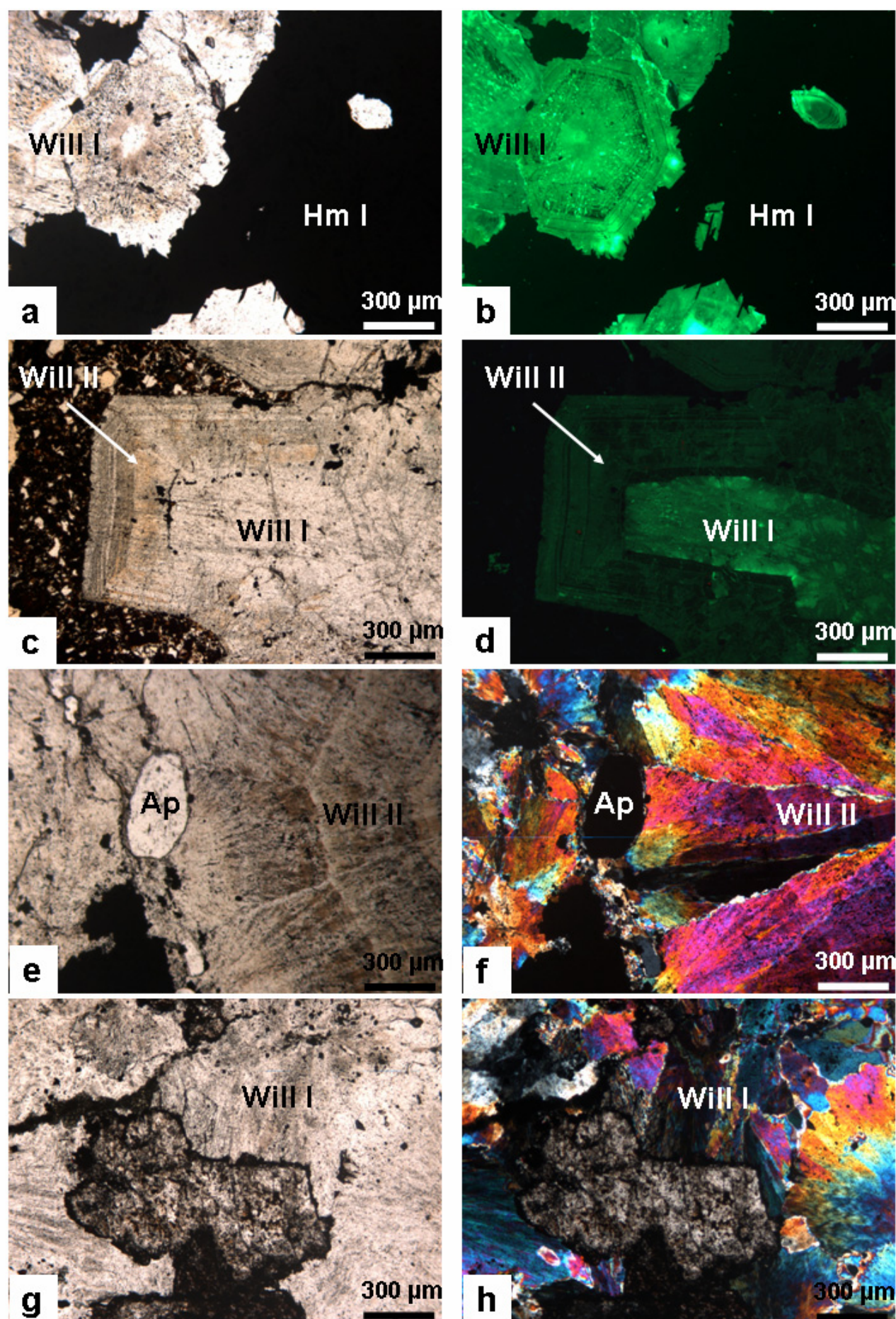
The mineral genthelvite also occurs in this first paragenetic stage. Genthelvite is a Zn-Be sulphosilicate occurring as accessory mineral in alkaline to peralkaline granites and related pegmatites and *greisen* (Burt, 1988). It is a mineral restricted to a low-S activity environment and in most cases it is transformed to sphalerite and willemite; free Be derives from Al saturation of feldspar in alkaline conditions (Burt, 1988). At Star Zinc genthelvite may be present as exsolution product in willemite (figure 6.29a) or as directly precipitated aggregates (figure 6.29d); genthelvite may also contains micrometric inclusions of Fe-Sr-Ba-Fe sulphates.

A second willemite generation (willemite II) postdates the above succession, usually filling the hostrock joints/fractures with a veins-like texture (figure 6.23d). According to Matthews (personal communication, 2005) two fracture systems are present in the marble hostrock (broadly N-S and E-W) and both of them are related to the Mwembeshi shear zone.

Profusely zoned willemite concretions can be observed in thin section under both polarized and cathodic light. A strong luminescence with colours ranging from dull to bright green is distinctive of each willemite layer.

At the top of the Star Zinc orebody, late karstification of the host rock produced an articulated morphology, where small “calamine” infillings with abundant hemimorphite and sauconite took place (figure 6.23g); goethite may occur as both kidney-like, hematite replacing, aggregates or as dissemination, giving to the “calamine” a reddish colour. The schematic paragenesis of Star Zinc is depicted in figure 6.30.

Figure 6.27: Images (polarized and cathodic light) of willemite ore from Star Zinc. a) massive willemite I after hematite I (NII); b) same as a in CL; c) zoned willemite II after massive willemite I (NII); d) same as c in CL; e) zoned willemite II and rounded (partially corroded) apatite crystal (NII); f) same as e at N+; g) remnants of carbonate hostrock in willemite I (NII); h) same as g in N+.



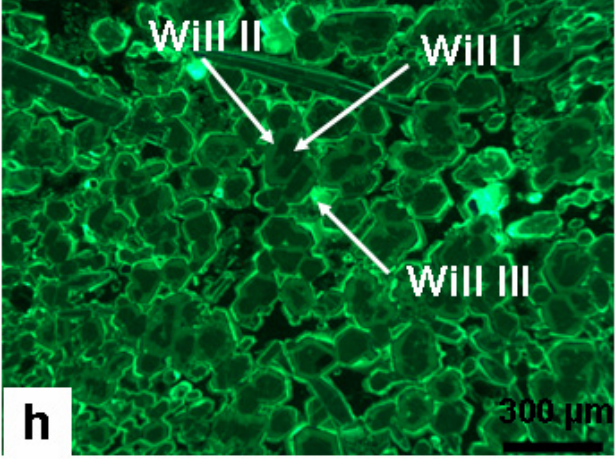
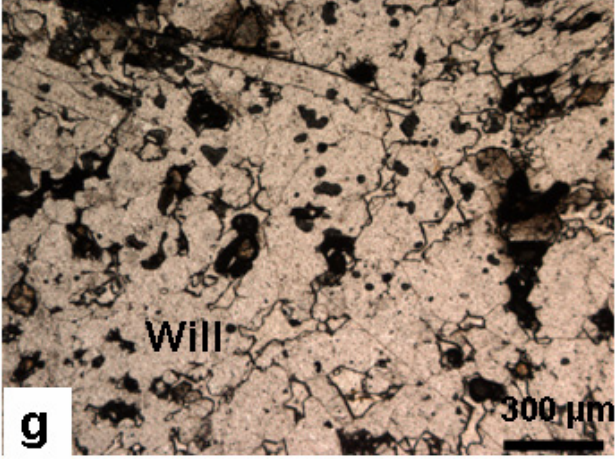
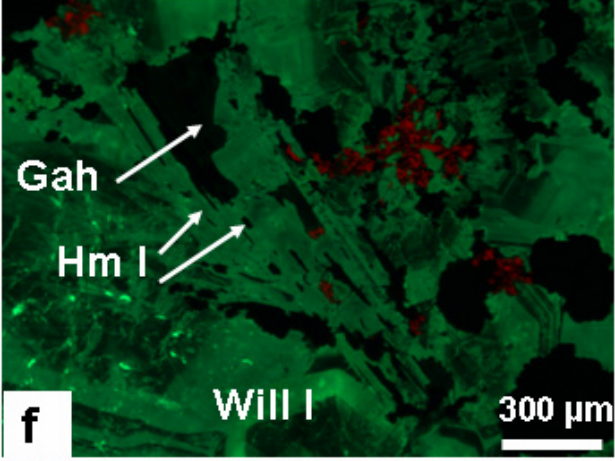
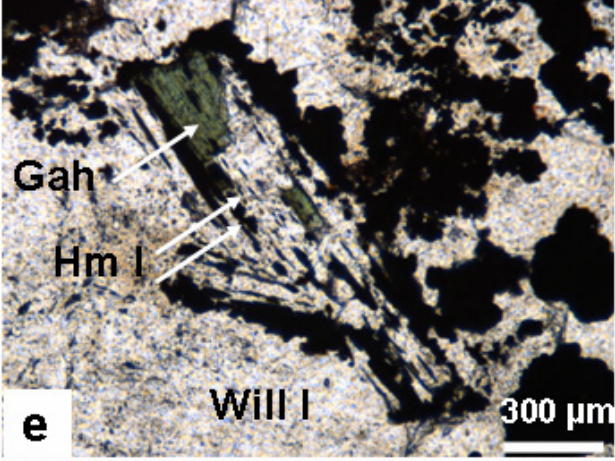
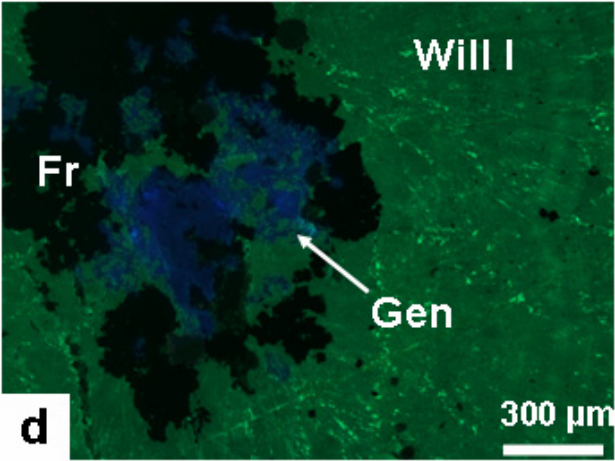
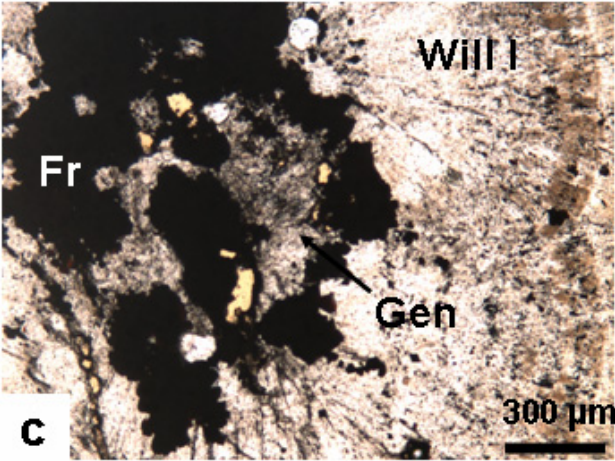
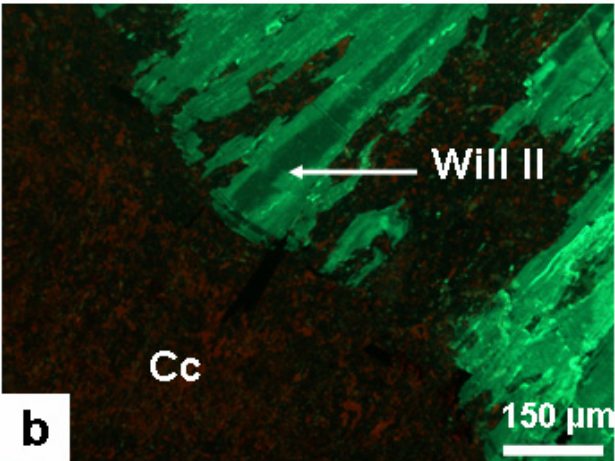
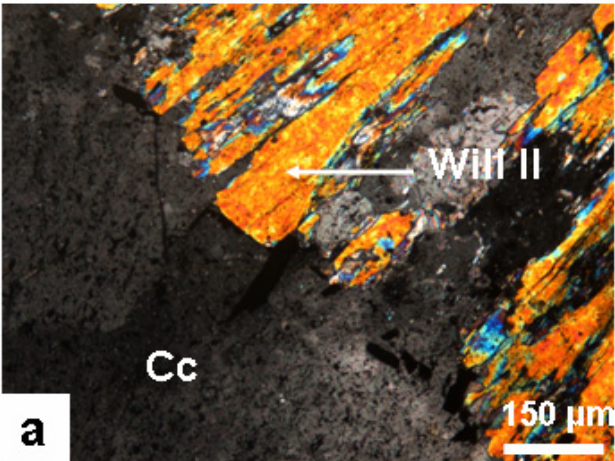
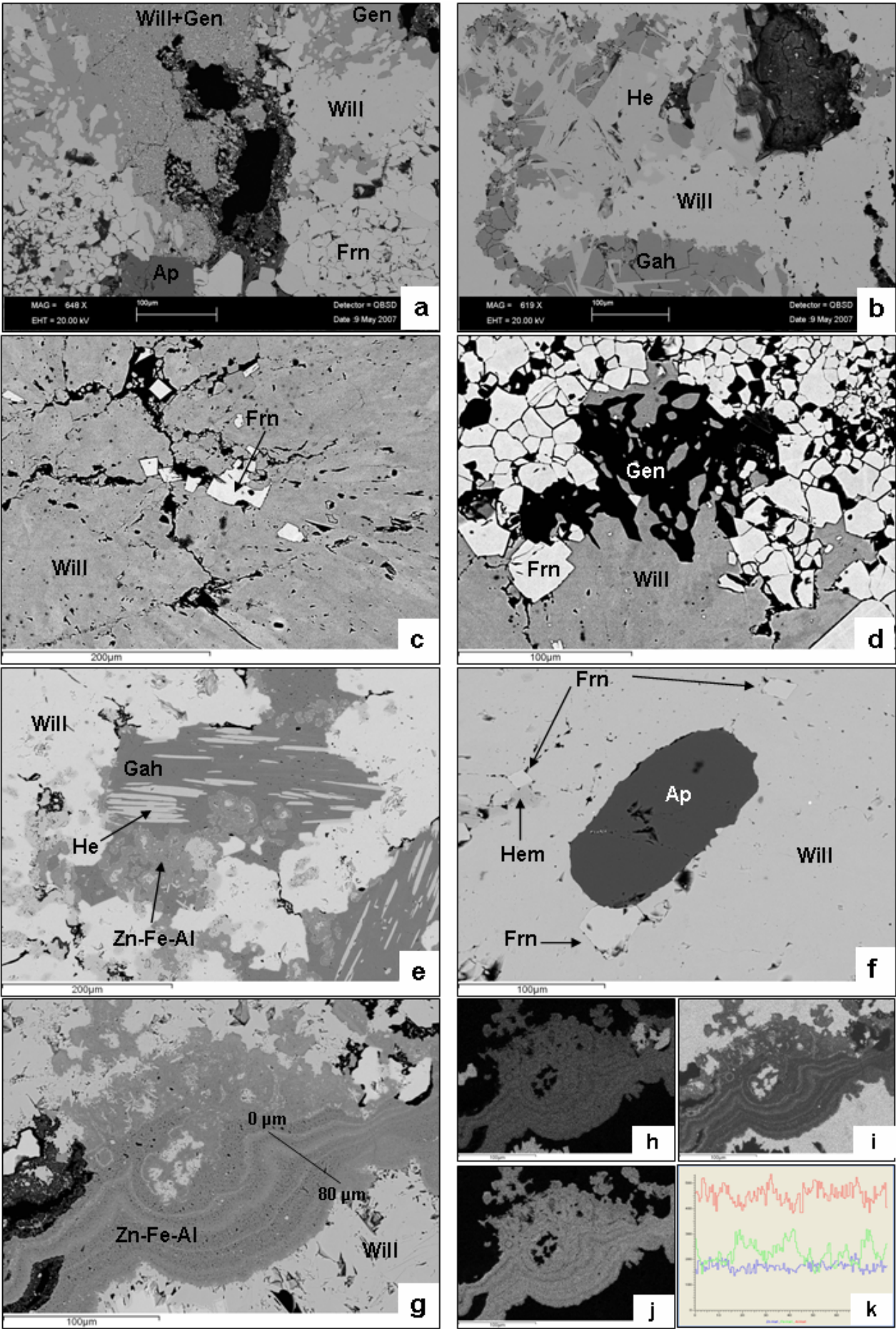


Figure 6.28: Images (polarized and cathodic light) of the willemite ore from Star Zinc (a to f) and Excelsior (g and h); a) willemite II replaced by calcite in the “zebra” ore (NII); b) same as a in CL; c) genthelvite (grey) intergrown with franklinite (black) and willemite I (whitish) (NII); d) same as c in CL; e) greenish crystal of gahnite and replacing hematite I lamellae and white willemite I (NII); f) same as e in CL g) willemite I, II and III (NII); h) same as g in CL, with the three willemite generations corresponding to the three green colour shades arranged with the darker in the core and the brighter at the rim.

Figure 6.29: BSE images on selected ore samples (ZA0512, a to d, and ZA0518, e to f) from Star Zinc. a) willemite I replacing franklinite and genthelvite occurring as disseminations in willemite; b) hematitised gahnite strongly replaced in turn by willemite I; c) dissemination of tiny franklinite cubes in willemite I; d) genthelvite after franklinite, both followed by willemite; e) hematite lamellae in gahnite replaced by willemite I; f) franklinite cubes growing on apatite, which shows a reaction rim with willemite I; g) micro zonations of Zn-bearing Fe-Al-hydroxides; h), i), j) Zn, Fe and Al, respectively, interference maps from figure g; k) Zn, Fe and Al variation pattern along the 0 - 80µm profile of figure g.



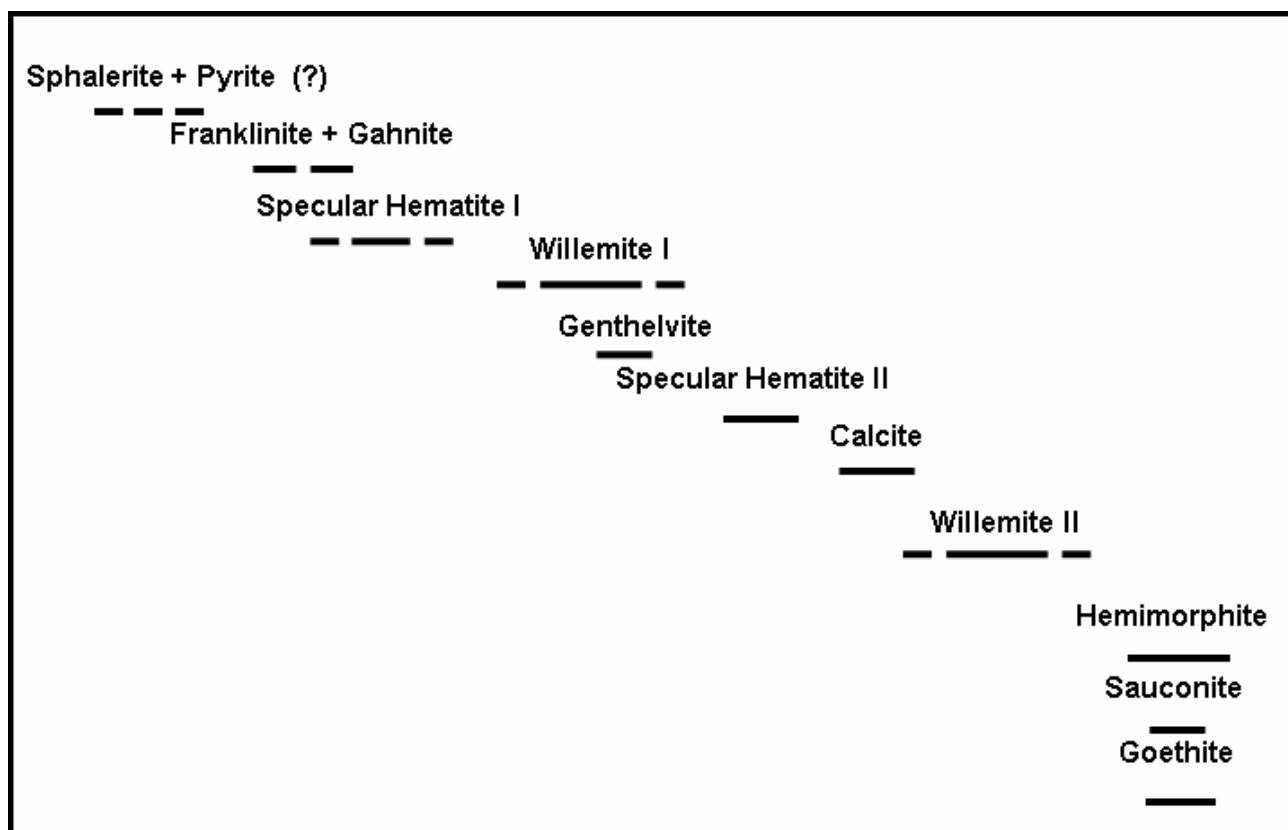


Figure 6.30: Mineral paragenesis of the Star Zinc orebody.

6.4.6 Major and trace element geochemistry of the willemite ore assemblage from Star Zinc

The willemite >> franklinite/gahnite ore at Star Zinc usually occurs with a total Zn grade higher than 20 wt%. The Fe wt%, associated with hematite and much less with spinels, generally does not exceed 5%.

In this section are presented several (WDS) geochemical analyses of the minerals occurring in the Star Zinc paragenesis: willemite (table 6.6), gahnite (table 6.7) and fluoroapatite (table 6.9). WDS franklinite analyses showed usually low totals (below 90-95%); in table 6.8 are presented the few analyses with the best-obtained data.

In performing the willemite analyses, Zn, Si, Mn, Mg and Cd were selected as standard elements to be compared with quoted values for the main, minor and trace elements in similar deposits. No substantial geochemical variation was found between the analytical values for willemite I and willemite II, which are remarkably precise in their stoichiometry. In fact, the ideal chemical values for willemite are as follows: $\text{ZnO} = 73.04\%$ and $\text{SiO}_2 = 26.96\%$, with 2 apfu Zn and 1 apfu Si.

Star Zinc willemites (table 6.6) show ZnO values ranging between 70.59% and 72.93% with a mean value of 72.12%. FeO can reach a maximum of 1.31% (minimum 0.16%, mean 0.12). The MnO,

Table 6.6: WDS analyses (% oxide) of willemite from Star Zinc (sample ZA0512).

	ZA12-1	ZA12-2	ZA12-3	ZA12-4	ZA12-5	ZA12-6	ZA12-7	ZA12-8	ZA12-9	ZA12-10	ZA12-11	ZA12-12
CdO	0.01			0.01	0.01	0.02		0.01	0.02			0.03
MnO	0.02	0.01				0.01				0.03		0.02
FeO	0.29	0.90	0.16	1.14	0.62	0.56	0.80	0.07	0.21	0.19	0.41	0.53
ZnO	71.84	72.39	72.22	71.60	72.90	72.12	72.87	71.98	72.80	72.53	72.93	72.26
MgO						0.01	0.05					
SiO₂	26.56	26.92	27.09	26.69	26.88	26.79	26.82	26.38	26.64	26.88	26.87	27.02
Total	98.71	100.23	99.47	99.43	100.40	99.50	100.54	98.44	99.66	99.63	100.20	99.87

	ZA12-13	ZA12-14	ZA12-15	ZA12-16	ZA12-17	ZA12-18	ZA12-19	ZA12-20	ZA12-21	ZA12-22	Mean
CdO	0.03	0.03	0.02	0.02	0.02						0.01
MnO	0.04						0.01		0.01	0.02	0.01
FeO	1.02	0.94	1.31	1.01	0.34	0.35	0.95	0.48	0.29	0.47	0.59
ZnO	71.40	72.15	71.00	70.59	72.64	72.47	72.03	72.23	72.14	71.47	72.12
MgO		0.02		0.01					0.01	0.01	0.01
SiO₂	26.70	26.88	26.83	27.04	26.93	26.73	26.88	26.84	26.66	26.83	26.81
Total	99.19	100.02	99.17	98.68	99.93	99.56	99.87	99.55	99.10	98.79	99.54

Table 6.7: WDS analyses (% oxide) of gahnite relicts in willemite ore from Star Zinc (sample ZA0512).

	ZA12-1	ZA12-2	ZA12-3	ZA12-4	ZA12-5	ZA12-6	ZA12-7	ZA12-8	ZA12-9	ZA12-10	ZA12-11	ZA12-12
MgO	0.01	0.01		0.03	0.01	0.01		0.01			0.02	0.04
Al₂O₃	49.32	48.93	49.23	49.14	48.98	50.26	50.19	50.03	49.39	48.52	49.15	50.64
SiO₂	0.59	0.49	0.5	0.8	0.85	0.44	0.14	0.15	0.13	0.13	0.54	0.96
CaO	0.01	0.01	0.01	0.01	0.01			0.01	0.01	0.02	0.01	0.01
TiO₂	0.03	0.01	0.02	0.02	0.02	0.03	0.04	0.02	0.03	0.04	0.07	0.07
V₂O₅	0.01	0.02	0.02	0.03	0.01	0.01	0.02	0.02	0.03	0.02		
Cr₂O₃	0.02		0.01	0.04		0.03	0.01	0.01	0.03	0.03	0.01	
MnO	0.01					0.02	0.02		0.01	0.03	0.02	0.01
FeO	7.7	7.67	7.68	6.79	7.17	6.81	6.89	7.27	7.7	8.69	7.85	5.83
NiO	0.04		0.04	0.08	0.03	0.01	0.05	0.02	0.06	0.01	0.02	0.01
ZnO	42.78	42.96	42.92	42.54	42.65	43.06	43.08	43.13	42.96	42.6	43.33	43.98
Total	100.50	100.11	100.43	99.47	99.74	100.69	100.43	100.64	100.33	100.09	101.51	102.05

	ZA12-13	ZA12-14	ZA12-15	ZA12-16	ZA12-17	ZA12-18	ZA12-19	ZA12-20	ZA12-21	ZA12-22	Mean
MgO	0.01	0.01	0.01	0.01	0.02		0.01	0.04	0.04	0.01	0.02
Al₂O₃	50.1	49.81	50.02	49.02	48.94	49.86	49.78	50.15	49.82	49.11	49.48
SiO₂	0.53	0.59	0.43	0.65	0.53	0.44	0.17	0.69	0.99	0.10	0.48
CaO				0.01	0.01		0.01	0.02	0.01		0.01
TiO₂	0.06	0.06	0.05	0.03	0.01	0.01	0.02	0.03	0.03	0.01	0.03
V₂O₅				0.02		0.02	0.02	0.01	0.02	0.03	0.02
Cr₂O₃			0.01	0.01	0.03	0.01	0.03		0.02		0.02
MnO	0.01	0.01	0.01		0.01	0.01		0.01	0.01		0.02
FeO	7.3	6.74	6.84	7.75	7.74	6.80	7.48	6.19	6.16	8.55	7.34
NiO	0.03	0.04	0.05	0.02	0.05	0.01	0.06	0.01	0.01	0.04	0.03
ZnO	43.61	43.32	43.85	43.44	43.29	43.42	43.46	43.97	43.77	43.18	43.00
Total	101.84	101.13	101.77	100.94	100.62	100.57	101.04	101.11	100.86	101.03	100.50

Table 6.8: WDS analyses (% oxide) of franklinite in willemite ore from Star Zinc (sample ZA0512).

	ZA12-1	ZA12-2	ZA12-3	ZA12-4	ZA12-5	ZA12-6	Mean
TiO₂			0.11	0.12	0.07	0.08	0.095
Al₂O₃	1.74	1.66	1.71	1.64	1.76	1.76	1.71
Fe₂O₃	63.6	63.74	62.87	62.59	61.67	61.67	62.69
FeO	0.09	0.29	0.79	0.84	0.89	1.23	0.69
MnO	0.03	0.05	0.02	0.03	0.04	0.04	0.04
MgO	0.02	0.01	0.02				0.02
Cr₂O₃			0.04	0.04	0.04	0.01	0.03
ZnO	33.61	33.41	32.69	32.49	31.95	31.57	32.62
Total	99.07	99.16	98.25	97.75	96.42	96.36	97.84

Table 6.9: WDS analyses (% oxide) of fluoroapatite inclusion in willemite ore from Star Zinc (sample ZA0512).

	ZA12-1	ZA12-2	ZA12-3	ZA12-4	ZA12-5	ZA12-6	ZA12-7	ZA12-8	ZA12-9	ZA12-10	ZA12-11	ZA12-12	ZA12-13	ZA12-14	ZA12-15	ZA12-16	Mean
Na ₂ O	0.03	0.02	0.04				0.01						0.02		0.02		
F	3.85	3.88	3.87	3.84	3.83	3.79	3.91	3.86	3.45	3.61	3.56	3.93	3.97	3.38	3.62	3.75	
MgO	0.01						0.01					0.01			0.04		
Al ₂ O ₃								0.02	0.02	0.02	0.01						
SiO ₂	0.06				0.02		0.04	0.05		0.01	0.06	0.02		0.03	0.02		
P ₂ O ₅	43.48	42.01	42.76	43.06	42.76	41.72	43.05	41.78	42.62	42.17	43.98	42.62	41.55	43.15	42.68	42.61	
CaO	55.09	54.19	54.90	54.90	54.77	55.58	54.65	54.65	55.16	55.29	54.88	54.91	54.51	55.55	55.01	54.99	
SO ₃	0.05	0.13	0.06	0.10				0.03			0.11				0.12		
Cl			0.01					0.12		0.01	0.06	0.02	0.03	0.06	0.12		
K ₂ O	0.01			0.05	0.05		0.02	0.02	0.01			0.01		0.01			
MnO	0.16	0.05			0.23	0.14			0.18			0.11	0.01	0.04	0.16	0.07	
FeO	0.08	0.18	0.09		0.42		0.57					0.16	0.81	0.03	0.12	0.15	
SrO				0.06	0.06	0.05	0.02						0.11				
La ₂ O ₃	0.13	0.14		0.05		0.02			0.06	0.11		0.14		0.13	0.07	0.07	
Ce ₂ O ₃				0.02			0.03	0.03	0.07	0.13	0.15						
Total	102.54	100.78	101.90	102.13	102.14	101.28	102.30	100.55	101.55	101.34	102.82	101.92	101.00	101.73	102.59	101.98	101.57
O=F	1.62	1.63	1.63	1.62	1.61	1.59	1.65	1.63	1.45	1.52	1.50	1.65	1.67	1.51	1.42	1.53	1.58
TOTAL	100.92	99.15	100.27	100.51	100.52	99.69	100.65	98.93	100.10	99.82	101.32	100.27	99.33	100.21	101.17	100.45	100.21

MgO and CdO mean values never exceed 0.01%, with a maximum for Mn at 0.05%. The average total of the analysis is 99.54, the mean total stoichiometry ($\text{Si}+\text{Zn}+\text{Mn}+\text{Mg}+\text{Cd} = 3$ apfu) is 3 with the following mean values: Zn 1.98 apfu, Si 1 apfu and Fe 0.02 apfu. The structural formula for willemite from Star Zinc shows only negligible variation: $[(\text{Zn}^{2+}_{1.96-2.00}\text{Fe}^{2+}_{0.04-0.00})(\text{Si}_{0.99-1.00})\text{O}_4]$ and appear even more pure (almost no Mn or Cd and lower Fe) than the Kabwe area willemites analysed, thus the lower iron content may not inhibit the green luminescence produced by poor (mean 0.01% and less than 0.01apfu) Mn concentration.

The ZnO content in gahnite (table 6.7) ranges between 42.54% and 43.97%, with a mean value of 43.24%. Al_2O_3 varies between 48.52% and 50.64% (mean 49.56%). Star Zinc gahnite is particularly iron-rich with the following FeO values: minimum 5.83%, maximum 8.69% and mean 7.24. SiO_2 has a mean value of 0.49%.

ZnO content in franklinite (table 6.8) ranges between 31.97% and 33.61%, with a mean value of 32.62%. According to Carmichael (1967), recalculated Fe_2O_3 varies from 61.67 to 63.74% (mean 62.69%) whilst just minor FeO has been detected. Star Zinc franklinite is particularly Al-rich with the following Al_2O_3 values: minimum 1.64%, maximum 1.76% and mean 1.71%. Unlike the ideal franklinite, only a negligible MnO content (<0.02%) has been detected in the Zambia mineral. Based on 32 oxygens and 24 cations (Carmichael, 1967), the structural formula of the Star Zinc franklinite is as follows: $(\text{Zn}^{2+}_{7.81}\text{Fe}^{2+}_{0.19}\text{Mn}^{2+}_{0.01})_{8.01}(\text{Fe}^{3+}_{15.31}\text{Al}^{3+}_{0.66}\text{Ti}^{3+}_{0.02})_{15.99}\text{O}_{32}$.

Several apatite grains (table 6.9) were analysed in order to discover their nature and provenance. They contain average values of 3.75% F, which could point to a magmatic origin. Spot EDS analyses have also revealed a low (3%) Zn content. After Charlet et al. (2006), the production of Zn-complexes on the surface can drastically reduce the dissolution rate of apatite in acid solution.

A few analyses have also been carried out on the recent supergene karst infillings around the main body, in order to obtain the Zn content of the grade of its eluvial cover. Bulk analyses carried out by ICP-MS on this “*calamine*” ore, show a Zn content of 45 wt %, 35 wt % Fe and Ag @ 5gm/t. Ag could originate from the degradation of the minute silver-rich sphalerite inclusions commonly detected in franklinite (EDS analyses showed a 0.7 wt% Ag grade).

6.5 Thermometric analysis of fluid inclusions

A fluid inclusions study of suitable willemite phases (transparent) from Star Zinc and Excelsior prospects (Lusaka area), and of the sphalerite from the Millberg prospect (Kabwe area) has been carried out. The inclusions assemblage was defined by a preliminary petrographic study on willemite I, willemite II and late calcite from Star Zinc (cfr § 6.4.5.1), on the only available willemite generation from Excelsior (cfr § 6.4.5) and on the Millberg sphalerite (cfr § 6.4.2.4). The

measurements were conducted through a heating-cooling procedure with observation of the homogenisation temperature (T_h), as well as the ice melting (T_m) temperature has been determined for most inclusions. The eutectic temperature (T_e) was established only in few cases, due to the optical limits preventing the identification of phase changes.

No fluid inclusion study has been produced so far on the Kabwe willemite, while for the Star Zinc prospect the following data have been published by Sweeney et al. (1991): homogenization temperature 150-250° C, salinity 7-12 eq wt% NaCl.

The willemites from the Kabwe area (Kabwe deposit, Airfield and Kashitu prospects) contain usually small (5 to 10 μm), monophase primary inclusions and two phase (liquid + vapour) secondary inclusions. These inclusions are generally not suitable for microthermometry, and have been only randomly analysed with disappointing results. Fluid inclusions on primary sulphides in the Kabwe mining district had been measured by Kamona et al. (2007). Two FI populations have been reported from a mineralised sphalerite+dolomite vein: type I has T_h between 98 and 178° C and salinity corresponding to 11.5 eq wt% NaCl, while type II shows T_h between 257 and 385° C and 31 eq wt% NaCl.

Willemite I generation (figure 6.31) at Star Zinc contains clouds of relatively small (10 to 25 μm), primary two phase (L+V) and monophase (L) inclusions (figure 6.32), usually subhexagonal to rounded in shape, localised at the core of the crystals (figure 6.27a and 6.27b). These are the same crystals that are usually disseminated with minute solid inclusions of franklinite (figure 6.29c, 6.31a and 6.31d). Secondary, monophase and two-phase (L+V) elongate inclusions (sizes exceeding 20 μm) have been also detected (figure 6.32d). They usually follow the direction of the crystallographic axis (c axis). A well-defined cleavage along this direction may lead to leaking and necking down phenomena (figure 6.32c).

Willemite II (figure 6.32c and 6.32d) contains predominantly secondary, mainly monophase inclusions at Star Zinc. The primary inclusions are too small to allow an accurate and systematic measurement. In the calcite replacing willemite I at Star Zinc (figure 6.25a and 6.25b), both primary (rare) and secondary (common) inclusions occur, which are generally monophase.

Fluid inclusions in the willemite from the Excelsior prospect (figure 6.32a and 6.32b) are randomly distributed in the crystals. Both primary and secondary inclusions occur (monophase and two-phase), frequently distributed with the same pattern as in the Star Zinc willemite I.

Green-yellowish crystals of sphalerite from Millberg have also been measured for their fluid inclusions, to compare their data with those of the Kabwe sulphides and with those of the willemites. Two-phase (L+V) primary inclusions prevail at Millberg (figure 6.32e and 6.32f), whose maximum size reaches up to 25 μm . The fluid inclusions are mainly located in the crystal cores. Temperatures

and salinities from Millberg sphalerite (figure 6.35a and 6.35b) have a very narrow spread, where T_h is constrained between 200 and 240° C, and salinity varies from 10 to 16 eq. wt% NaCl. No data exist about the eutectic temperature of this sphalerite, due to the optical limits of observation.

The microthermometric data for Star Zinc willemite and calcite are presented in table 6.10; the data for the Excelsior willemite and Millberg sphalerite are grouped in table 6.11.

Primary inclusions (figure 6.33a and 6.33b) in willemite I at Star Zinc show T_h between 210 and 250° C, and salinities between 12 and 16 eq. wt% NaCl. Secondary inclusions (figure 6.33c and 6.33d) have T_h between 170 and 210° C and salinities between 6 and 10 eq. wt% NaCl. Secondary inclusions in willemite II generation are supposed to have been trapped below 50° C (Goldstein and Reynolds 1994) and they show salinities close to 0 eq. wt% NaCl.

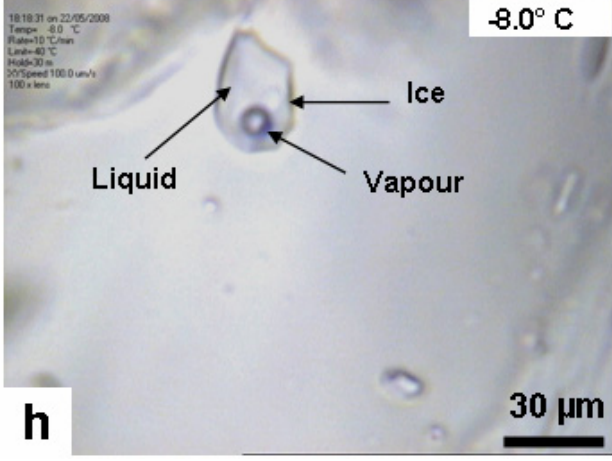
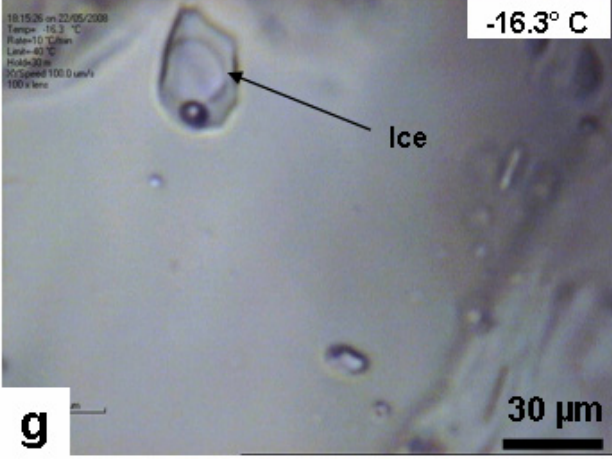
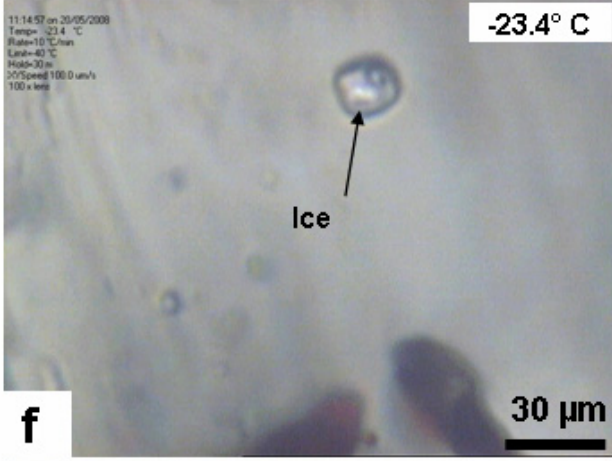
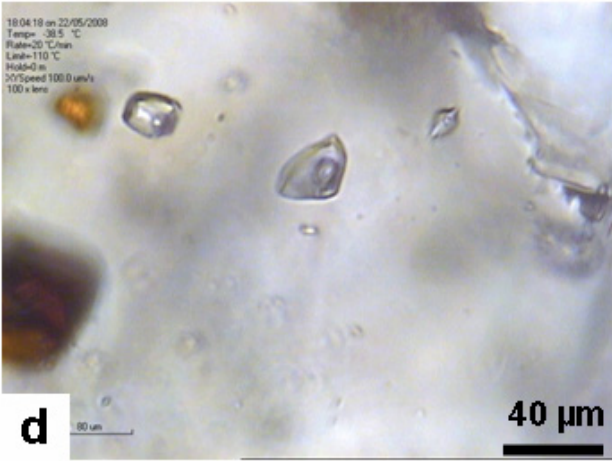
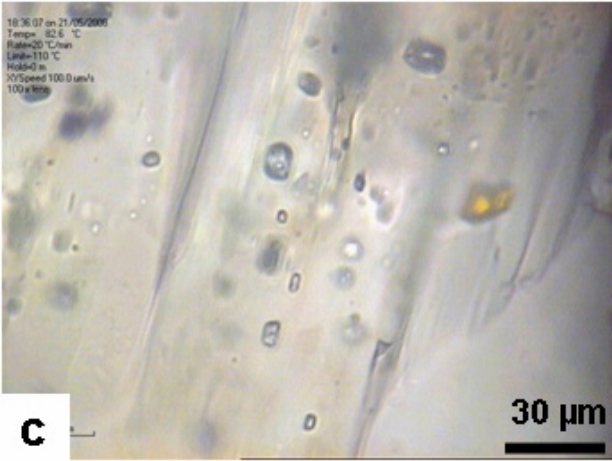
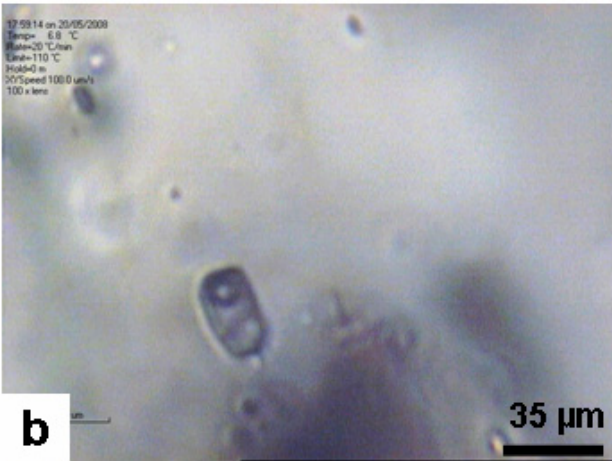
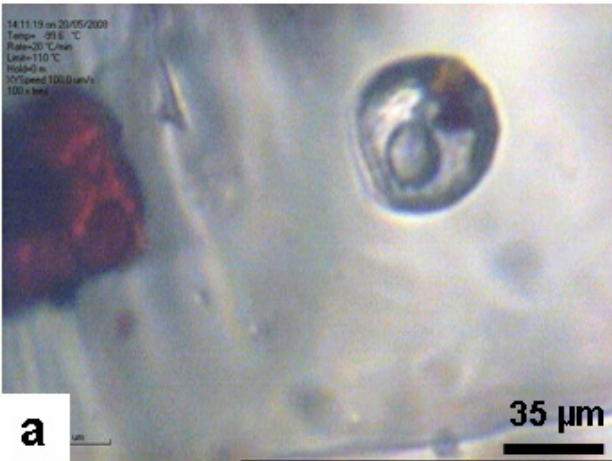
The few data collected in the Star Zinc calcite (T_h ca 50-60° and salinities always below 1 eq wt% NaCl) point to a meteoric/very low-temperature hydrothermal origin of these late fluids.

The homogenization temperatures (T_h) of the primary inclusions (figure 6.33e and 6.33f) of Excelsior willemite are grouped mainly around 190-230° C, with a spread from 160 to 250° C. The salinities show a lower dispersion and are concentrated between 10 and 16 eq. wt% NaCl. The secondary inclusions show a fair amount of dispersion in the homogenization data (figure 6.33g and 6.33h), with T_h ranging between 170 and 250° C, and salinities corresponding to an interval of 2-6 eq. wt% NaCl.

The fluid inclusion data presented in this paragraph support the conclusion that low temperature fluids (supergene?) have deposited the willemite in the Kabwe area. In the prospects from the Lusaka area (Star Zinc and Excelsior, fig 6.34) the most relevant FIs populations of the willemite are: I) T_h 200-250° C and the salinity 10-16 eq wt% NaCl (primary FIs), II) T_h 150-200° C with salinities of 2 - 10 eq wt% NaCl (secondary FIs).

Only few eutectic temperatures have been detected from willemite FIs at Star Zinc. T_e (figure 9.28f, 9.28g and 9.28h) is comprised between -23.4° and -16.3° C, close to NaCl-H₂O eutectic temperature.

Figure 6.31: Microphotograph of two-phase fluid inclusions from Star Zinc willemite (sample ZA0533 from Western Orebody). a) primary rounded inclusion near an opaque red franklinite grain; b) primary inclusion c) aligned secondary inclusions; d) primary inclusions near an opaque red franklinite grain; e) secondary inclusion; f) start of ice melting in a primary inclusion; g) start of ice melting in another primary inclusion; h) g at -8.0° C.



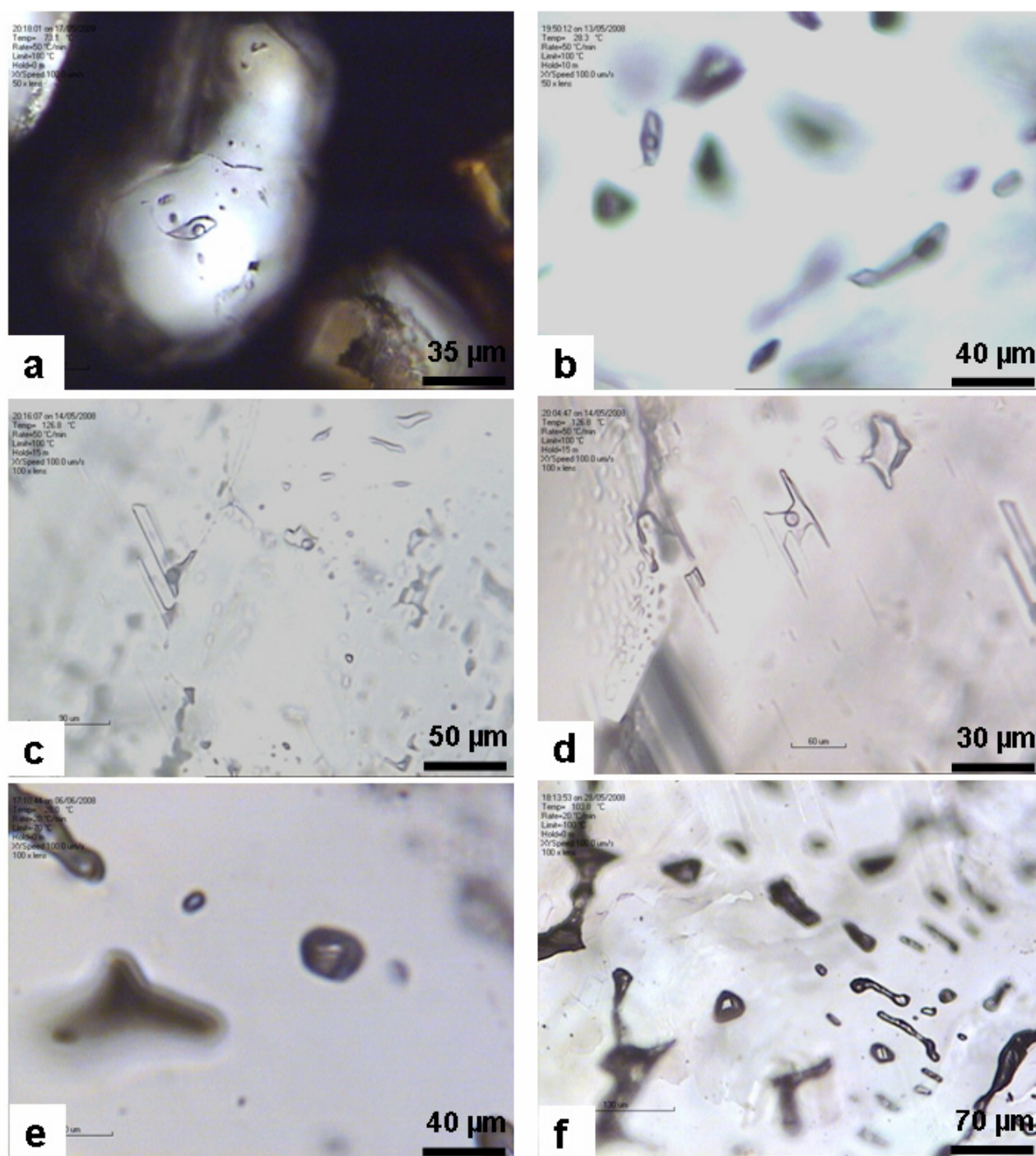


Figure 6.32: Microphotograph of two-phase fluid inclusions from the Excelsior willemite (a and b, sample ZA0538), Star Zinc (c and d, sample ZA0524A, Eastern Orebody) and Millberg sphalerite (e and f, sample KM19109). a) primary inclusion of an hexagonal willemite crystal; b) primary inclusions in range; c) necking-down in secondary inclusions ; d) secondary inclusions e) primary rounded V-rich inclusion; f) primary and secondary inclusions;

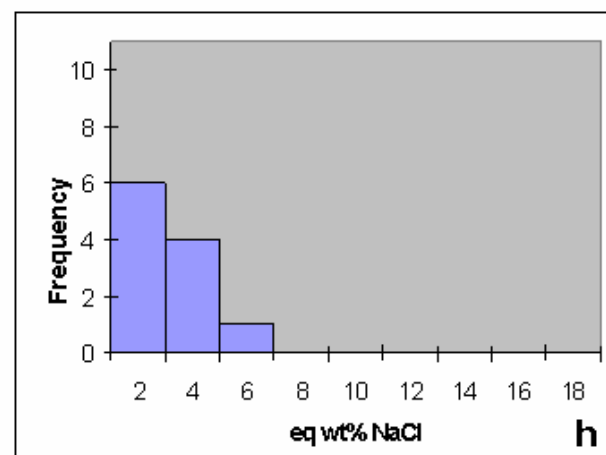
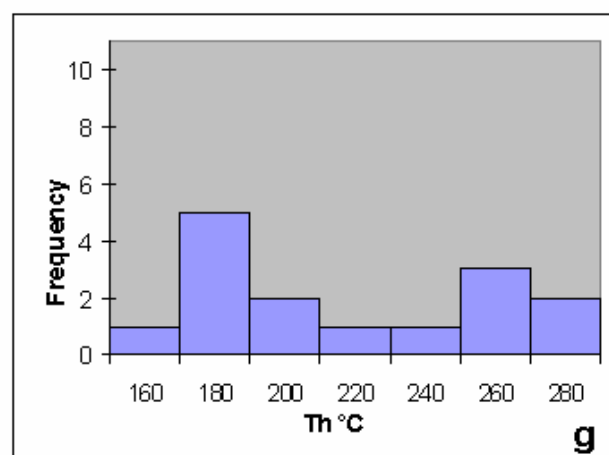
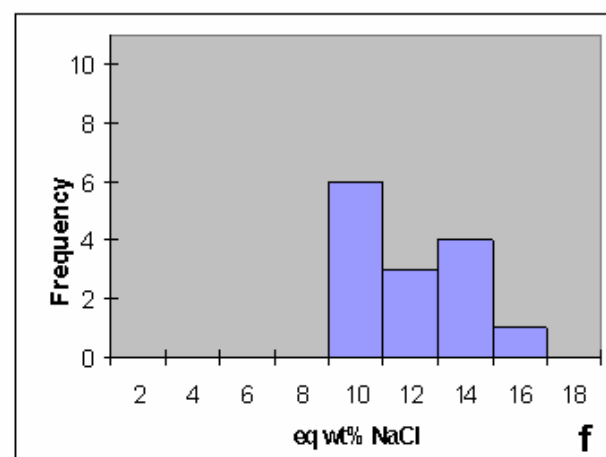
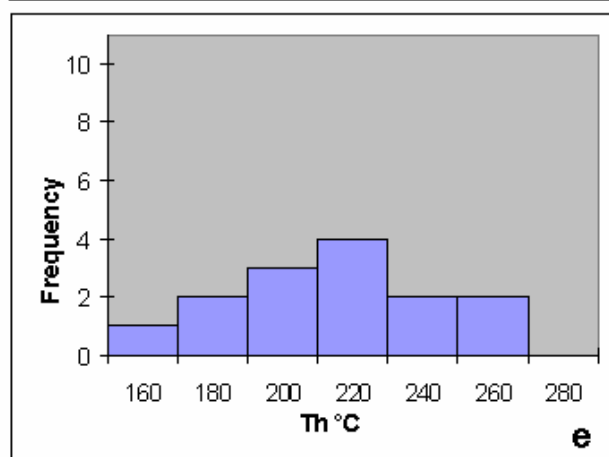
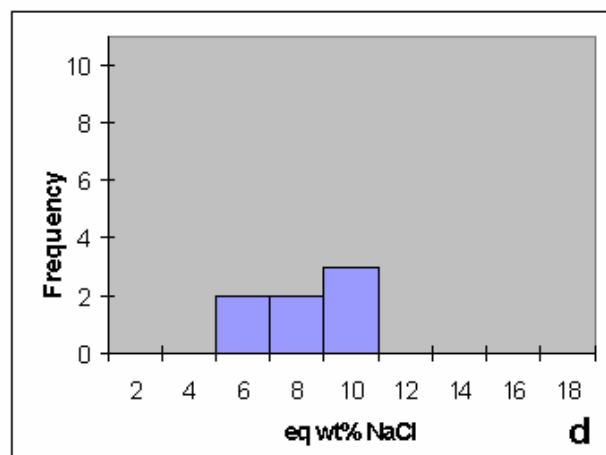
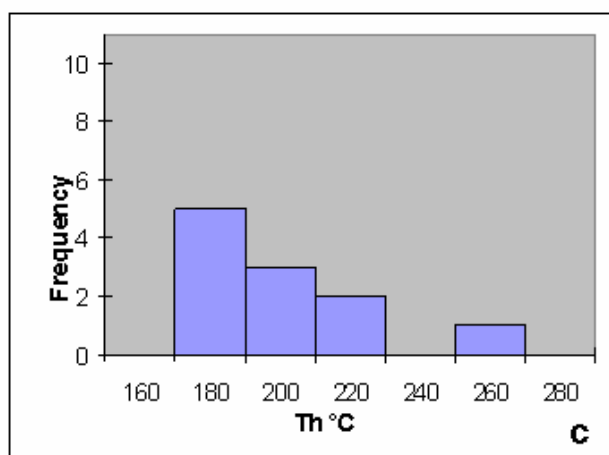
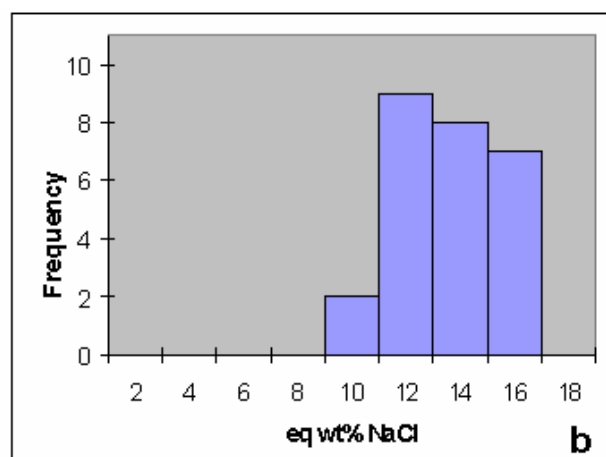
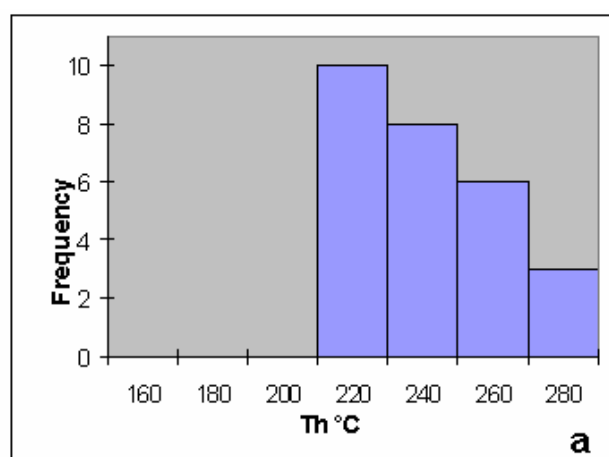
Table 6.10: Microthermometric analyses on willemite from Star Zinc.

Sample	Mineral	I. no	Tm T°	Salinity eq. wt% NaCl	Th T°	Type	Sample	Mineral	I. no	Tm T°	Salinity eq. wt% NaCl	Th T°	Type
ZA0533	Willemite I	1.a1	n.d.	n.d.	161.7	secondary	ZA0533	Willemite I	15c	-7.1	10.61	203.4	primary
ZA0533	Willemite I	1.a2	n.d.	n.d.	179.3	secondary	ZA0533	Willemite I	16	-5.8	8.95	164.5	secondary
ZA0533	Willemite I	1.b1	n.d.	n.d.	181.4	secondary	ZA0533	Willemite I	17	-9.7	13.62	215.4	primary
ZA0533	Willemite I	1.b2	n.d.	n.d.	169.5	secondary	ZA0533	Willemite I	21	-8.8	12.62	267.3	primary
ZA0533	Willemite I	1.b3	n.d.	n.d.	177.3	secondary	ZA0533	Willemite I	22	-9.9	13.83	233.7	primary
ZA0533	Willemite I	1.c	-3.3	5.41	185.7	secondary	ZA0533	Willemite I	23a	-10.8	14.77	216.8	primary
ZA0533	Willemite I	1.d1	-2.6	4.34	111.7	secondary	ZA0533	Willemite I	23b	-10.1	14.04	227.2	primary
ZA0533	Willemite I	1.d2	-4.6	7.31	253.7	secondary	ZA0533	Willemite I	23c	-8.2	11.93	237.1	primary
ZA0533	Willemite I	2a	n.d.	n.d.	66.8	secondary	ZA0533	Willemite I	24	-11.4	15.37	200.9	primary
ZA0533	Willemite I	2b	-10.4	14.36	203.6	primary	ZA0533	Willemite I	25	-7.7	11.34	242.5	primary
ZA0533	Willemite I	2c	-6.5	9.86	215.3	primary	ZA0533	Willemite I	26	-6.9	10.36	236.6	primary
ZA0533	Willemite I	3	-4.3	6.88	207.1	secondary	ZA0533	Willemite I	27	-9.5	13.4	248	primary
ZA0533	Willemite I	4	n.d.	n.d.	240.7	primary	ZA0533	Calcite	18	n.d.	n.d.	162.6	primary
ZA0533	Willemite I	5	-8.8	12.62	278.7	primary	ZA0533	Calcite	19	n.d.	n.d.		primary
ZA0533	Willemite I	6a	-10.3	14.25	244.3	primary	ZA0533	Calcite	20	n.d.	n.d.	167.9	primary
ZA0533	Willemite I	6b	-8.2	11.93	239.3	primary	ZA0533	Calcite	28	-0.2	0.35	<50°	secondary
ZA0533	Willemite I	7	-11.3	15.27	216.8	primary	ZA0533	Calcite	29	-0.5	0.88	<50°	secondary
ZA0533	Willemite I	8	-11.7	15.67	200.9	primary	ZA0533	Calcite	30	-0.2	0.35	<50°	secondary
ZA0533	Willemite I	9	-7.5	11.1	235.7	primary	ZA0533	Calcite	31	-0.6	1.05	<55°	secondary
ZA0533	Willemite I	10a	-7.2	10.73	249.6	primary	ZA0533	Calcite	32	-0.3	0.53	134.8	primary
ZA0533	Willemite I	10b	-8	11.7	235.1	primary	ZA0533	Calcite	32	-0.5	0.88	121.4	primary
ZA0533	Willemite I	10c	-9.5	13.4	214.2	primary	ZA0533	Calcite	30	-0.2	0.35	<50°	secondary
ZA0533	Willemite I	11	-9.1	12.96	263	primary	ZA0533	Calcite	31	-0.6	1.05	<55°	secondary
ZA0533	Willemite I	12	-6.5	9.86	207.6	secondary							
ZA0533	Willemite I	13	-6.6	9.98	194.5	secondary	ZA0524A	Willemite II	1	-0.2	0.35	n.d.	secondary
ZA0533	Willemite I	14	-7.1	10.61	211.5	primary	ZA0524A	Willemite II	2	-0.3	0.53	61.1	secondary
ZA0533	Willemite I	15a	-6	9.21	258.3	primary	ZA0524A	Willemite II	5	-0.3	0.53	n.d.	secondary
ZA0533	Willemite I	15b	-8.4	12.16	221.7	primary	ZA0524A	Willemite II	7	0	0	n.d.	secondary

Table 6.11: Microthermometric analyses on willemite from Excelsior and sphalerite from Millberg..

Sample	Mineral	I. no	Tm T°	Salinity eq.wt% NaCl	Th T°	Type	Sample	Mineral	I. no	Tm T°	Salinity eq.wt% NaCl	Th T°	Type
ZA0538	Willemite	1a	n.d.	n.d.	n.d.	secondary	ZA0538	Willemite	23	-2.1	3.55	169.2	secondary
ZA0538	Willemite	1b	n.d.	n.d.	71.8	secondary	ZA0538	Willemite	24	-0.5	0.88	145.4	secondary
ZA0538	Willemite	1c	n.d.	n.d.	103.9	secondary	ZA0538	Willemite	25	-9.7	13.62	201.3	primary
ZA0538	Willemite	1d	n.d.	n.d.	n.d.	secondary	ZA0538	Willemite	26	-0.6	1.05	185.8	secondary
ZA0538	Willemite	1e	n.d.	n.d.	n.d.	secondary	ZA0538	Willemite	27	-10.4	14.36	159.8	primary
ZA0538	Willemite	1f	n.d.	n.d.	n.d.	secondary	ZA0538	Willemite	28	-3.2	5.26	171.7	secondary
ZA0538	Willemite	1g	n.d.	n.d.	n.d.	secondary	ZA0538	Willemite	29	-8.2	11.93	217.8	primary
ZA0538	Willemite	2a	n.d.	n.d.	n.d.	secondary	ZA0538	Willemite	30	-5.7	8.81	237.3	primary
ZA0538	Willemite	2b	n.d.	n.d.	n.d.	secondary	ZA0538	Willemite	31	-6.3	9.6	199.3	primary
ZA0538	Willemite	2c	n.d.	n.d.	114.8	secondary	ZA0538	Willemite	32	-0.7	1.23	161.9	secondary
ZA0538	Willemite	3b	n.d.	n.d.	261.5	secondary							
ZA0538	Willemite	3a	n.d.	n.d.	200.6	secondary							
ZA0538	Willemite	4	-0.5	0.88	241.5	secondary	KM191	Sphalerite	1	-10.2	14.15	210.1	primary
ZA0538	Willemite	5	-0.9	1.57	187.7	secondary	KM191	Sphalerite	2	-7.2	10.73	229.1	primary
ZA0538	Willemite	6a	n.d.	n.d.	240.2	secondary	KM191	Sphalerite	3a	-6.6	9.98	201.6	primary
ZA0538	Willemite	6b	n.d.	n.d.	n.d.	secondary	KM191	Sphalerite	3b	-10.3	14.25	203.4	primary
ZA0538	Willemite	7	n.d.	n.d.	n.d.	secondary	KM191	Sphalerite	3c	-9.7	13.62	207.8	primary
ZA0538	Willemite	8	-0.5	0.88	175.6	secondary	KM191	Sphalerite	4	-9.2	13.07	220.3	primary
ZA0538	Willemite	9a	-9.3	13.18	161.7	primary	KM191	Sphalerite	5	-8.9	12.73	246.5	primary
ZA0538	Willemite	9b	-5.4	8.41	208.3	primary	KM191	Sphalerite	6a	-11.2	15.17	191.6	primary
ZA0538	Willemite	10a	-7.4	10.98	187.2	primary	KM191	Sphalerite	6b	-9.4	13.29	195	primary
ZA0538	Willemite	10b	-6.3	9.6	242.5	primary	KM191	Sphalerite	6c	-5.3	8.28	193.8	primary
ZA0538	Willemite	11	n.d.	n.d.	246.3	secondary	KM191	Sphalerite	7	-7.9	11.58	208.7	primary
ZA0538	Willemite	12	-2.1	3.55	n.d.	secondary	KM191	Sphalerite	8	-6.1	9.21	231.8	primary
ZA0538	Willemite	13	n.d.	n.d.	222.8	secondary	KM191	Sphalerite	9a	-7.8	11.46	198.7	primary
ZA0538	Willemite	14	-8.7	12.51	227.3	primary	KM191	Sphalerite	9b	-6.3	9.6	221.2	primary
ZA0538	Willemite	17	-8.9	12.73	187.9	primary	KM191	Sphalerite	9c	-7.2	10.73	191.3	primary
ZA0538	Willemite	18	-7.7	11.34	171.6	primary	KM191	Sphalerite	10	-8.7	12.51	218.3	primary
ZA0538	Willemite	19	-6.2	9.47	241.9	primary	KM191	Sphalerite	11	-10.8	14.77	217.3	primary
ZA0538	Willemite	20	-5.9	9.08	201.3	primary	KM191	Sphalerite	12	-6.7	10.11	211.4	primary
ZA0538	Willemite	21	-1.3	2.24	167.6	secondary	KM191	Sphalerite	13	-8.3	12.05	233.7	primary
ZA0538	Willemite	22	-2.3	3.87	272.4	secondary	KM191	Sphalerite	14	-11	14.97	199.3	primary

Figure 6.33: Star Zinc (a to d) and Excelsior (e to h) willemite FI frequency histogram (fh). a) fh of the T_h in primary FIs in willemite I from Star Zinc (T_h 210 and 250° C); b) fh of salinity in primary FIs in willemite I from Star Zinc (salinity 12-16 eq. wt% NaCl); c) fh of T_h in secondary FIs in willemite I from Star Zinc (T_h 170 and 210° C); d) fh of salinity in secondary FIs in willemite I from Star Zinc (salinity 6-10 eq. wt% NaCl); e) fh of the T_h in primary FIs in willemite from Excelsior (T_h 190-250° C); f) fh of salinity in primary FIs in willemite from Excelsior (salinity 10 and 16 eq. wt% NaCl); g) fh of T_h in secondary FIs in willemite from Excelsior (T_h 170 and 250° C); h) fh of salinity in secondary FIs in willemite from Excelsior (salinity 2-6 eq. wt% NaCl);



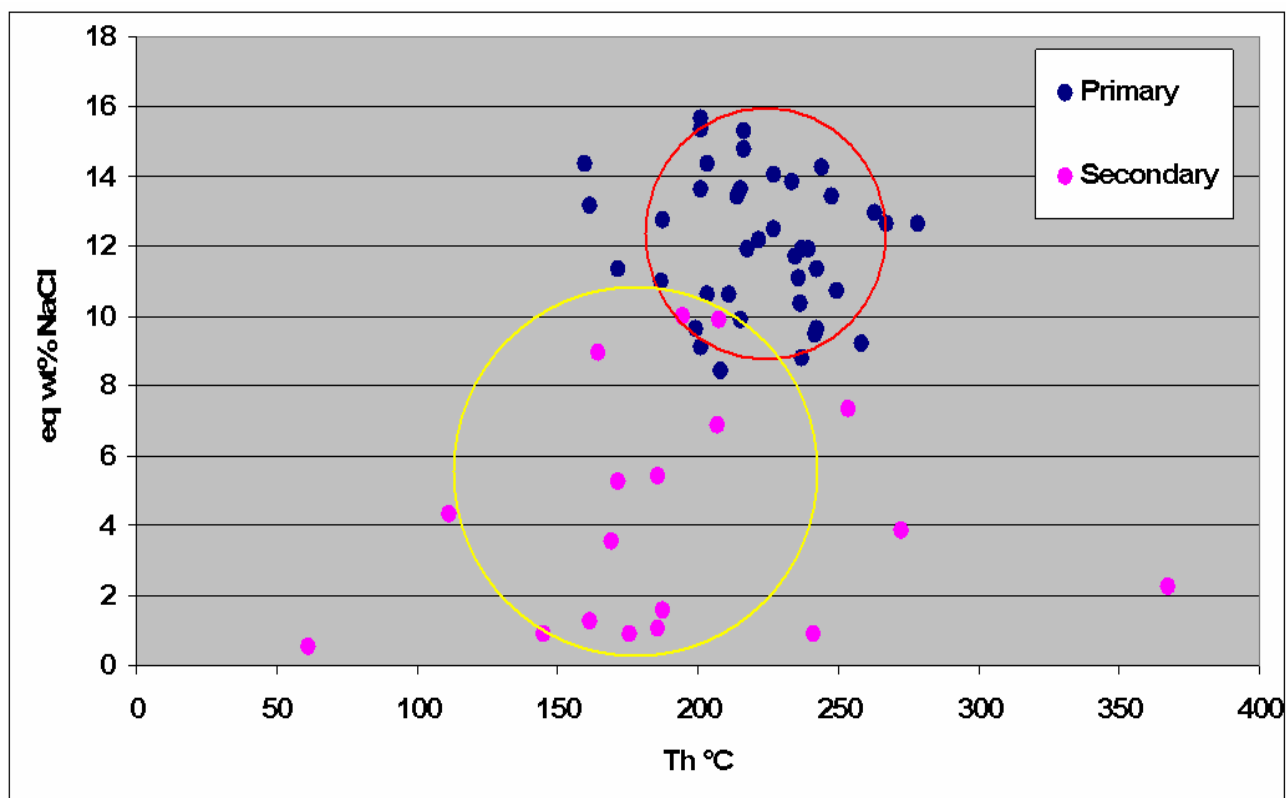


Figure 6.34: Correlation diagram Temperature-Salinity of the FIs in the willemite from the Lusaka area, where two distinct fields are clearly distinguished. The data of the primary FIs are: T_h 200-250° C - 10-16 eq wt% NaCl, those of the secondary FIs are: T_h 150-200° C – 2 - 10 eq wt% NaCl.

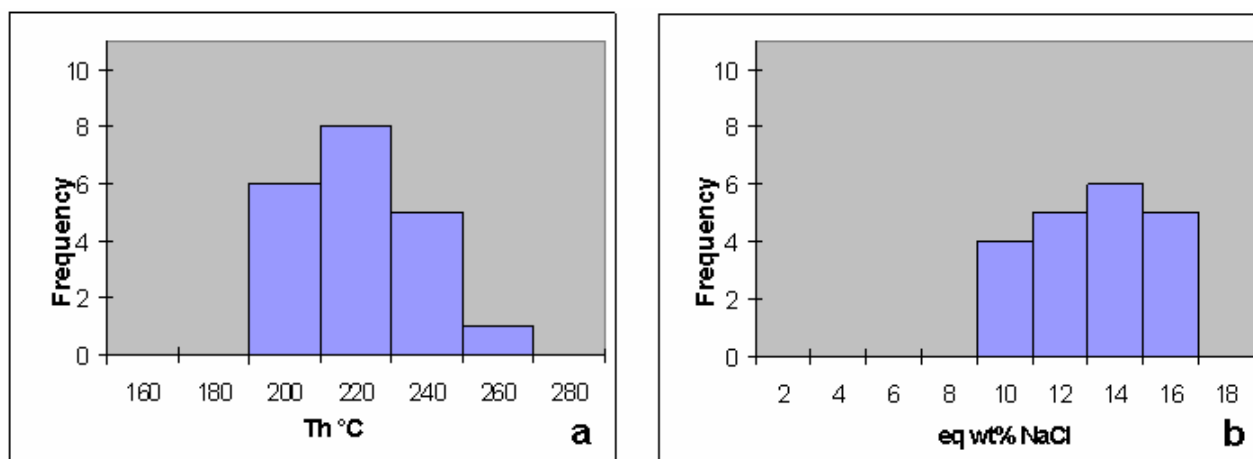


Figure 6.35: Millberg sphalerite FI frequency histogram (fh). a) fh of the temperature of homogenisation in primary inclusions; b) fh of the salinity of primary fluid inclusions.

7 Age constraints of Willemite mineralisation

7.1 Introduction

Only little information exists on willemite age dating in the world (e.g., Dejonghe and Boni, 2005, Groves et al., 2003, Schneider et al., 2008). This is due mainly to the paucity of well-datable minerals in the willemite paragenesis. Most of the currently accepted willemite ages are derived from a series of indirect evidences comprehending: 1) the timing of primary sulphides mineralisation, 2) the age of tectonic or metamorphic events in the region (that may or may not be related to the deposition of the willemite ores), and 3) the timing of major weathering events at a regional scale.

Of course, direct radiometric dating of the mineral associations is the prime tool that should be used, when possible. Direct dating can be decisive to understand the genesis of nonsulphide Zn-Pb mineralisation, as was the case of the Namibia willemite, dated by Schneider et al. (2008) with the Rb-Sr isotopic method. Zambian willemites are currently being dated, using the same Rb-Sr method. The results, so far, have only produced ambiguous ages.

Groves et al. (2003) obtained K-Ar ages of 437 ± 5 and 430 ± 5 Ma (cfr §2.3.2), for the mineral coronadite ($\text{MnPbMn}_6\text{O}_{14}$), which occurs in the late (post willemite) mineralisation stages of the Beltana deposit (northern Flinders Ranges, Australia). Willemite ore at Beltana should therefore have a minimum age corresponding to early Silurian.

7.2 OML willemite age and constraints

The Rb-Sr dating was applied from Schneider et al. (2008) to a few samples from Berg Aukas and Abenab West mines, where willemite occurs in several generations and complex textural assemblages (cfr §5.6). The selected samples were: a. massive, fine-grained red willemite I at Abenab West (cfr §5.6.2) and b. coarse grained, well crystallised, idiomorphic willemite I at Berg Aukas (cfr §5.6.1).

Rb-Sr analytical data for willemite, depicted in Figures 7.1 and 7.2, show isochron model ages in the range of ca. 480 to 580 Ma, obtained using different combinations of willemite samples. The 570 Ma Rb-Sr age obtained for Abenab West may represents only in a first approximation the maximum age of willemite mineralisation. No possibly contaminating mineral phases have been observed in thin section, which could be responsible for the high Rb-Sr isotopic ratios (Schneider et al., 2008).

Willemite ages can also be evaluated by comparison with other (already dated) geological events that have affected the study area. Ages in the range of 500 to 570 Ma for the willemite mineralisation could be related to the early Mulden karst phenomena and/or to the hydrothermal

fluid flow during D2 deformation and metamorphism (Miller, 1983). The 570 Ma age could envisage the formation of the Abenab nonsulphide deposit during the first Damaran metamorphic phase D1 (Haack et al., 1988). This, however, would conflict with the observation that willemite precipitation at Abenab West appears to postdate the major, D2-related structural elements (figure 4.4). The ages of ca. 500 to 480 Ma, obtained for the willemites at the Berg Aukas deposit would be consistent with the waning stages of the Damaran orogeny and subsequent uplift phase (Haack, 1976).

If the timing of willemite I mineralisation at Abenab and Berg Aukas can be plausibly linked to the different phases of the tectonothermal evolution of the Damara belt, then this may indicate an overprint of primary Zn-Pb sulphides on hydrothermal nonsulphide ores, rather than a typical supergene alteration of preexisting sulphides due to weathering processes (Schneider et al., 2008).

The multigenic willemite mineralisation predates in the OML the deposition of the widespread vanadates (descloizite-mottramite) ores. The oldest age obtained by Boni et al. (2007) for descloizite occurring in the Abenab Pipe stands between 45 and 65 Ma (late Cretaceous), which would correspond therefore to the uppermost possible time limit for the willemite formation.

7.3 *Zambia willemite age and constraints*

Rb-Sr dating is being carried out also on the willemites from Kabwe, Star Zinc and Excelsior in Zambia. Only few preliminary data are available for the Kabwe (cfr §6.4.2.1) and Star Zinc (cfr §6.4.5.1) willemite I. All analysed samples plotted together produced a preliminary age around 392 ± 2.3 Ma (Devonian). These data, however, are rather dubious, when considering the highlighted differences (mineralogy, petrography and fluid inclusion data) between the Kabwe willemites (which have been generally considered of supergene origin) and the Star Zinc ones (presumably hypogene). The data plot derived from the Star Zinc willemites only, suggests a possible age around 550-560 Ma. However, even if this time interval broadly fits within some of the previously calculated geochronological data for the Namibian willemites, the measures still lack of a robust statistical support (J. Schneider personal communication, 2008).

Other indirect age constraints for the willemite ores in Zambia can be derived from the age data of the primary sulphides at Kabwe. On the basis of structural relationships, Kamona and Friedrich (1994) considered the Zn-Pb mineralisation at Kabwe to have occurred prior to the last deformational phase of the Lufilian orogeny (ca. 650 to 500 Ma). On the other side, Boni et al. (2007) were able to date with the U/Th-He method the Kabwe descloizite, obtaining an age of 20-37 Ma (cfr figure 6.12). As in Namibia, the age of the vanadates can represent the upper temporal limit of deposition for the willemites.

Precise age constraints are currently lacking for the Star Zinc deposit. Since no tectonic deformation is affecting the willemite crystals, and no datable geological formation has been found covering the deposit, the only possible temporal constraint for the ores may involve the emplacement of the Hook granite, dated at 559 ± 18 Ma (Hanson et al., 1993, Johnson et al., 2005). The Hook granite is a major intrusion, supposed to be coeval with the main Mwembeshi dislocation zone, which is considered a major geotectonic boundary between the Lufilian Arc and the Zambezi Belt (cfr §4.3.3), and whose lineaments are also controlling the Star Zinc deposit.

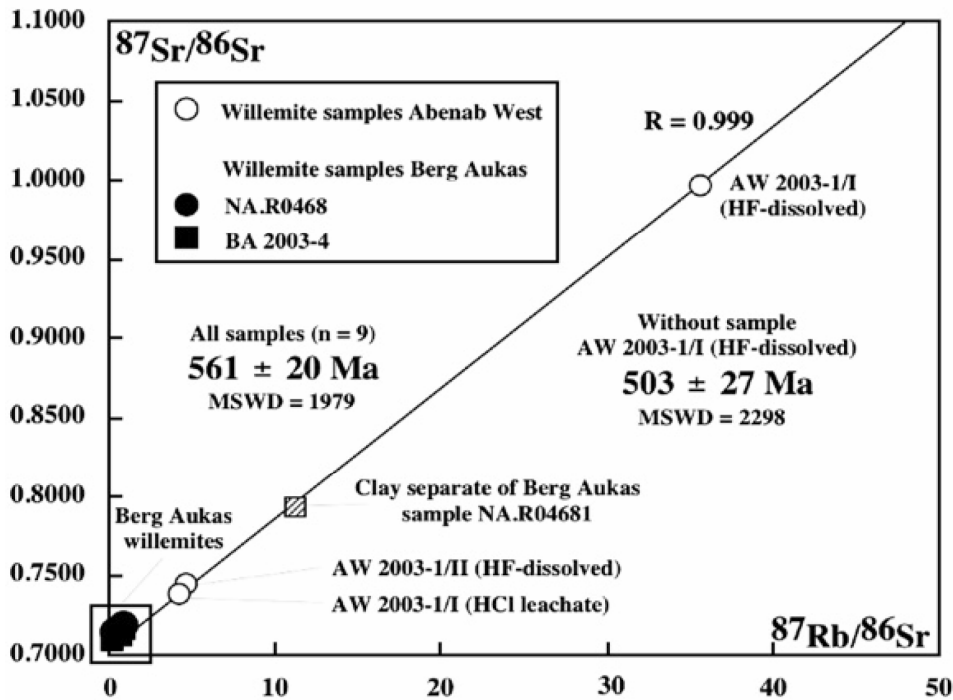


Figure 7.1: $^{87}\text{Sr}/^{86}\text{Sr}$ vs. $^{87}\text{Rb}/^{86}\text{Sr}$ diagram where all Berg Aukas and Abenab West samples are correlated along a straight line ($R=0.999$), with a slope corresponding to an Rb-Sr isochron model age of 561 ± 20 Ma (Schneider et al., 2008).

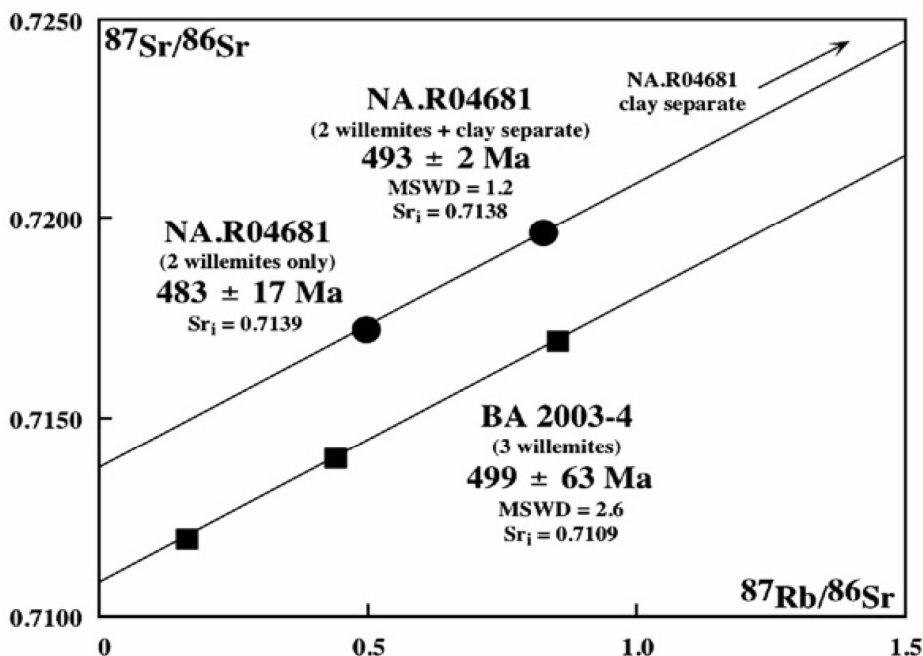


Figure 7.2: $^{87}\text{Sr}/^{86}\text{Sr}$ vs. $^{87}\text{Rb}/^{86}\text{Sr}$ correlation diagram for the Berg Aukas samples (Schneider et al., 2008).

8 Discussion

The African willemite ores have been deposited during multiple mineralisation stages. On the basis of mineralogical, petrographic, geochemical and geological evidence, two main groups of ore types can be distinguished, broadly corresponding to the groups described by Hitzman et al. (2003):

- “supergene” willemite, possibly generated through weathering and oxidation of primary sulphide deposits;
- “hypogene” willemite, generated by hydrothermal fluids.

The main characteristics of the two different mineralisation types will be discussed in the next paragraphs.

8.1 “Supergene” willemite

This kind of willemite usually occurs among the products of sulphide oxidation, characterised by a complex mineralogical assemblage. Willemites from the Namibian mines (Berg Aukas and Abenab West) and from the Kabwe area (Kabwe no. 2, no. 5/6, Airfield, Kashitu and Millberg) belong to this kind of “supergene” ores (cfr §5.5 and §6.4.1).

Willemite occurs in fractures, in veins and boxworks with replacement textures on both primary sulphides and host rocks. It occurs also in proper *gossans* together with Fe- and Mn-hydroxides. Massive bodies and blebs of fine- to coarse-grained willemite are commonly generated by the interaction of mineralising fluids with the carbonate (silica-rich) host-rock. No mineralogical or geochemical difference has been evidenced by XRD analyses between the different willemite generations.

In all the sites (except at Millberg) where a dense network of dark willemite veins replaces primary sulphides (*direct replacement*), a smithsonite-cerussite rim grows around the sphalerite grains. The incompatibility of Pb, Cu and Cd to be included within the willemite crystals, is responsible for the precipitation of secondary sulphides such as galena, covellite and greenockite, which occur also as distinct neoformed grains or as disseminations in willemite. None of these elements has been found in the willemite lattice, as confirmed by WDS and EDS analyses.

The interaction of the Zn-bearing (or Zn-enriched) fluids with the carbonate host rock has generally produced botryoidal replacive aggregates, characterised by idiomorphic hexagonal and thinly zoned willemite crystals.

Carbonate minerals, particularly dolomite, represent the most abundant non-metallic phases. Zn-Pb-

bearing saddle dolomite, postdating all willemite generations has been recognized in most mineral districts as ore gangue. Petrographic evidence has shown that this dolomite, characterised by a zoned blue CL luminescence, is a late mineral phase, genetically not related with willemite and locally replacing it. EDS spot analyses of this saddle dolomite revealed a Zn and Pb combined concentration up to 10-12 wt% maximum, with substitution of respectively Mg and Ca. Boni et al. (2007) reported this saddle dolomite following the main Vanadium ore stage in the OML dated at late Cretaceous. Sparry calcite represents the last precipitated phase in the Namibian willemite occurrences.

Widespread goethite and hematite characterize some of the willemite generations (as at Abenab West). In most mining districts, goethite/hematite occurring as disseminations in the Zn silicate, represents a minor, but always present ingredient of the ore, giving the willemite its deep reddish colour (i.e. Abenab West willemite I and Millberg willemite II). Under cathodic light “supergene” willemite (cfr §8.3) displays commonly blue colours (dull to bright), with only few cases (remnants?) of green luminescence, as at Berg Aukas (Namibia) and Millberg (Zambia).

Fluid inclusions from all Namibian and Kabwe area willemites (cfr §6.5) are predominantly monophasic. The measured homogenisation temperatures range from ca 50 to 70° C and the salinities never exceed values of 0.5 eq wt% NaCl. These values point to a supergene (meteoric?) origin of the mineralizing fluids, or at the least to low-temperature hydrothermal fluids.

In the mineral association of “supergene” willemite ore, a high number of typical *gossan* minerals and secondary alteration products are always present, representing the last deposited phases. Smithsonite and hemimorphite, as well as local sauconite occurrences have been commonly detected in the late weathering stages of the sulphide/willemite bodies. Late vanadates (descloizite) and phosphates (tarbuttite) are also quite common both in Namibian and Zambian “supergene” occurrences. Descloizite/mottramite ores represented an important economic vanadium resource in the OML (Namibia) (Boni et al., 2007).

Direct dating of Namibian and Zambian willemites has been performed only recently. Using willemite as Rb-Sr geochronometer Schneider et al. (2008) obtained a prevailing Ordovician age (ca. 480 Ma) for the Berg Aukas main willemite phase. This age is shortly postdating the metamorphic peak in the OML (Haack et al., 1980). Precise age data of the Zambian low-temperature willemites are still missing, but indirect age constraints place the main willemite event after the emplacement of the primary sulphide mineralisation at Kabwe (which has been dated to ca. 550 Ma by Kamona et al., 2007).

8.2 “Hypogene” willemite

Hypogene willemite ore has been identified at Star Zinc and Excelsior, located in the Lusaka region

(Zambia). Both the mineral paragenesis and fluid inclusion microthermometry (cfr § 6.5) point to a polycyclic, hydrothermal origin for these willemite deposits, not derived from the weathering of preexisting sulphides.

Willemite textures for this kind of ores are mainly massive, with locally developed prismatic crystals, and zoned crystalline aggregates. A preliminary mineral association, consisting of franklinite and gahnite is then replaced by willemite and hematite.

Franklinite and gahnite are zinc spinels, commonly associated with willemite in several hypogene nonsulphide zinc deposits (Hitzman et al., 2003, Monteiro et al., 2006). The better-known occurrences are in the Franklin Marbles of the Greenville Province in New Jersey (Larivière et al., 2007), with the best example represented by the Franklin-Sterling Hill deposit (Johnson et al., 2003). In the latter deposit the franklinite-gahnite-willemite ore association is considered as having been originated by amphibolite-granulite facies metamorphism from a previous zinc sulphide/nonsulphide mineralisation (Metsger, 1962; Johnson et al., 2003). Moreover, Stalder and Rozendaal (2005) have reported abundant franklinite from the Gamsberg Zn-Pb deposit (Namaqua province, South Africa), which has been also metamorphosed to amphibolite facies. The origin of the franklinite-gahnite *protore* in the Lusaka area is far to be clear and it could represent a metamorphosed occurrence derived from (now completely disappeared) primary sulphide concentrations. Several other sulphide deposits are known in the Zambezi metamorphic belt, as the metacarbonate-hosted Nampundwe volcanogenic massive pyrite deposit, representing a major exhalative stratiform deposit formed at 908.48 Ma (Burnard, 1990; Burnard et al., 1993). According to Hicks et al. (1985) green gahnite is usually formed during prograde metamorphism up to granulite facies of a Zn-rich precursor assemblage. In the Zambezi belt an eclogite facies metamorphism, which may be responsible for the green gahnite occurring at Star Zinc, occurred at ca. 600 Ma (John et al., 2003).

Monteiro et al. (2006) reported less than 5% franklinite from the Vazante (Brazil) ore deposit, where several willemite bodies are tectonically imbricated with small sulphide ones. The willemite is located at Vazante along the mylonitic foliation and is petrographically cogenetic with franklinite.

At Star Zinc franklinite and gahnite are clearly replaced by the willemite + hematite (specularite) association. At first, the hematite lamellae start to replace the greenish gahnite crystals and, further on in the process, the both hematite and willemite totally overprint the spinel. Franklinite seems to be more resistant to willemitisation than gahnite, since small cubic franklinite crystals may still be seen in the core of the willemite crystals or are randomly disseminated through it. Franklinite may also contain minute (μm sized) grains of Ag-bearing sphalerite, possibly as primary exsolutions rather than remnants. Apart from this, at Star Zinc and Excelsior only negligible sphalerite has been detected in this study.

Another peculiar feature of the hypogene willemite mineralisation at Star Zinc is the occurrence of the mineral pair willemite-genthelvite ($\text{Zn}_4\text{Be}_3(\text{SiO}_4)_3\text{S}$), which commonly show coprecipitation/exsolution textures. Genthelvite, showing at Star Zinc a dull blue colour under CL, is referred as the only silicate in which Zn and Be occur together and is a rare accessory in alkaline to peralkaline granites, syenites, and related pegmatites and greisens (Burt, 1988, Finch, 1990). Genthelvite has been also described in the Gamsberg orebody by Rozendaal (2008, personal communication). Genthelvite is a Zn-member belonging to the Helvite group $[(\text{Mn},\text{Zn},\text{Fe})_4\text{Be}_3(\text{SiO}_4)_3\text{S}]$ that comprises beryllium- and sulphur-bearing silicates (Zaw et al., 1997). According to Burt (1980) the minerals of the Helvite group are sensitive to hypogene oxidation and S-O exchange [i.e., variation in $\log f(\text{O}_2)/f(\text{S}_2)$]. Thus, the close association between genthelvite and willemite, points to low-sulphur activity oxidizing conditions.

Burt (1980) suggested the following reactions for equilibration of danalite ($\text{Fe}_4\text{Be}_3(\text{SiO}_4)_3\text{S}$) with pyrite (FeS_2), hematite (Fe_2O_3), magnetite ($\text{Fe}^{2+}\text{Fe}^{3+}_2\text{O}_4$), phenakite (Be_2SiO_4), and quartz (SiO_2):



Even if no experimental data exist for such a rare paragenesis in a Zn-rich contest, the equation [1] may be applied to the Star Zinc paragenesis involving genthelvite ($\text{Zn}_4\text{Be}_3(\text{SiO}_4)_3\text{S}$), franklinite $[(\text{Zn}, \text{Fe}^{2+})(\text{Fe}^{3+})_2\text{O}_4]$, sphalerite $[(\text{Zn},\text{Fe})\text{S}]$ and willemite (Zn_2SiO_4) -instead of danalite, magnetite and phenakite respectively-.

Thus, as shown by petrographic evidence, our small occurrence of genthelvite may reflect the interaction of Be-rich fluids with the franklinite/willemite association (figure 6.29d), acknowledging the high SiO_2 activity in the formation of willemite (Brugger et al., 2003) and the very minor pyrite/sphalerite (which as been found in negligible amount in the XRD analysis, cfr table 6.5) acting as a local sulphur source.

The hypogene willemite under cathodic light shows a strong green colour in all associations, with little variation in shades, following the mineral zonations. WDS analyses of the willemite from Star Zinc revealed only a negligible enrichment in trace elements (mainly Fe and Mn < 0.05%). According to Monteiro et al. (2006), this same purity of the willemite could be held responsible for the strong green CL observed in this mineral, because impurities can be inhibitors of the CL effects (cfr §6.4.6).

The microthermometric data from Star Zinc and Excelsior also speak for a high temperature, hydrothermal origin of the mineralising fluids. Measured fluid inclusions in willemite I (figure 6.34) show homogenisation temperatures mainly concentrated around 220-260° C and salinities of ca 10-

16 eq wt% NaCl.

Direct dating of Star Zinc willemite with the Rb-Sr method are still in a preliminary stage. A possible age of 550-560 Ma needs to be confirmed by further analyses and statistic elaboration.

However, hypogene willemite at Star Zinc and Excelsior may have been formed within a period possibly shortly postdating the Mwembeshi dislocation (551 Ma, Hanson et al., 1993). Be-bearing, oxidizing hydrothermal fluids, related to the waning stages of the regional metamorphism in the Zambezi belt, may have been responsible for the (hematite)-willemite-genthelvite association replacing a franklinite-gahnite *protore*..

8.3 *Common and general remarks*

A number of common features occur within the studied supergene and hypogene willemite deposits. In both Namibian and Zambian ores (supergene or hypogene), willemite occurs in carbonate host rocks owing to the high reactivity of carbonate minerals with the acidic, oxidized, zinc-rich fluids derived from the oxidative destruction of sphalerite-bearing sulphide bodies (for the “supergene” deposits) or for the buffering properties of the carbonate rocks toward the zinc-enriched solutions (for the hypogene deposits).

The green luminescence of willemite has been commonly assumed to have been generated by Mn substituting for Zn in the silicate lattice. Harper et al. (2005) referred willemite luminescence at 0.26 apfu Mn; however, the WDS analyses carried out for both the Namibian and Zambian willemites show a maximum of 0.01 apfu Mn for both green- and blue-luminescent willemite. Therefore, at least for the blue willemites, the luminescence colour seems to be related to the presence of abundant solid inclusions (particularly goethite/hematite) or to the high FeO content in the willemite lattice, which can reach up to 2% and may act as a luminescence quencher. Another possibility for the variability in the cathodoluminescence colours could be related to the different orientation of the willemite crystals. Bhalla et al. (1972) mentioned a shifting of 100 Å in the emission peak position of willemite under spectroscopic cathodoluminescence, with the maximum value corresponding to the direction parallel to the c-axis.

8.4 *Non African Willemite mineralisation ages and comparisons*

The currently known, major economic willemite deposits that have been recently reinterpreted to originate from structurally controlled, hypogene-hydrothermal fluid flows are confined to the southern hemisphere, located roughly at the same latitude (plate 2.1). These are Vazante (Brazil), Kabwe and Star Zinc (Zambia), Berg Aukas and Abenab West (Namibia), and Beltana-Aroona (Australia). They all occur in tectonized and mostly dolomitized, Neoproterozoic carbonate

successions (Hitzman et al., 2003), with the exception of Beltana, which is hosted by Lower Cambrian carbonates overlying a Neoproterozoic succession (Groves et al., 2003). The common Late Proterozoic to Early Cambrian age of the carbonate rocks that host this type of hypogene willemite mineralisation worldwide provide also a background for the constraints on the timing of these nonsulphide deposits relative to each other. No direct radiometric age constraints are available for the willemite mineralisation at Vazante (Brazil) yet and only poorly reliable data are available from Kabwe/Star Zinc (Zambia). Monteiro et al. (2006) related the formation of sulphide ores and willemite in the Vazante district to the late stages of the Brasiliano orogeny (ca. 630 to 500 Ma). Groves et al. (2003) proposed a younger, early Silurian age of about 435 Ma for the formation of the late stages at the Beltana-Aroona willemite deposit in the Adelaide basin in the northern Flinders Ranges (Australia). The same authors have related this mineralisation age to an exhumation period, which followed the Delamerian orogeny (523 to 490 Ma).

In the general absence of direct radiometric ages for all known willemite deposits, the local evidence for the timing of epigenetic willemite deposits at Vazante, Kabwe and Beltana may indicate mineralisation events in the broad range of ca. 490 to 550 Ma. These general ages would be in good agreement with the first Rb-Sr ages directly obtained for the willemite in the Abenab West and Berg Aukas deposits (Namibia) by Schneider et al. (2008). These ages may also point to a global period of hydrothermal activity between Cambrian and early Ordovician that favoured the formation of willemite deposits.

9 Conclusions

Several mineralogical, petrographic and geochemical methods have been used in order to characterise the willemite mineralisation of Namibia and Zambia. Willemite occurs in several mining districts throughout both countries as low tonnage, high grade (15-20% Zn), carbonate-hosted deposits. Suitable conditions for willemite crystallisation are oxidising (hematite stable) conditions with high SiO₂ and low sulphur activity. The different characteristics of the deposits have allowed the definition of two main groups: A. “supergene” mineralisation (Berg Aukas, Abenab West and Baltika in Namibia and Kabwe deposits in Zambia) and B. hypogene mineralisation (Star Zinc and Excelsior in Zambia).

The main features of “supergene” *** willemite are:

1. Typical *gossan* textures and complex mineralogy, derived from multiple oxidation/weathering stages of primary sulphide bodies;
2. Willemite with dominant blue cathodoluminescence colours, induced by goethite/hematite inclusions and Fe substitution in the mineral lattice;
3. Monophase fluid inclusions, pointing to supergene-meteoric (or very low temperature hydrothermal) fluids;
4. Late to post orogenic-post metamorphism, probably associated with paleoweathering processes, which followed the Cambro-Ordovician uplifts (530-490 Ma);
5. Carbonate gangue, frequently Zn-Pb bearing saddle dolomite.

***ALL the quoted characteristics could be also derived for willemite deposition by low-temperature hydrothermal, oxygen-rich fluids.

The main features of hypogene willemite are:

1. Typical direct replacement textures as discordant bodies;
2. Close association with zinc spinels, particularly franklinite and gahnite; minerals deposited in the late stages of metamorphism such as genthelvite; hematite-specularite association;
3. Willemite with dominantly green cathodoluminescence colours, with stronger colours along the c mineral axis;
4. Dominant two-phase fluid inclusions with medium/high temperatures (>200-250° C) and salinities (>10-12 eq wt% NaCl);
5. Late-orogenic metamorphism, possibly associated with late granitic intrusions related to local scale tensional tectonic;

References

- Ahrendt, H., Behr, H.J., Clauer, N., Hunziker, J.C., Porada, H., Weber, K., 1983. The Northern Branch; depositional development and timing of the structural and metamorphic evolution within the framework of the Damara Orogen. In: H. Martin, Eder, F.W. (Editor), *Intracontinental Fold Belts - Case studies in the Variscan Belt and Damara Belt*, pp. 723-743.
- Allsopp, H.L., Welke, H.J. and Hughes, M.J., 1981. Shortening the odds in exploration. *Nuclear Active*, 24, 8-12.
- Amaral, G., 1968. *Geologia e depósitos de minério da região de Vazante*: Unpublished Ph.D. dissertation, Estado de Minas Gerais, São Paulo, Universidade de São Paulo, 103 p.
- Annels, A. E. 1974. Some aspects of the stratiform ore deposits of the Zambian Copperbelt and their genetic significance. In Bartholomé, P., ed. *Gisements stratiformes et provinces cupifères*. Liège, Société Géologique Belgique, p. 235-254.
- Armstrong, R.A., Robb, L.J., Master, S., Kruger, F.J., Mumba, P.A.C.C., 1999. New U-Pb age constraints on the Katangan Sequence, Central African Copperbelt. *Journal of African Earth Sciences* 28(4A), 6-7.
- Arthurs, J.W., Newman, D., Smith, A.G., 1995. Geology of the Chipembi area: explanation of degree sheet 1438, SE quarter. Geological Survey of Zambia, Report 58, 37.
- Avery, D.M., 2003. Early and Middle Pleistocene environments and hominid biogeography; micromammalian evidence from Kabwe, Twin Rivers and Mumbwa Caves in central Zambia. *Palaeoecology*, 189, 55-69.
- Barr, M. W. C., Cahen, L., and Ledent, D., 1977. Geochronology of syntectonic granites from central Zambia: Lusaka Granite and granite NE of Rufunsa. *Annales Société Géologique Belgique*, 100, 47-54.
- Bayley, W.S., 1910. Iron mines and mining in New Jersey: Volume VII of the Final Report Series of the State Geologist: Trenton. Geological Survey of New Jersey, 512 p.
- Bhalla, R.J. and White, E.W., 1972. Cathodoluminescence Characteristics of Mn²⁺-Activated Willemite (Zn₂SiO₄) Single Crystals. *Journal of Electrochemical Society*, 119(6), 740-743.
- Binda, P. L. 1994. Stratigraphy of the Zambian Copperbelt orebody. *Journal of African Earth Science*, 19, 251-264.
- Birch, A., 1999. Kabwe mine, prospecting license PLLS28 exploration programme and results for 1997 and 1998 with residual prospectivity volume I and II. Billiton exploration and development Central Africa, unpublished report, 49p.
- Bodnar, R.J., 1993. Revised equation and table for determining the freezing point depression of H₂O-NaCl solutions. *Geochimica et Cosmochimica Acta*, 57, 683-684.
- Boni, M., 2003. Nonsulfide Zinc Deposits: A New-(Old) Type of Economic Mineralisation", M. Chiaradia, Ed., SGA Newsletter, 15, 1 & 6-11.

- Boni, M., and Large, D., 2003. Nonsulfide zinc mineralisation in Europe: an overview. *Economic Geology*, 98(4), 715-729.
- Boni, M., 2005. The Geology and Mineralogy of Non Sulfide Zinc Ore Deposits. Proceedings of Lead & Zinc '05, Kyoto 17-19 October 2005, 15 p.
- Boni, M., Terracciano, R., Evans, N.J., Laukamp, C., Schneider, J. and Bechstadt, T., 2007. Genesis of Vanadium Ores in the Otavi Mountainland, Namibia. *Economic Geology*, 102, 441-469.
- Brugger, J., McPhail, D.C., Wallace, M. and Waters, J., 2003. Formation of Willemite in Hydrothermal Environments. *Economic Geology*, 98(4), 819-835.
- Burdett, M., 2000. Origin of the Beltana and Aroona willemite deposits, Flinders Ranges, South Australia. Unpublished B.Sc. thesis, University of Melbourne, Australia, 58 p.
- Burnard, P.G., 1990. The nature, origin and regional implications of the Nampundwe ores, southern Zambia. PhD Dissertation, University of Manchester, Manchester, England, 316p.
- Burnard, P.G., Sweeney, M.A., Vaughan, D.J., Spiro, B. and Thirwall, M.F., 1993. Sulfur and lead isotope constraints on the genesis of a southern Zambian massive sulfide deposit. *Economic Geology*, 88, 418-436.
- Burt, D.M., 1980. The stability of danalite, $(\text{Fe}_4\text{Be}_3(\text{SiO}_4)_3\text{S})$. *American Mineralogist*, 65, 355-360.
- Burt, D.M., 1988. The stability of genthelvite $(\text{Zn}_4\text{Be}_3(\text{SiO}_4)_3\text{S})$: an exercise in calcophilicity using operators. *American Mineralogist*, 73, 1384-1394.
- Cahen, L., Snelling, N.J., Delhal, J., Vail, J.R., 1984. The Geochronology and Evolution of Africa. Clarendon Press, Oxford. 512 pp.
- Cairncross, B., 1997. The Otavi Mountain Land Cu-Pb-Zn-V deposits. *Mineralogical Record*, 28, 109-157.
- Cairney, T., Kerr, C.D., 1998. The geology of the Kabwe area: explanation of degree sheet 1428, NW quarter. Geological Survey of Zambia, Report 47, 40.
- Charlet, L., Peaudecerf, A., Van Cappelen, P., Reiche, I. and Chapron, Y., 2006. Surface complexation of zinc cation with hydroxyapatite, molecular dynamics and surface durability. In *Surface Complexation Modelling* J.H. Lutzenkirchen - Science – 638p ed., 301-321.
- Clifford, T.N., Rooke, J.M. and Allsopp, H.L., 1969. Petrochemistry and age of the Franzfontein granitic rocks of northern South-West Africa. *Geochimica and Cosmochimica Acta*, 33, 973-986.
- Clauer, N. and Kroener, A., 1979. Strontium and argon isotopic homogenization of pelitic sediments during low-grade regional metamorphism; the Pan-African Upper Damara Sequence of northern Namibia (South West Africa). *Earth and Planetary Science Letter*, 43(1), 117-131.
- Coppola, V., 2007. The main nonsulphide Zn deposits in Europe: Characterisation, timing and paleoclimatic control. Unpublished PhD thesis, Universit di Napoli "Federico II", 236 p.

- Coppola, V., Boni, M., Gilg, H.A., Balassone, G., Dejonghe, L., 2008. The "calamine" nonsulfide Zn–Pb deposits of Belgium: Petrographical, mineralogical and geochemical characterization. *Ore Geology Reviews*, 33 (2), 187-210.
- Cosi M., De Bonis, A., Gosso, G., Hunziker, J., Martinotti, G., Moratto, S., Robert, J.P. and Ruhlman, F., 1992. Late proterozoic thrust tectonics, high-pressure metamorphism and uranium mineralisation in the Domes Area, Lufilian Arc, northwestern Zambia. *Precambrian Research*, 58, 215-240.
- Coward, M.P., 1981. The junction between Pan African mobile belts in Namibia: its structural history. *Tectonophysics*, 76, 59-73.
- Chadwick, P.J., 1993. A study of the Berg Aukas-Type Pb-Zn-V deposits in the Otavi Mountain Land, Namibia. Master of Science Thesis, University of Cape Town, South Africa.
- Chadwick, P.J., 1993. A study of the Berg Aukas-type Pb-Zn-V deposits in the Otavi Mountain Land, Namibia. MSC Thesis, University of Cape Town, Cape Town, 138 p.
- Chetty, D. and Frimmel, H.E., 2000. The role of evaporites in the genesis of base metal sulphide mineralisation in the northern platform of the Pan-African Damara Belt, Namibia; geochemical and fluid inclusion evidence from carbonate wall rock alteration. *Mineralium Deposita*, 35(4), 364-376.
- Daly, M.C., 1986, Crustal shear zone and thrust belts: their geometry and continuity in Central Africa: *Philosophical Transactions Royal Society London*. A317, 11-128.
- Deane, J.G., 1993. The controls on "contact type" Cu-Pb (Ag) mineralisation within the Tsumeb Subgroup of the Otavi Valley Syncline, Northern Namibia. Master of Science Thesis, University of Cape Town, South Africa.
- Deane, J.G., 1995. The structural evolution of the Kombat deposits, Otavi Mountainland, Namibia. *Communications of the Geological Survey of Namibia*, 10, 99-107.
- Drexel, J.F., and Preiss, W.V., eds., 1995. The geology of South Australia, v. 2: The Phanerozoic. *Geological Survey of South Australia Bulletin* 54, 347 p.
- Drysdall, A.R., 1962. Central brickfields, Broken Hill as a possible site for salt-glaze ware and face brick industries . Technical report of the Geological Survey of Northern Rhodesia, 74.
- Dürr, S.B., Dingeldey, D.P., 1996. The Kaoko belt (Namibia): Part of a late Neoproterozoic continental-scale strike-slip system. *Geology*, 24(6), 503-506.
- Finch, A., 1990. Genthelvite and willemite, zinc minerals associated with alkaline magmatism from the Motzfeldt centre, South Greenland. *Mineralogical Magazine*, 54, 407-412.
- Freeman, P.V., Description of mineral deposits in the Copperbelt (and Kabwe, Nampundwe). Zambia Consolidated Copper Mines (unpublished report).
- Frimmel, H.E., Deane, J.G. and Chadwick, P.J., 1996. Pan-African tectonism and the genesis of base metal sulfide deposits in the northern foreland of the Damara Orogen, Namibia. In Sangster, D. F., ed., *Carbonate-hosted lead-zinc deposits*, Littleton, Society of Economic Geologists, 4, 204-217.

- Frimmel, H.E., 2004. Formation of a late Mesoproterozoic Supercontinent: the South Africa - East Antarctica connection. In: P.G. Eriksson, Altermann, W., Nelson, D.R., Mueller, W.U., Catuneanu, O. (Editor), *The Precambrian Earth: Tempos and Events. Developments in Precambrian Geology*, 12, 240-255.
- Frimmel, H.E., Jonasson, I.R. and Mubita, P., 2004. An Eburnean base metal source for sediment-hosted zinc-lead deposits in Neoproterozoic units of Namibia: Lead isotopic and geochemical evidence. *Mineralium Deposita*, 39, 328-343.
- Fron del, C., and Baum, J.L., 1974. Structure and mineralogy of the Franklin zinc-iron-manganese deposit, New Jersey. *Economic Geology*, 69, 157-180.
- Goldstein, R.H. and Reynolds, T.J., 1994. Systematics of fluid inclusions in diagenetic minerals. *Society for Sedimentary Geology, Short Course*, 31, 87-121.
- Goscombe, B., Gray, D., Hand, M., 2004. Variation in Metamorphic Style along the Northern Margin of the Damara Orogen, Namibia *Journal of Petrology*, 45(6), 1261-1295.
- Goscombe, B., Gray, D., Armstrong, R., Foster, D.A., Vogl, J., 2005. Event geochronology of the Pan-African Kaoko Belt, Namibia. *Precambrian Research*, 140, 103-131.
- Goscombe, B.D., Hand, M., Gray, D., 2003. Structure of the Kaoko Belt, Namibia: progressive evolution References n 150 of a classic transpressional orogen. *Journal of Structural Geology*, 25, 1049-1081.
- Gray, D.R., Foster, D.A., Goscombe, B., Passchier, C.W. and Trouw, R.A.J., 2006. $^{40}\text{Ar}/^{39}\text{Ar}$ thermochronology of the Pan-African Damara Orogen, Namibia, with implications for tectonothermal and geodynamic evolution. *Precambrian Research*, 150, 49-72.
- Groves, I., Gregory, I., and Carman, C., 2002. A new high-grade zinc silicate-oxide discovery in the Flinders Ranges. *Mines and Energy South Australia Journal*, 25, 6-10.
- Groves, I.M., Carman, C.E. and Dunlap, W.J., 2003. Geology of the Beltana Willemite Deposit, Flinders Ranges, South Australia. *Economic Geology*, 98(4), 797-818.
- Grubb, P.L.C., 1971. Mineralogy and genesis of the Beltana zinc-lead deposit, Putlapa, South Australia. *Journal Geological Society of Australia*, 18, 165-171.
- Haack, U., 1976. Rekonstruktion der Abkühlungsgeschichte des Damara-Orogens in Südwest-Afrika mit Hilfe von Spaltspuren. *Geologische Rundschau*, 65, 967-1002.
- Haack, U., Martin, H., 1983. Geochronology of the Damara Orogen: a review. In: Martin, H., Eder, F.W. (Eds.), *Intracontinental Fold Belts*, Springer, Berlin, 839-846.
- Haack, U., Gohn, E., Brandt, R., Feldmann, H., 1988. Rb-Sr data on the Otjimbingwe Alkali Complex in the Damara Orogen, South West Africa, Namibia. *Chemie der Erde*, 48, 131-140.
- Haack, U., 1993. Critical note on lead-lead model ages. In: P. Möller, Lüders, V. (Editor), *Formation Hague*, J.M., Baum, J.L., Herrmann, L.A., and Pickering, R.J., 1956, *Geology and structure of the Franklin-Sterling area*, New Jersey. *Bulletin of the Geological Society of America*, 67, 436-474.

- Haldane, R., 1989. Kabwe-mine – compilation of geological work in the Airfield area: Zambia Consolidated Copper Mines technical service unpublished report, Kalulushi, Zambia, 36p.
- Hallam, J., 2000. The geology of the Pultapa willemite deposit. Unpublished B.Sc. thesis, Melbourne, Australia, University of Melbourne, 65 p.
- Hanson, R. E., Wilson, T. J., and Munyanyiwa, H. 1994. Geologic evolution of the Neoproterozoic Zambezi orogenic belt in Zambia. *Journal of African Earth Science*, 18, 135-150.
- Hanson, R. E., Wilson, T. J., and Wardlaw, M. S. 1988. Deformed batholiths in the Pan-African Zambezi belt, Zambia: age and implications for regional Proterozoic tectonics. *Geology*, 16, 1134-1137.
- Hanson, R.E., Wardlaw, M.S., Wilson, T.J. & Mwale, G. 1993. U-Pb zircon ages from the Hook Granite massif and Mwembeshi Dislocation: constraints on Pan-African deformation, plutonism, and transcurrent shearing in central Zambia. *Precambrian Research*, 63, 189-209.
- Harper, K. and Griffen, D., 2005. Crystallographic consequences of Mn substitution in willemite. Salt Lake City Annual Meeting, 126-15.
- Hedberg, R.M., 1979. Stratigraphy of the Ovamboland Basin, South West Africa. *Bulletin - University of Cape Town, Department of Geology, Chamber of Mines Precambrian Research Unit*, 24, 324.
- Hicks, J.A., Moore, J. M. and Reid, A.M., 1985. The occurrence of green and blue gahnite in the Namaqualand Metamorphic Complex, South Africa. *Canadian Mineralogist*, 23, 535-542.
- Hitzman, M.W., 1997. Sediment-hosted Zn, Pb, and Au deposits in the Proterozoic Paracatu-Vazante fold belt, Minas Gerais, Brazil [abs.]: Denver Region Exploration Geologists Society.
- Hitzman, M.W., Reynolds, N.A., Sangster, D.F., Allen, C.R. and Carman, C.E., 2003. Classification, genesis, and exploration guides for nonsulfide Zinc deposits. *Economic Geology*, 98(4), 685-714.
- Hitzman, M.W., 1999. Geology of the Kabwe district and exploration potential in Billiton Development (Zambia) Limited's, Kabwe Prospecting Licenses (LS 28 and 1060). Billiton exploration and development Central Africa, unpublished report, 41p.
- Hoffman, P.F., Hawkins, D.P., Isachsen, C.E. and Bowring, S.A., 1996. Precise U-Pb zircon ages for early Damara magmatism in the Summas Mountains and Welwitschia Inlier, northern Damara belt, Namibia. *Geological Survey of Namibia Communications*, 11, 47-52.
- Hoffmann, K.H., Condon, D.J., Bowring, S.A. and Crowley, J.L., 2004. U-Pb zircon date from the Neoproterozoic Ghaub Formation, Namibia: Constraints on Marinoan glaciation. *Geology*, 32(9), 817-820.
- Horn, R.A., 1975. Beltana and Aroona willemite orebodies, *in* Knight, C.L., ed., *Economic geology of Australia and Papua New Guinea*, 1. Metals. Parkville, Australia, Australasian Institute of Mining and Metallurgy, 548-553.
- Hughes, M.J., 1979. Some aspects of the genesis of the Tsumeb ore body, South West Africa, and of

its subsequent deformation, Geokongres 79, 18th congress of the geological society of S.A., 200-206.
James, N.P., and Gravestock, D.I., 1990, Lower Cambrian shelf and shelf margin buildups, Flinders Ranges, South Australia. *Sedimentology*, 37, 455-480.

Hughes, M.J., Welke, H.J. and Allsopp, H.L., 1984. Lead isotopic studies of some late Proterozoic stratabound ores of central Africa. *Precambrian Research*, 25(1-3), 137-139.

Innes, J., Chaplin, R.C., 1986. Ore bodies of the Kombat mine, South West Africa/Namibia. In: Anhaeusser, C.R., Maske, S. (Eds.), *Mineral Deposits of Southern Africa*. Geological Society of Southern Africa, vol. II, 1789-1805.

Jackson, M.P.A., Warin, O.N., Woad, G.M., and Hudec, M.R., 2003. Neoproterozoic allochthonous salt tectonics during the Lufilian orogeny in the Katangan Copperbelt, central Africa. *Geological society of America Bulletin*, 115, 314-330.

John, T. and Schenk, V. 2003. Partial eclogitisation of gabbroic rocks in a late Precambrian subduction zone (Zambia): prograde metamorphism triggered by fluid infiltration. *Contribution to Mineralogy and Petrology*, 146, 174-191.

John, T., Schenk, V., Haase, K., Scherer, E., and Tembo, F. 2003. Evidence for a Neoproterozoic ocean in south-central Africa from mid-oceanic-ridge-type geochemical signatures and pressure-temperature estimates of Zambian eclogites. *Geology*, 31, 243-246.

John, T., Scherer, E. E., Haase, K., and Schenk, V. 2004. Trace element fractionation during fluid-induced eclogitization in a subducting slab: trace element and Lu-Hf-Sm-Nd isotope systematics. *Earth Planetary Science Letter*, 227, 441-456.

Johns, C.C., Liyungu, K., Mabuku, S., Mwale, G., Sakungo, F., Tembo, D., Vallance, G., 1989. The stratigraphic and structural framework of Eastern Zambia: results of a geotraverse. *Journal of African Earth Science*, 9(1), 123-136.

Johnson, C.A., 2001. Geochemical constraints on the origin of the Sterling Hill and Franklin zinc deposits, and the Furnace magnetite bed, northwestern New Jersey. *Society of Economic Geologists Guidebook Series*, 35, 89-97.

Johnson, S.P. and Oliver, G.J.H., 2000. Mesoproterozoic oceanic subduction, island-arc formation and the initiation of back-arc spreading in the Kibaran belt of central, southern Africa: evidence from the ophiolite terrane, Chewore inliers, northern Zimbabwe. *Precambrian Research*, 103, 125-146.

Johnson, C.A., and Skinner, B.J., 2003. Geochemistry of the Furnace magnetite bed, Franklin, New Jersey, and the relationship between stratiform iron oxide ores and stratiform zinc oxide-silicate ores in the New Jersey Highlands. *Economic Geology*, 98, 837-854.

Johnson, S.P., Rivers, T., and De Waele, B., 2005. A review of the Mesoproterozoic to early Palaeozoic magmatic and tectonothermal history of south-central Africa: implications for Rodinia and Gondwana. *Journal of the Geological Society, London*, 162, 433-450.

Johnson, S.P., De Waele, B., Evans, D., Banda, W., Tembo, F., Milton, J.A. and Tani, K., 2007. Geochronology of the Zambezi Supracrustal Sequence, Southern Zambia: A Record of

- Neoproterozoic Divergent Processes along the Southern Margin of the Congo Craton. *The Journal of Geology*, 115, 355-374.
- Kamona, A.F., 1993. The carbonate hosted Kabwe Pb-Zn deposit, Central Zambia. *Mitteilungen zur Mineralogie und Lagerstättenlehre der RWTH Aachen*, 44.
- Kamona, F., and Friedrich, G., 1994. Die Blei-Zink-Lagerstätte Kabwe in Zentral Sambia. *Erzmetall*, 47, 34-44.
- Kamona, A.F., L  veque, J., Friedrich, G., Haack, U., 1999. Lead isotopes of the carbonate-hosted Kabwe, Tsumeb, and Kipushi Pb-Zn-Cu sulphide deposits in relation to Pan African orogenesis in the Damaran-Lufilian Fold Belt of Central Africa. *Mineralium Deposita*, 34, 273-283.
- Kamona, A.F. and Friedrich, G.H., 2007. Geology, mineralogy and stable isotope geochemistry of the Kabwe carbonate-hosted Pb-Zn deposit, Central Zambia. *Ore Geology Reviews*, 30, 217-243.
- Katongo, C., K  ller, F., Kl  tzli, U., Koeberl, C., Tembo, F., and De Waele, B. 2004. Petrography, geochemistry and geochronology of granitoid rocks in the Neoproterozoic-Paleozoic Lufilian-Zambezi belt, Zambia: implications for tectonic setting and regional correlation. *Journal of African Earth Science*, 40, 219-244.
- Kampunzu, A.B., and Cailteux, J., 1999. Tectonic exsolution of the Lufilian Arc (Central Africa Copper Belt) during Neoproterozoic Pan African orogenesis: *Gondwana Research*, 2, 401-421.
- Key, R. M., Liyungu, A. K., Njamu, F. M., Somwe, V., Banda, J., Mosley, P. N. and Armstrong, R. A., 2001. The western arm of the Lufilian Arc in NW Zambia and its potential for copper mineralisation. *Journal of African Earth Science*, 33, 503-528.
- K  rner, K., 2006. The Metallogeneses of the Skorpion Non-Sulphide Zinc Deposit, Namibia. PhD thesis, Martin-Luther-Universit  t Halle-Wittenberg. 252p.
- King, L.C., 1951. South African scenery, Edinburgh, 379 pp.
- Kortman, C.R., 1972. The geology of the Zambia Broken Hill Mine, Kabwe. *Geologie en Mijnbouw*, 51(3), 347.
- Large, D., 2001. The Geology of Non-Sulphide Zinc Deposits - An Overview. *Erzmetall*, 54(5), 264-276.
- Laukamp, C., 2006. Structural and Fluid System Evolution in the Otavi Mountainland (Namibia) and its significance for the genesis of sulphide and nonsulphide mineralisation. PhD thesis, University of Heidelberg, 167 p.
- Lombaard, A.F., G  nzel, A., Innes, J., Kr  ger, T.I., 1986. The Tsumeb Lead-Copper-Zinc-Silver Deposit, South West Africa/Namibia. *Mineral Deposits of Southern Africa*, I & II, 1761-1787.
- Madalosso, A., 1979. Stratigraphy and sedimentation of the Bambu   Group in Paracatu region, MG, Brazil: Unpublished M.A. thesis, Rolla, University of Missouri, 127 p.
- Mallick, D. I. J., 1966. The stratigraphy and structural development of the Mpande Dome, Southern Zambia. *Geological Society of South Africa*, 69, 211-230.

- Maloof, A.C., 2000. Superposed folding at the junction of the inland and coastal belts, Damara Orogen, NW Namibia. Communications of the Geological Survey of Namibia. Department of Economic Affairs, 12, 89-98.
- Markham, N.L., 1958. Mineralogy of the Berg Aukas vanadium and secondary lead-zinc ores. South West Africa Company Limited.
- Marsh, J.S., Swart, R.S., Philips, D., 2003. Implications of a new $^{40}\text{Ar}/^{39}\text{Ar}$ age for a basalt flow interbedded with the Etjo Formation, Northeast Namibia. South African Journal of Geology, 106, 281-286.
- Martin, H., 1965. The Precambrian Geology of South West Africa and Namaqualand. The Precambrian Research Unit, 159.
- Matthews, A., 2005. Star Zinc deposit, Zambia, Africa. Unpublished, 2p.
- Melcher, F., 2003. The Otavi Mountain Land in Namibia: Tsumeb, Germanium and Snowball Earth. Mitteilungen der Österreichischen Mineralogischen Gesellschaft, 148, 413-435.
- Melcher, F., Oberthür, T., Vetter, U., Gross, C., Vollbrecht, A., Brauns and M., Haack, U., 2003. Germanium in carbonate-hosted Cu-Pb-Zn mineralisation in the Otavi Mountain Land, Namibia.
- Melcher, F., Oberthür, T., Rammlmair, D., 2006. Geochemical and mineralogical distribution of germanium in the Khusib Springs Cu-Zn-Pb-Ag sulfide deposit, Otavi Mountain Land, Namibia. Mineralium Deposita, 42(7), 791-797.
- Metsger, R.W., 1962. Notes on the Sterling Hill ore body, Ogdensburg, N.J., in Northern field excursion guidebook: International Mineralogical Association third general congress: Washington, D.C., Mineralogical Society of America, 12-21.
- Metsger, R.W., 2001. Evolution of the Sterling Hill zinc deposit, Ogdensburg, Sussex County, New Jersey: Society of Economic Geologists Guidebook Series, 35, 75-87.
- Metsger, R.W., Tennant, C.B., and Rodda, J.L., 1958. Geochemistry of the Sterling Hill zinc deposit, Sussex Co., N.J.. Geological Society of America Bulletin, 69, 775-788.
- Miller, R.McG., 1983. The Pan-African Damara orogen of South West Africa/Namibia, in: Miller, R.McG., Evolution of the Damara orogen of South West Africa/Namibia. Special publication of the Geological Society of South West Africa, 11, 431-515.
- Miller, R.M., 1997. The Owambo Basin of Northern Namibia. In: R.C. Selley (Editor), Sedimentary Basins of the World, 237-268.
- Misi, A., Veizer, J., Kawashita, K., and Dardenne, M.A., 1997. The age of the Neoproterozoic carbonate platform sedimentation based on $^{87}\text{Sr}/^{86}\text{Sr}$ determinations, Bambuí and Una groups, Brazil [abs.]: South American Symposium on Isotope Geology in Brazil, Abstracts, 199-200.
- Misiewicz, J.E., 1988. The Geology and Metallogeny of the Otavi Mountain Land, Damara Orogen, SWA/Namibia, with particular reference to the Berg Aukas Zn-Pb-V deposit - A model or ore

genesis. MSC Thesis, Rhodes University, Grahamstown, 147p.

Monteiro, L.V.S., Bettencourt, J.S., Juliani, C. and de Oliveira, T.F., 2006. Geology, petrography, and mineral chemistry of the Vazante non-sulfide and Ambrósia and Fagundes sulfide-rich carbonate-hosted Zn-(Pb) deposits, Minas Gerais, Brazil. *Ore Geology Reviews*, 28, 201-234.

Monteiro, L.V.S., Bettencourt, J.S., Spiro, B., Graca, R. and de Oliveira, T.F., 1999. The Vazante zinc mine, Minas Gerais, Brazil: Constraints on willemitic mineralisation and fluid evolution. *Exploration and Mining Geology*, 8, 21-42.

Moore, S.J., 1956. Zinc and copper deposits of the Vazante area, Minas Gerais, Brazil. U.S. Geological Survey Bulletin 386, 16 p.

Moore, T.A., 1964. The geology of the Chisamba area: explanation of degree sheet 1428, SW quarter. Geological Survey of Zambia, report no.5.

Mulcahy, S., 1996. Lithological and structural controls of the Kabwe lead zinc deposits, Zambia. Unpublished PhD thesis, 93p.

Muller, D.W., 1972. The geology of the Beltana willemite deposits. *Economic Geology*, 67, 1146-1167.

Olesch, M., Doroshev, A.M., and Nechaev, P.J., 1982. Low pressure stability of zinc clinopyroxene ZnSiO_3 and the possible stable occurrence of zinc orthopyroxene: *Neues Jahrbuch fuer Mineralogie, Monatshefte*, 7, 312-320.

Pagel, M., Barbin, V., Blanc, P. and Ohnenstetter, D., 2000. Cathodoluminescence in geosciences: an introduction. Springer, Heidelberg, 514 p.

Partridge, T.C. and Maud, R.R., 1987. Geomorphic evolution of southern Africa since the Mesozoic. *South African Journal of Geology*, 90, 179-208.

Pickford, M., 1993. Age of supergene ore bodies at Berg Aukas and Harasib 3a, Namibia. *Communications of the Geological Survey of Namibia*, 8, 147-150.

Pickford, M., 2000. Neogene and Quaternary vertebrate biochronology of the Sperrgebiet and Otavi Mountainland, Namibia. *Communications of the Geological Survey of Namibia*, 12, 359-365.

Pirajno, F. and Joubert, B.D., 1993. An overview of carbonate-hosted mineral deposits in the Otavi Mountain Land, Namibia: implications for ore genesis. *Journal of African Earth Science*, 16, 265-272.

Pirajno, F., 1993. Hydrothermal ore deposits - Principles and fundamental concepts for the Exploration Geologist. Springer Verlag, 708 p.

Porada, H. 1989. Pan-African rifting and orogenesis in southern to equatorial Africa and eastern Brazil. *Precambrian Research*, 44, 103-136.

Porada, H., and Berhorst, V. 2000. Towards a new understanding of the Neoproterozoic–Early Palaeozoic Lufilian and Zambezi belts in Zambia and the Democratic Republic of Congo. *Journal of*

African Earth Science, 30, 717–771.

Prave, A.R., 1996. Tale of three cratons; Tectonostratigraphic anatomy of the Damara Orogen in northwestern Namibia and the assembly of Gondwana. *Geology*, 24(12), 1115–1118.

Preiss, W.V., ed., 1987. The Adelaide geosyncline: Late Proterozoic stratigraphy, sedimentation, paleontology, and tectonics. *Geological Survey of South Australia Bulletin* 53, 438 p.

Raab, M.J., Brown, R.W., Gallagher, K., Carter, A. and Weber, K., 2002. Late Cretaceous reactivation of major crustal shear zones in northern Namibia: constraints from apatite fission track analysis. *Tectonophysics*, 349, 75–92.

Rainaud, C.L., Armstrong, R.A., Master, S., Robb, L.J. & Mumba, P.A.C.C. 2002. Contributions to the geology and mineralisation of the central African Copperbelt: I. Nature and geochronology of the pre-Katangan basement. Abstracts, 11th IAGOD Quadrennial Symposium and Geocongress, Windhoek, 5.

Rainaud, C., Master, S., Armstrong, R.A., and Robb, L.J., 2005. Geochronology and nature of the Palaeoproterozoic basement in the Central African Copperbelt (Zambia and the Democratic Republic of Congo), with regional implications. *Journal of African Earth Science*, 42, 1–31.

Ramsay, C.R., Ridgway, J., 1977. Metamorphic patterns in Zambia and their bearing on problems of tectonic history. *Precambrian Research* 4, 321–337.

Reynolds, N.A., Chisnall, T.W., Kaewsang, K., Keesaneyabutr, C. and Taksavas, T., 2003. The Padaeng supergene nonsulfide zinc deposit, Mae Sod, Thailand. *Economic Geology*, 98(4), 773–785.
Roedder, E., 1984. Fluid inclusions. *Reviews in Mineralogy*, 12, 646p.

Schneider, J., Boni, M., Laukamp, C., Bechstädt, T. and Petzel, V., 2008. Willemite (Zn_2SiO_4) as a possible Rb–Sr geochronometer for dating nonsulfide Zn–Pb mineralisation: Examples from the Otavi Mountainland (Namibia). *Ore Geology Reviews*, 33, 152–167.

Schneider, J., Melcher, F. And Brauns, M., 2007. Concordant ages for the giant Kipushi base metal deposit (DR Congo) from direct Rb–Sr and Re–Os dating of sulfides. *Mineralium Deposita*, 42(7), 791–797.

Schneiderhöhn, H., 1929. Das Otavi-Bergland und seine Erzlagerstätten - Ein Führer für die Exkursionen anlässlich des XV. Internationalen Geologen Kongresses 1929. *Zeitschrift für praktische Geologie*, 37, 85–116.

Selley, D., Broughton, D., Scott, R., Hitzman, M., Bull, S., Large, R., McGoldrick, P., Croaker, M., Pollington, N. and Barra, F., 2005. A new look at the geology of the Zambian Copperbelt, in Hedenquist, J. W., Thompson, J.F.H., Goldfarb, R. J., and Richards, J.P, eds., *Economic Geology*, 100th Anniversary Volume, 965–1000.

Simonov, M.A., Sandomirskii, P.A., Egorov-Tismenko, Y.K. and Belov, N.V., 1977. The crystal structure of willemite $\text{Zn}_2[\text{SiO}_4]$. *Soviet Physics Doklady*, 22, 622–623.

Simpson, J. G., Drysdall, A. R. and Lambert, H. H., 1963. The geology and groundwater resources of the Lusaka area: explanation of degree sheet 1528, NW quarter, Lusaka. *Geological Survey of*

Northern Rhodesia, 59 p.

Smith, A. G. 1963. The geology of the country around Mazabuka and Kafue: explanation of degree sheets 1527, SE quarter and 1528, SW quarter, Lusaka. Geological Survey of Northern Rhodesia, 52 p.

Sims, P.K., 1958. Geology and magnetite deposits of Dover district, Morris County, New Jersey. U.S. Geological Survey Professional Paper 287, 162 p.

Singletary, S.J., Hanson, R.E., Martin, M.W., Crowley, J.L., Bowring, S.A., Key, R.M., Ramokate, L.V., Direng, B.B., Krol, M.A., 2003. Geochronology of basement rocks in the Kalahari Desert, Botswana, and implications for regional Proterozoic tectonics. *Precambrian Research*, 121, 47-71.

Söhnge, P.G., 1957. Geology of the Otavi Mountain Land, Tsumeb Corporation Ltd.

Söhnge, P.G., 1964. The geology of the Tsumeb mine. *Geological Society of South Africa*, 65, 367-382.

Söhnge, P.G., 1967. Tsumeb. A historical sketch. *Scientific Research in South West Africa*, 5th series. Committee of the S.W.A. Scientific Society, Windhoek, 94 p.

Stalder, M. and Rozendaal, A., 2005. Calderite-rich garnet and franklinite-rich spinel in amphibolite-facies hydrothermal sediments, Gamsberg Zn-Pb deposit, Namaqua Province, South Africa. *The Canadian Mineralogist*, 43, 585-599.

Sweeney, M.A., Patrick, R.A.D. and Vaughan, D.J., 1991. The nature and genesis of Willemite deposits of Zambia. *Source, Transport, and Ore Deposition of Metals*. M. Pagel and J. Leroy, Eds., First Biennial SGA Meeting, Nancy, Rotterdam, Balkema, 139-142.

Taylor, J.H., 1953. The lead-zinc-vanadium deposits at Broken hill, Northern Rhodesia. *Colonial Geology and Mineral Resources*, 4, 335-365.

Tegtmeyer, A. and Kröner, A., 1985. U-Pb zircon ages for granitoid gneisses in northern Namibia and their significance for Proterozoic crustal evolution of south-western Africa. *Precambrian Research*, 28, 311-326.

Teal exploration and mining company, 2001. An introduction to Teal's Kabwe Exploration. unpublished report, 23p.

Thomas, L., 1968. The geochemistry of the carbonate rocks associated with the Pultapa (Beltana) zinc deposit, northern Flinders Ranges, South Australia. Unpublished B.Sc. thesis, Adelaide, Australia, University of Adelaide, 73 p.

Thorman, C.H., and Nahas, S., 1979. Reconnaissance geological study of the Vazante zinc district, Minas Gerais, Brazil. U.S. Geological Survey Prof. Paper 1126-I, 12 p.

Unrug, R. 1988. Mineralisation controls and source of metals in the Lufilian fold belt, Saba (Zaire), Zambia and Angola. *Economic Geology*, 83, 1247-1258.

Van der Westhuizen, W.A., 1984. The nature, genesis and geochemistry of the supergene vanadium ores of the Otavi Mountain Land. MSC University Orange Free State, Bloemfontein, 196 p.

Verwoerd, W.J., 1953. The mineralogy and genesis of the lead-zinc-vanadium deposit of Abenab West in the Otavi Mountains, South West Africa. Ann. University of Stellenbosch, 33, Section A, 1-11, 235-329.

Verwoerd, W.J., 1957. The mineralogy and genesis of the lead-zinc- vanadium deposit of Abenab West in the Otavi mountains, South West Africa. Annale Universiteit van Stellenbosch, Serie A, 33, 235-319.

Vinyu, M.L., Hanson, R.E., Martin, M.W., Bowring, S.A., Jelsma, H.A., Krol, M.A. and Dirks, P. H. G. M., 1999. U/Pb and $^{40}\text{Ar}/^{39}\text{Ar}$ geochronological constraints on the tectonic evolution of the easternmost part of the Zambezi orogenic belt, northeast Zimbabwe. Precambrian Research, 98, 67-82.

Volkert, R.A., 2001. Geologic setting of Proterozoic iron, zinc, and graphite deposits, New Jersey Highlands. Society of Economic Geologists Guidebook Series, 35, 59-73.

Vràna, S.; Prasad, R.; and Fediukova, E. 1975. Metamorphic kyanite eclogites in the Lufilian Arc of Zambia. Contribution to Mineralogy and Petrology, 51, 139-160.

Wartha, R.R. and Schreuder, C.P., 1992. Minerals Resource Series - Vanadium. Ministry of Mines and Energy, Geological Survey of Namibia, Windhoek, 16 p.

Weilers, B.F., 1959. A contribution to the geology of the lead-zinc-vanadate mine at Berg Aukas, South Western Africa Company Limited.

Wilson, T. J., Hanson, R. E. and Wardlaw, M. S., 1993. Late Proterozoic evolution of the Zambezi belt: implications for regional Pan-African tectonics and shear displacements in Gondwana. *In* Findlay, R. H.; Unrug, R.; Banks, M. R.; and Veevers, J. J., eds. Gondwana eight: assembly, evolution and dispersal. Rotterdam, Balkema, 69–82.

Woollett, A., 2005. The Processing of Non-Sulfide Zinc Deposits. Paper presented at the ESF Workshop: Nonsulfide Zn-Pb Deposits, M. Boni and H.A. Gilg, Eds., Iglesias, Italy, 21-23 April, 2005.

Ypma, P.J.M., 1978. Fluid inclusions and ore genesis in the Otavi Mountains, South West Africa. Part I: Geothermometry and barometry. Unpublished Report, Dept. of Economic Geology, University of Adelaide, Australia.

Zaw, K., Large, R.R., Huston, D.L., 1997. Petrological and geochemical significance of a Devonian replacement zone in the Cambrian Rosebery massive sulphide deposit, Western Tasmania. The Canadian Mineralogist, 35, 1325-1349.

Zheng, Y.F., 1996. Oxygen isotope fractionation in zinc oxides and implications for zinc mineralisation in the Sterling Hill deposit, USA. Mineralium Deposita 31, 98-103.